LBL-13604

Lawrence Berkeley Laboratory
UNIVERSITY OF CALIFORNIA

Materials & Molecular
Research Division

NMR STUDIES OF ORIENTED MOLECULES

Steven Williams Sinton
(Ph.D. thesis)

November 1981

Prepared for the U.S. Department of Energy under Contract W-7405-ENG-48

LBL 13604

NMR Studies of Oriented Molecules

By

Steven Williams Sinton
Ph.D. Thesis

November 1981

Materials and Molecular Research Division
Lawrence Berkeley Laboratory
University of California
Berkeley, CA 94720

This work was supported by the Director, Office of Energy Research, Office of Basic Energy Sciences, Materials Sciences Division of the U. S. Department of Energy under Contract Number W-7405-ENG-48.

NMR STUDIES OF ORIENTED MOLECULES

Steven Williams Sinton

Abstract

The properties of liquid crystalline mesophases have been of continuing interest in physics and chemistry since the discovery of these novel compounds. Recently, nuclear magnetic resonance (NMR) spectroscopy has been extensively used to probe the microscopic nature of liquid crystal samples. The NMR spectra contain information which is sensitive to internal molecular parameters and reflect the anisotropic potential in which the molecules reorient. Fast diffusion and rotational motion remove the effects of couplings between molecules.

In this work, deuterium and proton magnetic resonance are used in experiments on a number of compounds which either form liquid crystal mesophases themselves or are dissolved in a liquid crystal solvent. The nature of the information available from the spectra and limitations imposed by assumptions necessary in their analyses are discussed. The new technique of proton multiple quantum NMR is employed as a means to simplify complicated spectra without the need for selective isotopic substitution. In a multiple quantum experiment, the change of the total magnetic quantum number, M, associated with observed spectral lines may be any integer allowed by the number of coupled spins; e.g., $\Delta M = 0, \pm 1, \ldots, \pm N$ for N coupled spin-1/2 nuclei. This experiment also retains the higher sensitivity and precision in structural information available from proton NMR compared with other nuclei. The theory of non-selective multiple quantum NMR is briefly reviewed. Experimental examples with benzene dissolved in a liquid crystal are used to demonstrate several

outcomes of the theory. Possible complications in the analysis of spin echo spectra when chemical shifts and heteronuclear couplings are present in a strongly coupled spin system are discussed.

Experimental studies include proton and deuterium single quantum ($\Delta M = \pm 1$) and proton multiple quantum spectra of several molecules which contain the biphenyl moiety. The number of multiple quantum transitions in the spectrum can be easily predicted from simple symmetry arguments for para-substituted biphenyl. These predictions and the extraordinary simplicity of parts of the multiple quantum spectrum allow unambiguous line assignments and tests of simple models to be made in the analysis.

4-Cyano-4'-n-pentyl-d_{11}-biphenyl (5CB-d_{11}) is studied as a pure compound in the nematic phase. Assignments of the proton decoupled deuterium single quantum spectrum of the alkyl chain are made to obtain the chain order parameters and dipolar couplings. These are found to be in close agreement with previously reported results. The undecoupled and deuterium decoupled proton multiple quantum NMR spectra are analyzed for the aromatic core order tensor and structural parameters. A number of models for the effective symmetry of the biphenyl group in 5CB-d_{11} are tested against the experimental spectra. Most of the features are reproduced by the simplest model and possible causes of additional structure in the spectra are discussed. The dihedral angle, defined by the planes containing the rings of the biphenyl group, is found to be $30 \pm 2°$ for 5CB-d_{11}. Experiments are also described for 4,4'-d_2-biphenyl, 4,4'-dibromo-biphenyl, and unsubstituted biphenyl. Complete descriptions are given of the NMR spectrometer and computer programs used to obtain and analyze these spectra.

TO MY FAMILY

Acknowledgments

Graduate school at Berkeley is an extraordinary time for all those who have the opportunity to experience it. I will certainly always look back on this period as one of special significance in my life. Many people have been crucial to my work and it would be difficult to name all those who, by their support and services, richly deserve acknowledgment.

It has been a great pleasure to work with Professor Alexander Pines during my stay at Berkeley. I have had the rare opportunity to observe his laboratory evolve and become a truly unique and productive force in the College of Chemistry. Alex's seemingly limitless energy and personal drive receive the credit for this evolution and the constant evaluation of past and future goals which keeps the group at the forefront of the field and chemical physics in general. The group has always attracted capable graduate students and postdocs whose variety of interests and personalities have constantly generated new ideas and made the lab an exciting forum for their exchange.

Several other people deserve special mention for their involvement in my research. Dr. David Wemmer's scientific insights were invaluable during my initial years and his friendship is deeply appreciated. Dan Weitekamp, Gary Drobny, Jim Murdoch and Joel Garbow have been very generous in the time they have devoted to problems related to my research. Together they have provided the lab with many of its special qualities and I consider each a personal friend. There are many others whom I have either worked closely with, or whose contributions have proved important in shaping and defining this work. I have been fortunate to have worked with Dr. Zeev Luz, whose brilliance in the field of liquid

crystals underlies much of this work. I have also had many enlightening discussions with Dr. Soemi Emid on solid state physics and NMR in general. Drs. David Ruben, Jerome Ackerman and Luciano Muller have been very helpful during their stays as postdocs in the group. I would like to extend special thanks to Jau Tang, Yu-sze Yen, Warren Warren, Larry Sterna, Dick Eckman, Rob Tycko, David Zax, Jean Baum and John Millar. The wizardry of Sidney Wolfe was responsible for the synthesis of most of the compounds described in this work. Dr. Melvin Klein and his group have provided many hours of fruitful discussion on NMR and related topics.

The efforts of Don Wilkinson and members of the electronics shop of the College of Chemistry have been crucial in the design and construction of equipment needed for this work. I am indebted to Drs. P. Diehl and H. Bosiger for providing a copy of their program SHAPE which has been the basis for some of the computational approaches used in this work.

A generous contribution of computer time from the Melvin Calvin Laboratory is gratefully acknowledged as are the myriad of personnel and services of the Lawrence Berkeley Laboratory without which this thesis could not have been written. For their patient deciphering of my handwritten manuscript and professionalism in typing the first and final drafts, Mrs. Dione Carmichael and Ms. Cordelle Yoder deserve well earned thanks.

The most important contributions to bringing about a completion of this work were the understanding and unwaivering support I received from my family. I know of no way that I can adequately express my thanks to them. I only hope that by dedicating this thesis to my family, they can share something of my sense of accomplishment in return for all they have done for me.

This research was supported in part by the Division of Materials Sciences, Office of Basic Energy Sciences, U. S. Department of Energy under Contract W-7405-ENG-48.

TABLE OF CONTENTS

TABLE OF CONTENTS (continued)

TABLE OF CONTENTS (continued)

TABLE OF CONTENTS (continued)

Chapter 1

Fundamentals

1.1 Introductory Remarks

It is usual to begin a discussion of experiments which employ a spectroscopic technique with a description of the basic interactions involved and their relation to quantities of interest. In this work, the spectroscopy of nuclear magnetic resonance (NMR) is used to study anisotropic molecular ordering, structure and internal motion in liquid crystals. The two major areas to be considered are the use of NMR (1) as a tool to probe the chemical nature of the compounds and (2) in the ongoing investigation of basic spectroscopic physics. For this work, the first part is found in the sensitivity of nuclear magnetic resonance to the interaction between the individual dipole moments of nuclei. This phenomenon is in turn important in elucidating internuclear distances and ordering in condensed matter, particularly liquid crystals. The second area, that of understanding a new spectroscopic process, is found in the development of a technique known as multiple quantum NMR spectroscopy. The usefulness of this technique in our work lies in the tremendous aid in spectral assignment possible from a multiple quantum experiment.

Several aspects of theory and experiment for multiple quantum NMR spectroscopy and its application to liquid crystals and solutions of small molecules dissolved in liquid crystals are described in the following chapters. The next few sections of this chapter present the basic interactions important in liquid crystal NMR and a brief description of the properties of multiple quantum transitions with reference to the energy level diagram. Chapter 2 gives a detailed description of the

information available in the NMR spectrum of an ordered medium such as a liquid crystal. The limitations of this approach are also discussed. Chapter 3 describes the basic multiple quantum experiment. A review of density matrix formalism is held off until then. The rotational properties of the multiple quantum density matrix are explored with experimental examples of benzene partially ordered in a liquid crystal solution. Chapter 4 presents a specific example of multiple quantum NMR of biphenyl groups which demonstrates some of the principles developed in earlier chapters. Finally, a complete description of one of the two 180 MHz Fourier transform spectrometers used for all experiments is found in Chapter 5. The Appendices contain the details of computer programs used for calculations and data preparation and complete listings of each.

1.2 The Nuclear Spin Hamiltonian

Usually, the strongest nuclear spin interaction present for a sample in a high magnetic field is the Zeeman interaction. Classically, the energy of this interaction (for a single spin) is

$$E = -\vec{\mu}\cdot\vec{H} \tag{1.1}$$

where $\vec{\mu}$ is the magnetic moment of the nucleus and $\vec{H}$ is the large static field. The moment arises from the intrinsic angular momentum of the electrically charged nucleus; hence the term spin. Quantum mechanically, this energy is related to the angular momentum operator $\vec{I}$ through Equation (1.2).

$$\vec{\mu} = \gamma\hbar\vec{I}, \tag{1.2}$$

where $\hbar$ is Plank's constant divided by 2π.

It is well known that $\vec{I}^2$ and one of the components of $\vec{I}$ may have simultaneous eigenvalues for the wavefunction of the spin [1]. The total angular momentum is $\hbar I(I+1)$ where I is the eigenvalue of $\vec{I}^2$. By convention, I_z is the component of $\vec{I}$ taken to commute with $\vec{I}^2$. The eigenvalues of I_z are the $(2I+1)$ values $m\hbar$ where $m = I, I-1,\ldots-I+1,-I$. Taking the magnetic field to be $\vec{H} = (0,0,H_0)$ gives

$$E = -\gamma\hbar H_0 m. \tag{1.3}$$

The constant γ is known as the gyromagnetic ratio and its value is tabulated for every nucleus of interest in NMR. It is not the purpose of this work to measure γ and so the important interactions are perturbations of the Zeeman energy given in Equation (1.3).

Before proceeding with a discussion of these interactions, it is worthwhile to point out some of the important consequences of Equation (1.3). The quantization of the z axis component of angular momentum in the static field, described by the operator I_z and having discrete values $m\hbar$, means that the energies are bounded by the $(2I+1)$ values of m. The result is that the density matrix approach is particularly useful in the description of pulsed NMR experiments.

Although the measurement of the energy level diagram for single nuclei when $I \geq 1$ provides information from quadrupole perturbations to Equation (1.3), it is often more useful to consider a collection of nuclei. For our purposes, a collection of interacting protons is relevant. For N such spin ½ nuclei, the total z component of angular momentum is described by the quantum number $M = \sum_i m_i$. Here the sum runs over all nuclei which together are sufficient to describe the energy level diagram of the system. There are $N+1$ possible unique values of M

from M = +N/2 to M = -N/2 differing by 1. There are a total of 2^N states for the entire N spin ½ system. The energy differences among states for a particular value of M (termed a Zeeman manifold) are determined by the perturbative Hamiltonians described below.

1.2.1 The Zeeman Hamiltonian

The Zeeman interaction has already been given for a single spin in Equation (1.3). For an N spin system, setting $\hbar = 1$ and measuring energies in frequency units, the general Zeeman Hamiltonian is written

$$\begin{aligned} H_Z &= -H_0 \sum_i \gamma_i I_{zi}, \\ &= -\omega_0 \sum_i I_{zi}, \\ &= -\omega_0 I_z, \end{aligned} \tag{1.4}$$

where ω_0 is the angular Larmor frequency ($\omega_0 = 2\pi\nu_0$). At magnetic field strengths of about 42 kG, ν_0 is approximately 185 MHz for protons.

1.2.2 Radio Frequency Hamiltonian

The interaction of nuclear spins with an externally applied radio frequency magnetic field is quite similar to the Zeeman term above. Assuming this field to be oscillating along the x axis of the laboratory frame, the r.f. Hamiltonian becomes

$$H_{rf} = -H_1(t)\cos(\omega t + \phi(t)) \sum_i \gamma_i I_{xi}. \tag{1.5}$$

$I_x = \sum_i I_{xi}$ is the operator for the x component of the spin angular momentum. $H_1(t)$ is the time dependent field amplitude oscillating at frequency ω with phase $\phi(t)$. The usual approach at this point is to transform to an interaction frame known as the rotating frame [2]. This is accomplished by the following equation:

$$H_{rf}^{R} = e^{-i\omega t I_z} H_{rf} e^{i\omega t I_z} \tag{1.6}$$

where the exponential operator is defined by [2,3]

$$e^{-i\omega t I_z} = 1 - i\omega t I_z + \frac{(\omega t)^2}{2} I_z^2 - \frac{i(\omega t)^3}{6} I_z^3 + \ldots . \tag{1.7}$$

The transformation of Equation (1.6) effectively removes the time dependence of the frequency part of the cosine term in Equation (1.5). The result is given in Equation (1.8) (dropping terms oscillating at higher frequencies [4]).

$$H_{rf}^{R} = -\omega_1(t)[I_x \cos\phi(t) + I_y \sin\phi(t)]. \tag{1.8}$$

In this equation $\omega_1(t) = \gamma H_1(t)$ is the r.f. field amplitude in angular frequency units. The occurrence of the operators I_x and I_y in Equation (1.8) comes about from the definition of the exponential operator and commutation properties of the angular momentum operators [3,5].

If we also transform observable quantities, such as the Zeeman interaction to this rotating frame, the spin system will appear to evolve as though it were observed from a frame rotating about the z axis at angular velocity ω (hence the name). When the transformation is applied to the Zeeman Hamiltonian Equation (1.4) the result is

$$H_Z^{R} = -(\omega_0 - \omega)\ I_z = -\Delta\omega I_z. \tag{1.9}$$

The factor $\Delta\omega$ is called the offset. Throughout this work, the rotating frame transformation will be assumed and the superscript R dropped.

The remaining interactions described below all take the form of spatial and spin tensor products [6]. The spatial tensors involving just one spin are the chemical shift and quadrupolar tensors. The scalar

(or spin-spin) and dipolar (or direct) tensors involve the interaction of spins with magnetic fields generated by their neighbors. All are second rank tensors which may be described in a cartesian or spherical basis [7,8]. Under different conditions, each of these tensor interactions can be reduced in rank or removed by "averaging". As an example, the anisotropic chemical shift interaction, the dipolar interaction and the quadrupolar interaction are all unobservable in non-viscous liquid samples. This comes about from rapid, isotropic motion of the spins attached to tumbling molecules. By rapid it is meant that the motion is fast on the time scale of the interactions and by isotropic it is meant that the average over all possible orientations for the spatial part of the tensor is zero.

Besides the use of an isotropic liquid, there exists a number of ways for selectively averaging the interactions below. Since the Hamiltonian for each consists of a product of spatial and spin terms, this averaging may be done in either coordinate or spin space. These selective techniques are fully described elsewhere [6] and are only indirectly relevant to an understanding of this work. The isotropic and, for liquid crystals, anisotropic averaging of spatial quantities provided by nature are very important in our experiments and will be described briefly here and in more detail in latter chapters.

In the equations of the next few sections, the second rank interaction tensors are written in a cartesian coordinate system basis with axes X, Y, Z. Thus, they may be expressed as 3 x 3 matrices and the Hamiltonians become scalar products of these with spin operator vectors such as $\vec{I} = (I_x, I_y, I_z)$ and $\vec{S} = (S_x, S_y, S_z)$. The X, Y, Z system is fixed in space. If we take the Z axis to be along the main field direction, then the subscripts on tensor elements below refer to components observed

in the laboratory frame. To describe the interaction tensors in some other coordinate system, such as one fixed in the molecules, requires transformations of the spatial part of the Hamiltonian as covered in Chapter 2 and detailed elsewhere [7,8].

There will always exist some coordinate system in which a spatial interaction tensor is diagonal. In general, this principle axis system (PAS) will not be the same for different interactions. Often, one writes each of the Hamiltonians below in a PAS and then the tensor elements are the principle components of the interaction. In this case, the transformation required to relate the Hamiltonian to an NMR spectrum is from the PAS to lab frame. Depending on the nature of the sample, the PAS components of the tensor may be found from lab frame measurements. For a sample consisting of a single crystal, rotation plots of the frequencies measured from the spectrum reveal the principle components [14,15]. If the sample is a polycrystalline solid, then a "powder pattern" line shape will result. An example is the well known asymmetric chemical shift powder pattern observed for many samples [14]. In the following chapters, whenever the Hamiltonian refers to a particular coordinate system, that system will be identified. We will always state the nature of any coordinate transformations performed.

In considering the perturbations to H_Z below, reference is made to the secular part of the Hamiltonian. This refers to the usual truncation of some parts of the total Hamiltonian to those terms which commute with I_z. This approximation is valid for all cases in this work as non-commuting parts of the quadrupolar, dipolar, spin-spin, and chemical shift interactions are all small compared to the Zeeman term (the "high field approximation").

1.2.3 The Quadrupolar Hamiltonian

When a nucleus with spin $I \geq 1$ is present at a site with non-zero electric field gradients, the total energy depends on its orientation. This is expressed by the quadrupolar Hamiltonian in Equation (1.10).

$$H_Q = \frac{eQ}{6I(2I-1)} \vec{I} \cdot \underset{\approx}{V} \cdot \vec{I} \tag{1.10}$$

Q is called the quadrupole moment of the nucleus and is related to the quadrupole term of a multipole expansion for the charge distribution of the nucleus. The tensor $\underset{\approx}{V}$ is the field gradient tensor with elements $V_{\alpha\beta} = \frac{\partial^2 V}{\partial\alpha\partial\beta}$ for α,β = X, Y, Z. That $\underset{\approx}{V}$ is traceless and symmetric can be seen from Laplace's equation $\vec{\nabla}^2 V = 0$, and the symmetry of the partial derivatives, $V_{\alpha\beta} = V_{\beta\alpha}$. For a collection of spins, it can be shown [9] that Equation (1.10) becomes

$$H_Q = \sum_i \frac{eQ^i}{6I_i(2I_i-1)} \sum_{\alpha\beta}^{XYZ} V^i_{\alpha\beta}[\tfrac{3}{2}(I_{\alpha i}I_{\beta i} + I_{\beta i}I_{\alpha i}) - \delta_{\alpha\beta}(\vec{I}_i)^2]. \tag{1.11a}$$

Truncating Equation (1.11a) to the secular terms gives

$$H_Q = \sum_i \frac{eQ^i}{4I_i(2I_i-1)} [V^i_{ZZ}(3I^2_{zi} - I^2_i) + (V^i_{XX} - V^i_{YY})(I^2_{xi} - I^2_{yi})]. \tag{1.11b}$$

$$H_Q = \sum_i \frac{eqQ^i}{4I_i(2I_i-1)} \{[3I^2_{zi} - I_i(I_i+1)] + \eta(I^2_{xi} - I^2_{yi})\}. \tag{1.11c}$$

In Equation (1.11) the quantity Q^i is the quadrupole moment of nucleus i. In Equation (1.11c) the gradient $eq = V_{ZZ}$ and the asymmetry parameter $\eta = \frac{(V_{XX}-V_{YY})}{V_{ZZ}}$ have been introduced. Usually, the electric field gradient is axially symmetric (or nearly so) and η is taken to be zero. That the quadrupolar Hamiltonian vanishes for nuclei with spin $I = \frac{1}{2}$ can be seen

from a consideration of the expectation value of the spin part of H_Q, i.e.,

$$\langle 3I_z^2 - I(I+1) \rangle = 0.$$

1.2.4 The Dipolar Hamiltonian

The energy of the interaction of spins with the local field caused by the dipole moments of neighboring nuclei is given classically by [10],

$$E_D = + \sum_{i<k} \left[\frac{\vec{\mu}_i \cdot \vec{\mu}_k}{r_{ik}^3} - \frac{3(\vec{\mu}_i \cdot \vec{r}_{ik})(\vec{\mu}_k \cdot \vec{r}_{ik})}{r_{ik}^5} \right] \tag{1.12}$$

which results in the quantum mechanical Hamiltonian (in frequency units)

$$H_D = + \sum_{i<k} \vec{I}_i \cdot \underset{\approx}{D}^{ik} \cdot \vec{S}_k. \tag{1.13}$$

In Equation (1.13) the dipolar interaction tensor, $\underset{\approx}{D}^{ik}$, is traceless and symmetric and $\vec{I}_i$, $\vec{S}_k$ are the spin angular momentum operators for spins i and k. The elements of $\underset{\approx}{D}^{ik}$ are $- \frac{\gamma_i \gamma_k}{r_{ik}^3} (3e_p e_q - \delta_{pq})$ where e_p, e_q (p,q = X,Y,Z) are direction cosines for the internuclear vector $\vec{r}_{ik}$. If the two spins i and k are of the same species ($\gamma_i = \gamma_k$) then, truncating H_D to the secular terms (terms which commute with H_Z) and noting that $\underset{\approx}{D}^{ik}$ is axially symmetric [11] makes Equation (1.13) become (with the Z axis along the main field)

$$H_D = + \sum_{i<k} D_{ZZ}^{ik} (3I_{zi}I_{zk} - \vec{I}_i \cdot \vec{I}_k) \tag{1.14a}$$

$$= + \sum_{i<k} D_{ZZ}^{ik} [I_{zi}I_{zk} - \tfrac{1}{4} (I_{+i}I_{-k} + I_{-i}I_{+k})], \tag{1.14b}$$

where

$$D_{ZZ}^{ik} = - \frac{\gamma_i \gamma_k (3\cos^2\theta_{ikZ} - 1)}{r_{ik}^3} . \qquad (1.15)$$

In Equation (1.15) the angle θ_{ikZ} is between the internuclear vector $\vec{r}_{ik}$ and the laboratory z axis. For Equation (1.14) we have introduced the well known raising and lowering (or "ladder") operators:

$$I_{+k} = I_{xk} + iI_{yk} \qquad (1.16a)$$

$$I_{-k} = I_{xk} - iI_{yk} \qquad (1.16b)$$

$$i = \sqrt{-1}.$$

For liquid crystal samples we will see that the angular part of Equation (1.15), averaged over all molecular orientational possibilities, becomes what is known as the ordering tensor [12]. The D_{ZZ}^{ik} of Equation (1.15) is in a space fixed axis system. For liquid crystals, transformation to a molecular axis system will be required. For an isotropic liquid (or a gas), $\langle 3\cos^2\theta_{ikZ} - 1 \rangle$ vanishes and dipolar interactions are not observed. We note here that there exists effectively two definitions of the coupling teasor $\underset{\approx}{D}^{ik}$ in the literature. These definitions differ only in the use of $P_2(\cos\theta)$ or $2P_2(\cos\theta)$ for the angular portion of Equation (1.15) where $P_2(\cos\theta)$ is the second legendre polynomial. We will consistently use the larger of the two forms of $\underset{\approx}{D}^{ik}$ and attempt to make note of any conversions required to relate couplings to literature values.

When the spins i and k are different nuclear species, then the secular part of Equation (1.13) becomes

$$H_D = \sum_{i<k} D_{ZZ}^{ik} I_{zi} S_{sk}. \qquad (1.17)$$

1.2.5 The Indirect Spin-Spin Hamiltonian

The interaction of Equation (1.12) is the "through space" or direct energy of spins in the magnetic field of neighbors. In addition, there is a "through bonds" or indirect interaction in which a nucleus feels the presence of its neighbors via the interactions each has with the electrons making up their common chemical bonds. This is given by

$$H_J = \sum_{j<k} \vec{I}_i \cdot \underset{\approx}{J}^{ik} \cdot \vec{S}_k . \tag{1.18}$$

Although the form of H_J is similar to H_D given in Equation (1.13), several differences exist. Whereas $\underset{\approx}{D}^{ik}$ is traceless, $\underset{\approx}{J}^{ik}$ is not, and the isotropic average,

$$J_{ik}^{iso} = \frac{1}{3} \mathrm{Tr}(\underset{\approx}{J}^{ik}) \equiv J_{ik}, \tag{1.19}$$

is the quantity measured as the "scalar" coupling in high resolution NMR of liquid samples. Also, $\underset{\approx}{J}^{ik}$ may have an antisymmetric component, but this cannot be measured in NMR [13]. The total indirect spin-spin Hamiltonian, for like spins i and k, may be written

$$H_J = \sum_{i<k} \{J_{ZZ}^{ik} I_{zi} I_{zk} + \frac{1}{2} (J_{XX}^{ik} + J_{YY}^{ik})(I_{xi} I_{xk} + I_{yi} I_{yk})\} \tag{1.20a}$$

$$H_J = \sum_{i<k} \{J_{ik} \vec{I}_i \cdot \vec{I}_k + \frac{1}{2} (J_{XX}^{ik} + J_{YY}^{ik})(3 I_{zi} I_{zk} - \vec{I}_i \cdot \vec{I}_k)\} \tag{1.20b}$$

where Equation (1.19) has been used. Equation (1.20b) is sometimes rewritten in the forms

$$H_J = \sum_{i<k} \{J_{ik} \vec{I}_i \cdot \vec{I}_k + J_{ik}^{aniso} (3 I_{zi} I_{zk} - \vec{I}_i \cdot \vec{I}_k)\} \tag{1.20c}$$

$$H_J = \sum_{i<k} \{J_{ik}[I_{zi}I_{zk} + \frac{1}{2}(I_{+i}I_{-k} + I_{-i}I_{+k})]$$

$$+ J_{ik}^{aniso}[I_{zi}I_{zk} - \frac{1}{4}(I_{+i}I_{-k} + I_{-i}I_{+k})]\} \qquad (1.20d)$$

The quantity J_{ik}^{aniso} above is usually much smaller than D_{ZZ}^{ik}. Because it multiplies spin operators in the same form as the dipolar Hamiltonian, J_{ik}^{aniso} is sometimes referred to as the pseudo-dipolar coupling. For liquid crystals J_{ik}^{aniso} cannot be measured independently of D_{ZZ}^{ik} by NMR, but may be estimated from theory or from a model for the D_{ZZ}^{ik} values.

1.2.6 The Chemical Shift Hamiltonian

The chemical shift interaction in nuclear magnetic resonance arises from the screening affect the electrons surrounding a nucleus have on the external magnetic field it experiences. Methods exist for calculating or estimating its value theoretically but will not be required in this work. The chemical shift Hamiltonian is presented here partly for consistency, but also because an important consideration for multiple quantum NMR as a high resolution technique has its origin in the "interference" of the chemical shift and dipolar Hamiltonians.

The chemical shift takes the form of a product of the second rank tensor $\underset{\approx}{g}$, the first rank spin operator vector $\vec{I}$, and $\vec{H}$ (once again taking Z to be along the main field),

$$H_{cs} = \sum_i \gamma_i \vec{I} \cdot \underset{\approx}{g} \cdot \vec{H} \qquad (1.21)$$

$$= \sum_i \gamma_i \sigma_{ZZ}^i I_z H_0 \text{ (secular term)},$$

where σ_{ZZ}^i is the ZZ component of the tensor $\underset{\approx}{g}^i$ for spin i. Often, the

product $\gamma_i H_0$ is included in σ^i_{ZZ} so that $H_{cs} = \sum_i \sigma^i_{ZZ} I_{zi}$. As with the spin-spin coupling, $\underset{\approx}{\sigma}^i$ is not traceless and σ^i_{ZZ} may contain an anisotropic component:

$$H_{cs} = \sum_i \gamma_i \sigma_i^{iso} H_0 I_{zi} + \sum_i \gamma_i \sigma_i^{aniso} H_0 I_{zi},$$

where

$$\sigma_i^{iso} = \frac{1}{3} \mathrm{Tr}(\underset{\approx}{\sigma}^i) \equiv \sigma_i.$$

1.2.7 Summary of the Spin Hamiltonian

Collecting all the interactions written above into the total spin Hamiltonian, we have

$$H = H_Z + H_{cs} + H_{rf} + H_Q + H_D + H_J \tag{1.22}$$

In the rotating frame and under the high field approximation:

$$\begin{aligned} H = & -\Delta\omega I_z + \sum_i \sigma^i_{ZZ} I_{zi} \\ & - \omega_1(t)[\cos(\phi(t))I_x + \sin(\phi(t))I_y] \\ & + \sum_i \frac{eqQ^i}{4I_i(2I_i-1)} \{[3I^2_{zi} - I_i(I_i+1)] + \eta(I^2_{xi} - I^2_{yi})\} \\ & + \sum_{i<k} D^{ik}_{ZZ} [I_{zi}I_{zk} - \frac{1}{4}(I_{+i}I_{-k} + I_{-i}I_{+k})] \\ & + \sum_{i<k} \{J^{ik}_{ZZ} I_{zi} I_{zk} + \frac{1}{4}(J^{ik}_{XX} + J^{ik}_{YY})(I_{+i}I_{-k} + I_{-i}I_{+k})\}. \end{aligned} \tag{1.23a}$$

Equation (1.23a) is sometimes written

$$H = -\Delta\omega I_z + \sum_i \sigma^i_{ZZ} I_{zi} - \omega_1(t)[\cos(\phi(t))I_x + \sin(\phi(t))I_y] \tag{1.23b}$$

$$+ \sum_i \frac{eqQ^i}{4I_i(2I_i-1)} \{[3I_{zi}^2 - I_i(I_i+1)] + \eta(I_{xi}^2 - I_{yi}^2)\}$$

$$+ \sum_{i<k} D_{ZZ}^{ik}(3I_{zi}I_{zk} - \vec{I}_i \cdot \vec{I}_k)$$

$$+ \sum_{i<k} \{J_{ZZ}^{ik} \vec{I}_i \cdot \vec{I}_k + \frac{1}{2}(J_{XX}^{ik} + J_{YY}^{ik})(3I_{zi}I_{zk} - \vec{I}_i \cdot \vec{I}_k)\}.$$

It is often assumed that the asymmetry parameter for the quadrupolar Hamiltonian is small, i.e., that this tensor is axially symmetric. For alkyl deuterons, the case of interest here, η is about .01 and this is a good assumption. If we also assume that the anisotropic parts of the chemical shift and spin-spin couplings are negligible, Equation (1.23b) becomes

$$H = -\Delta\omega I_z + \sum_i \sigma_i I_{zi} - \omega_1(t)[\cos(\phi(t))I_x + \sin(\phi(t))I_y] \qquad (1.23c)$$

$$+ \sum_i \frac{eqQ^i}{4I_i(2I_i-1)} (3I_{zi}^2 - I_i(I_i+1)) + \sum_{i<k} D_{ZZ}^{ik}(3I_{zi}I_{zk} - \vec{I}_i \cdot \vec{I}_k)$$

$$+ \sum_{i<k} J_{ik} \vec{I}_i \cdot \vec{I}_k,$$

where the definitions of the isotropic chemical shift and scalar coupling have been used. Often, the ZZ subscript on the dipolar term is dropped and the coupling is denoted simply as D_{ik}. This will be adopted heretofore except when the distinction of a particular component of the dipolar tensor is required.

All the NMR measurements analyzed in this work were taken with liquid crystal samples in a nematic mesophase. As we shall see, a liquid crystal is like a polycrystalline sample of rigid molecules in some respects but quite different in others. For one, the relation between

known or desired quantities of the molecules and the NMR spectrum is complicated by the need to average over a number of inter and intramolecular motions. Generally, the "ordering tensor" elements or "motional constants" are introduced to describe the average orientation of molecules with respect to some laboratory axis system. The elements of such an order tensor are actually the results of various transformations required to give the lab frame components of Equation (1.23c). We shall show how the symmetry properties of a uniaxial nematic liquid crystal reduce the number of elements required in the order tensor. Molecular symmetry will also become important in this consideration.

1.3 The Energy Level Diagram for Liquid Crystals

In Equation (1.23) we have written out the Hamiltonian for a collection of N spins.. In a non-dilute solid sample, N will be very large and, in general, none of the individual allowed transitions will be resolved. The usual approaches in this case include isotopic dilution or selective averaging to remove the largest contributions to line broadening. With liquid crystals (and molecules dissolved in a liquid crystal solution) nature does a good deal of averaging of the quadrupole and dipole terms to yield a spectrum with structure.

Liquid crystalline mesophases are generally characterized by some degree of long range order [16-18]. There are several types of mesophases which occur for thermotropic liquid crystals. Two of these are shown schematically in Figure 1.1. For the nematic mesophase, the long range order consists of an angular correlation of the long axes of the molecules. The preferred direction of these long axes is described by a unit vector called the "director". Smectic phases have a similar alignment of the director but in addition order into layers as shown in

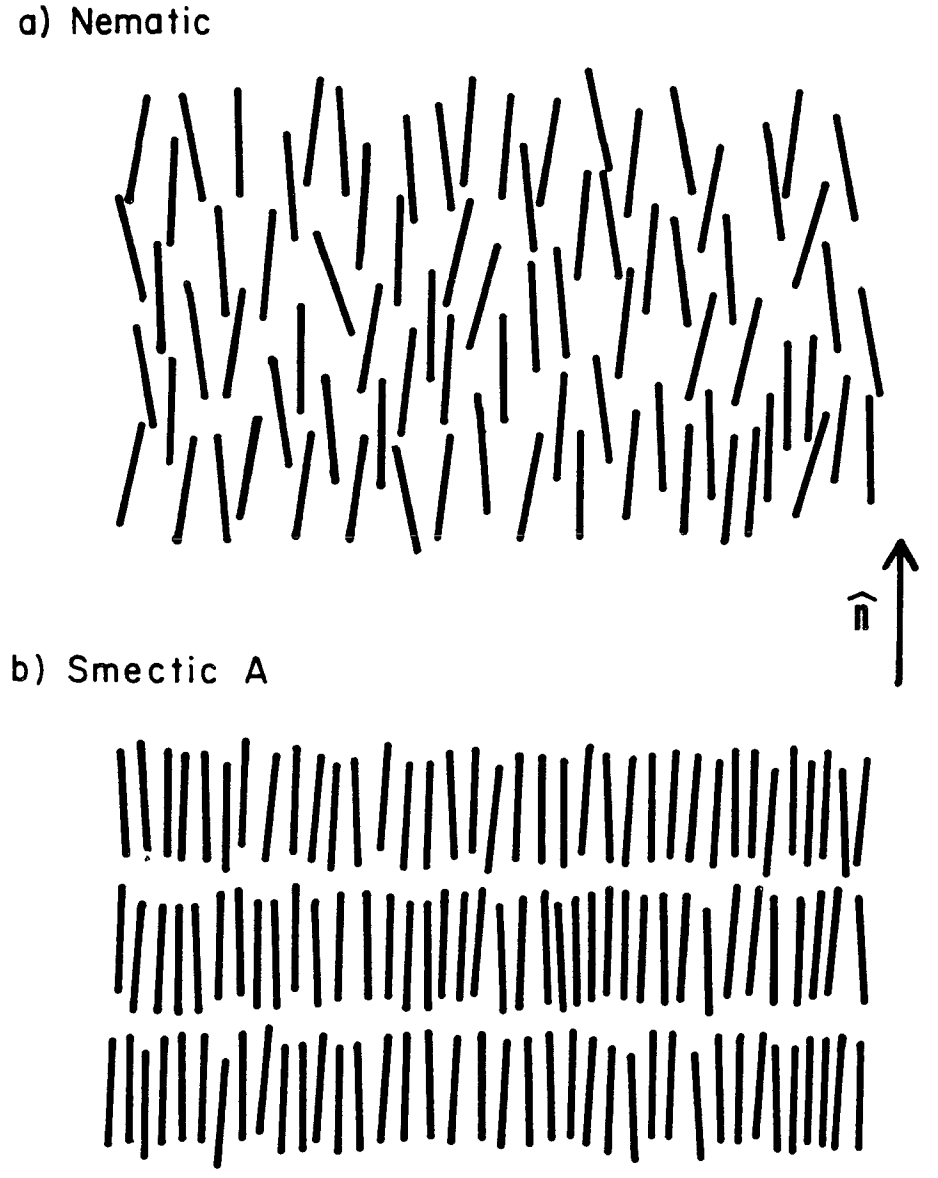

XBL 818-1765

Figure 1.1

Pictorial representation of the two common thermotropic liquid crystal phases. Liquid crystal molecules are viewed as rod-like particles whose long axes are preferentially aligned with respect to the crystal director, $\hat{n}$. In a), a nematic phase is depicted in which there is only this angular correlation of molecular long axes. In b), a smectic A phase is shown. In addition to an angular correlation, one translational degree of freedom for the center of mass of each molecule is correlated with the ensemble. Molecules then become ordered in planes as shown.

Figure 1.1. There is rotational symmetry about the director in the nematic phase which means that it is uniaxial. All of the NMR spectra taken in this work are in the nematic or isotropic phase and so further discussion will be directed to these phases.

When there are no external constraints on a nematic liquid crystal, the long axes of individual molecules and the director are not always colinear but fluctuate in relative orientation. The long range order extends over domains of many molecules (10^6). This order only consists of angular correlations with complete freedom of translational diffusion for the molecules (at least on the NMR time scale). When the nematic crystal is placed in a sufficiently high magnetic field, the director becomes aligned along the field direction. This is a result of the anisotropy of the magnetic susceptibility. The free energy for this interaction is [18]

$$F = -\Delta\chi H_0^2(3\cos^2\alpha - 1)/6, \tag{1.24}$$

where

$$\Delta\chi = \chi_{\parallel} - \chi_{\perp}$$

is the susceptibility anisotropy. The angle α is between the director and $\vec{H}_0$. For nematics studied in this work (and indeed most thermotropics), $\Delta\chi$ is positive which means the minimum free energy contribution occurs with the director along $\vec{H}_0$. For liquid crystals, this contribution is significant when compared to the thermal energy and so the director becomes aligned along $\vec{H}_0$.

When a small molecule is dissolved in a nematic solution it experiences the local potential of the liquid crystal matrix. If the molecule

is not completely symmetric itself, then clearly it will also seek a minimum free energy situation in which it orients with respect to the director. Unlike an isotropically tumbling molecule, interactions such as the quadrupolar and dipolar Hamiltonians will be present. Because the molecule is free to diffuse, intermolecular interactions are averaged away and the NMR spectrum displays only the intramolecular couplings. Even for a molecule which is highly symmetric, for example, a molecule with tetrahedral symmetry, dipolar and quadrupolar couplings have been observed in the NMR spectrum [19,20]. The exact mechanism for the ordering in this case is a matter of debate in the literature [21-23].

A generalized picture of the nuclear spin energy level diagram is shown in Figure 1.2. For the liquid crystal case the number of interacting spins, N, refers to those of each molecule in the ensemble. The major splittings shown are from the Zeeman interaction. Each set of states with a common total magnetic quantum number, M, is termed a Zeeman manifold. Without the perturbations of H_Q, H_D, H_J, and H_{cs}, the states of one Zeeman manifold are degenerate. If the N nuclei are all spin ½ (e.g., protons) then the total number of states is 2^N and each manifold contains $N!/(N/2-M)!(N/2+M)!$ states. The extreme energy states correspond to the situations in which all spins are aligned with or against the external field. There are a total of $N+1$ manifolds and, if N is odd, the $M=0$ manifold does not exist.

1.4 Multiple Quantum Transitions in NMR

The "golden rule" of time-dependent perturbation theory states the probability per unit time that a perturbation V induces a transition from state s to state k is given by [24]

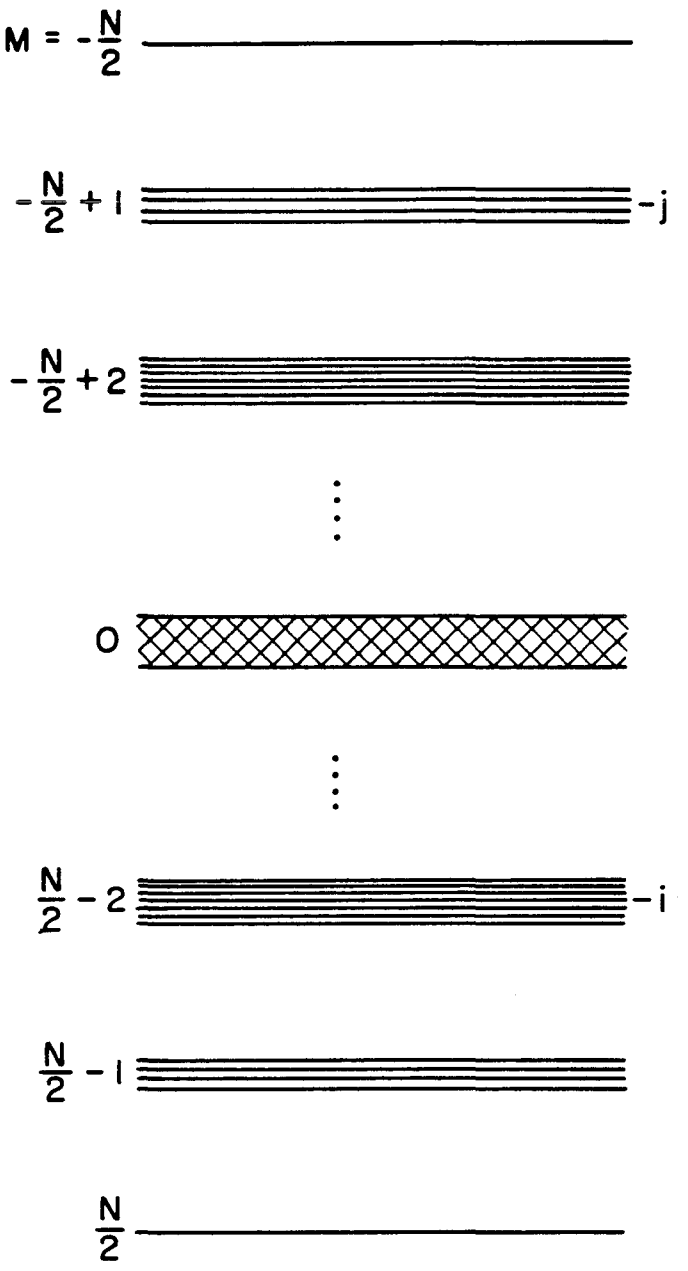

Figure 1.2

Energy level diagram for the spin Hamiltonian of a general system of N coupled spins each with spin quantum number ½. The total magnetic quantum number, M, is the sum of the Zeeman Hamiltonian quantum numbers $\pm$½ for each spin, and the large splittings are from the interaction energy of this Hamiltonian. Smaller splittings within each group of states with the same value of M arise from other spin interaction terms in the total Hamiltonian. A transition from state i to j represents a change in M of $\Delta M = N-3$. If N is odd, the group of states for M = 0 doesn't exist.

$$W_{ks} = \frac{2\pi}{\hbar}|\langle k|V|s\rangle|^2 \rho_f(E_s^{(0)}) \qquad (1.25)$$

where ρ_f is the density of states for the final (unperturbed) states. Referring to Figure 1.2 justifies the usual use of a delta function for ρ_f in NMR [25].

In NMR, we apply a perturbation to a sample at equilibrium by irradiating it with the oscillating magnetic field of the probe coil. Thus the perturbation takes the form of the r.f. Hamiltonian (Eq. (1.8)). The transition element is then $|\langle k|I_x|s\rangle|^2$ for the r.f. field along the x axis. The matrix elements can be evaluated in the usually spin product basis set (α's and β's) to yield the familiar selection rule that the change in the total magnetic quantum number is one ($\Delta M = \pm 1$) for allowed transitions. The intensity of these transitions is proportional to $|\langle k|I_x|s\rangle|^2$.

Equation (1.25) is from a first order treatment of perturbation theory. It was realized some years ago that higher order effects would cause multiple quantum ($\Delta M \geq 0$) transitions [26-28]. These non-linear effects were first demonstrated in the continuous wave observation of double quantum transitions in ethanol [29]. The technique has been used in the elucidation of spectral assignment of liquids [27].

The development of multiple quantum c.w. NMR was hampered by the technical difficulties associated with creating and observing this non-linear phenomenon. In addition, the strong r.f. fields required perturb the spin system in a manner that must be theoretically accounted for. The advent of pulsed Fourier transform techniques allowed the development of multiple quantum NMR without these problems. Theoretically, rather than dealing with photon absorption and emission processes, the FT

multiple quantum experiment can be described in terms of coherences and formulated with the density matrix. This approach will be covered in Chapter 3. The basics of the development of MQNMR is a rich subject and has been dealt with in an excellent review by Bodenhausen [30].

Referring to Figure 1.2, some of the terminology which will be used throughout this work can be defined. A multiple quantum "order" refers to all those transitions for which M changes by some integer. Thus, the zero quantum, one quantum, two quantum, ..., N quantum orders refer to transitions for which $M = 0, \pm 1, \pm 2, \ldots, \pm N$, respectively. Usually, the term single quantum will be used to mean the "normal" NMR spectrum although occasionally the one quantum order of a multiple quantum experiment may be meant. The only major differences between the two for this work will be in how the spectrum was obtained and thus the relative intensities of the single quantum lines.

Finally, a few words about the number of transitions expected for each order and the information content of the higher orders. The number of states in each Zeeman manifold is

$$\binom{N}{\frac{N}{2} - M} = \frac{N!}{(\frac{N}{2} - M)!\,(\frac{N}{2} + M)!} \tag{1.26}$$

where the common symbol for the binomial coefficient has been used. Thus, except for the zero quantum order and assuming no molecular symmetry, the number of p quantum transitions is given by

$$\sum_{k=0}^{N-p} \binom{N}{k}\binom{N}{k+p}, \quad p = 1, 2, \ldots, N \tag{1.27}$$

This is equivalent to the following expression [31].

$$\#\ \text{p quantum transitions} = \binom{2N}{N-p}, \quad p \neq 0 \tag{1.28a}$$

Also, for the zero quantum transition,

$$\text{Number zero quantum transitions} = \frac{1}{2}\left[\binom{2N}{N} - 2^N\right]. \tag{1.28b}$$

Using Sterling's approximation and an expansion for $\ell n(1+x)$, for large N Equation (1.28a) can be approximated as

$$4^N\, e^{-p^2/N}, \quad p = 1, 2, \ldots, N. \tag{1.29}$$

Thus we see that the number of transitions expected from a set of coupled spins with no symmetry has a Gaussian distribution with order.

The extreme states shown in Figure 1.2 have a special property. The bilinearity of spin operators in the dipolar, quadrupolar and spin-spin Hamiltonians given in Section 1.2 means that these states will only experience the sum of these interactions for all spins. For example, for N protons the extremes states correspond to all spins in either the α or the β state. The dipolar Hamiltonian matrix elements are

$$\langle\alpha(1)\ldots\alpha(N)|H_D|\alpha(1)\ldots\alpha(N)\rangle = \langle\beta(1)\ldots\beta(N)|H_D|\beta(1)\ldots\beta(N)\rangle = \sum_{i<k} D_{ik}$$

The chemical shift and Zeeman Hamiltonians are linear in spin operators and so a flip of all spins corresponds to a change in sign of the matrix elements. These matrix elements are

$$\begin{aligned}
&\langle\alpha(1)\ldots\alpha(N)|H_Z + H_{cs}|\alpha(1)\ldots\alpha(N)\rangle \\
&\quad = -\langle\beta(1)\ldots\beta(N)|H_Z + H_{cs}|\beta(1)\ldots\beta(N)\rangle \\
&\quad = \frac{1}{2}\,(N\Delta\omega - \sum_i^N \sigma_i).
\end{aligned}$$

As a consequence, the N quantum transition contains information only on the Zeeman offset $\Delta\omega$ and the sum of chemical shifts:

$$\Delta E_{\frac{N}{2}\rightarrow-\frac{N}{2}} = E_{\frac{N}{2}} - E_{-\frac{N}{2}} = N\Delta\omega - \sum_{i}^{N} \sigma_i . \qquad (1.30)$$

Equation (1.30) makes the important statement that complete removal of the dipolar interaction is effective in the observation of the N quantum transition. Thus the N quantum spectrum is similar to that obtained from the multiple pulse selective averaging technique known as WAHUHA [32] without reducing the chemical shift interaction.

To obtain information on the dipolar and spin-spin couplings, one has to consider the transitions of order less than N. In an anisotropically ordered sample, there are N(N-1)/2 dipolar couplings, N(N-1)/2 spin-spin couplings and N chemical shifts. Assuming that all lines are resolved, the (N-1) quantum spectrum gives N frequencies and N(N-1) are obtained from the (N-1) order. Thus, these orders generally contain enough transitions to solve for all dipolar and spin-spin couplings and chemical shifts. These and other counting arguments are presented in more detail elsewhere [33].

Of course, all the above arguments apply to a general spin system with no symmetry. Usually, molecules of interest will belong to a point group with more than one irreducible representation [34]. Each Zeeman manifold is factored into states of different irreducible representations. As we shall show, ultimately the multiple quantum coherences produced and detected in the experiments obey the symmetry selection rules for normal single quantum NMR. The well known result from group theory is that allowed transitions are those involving only states within the same

irreducible representation [35]. This is a result of the totally symmetric nature of the magnetic dipole transition operators of NMR [36]. The symmetry selection rule is written as

$$\langle i|V|j\rangle = 0 \text{ unless}$$

$$\Gamma^{(i)} \times \Gamma^{(V)} \times \Gamma^{(j)} \rightarrow \Gamma^{(A)}$$

where the usual symbols representing the irreducible representations of $|i\rangle$, V and $|j\rangle$ are used. Taking I_x, which is of the A representation, as the transition operator for NMR, the symmetry selection rule is given by the statement above.

The effect of molecular symmetry is two sided. On the one hand, the selection rule stated above reduces the number of transitions in each order and hence the available information. However, the number of unique couplings required to solve for is also reduced by symmetry. There is no general way to predict how many orders will have to be used for a specific molecule without considering symmetry. For each case, the permutational point group relevant to the spins will have to be considered. The results of the group theory for the cases of interest in this work are presented in the following chapters. It is interesting to note that there are counting schemes which make use of the behavior of some states under point group symmetry elements to predict the number of lines expected in the higher order spectra [37].

We have seen that the number of transitions corresponding to the p quantum order decreases as p increases ($p = |\Delta M|$). This comes about because the higher order transitions probe the Zeeman manifolds with the fewest number of states. The spread of energy shifts caused by perturbations to H_Z is roughly the same for each manifold and so the higher order

spectra contain splittings similar to the single quantum in magnitude. The result is more resolved spectra the higher the order observed. For the experiments of this work, the nature of the quantitative information relevant to molecular structure that is available in the high quantum orders is identical to the single quantum spectrum. However, from Equation (1.28) it is readily seen that the single quantum spectrum may contain a tremendous amount of redundancy of this information for large spin systems. The multiple quantum experiment has the effect of sampling the single quantum spectral information and presenting the data in an accessible manner (i.e., in the form of resolved transitions). As we shall demonstrate in Chapters 3 and 4, the high quantum spectra, together with a consideration of molecular symmetry, will elucidate the dependence of transition frequencies on the molecular parameters of interest.

Chapter 2

NMR Using Liquid Crystals

In this chapter, we present some details of the theory for NMR experiments with liquid crystals. The results here also pertain to solutes partially ordered in a liquid crystal solution. All the liquid crystal samples studied are thermotropic nematogens with positive magnetic susceptibilities. Thus, the director is taken to be parallel to the static field direction and the laboratory z axis.

Alkyl and aromatic quadrupole moments for deuterium are ~160-180 kHz and deuterium spectra from isotopically labeled nematogens are typically about 50 kHz wide. The scaling, as we show below, is due to the imperfect ordering of molecules in the matrix. The typical strength of the dipolar interaction for protons is 100 Hz to 10 kHz yielding a spectral width of ~10-100 kHz. Chemical shift values and scalar couplings are usually about the same size as their isotropic values. Indeed, they are quite often fixed at the latter during spectral analysis.

For asymmetric molecules as solutes in a nematic sample, proton linewidths are typically a few hertz wide. This means, with a small number of coupled spins or high enough molecular symmetry, most transitions will be resolved in the single quantum spectrum and an analysis may be possible. As an example, consider the highly symmetric six spin system for the proton spectrum of benzene dissolved in a nematogen. This is shown in Figure 2.1. The top trace is the benzene spectrum taken with a single pulse Fourier transform experiment under conditions of moderate field homogeneity. The center trace was produced by applying a two dimensional spin echo sequence [38]. Use of the spin echo technique

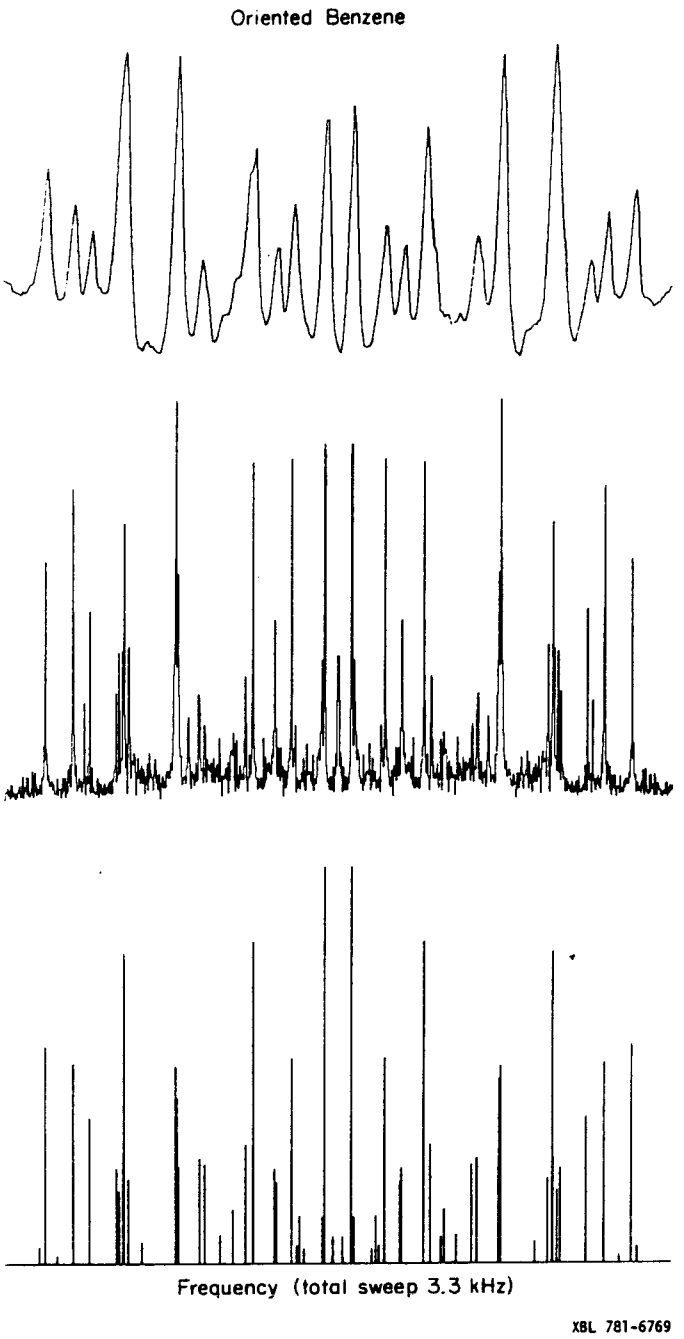

Figure 2.1

Proton NMR spectra of benzene dissolved in a nematic liquid crystal. The top trace was obtained from a single pulse FT NMR experiment under conditions of moderate field homogeneity (~.5 ppm). The middle trace demonstrates the enhanced resolution obtainable when a two-dimensional spin echo pulse sequence is used. A theoretical stick spectrum is shown at the bottom.

has removed line broadening due to magnetic field inhomogeneity. Also shown in the figure is a theoretical stick spectrum fitting the experimental frequencies. Because there are no chemical shift differences, the spectrum appears symmetric about its center. With complete resolution of all lines as shown in the center trace, all dipolar and scalar couplings can be determined. Perhaps the most complicated spectrum studied to date by single quantum NMR is that from the 10 spin spectrum of partially oriented ortho toluene [46].

As we shall see in Chapter 4, the proton spectrum of a pure liquid crystal is generally not as well resolved as benzene. Without isotopic substitution the number of protons per molecule is large and, with the higher degree of ordering, individual transition linewidths are greater than for solutes. The result is a large number of overlapping lines in the spectrum. Without a sufficient number of fully resolved peaks, the proton spectrum is usually intractable and no analysis may be possible.

Deuterium NMR of labeled liquid crystals has been somewhat successful in yielding quantitative information on ordering [39-44]. For example, methylene deuterons on an alkoxy or alkyl chain segment of a liquid crystal will give a resolved doublet [43]. Linewidths may be approximately 0.1 to 1 kHz, but splittings are 10 to 100 kHz. If the chain were allowed only to exist in an all trans configuration, all the methylene resonances would be related simply and contain the same information about ordering. Usually, one can assign individual resonances to specific segments [43] and it is possible to learn about conformational statistics. Dipolar splittings can be observed in a spectrum but are usually small due to the small deuterium dipole moment. Proton spectra are much richer in structure [39] than their deuterium analogs. In

addition, higher sensitivity and greater precision of structural information make proton NMR of liquid crystals attractive. Alkyl chain solutes partially oriented in a nematic liquid crystal have been studied by multiple quantum NMR [45].

Before going on to discuss the method of obtaining structure and ordering information from liquid crystal spectra, we pause now to review rotations of cartesian and spherical tensors. The results of the next section are relevant to the definition of an order tensor for a nematic sample and also apply to the spin tensor portion of the interaction Hamiltonians described in Chapter 1.

2.1 Coordinate Transformations for Tensors

The mathematical details of coordinate transformations for tensors are covered in a number of texts [7,8]. We give here only a brief summary of the results necessary for our purposes. The equations below will be useful for coordinate transformations of both the order tensor and the irreducible tensor representations of the spin Hamiltonians.

2.1.1 Cartesian Basis

In Chapter 1 we have given the interaction tensors in cartesian coordinates. To perform a rotation of tensor A,

$$\underset{\approx}{A} = \begin{pmatrix} A_{xx} & A_{xy} & A_{xz} \\ A_{yx} & A_{yy} & A_{yz} \\ A_{zx} & A_{zy} & A_{zz} \end{pmatrix}, \tag{2.1}$$

to $\underset{\approx}{A}^R$, we apply the transformation matrix $\underset{\approx}{R}$,

$$\underset{\approx}{A}^R = \underset{\approx}{R}\,\underset{\approx}{A}\,\underset{\approx}{R}^\dagger. \tag{2.2}$$

If $\underset{\approx}{A}$ is real, as in the case of the interaction Hamiltonians of Chapter 1, $\underset{\approx}{R}^{\dagger} = \underset{\approx}{R}^{-1}$. The usual convention is to break the transformation up into rotations about cartesian axes with Euler angles $\Omega = \alpha, \beta, \gamma$ [8]. The rotations are as follows. Rotate by angle α about the z axis to the intermediate frame x', y', z'. Rotate about y' by angle β to the frame x", y", z". Finally, rotate about z" by angle γ to the transformed axis system x"', y"', z"'. The complete rotation matrix is given by Equation (2.3).

$$\underset{\approx}{R} = \begin{pmatrix} \cos\alpha\cos\beta\cos\gamma-\sin\alpha\sin\gamma & \sin\alpha\cos\beta\cos\gamma+\cos\alpha\sin\gamma & -\sin\beta\cos\gamma \\ -\cos\alpha\cos\beta\sin\gamma-\sin\alpha\cos\gamma & -\sin\alpha\cos\beta\sin\gamma+\cos\alpha\cos\gamma & -\sin\beta\sin\gamma \\ \cos\alpha\sin\beta & \sin\alpha\sin\beta & \cos\beta \end{pmatrix} \quad (2.3)$$

2.1.2 Spherical Basis

In the previous section, we have written the second rank tensor A in cartesian coordinates for Equation (2.1). An alternate approach, and one convenient when considering several rotations of tensors, is to express $\underset{\approx}{A}$ in a spherical basis. One can then make use of the properties of irreducible spherical tensors to simplify calculations. Irreducible tensor methods and rotational properties of tensor operators are subjects covered in several texts, for example those by Rose [8] and Silver [7]. Only the results necessary for our analysis will be reviewed here.

Each of the interaction Hamiltonians of Chapter 1 can be written in the form of a scalar product of tensors:

$$H = \vec{X}\cdot\underset{\approx}{A}\cdot\vec{Y} = \sum_{ij}^{xyz} A_{ij}X_iY_j \quad (2.4)$$

where $\vec{X}$ and $\vec{Y}$ are first rank tensors (vectors) and $\underset{\approx}{A}$ is second rank.

To use a spherical basis instead of the cartesian basis of Equation (2.4), we make use of the scalar product of two irreducible tensors with components A^k_q and T^k_q,

$$\underset{\approx}{A}^k \cdot \underset{\approx}{T}^k = \sum_{q=-k}^{k} (-1)^q \, A^k_q T^k_{-q} \tag{2.5}$$

In Equation (2.5), the integer $k \geq 0$ is the rank and each tensor has $(2k+1)$ elements specified by $q = -k, -k+1, \ldots, +k$. In general, the Hamiltonian can be written as contributions from zero, first, and second rank tensors so that Equation (2.4) becomes

$$H = \sum_{k=0}^{2} \sum_{q=-k}^{k} (-1)^q \, A^k_q T^k_{-q} \tag{2.6}$$

We must now relate the irreducible tensors of Equation (2.5) to the cartesian components in Equation (2.4). In terms of the cartesian components (T_x, T_y, T_z), we can write the elements of the first rank irreducible spherical tensor as

$$T^1_0 = T_z \tag{2.7a}$$

$$T^1_{\pm 1} = \mp(1/\sqrt{2})(T_x \pm iT_y), \tag{2.7b}$$

and similarly

$$A^1_0 = A_z \tag{2.8a}$$

$$A^1_{\pm 1} = \mp(1/\sqrt{2})(A_x \pm iA_y) \tag{2.8b}$$

To find the elements of a second rank irreducible tensor, we make use of the product rule for two commuting tensors of rank k' and k":

$$T_q^{k,ij} = \{\underset{\approx}{T}^{k',i} \times \underset{\approx}{T}^{k'',j}\}$$

$$= \sum_{q'} C(k'k''k,q',q-q')T_{q'}^{k',i}\, T_{q-q'}^{k'',j} \qquad (2.8)$$

where the C coefficients are the Clebsch-Gordon coefficients. In Equation (2.8), we have introduced the superscripts i and j to indicate the tensors involve different parts of the system. For example, in the dipolar Hamiltonian, i and j refer to a particular nuclear pair.

Multiplying the first rank tensors of Equation (2.7b) gives the result [47]:

$$T_0^{0,ij} = \frac{1}{\sqrt{3}}[T_{+1}^{1,i}T_{-1}^{1,j} - T_0^{1,i}T_0^{1,j} + T_{-1}^{1,i}T_{+1}^{1,j}] \qquad (2.9)$$

$$T_{+1}^{1,ij} = \frac{1}{\sqrt{3}}[T_{+1}^{1,i}T_0^{1,j} - T_0^{1,i}T_{+1}^{1,j}]$$

$$T_0^{1,ij} = \frac{1}{\sqrt{2}}[T_{+1}^{1,i}T_{-1}^{1,j} - T_{-1}^{1,i}T_{+1}^{1,j}]$$

$$T_{-1}^{1,ij} = \frac{1}{\sqrt{2}}[T_{-1}^{1,i}T_0^{1,j} - T_0^{1,i}T_{-1}^{1,j}]$$

$$T_{+2}^{2,ij} = T_{+1}^{1,i}T_{+1}^{1,j}$$

$$T_{+1}^{2,ij} = \frac{1}{\sqrt{2}}[T_{+1}^{1,i}T_0^{i,j} + T_0^{1,i}T_{+1}^{1,j}]$$

$$T_0^{2,ij} = \frac{1}{\sqrt{6}}[T_{+1}^{1,i}T_{-1}^{1,j} + 2T_0^{1,i}T_0^{1,j} + T_{-1}^{1,i}T_{+1}^{1,j}]$$

$$T_{-1}^{2,ij} = \frac{1}{\sqrt{2}}[T_{-1}^{1,i}T_0^{1,j} + T_0^{1,i}T_{-1}^{1,j}]$$

$$T_{-2}^{2,ij} = T_{-1}^{1,i}T_{-1}^{1,j}.$$

Similarly, for the tensor $\underset{\approx}{A}^{2,ij}$ in terms of the cartesian components

of Equation (2.1) we find, from the product of first rank tensors (see Equation (2.8)),

$$A_0^{0,ij} = \frac{-1}{\sqrt{3}} \mathrm{Tr}(\underset{\approx}{A}^{ij}) = -\frac{1}{3}(A_{xx}^{ij} + A_{yy}^{ij} + A_{zz}^{ij}) \tag{2.10}$$

$$A_{+1}^{1,ij} = -\frac{1}{2}[A_{zx}^{ij} - A_{xz}^{ij} + i(A_{zy}^{ij} - A_{yz}^{ij})]$$

$$A_0^{1,ij} = -\frac{1}{\sqrt{2}}[A_{xy}^{ij} - A_{yx}^{ij}]$$

$$A_{-1}^{1,ij} = -\frac{1}{2}[A_{zx}^{ij} - A_{xz}^{ij} - i(A_{zy}^{ij} - A_{yz}^{ij})]$$

$$A_{+2}^{2,ij} = \frac{1}{2}[A_{xx}^{ij} - A_{yy}^{ij} + i(A_{xy}^{ij} + A_{yx}^{ij})]$$

$$A_{+1}^{2,ij} = -\frac{1}{2}[A_{xz}^{ij} + A_{zx}^{ij} + i(A_{yz}^{ij} + A_{zy}^{ij})]$$

$$A_0^{2,ij} = \frac{1}{\sqrt{6}}[3A_{zz}^{ij} - \mathrm{Tr}(\underset{\approx}{A}^{ij})]$$

$$A_{-1}^{2,ij} = +\frac{1}{2}[A_{xz}^{ij} + A_{zx}^{ij} - i(A_{yz}^{ij} + A_{zy}^{ij})]$$

$$A_{-2}^{2,ij} = \frac{1}{2}[A_{xx}^{ij} - A_{yy}^{ij} - i(A_{xy}^{ij} + A_{yx}^{ij})].$$

As an example particularly useful for our purposes, consider the dipolar Hamiltonians for like spins i and j. From Chapter 1, the elements of the dipolar tensor $\underset{\approx}{D}^{ij}$ are

$$D_{pq}^{ij} = +\gamma_i\gamma_j(\delta_{pq} - 3\vec{e}_p\cdot\vec{e}_q)/r_{ij}^3, \quad p,q = x,y,z. \tag{2.11}$$

The dipolar Hamiltonian may be considered as a scalar product of two second rank tensors. The elements in Equation (2.11) make up one tensor and, combining the spin operators, $\vec{I}_i$ and $\vec{I}_j$, we have the other. Recalling that $\underset{\approx}{D}^{ij}$ is traceless and symmetric, we get for the components

of the two tensors,

$$A_0^{0,ij} = A_{0,\pm 1}^{1,ij} = 0 \tag{2.12}$$

$$A_0^{2,ij} = \frac{3}{\sqrt{6}} D_{zz}^{ij}$$

$$A_{\pm 1}^{2,ij} = \mp (D_{xz}^{ij} \pm iD_{yz}^{ij})$$

$$A_{\pm 2}^{2,ij} = \frac{1}{2} (D_{xx}^{ij} - D_{yy}^{ij} \pm 2iD_{xy}^{ij})$$

$$T_0^{2,ij} = \frac{1}{\sqrt{6}} [2I_0^i I_0^j + I_{+1}^i I_{-1}^j + I_{-1}^i I_{+1}^j] \tag{2.13}$$

$$T_{+1}^{2,ij} = \frac{1}{\sqrt{2}} [I_{+1}^i I_0^j + I_0^i I_{+1}^j]$$

$$T_{-1}^{2,ij} = \frac{1}{\sqrt{2}} [I_{-1}^i I_0^j + I_0^i I_{-1}^j]$$

$$T_{+2}^{2,ij} = I_{+1}^i I_{+1}^j$$

$$T_{-2}^{2,ij} = I_{-1}^i I_{-1}^j .$$

In Equation (2.13) the first rank spin operators

$$I_0^i = I_{zi} \tag{2.14a}$$

$$I_{+1}^i = - \frac{1}{\sqrt{2}} (I_{xi} + iI_{yi}) \tag{2.14b}$$

$$I_{-1}^i = + \frac{1}{\sqrt{2}} (I_{xi} - iI_{yi}) \tag{2.14c}$$

have been introduced. From Equation (2.11), the spatial elements can be related to the spherical harmonics Y_m^ℓ by

$$A_q^{2,ij} = -\sqrt{6}\,\frac{\gamma_i\gamma_j\hbar}{r_{ij}^3}\sqrt{\frac{4\pi}{5}}\,Y_q^2. \tag{2.15}$$

If Equations (2.12) and (2.13) are combined according to Equation (2.6), we obtain the full dipolar Hamiltonian. Finally, we note that the secular truncation of H_D is equivalent to keeping those terms in the products $A_q^2 T_{-q}^2$ corresponding to $q = 0$. This is a result of the commutation relations of the angular momentum operators and irreducible tensor operators [47]:

$$[I_{\pm}, T_q^k] = T_{q\pm1}^k\,[(k\mp q)(k\pm q+1)]^{\frac{1}{2}}, \tag{2.16a}$$

$$[I_z, T_q^k] = qT_q^k. \tag{2.16b}$$

Now that we can write Hamiltonians in terms of irreducible tensor operators, we turn to the question of rotations. The coordinate transformation of an irreducible spherical tensor is given by

$$(T_q^k)^R = \underset{\approx}{R}\underset{q\approx}{T^k}\underset{\approx}{R}^{\dagger} = \sum_{q'} T_{q'}^k D_{q',q}^k(\Omega) \tag{2.17}$$

where the $D_{q',q}^k(\Omega)$ are elements of the Wigner rotation matrix and $\Omega = (\alpha,\beta,\gamma)$ is the set of Euler angles for the rotation. Properties of the Wigner rotation matrix, together with a description of how to calculate the elements $D_{q',q}^k(\Omega)$ can be found in the texts by Silver and Rose.

2.2 Order Parameters

We can now proceed to discuss the situation of an ensemble of anisotropically ordered molecules such as found in a liquid crystal. If only rigid molecules are considered, the Hamiltonian will contain an average over the orientation probability distribution of the ensemble. If a

number of conformations are possible for each molecule, then the Hamiltonian will also have to reflect an average over these, each weighted by a conformational probability. The probability distribution for orientations is then a function of the conformational states of the molecules. Roughly speaking, this takes into account the possibility that each conformation may orient differently. Approximations, based on arguments for the relative time scales for reorientation of the entire molecule and conformational changes, are often introduced to reduce the number of parameters required to describe the ordering of the ensemble. For the time being we will ignore such time scale arguments and assume a conformationally dependent probability distribution for ordering. Later, after introducing the Saupe order tensor, the question of separation of averaging for reorientation and conformational change will be re-examined. The problems with time scale arguments will be addressed and the approach for choosing a molecular axis system will be discussed.

2.2.1 Coordinate Transformations for Liquid Crystal Interactions

In Equation (2.6) we give the Hamiltonian as a scalar product of irreducible tensors. This equation is valid for a rigid molecule (or a non-rigid molecule in a single conformation) where the tensors $\underset{\approx}{T}^{k}$, describing the spin portion of H, and $\underset{\approx}{A}^{k}$, describing the spatial part, are related to some space fixed axis system. More rigorously, for an ensemble of non-rigid molecules, we must include the contribution from each conformation as expressed below.

$$H = \sum_{k=0}^{2} \sum_{s=-k}^{k} (-1)^{s} (T_{s}^{k})^{L} [\sum_{n} F_{n} (A_{s}^{k})_{n}^{L}] \qquad (2.18)$$

In Equation (2.18), the subscript n specifies a particular conformation with probability of occurring F_n. We have used the superscript L to indicate that we measure the spectrum in the lab frame. For the most general case, four coordinate systems and three transformations have to be considered to relate the microscopic molecular properties to lab frame tensor components. The axis systems and rotations are shown schematically below.

$$\left[\begin{array}{ccccc} \text{PAS} & \xrightarrow{\Omega_n} & \text{M} & \xrightarrow{\Omega_n'} & \text{D} \\ (X,Y,Z) & & (x,y,z) & & (x',y',z') \end{array}\right]_n \xrightarrow{\Omega''} \begin{array}{c} \text{L} \\ (x'',y'',z'') \end{array}$$

where the rotations involved are:

(1) Ω_n: Rotate from Principle Axis System (PAS) to a molecule fixed system (M).

(2) Ω_n': Rotate from M to the director axis system (D).

(3) Ω'': Rotate from D to the lab frame (L).

Rotations (1) and (2) with Euler angles $(\alpha_n, \beta_n, \gamma_n)$ and $(\alpha_n', \beta_n', \gamma_n')$, respectively, have to be done for all allowed conformations. The results are collected with the appropriate weights F_n and the final rotation, Ω'', performed.

Starting with the interaction Hamiltonian in the principle axis system, the rotations for the spatial portion of H are:

a) from PAS to M

$$(A_q^k)_n^M = \sum_{p=-k}^{k} (A_p^k)_n^{PAS} D_{pq}^k(\Omega_n), \tag{2.19a}$$

b) from M to D

$$(A_r^k)_n^D = \sum_{q=-k}^{k} (A_q^k)_n^M D_{qr}^k(\Omega_n'), \tag{2.19b}$$

c) from D to L

$$(A^k_s)^L = \sum_{r=-k}^{k} D^k_{rs}(\Omega'') \sum_n F_n (A^k_r)^D_n. \tag{2.19c}$$

The spin operators, T^k_s, are invariant to these rotations with spatial Euler angles. Combining Equations (2.19) and (2.18) we have for the interaction Hamiltonian

$$H = \sum_{ks} (-1)^s T^k_s \sum_r D^k_{rs}(\Omega'') \sum_{nqp} F_n D^k_{qr}(\Omega'_n) D^k_{pq}(\Omega_n) (A^k_p)^{PAS}_n, \tag{2.20}$$

where the superscript L on the spin operators has been dropped for brevity. Equation (2.20) is valid for a single orientation of the molecule fixed axis system relative to the director frame. Actually, there is a distribution of orientations described by the function $P(\Omega'_n)$. This function is usually expanded in terms of the generalized spherical harmonics [48]

$$P(\Omega'_n) = \left(\frac{2k+1}{8\pi^2}\right) \sum_{\mu\nu} C^k_{\mu\nu}(n) D^k_{\mu\nu}(\Omega'_n) \tag{2.21}$$

In Equation (2.21), we have explicitly indicated the dependence on conformation by the symbol n. The $C^k_{\mu\nu}(n)$ are independent of Ω'_n (but not of the conformation) and are known as the generalized order parameters or "motional constants" [49]. The average of the rotation matrix relating molecular and director frames is then

$$\langle D^k_{qr}(\Omega'_n)\rangle = \int P(\Omega'_n) D^k_{qr}(\Omega'_n) d\Omega'_n. \tag{2.22}$$

Making use of the relation for conjugates of the $D^k(\Omega)$,

$$D^k_{mn}(\Omega) = (-1)^{m-n} (D^k_{-m-n}(\Omega))^*, \tag{2.23}$$

and the orthogonality of the Wigner rotation matrices, we have

$$\langle D^k_{qr}(\Omega'_n)\rangle = (-1)^{r-q} C^k_{-q-r}(n). \tag{2.24}$$

We finally get for the general (averaged) interaction Hamiltonian

$$\bar{H} = \sum_{ks} (-1)^s T^k_s \sum_r D^k_{rs}(\Omega'') \sum_{npq} C^k_{q-r}(n)\, D^k_{pq}(\Omega_n) (A^k_q)^{PAS}_n. \tag{2.25}$$

We can begin to make reductions in the complexity of Equation (2.25). First, the interactions most important to the study of liquid crystal NMR are of rank two (e.g., dipolar and quadrupolar). Also, the usual high field approximation allows us to neglect terms for $s \neq 0$. The result is

$$\bar{H} = T^2_0 \sum_r D^2_{r0}(\Omega'') \sum_{nq} F_n (-1)^{1-q} C^2_{-q-r}(n)$$

$$\times \left[\sum_p D^2_{pq}(\Omega_n)(A^2_p)^{PAS}_n\right]. \tag{2.26}$$

Thus we see that there are 25 (complex) order parameters (for $q = -2, -1, 0, 1, 2$ and $r = -2, -1, 0, 1, 2$) required to describe the ordering for every allowed conformation. Henceforth, we will replace the final summation over p in Equation (2.26) with the tensor components in the molecule fixed axis system, $(A^2_q)^M$, and leave off the superscript M. This seems reasonable for the dipolar interaction where we can choose a molecule fixed axis system according to symmetry to reduce the number of order parameters. The dipolar interaction in its PAS is given by $D^{ij}_{\alpha\alpha} \propto (r_{ij})^{-3}$ and, applying the rotation of Equation (2.19a), we arrive at $\underset{\approx}{D}^{ij}$ given in Chapter 1 and Equation (2.11).

If we now consider the symmetry of a uniaxial nematic liquid crystal we can reduce the number of order parameters required. The uniaxial

nature of the phase means that $P(\Omega')$ (and the spectrum) are invariant to rotations about z' of the director frame by angle γ'. Thus, $r = 0$ and we only have five order parameters for each conformation. The first rotation matrix of Equation (2.26) then reduces to D^2_{00} (0, β'', 0) where β'' is the angle between the director frame z' axis and the magnetic field. Nematic mesogens order nearly perfectly so that $\beta'' = 0$. This may be a poor approximation if used for smectic phases with large tilt angles [48]. With these uniaxial properties, Equation (2.26) becomes

$$\bar{H} = T_0^2 \sum_n F_n \sum_q (-1)^q \, C^2_{-q0}(n)(A^2_q)_n . \tag{2.27}$$

2.2.2 The Saupe Order Tensor

An alternate description of order for a uniaxial liquid crystal is offered by Saupe [50]. In the high field approximation an NMR experiment measures the component of the Hamiltonian parallel to the main field. Considering just a single conformation in an ensemble of rigid molecules for now, the transformation of a second rank interaction tensor from lab frame to molecule fixed axis system is given by

$$A_{LAB} = \sum_{\alpha\beta}^{xyz} S_{\alpha\beta} A_{\alpha\beta} . \tag{2.28}$$

A_{LAB} is the lab frame component of $\underset{\approx}{A}$ parallel to the field (z" direction). In Equation (2.28) the elements of a traceless, symmetric tensor $\underset{\approx}{S}$ have been introduced,

$$S_{\alpha\beta} = \frac{1}{2} \langle 3\ell_\alpha \ell_\beta - \delta_{\alpha\beta} \rangle , \tag{2.29}$$

where ℓ_α, ℓ_β are the direction cosines between the molecule fixed axes α,β and the field direction. In Equation (2.29), the angle brackets imply an average over an orientational distribution function similar to that in

the last section. Equation (2.28) may be rewritten

$$A_{LAB} = A^{iso} + \frac{2}{3} \sum_{\alpha\beta}^{xyz} S_{\alpha\beta} A_{\alpha\beta}, \tag{2.30}$$

where

$$A^{iso} \equiv \frac{1}{3} \mathrm{Tr}(\underset{\approx}{A}) = \frac{1}{3} (A_{xx} + A_{yy} + A_{zz}) \tag{2.31}$$

is the isotropic average of the tensor. Re-introducing the dependence on conformation n, the elements of $\underset{\approx}{S}^n$ may be related to the motional constants of the last section by

$$S^n_{zz} = \langle D^2_{00}(\Omega'_n) \rangle = \frac{1}{2} \langle 3\cos^2\beta'_n - 1 \rangle \tag{2.32a}$$

$$(S^n_{xx} - S^n_{yy}) = \left(\frac{3}{2}\right)^{\frac{1}{2}} \langle D^2_{20}(\Omega'_n) + D^2_{-20}(\Omega'_n) \rangle$$

$$= \frac{\sqrt{3}}{2} \langle \sin^2\beta'_n \cos 2\alpha'_n \rangle \tag{2.32b}$$

$$S^n_{xy} = -i\left(\frac{3}{8}\right)^{\frac{1}{2}} \langle D^2_{-20}(\Omega'_n) - D^2_{20}(\Omega'_n) \rangle$$

$$= \frac{\sqrt{3}}{2} \langle \sin^2\beta'_n \sin 2\alpha'_n \rangle \tag{2.32c}$$

$$S^n_{xz} = \left(\frac{3}{8}\right)^{\frac{1}{2}} \langle D^2_{10}(\Omega'_n) - D^2_{-10}(\Omega'_n) \rangle$$

$$= \frac{\sqrt{3}}{2} \langle \sin\beta'_n \cos\beta'_n \cos\alpha'_n \rangle \tag{2.32d}$$

$$S^n_{yz} = -i\left(\frac{3}{8}\right)^{\frac{1}{2}} \langle D^2_{-10}(\Omega'_n) + D^2_{10}(\Omega'_n) \rangle$$

$$= \frac{\sqrt{3}}{2} \langle \sin\beta'_n \cos\beta'_n \sin\alpha'_n \rangle \tag{2.32e}$$

As an example of the use of $\underset{\approx}{S}^n$, the contribution to the lab frame dipolar coupling between spins i and j from the n^{th} conformation can be written:

$$D_{ij}^{n} = -\frac{\gamma_i\gamma_j h}{4\pi^2(r_{ij}^3)_n}\{S_{zz}^{n}(3\cos^2\theta_{ijz}-1)_n$$

$$+ (S_{xx}^{n}-S_{yy}^{n})(\cos^2\theta_{ijx}-\cos^2\theta_{ijy})_n$$

$$+ 4S_{xy}^{n}(\cos\theta_{ijx}\cos\theta_{ijy})_n + 4S_{xz}^{n}(\cos\theta_{ijx}\cos\theta_{ijz})_n$$

$$+ 4S_{yz}^{n}(\cos\theta_{ijy}\cos\theta_{ijz})_n\}, \qquad (2.33)$$

where $\cos\theta_{ijp}$, p = x,y,z are the projections onto the molecule fixed axes of a unit vector pointing from nucleus i to j and r_{ij} is the internuclear distance.

From the form of Equation (2.32) it is clear that the number of order parameters actually affecting the spectrum will be determined by molecular symmetry and the choice of molecular axes. The number of order parameters required for different molecular point groups is given elsewhere [51]. For example, the rigid molecule benzene, with D_6 symmetry for the proton spins and the z axis chosen along the six-fold axis, requires only S_{zz}. We find it convenient to use Equation (2.33) when actually calculating coupling constants in Chapter 4.

Now, using the probability for the occurrence of conformation n, F_n, the lab frame measurement can be written as

$$A_{LAB} = \sum_n F_n[(A^{iso})^n + \frac{2}{3}\sum_{\alpha\beta}^{xyz} S_{\alpha\beta}^{n}A_{\alpha\beta}^{n}] \qquad (2.34)$$

2.3 The Influence of Internal Motions on Molecular Ordering

In the last section we have demonstrated that, for molecules with no symmetry experiencing the ordering potential of a uniaxial liquid crystal,

the NMR spectrum will be sensitive to five independent order parameters for each conformation, weighted by conformational probabilities. Only a few assumptions have been made in arriving at this result. First, the correlation times for all types of molecular motion, including intramolecular vibration and rotation as well as reorientation, are assumed to be short compared to the inverse of the largest contribution to the interaction tensor involved. This is certainly a good approximation for NMR of liquid crystals. Reorientational correlation times for liquid crystals are usually shorter than a nanosecond. In contrast, quadrupolar and dipolar interactions for common nuclei observed in NMR are typically 10 to 10^6 sec^{-1}. Thus, the Hamiltonian reflects an average over intramolecular and reorientational motions.

The second assumption implicit in Equation (2.27) and (2.34) involves the manner in which the conformational average is treated. The use of a summation over conformational states implies that molecules exist for some time in well defined configurations which rapidly interconvert. This may be reasonable when the potential barriers involved are high and only states at the minima are appreciably populated. If this is not the case then, in principle, the summation over conformations may be replaced with an integration over a continuous motion or an ensemble average of quantum mechanical states. The summation is also usable, though perhaps not physically meaningful, when a continuum of conformational possibilities are related through molecular symmetry. This point will be discussed when considering oriented biphenyl groups in Chapter 4.

The most general approach in spectral analysis makes use of Equation (2.27) or (2.34) which contain only the approximations already mentioned.

The motional averaging in Equation (2.34) may be rewritten as

$$A_{LAB} = \sum_{\alpha\beta}^{xyz} \langle S_{\alpha\beta} A_{\alpha\beta} \rangle_{int,mole}, \tag{2.35}$$

where the complete averaging includes both internal motion (int) and motion which reorients the entire molecule (mole). In an attempt to reduce the number of parameters in a model used to analyze a spectrum, further approximations to Equation (2.35) are often made. A separation of the averaging of $\underset{\approx}{S}$ and $\underset{\approx}{A}$ is sometimes assumed based on arguments for the relative time scales for reorienting and internal motions [18]. Two extremes may be considered. The time for which a molecule is correlated with a particular orientation Ω' relative to the director is denoted τ_{mole}. The conformational states are characterized by a correlation time τ_{int}. In the first extreme conformational changes occur faster than a molecule can reorient ($\tau_{int} << \tau_{mole}$). A single order tensor should then describe the average orientation for all conformations:

$$A_{LAB} = \sum_{\alpha\beta}^{xyz} \langle S_{\alpha\beta} \rangle_{mole} \langle A_{\alpha\beta} \rangle_{int} \tag{2.36}$$

The distribution function, $P(\Omega')$, is then independent of conformation. This implies that the intermolecular potential determining orientations only depends on Ω' [52]. In the other relative time scale extreme ($\tau_{mole} << \tau_{int}$), when a molecule changes its conformational state, it is highly probable that it will completely reorient before undergoing another change of conformation. For this case, each conformation must be described by a separate order tensor $\underset{\approx}{S}^n$ as in Equation (2.34). The intermediate situation, for which $\tau_{int} \sim \tau_{mole}$, corresponds to replacing the discrete summations of Equation (2.27) and (2.34) with a treatment for continuous internal motion.

In an approach similar to the assumption $\tau_{int} << \tau_{mole}$, the average of Equation (2.35) is separated by assuming a non-rigid molecule is composed of rigid subunits with relative rotations making up the conformational changes [54]. Each rigid subunit i is described by its own order tensor, $\underset{\approx}{S}(i)$. If the relative timescales allow a separation of internal and reorientational averaging, then the $\underset{\approx}{S}(i)$ will be related to a single $\underset{\approx}{S}$ for the entire molecule. Otherwise, the $\underset{\approx}{S}(i)$ will be independent.

There seems to be no body of well founded experimental evidence to support the simplifying assumption $\tau_{int} << \tau_{mole}$. For large amplitude motions resulting in geometrically dissimilar configurations it is reasonable that the orientation distribution function $P(\Omega')$ will be at least weakly dependent on internal coordinates. Indeed, there are many examples in the literature in which the spectrum of non-rigid molecules cannot be adequately explained by assuming a single order tensor independent of conformation ([52-55] and references therein). In some cases it has been found that observed quadrupolar and dipolar splittings in the spectra of pure liquid crystals can only be explained by assuming a conformationally dependent $\underset{\approx}{S}$ [54]. Although it would seem that $P(\Omega')$ should be only weakly dependent on ground state vibrational modes of molecules, even this assumption may not be appropriate when analyzing a high resolution spectrum of oriented solute molecules. Emsley, et al. [52] and Burnell, et al. [53] have suggested that the anisotropic couplings observed from tetrahedral molecules dissolved in nematic phases may be explained by a correlation between molecular orientation and asymmetric vibrational modes.

Thus it would appear that one must always use the more complicated averaging procedure in Equation (1.35) to relate $\underset{\approx}{A}$ to A_{LAB}. This will present difficulties unless an adequate model exists to give the conformational probabilities. If, instead, these are to be determined from an experiment, then drastic simplifications or assumptions may have to be used concerning molecular structure. It has been suggested that a possible approach is to carefully choose the molecule fixed axis system to effectively "decouple" internal motions and reorientation [55]. In some cases this amounts to finding the principle axis system for $\underset{\approx}{S}$. Choosing the molecule axis system in this manner may be difficult if the conformations are not related by symmetry. The case of biphenyl discussed in Chapter 4 demonstrates this approach.

Chapter 3

Multiple Quantum NMR

3.1 Introduction

This chapter covers the basic theory of multiple quantum NMR. Most of the theoretical development of this technique is found elsewhere [31, 38,56-66,69]. No attempt is made to give a complete description of all aspects of multiple quantum spectroscopy. However, details given here are sufficient to understand all multiple quantum spectra presented in this and the next chapter. The radio frequency pulses used are sufficiently broadband to excite all allowed transitions of the spin systems studies. Aside from specific creation and detection of even quantum ($\Delta M = 0, \pm 2, \pm 4 \ldots$) or odd quantum ($\Delta M = \pm 1, \pm 3, \pm 5, \ldots$) transitions- a result of the bilinear spin coupling Hamiltonians - all pulse sequences used are non-selective. Selective sequences, which produce enhanced signals for specific multiple quantum orders, are the subject of separate work [64,66,69,33].

As an example of multiple quantum NMR, we again consider benzene partially ordered in a nematic liquid crystalline solution. A non-selective proton multiple quantum spectrum of benzene in Eastman Kodak liquid crystal #15320 is shown in Figure 3.1. All orders, from zero quantum transitions to the six quantum, are present. Each order is composed of a group of lines separated from neighboring orders and extending from zero quantum on the left to six quantum on the right. The method of separating transitions by order (time proportional phase incrementation) is given below.

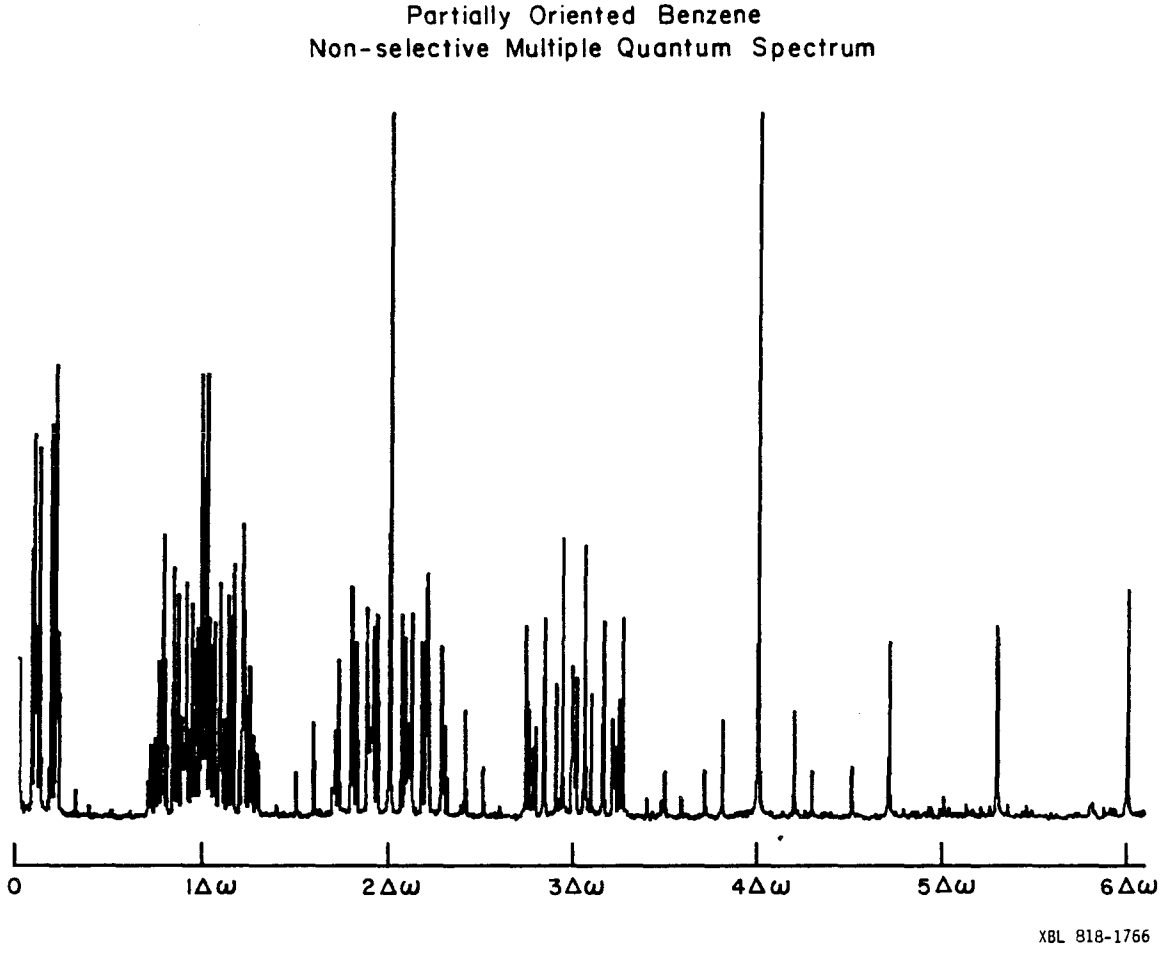

Figure 3.1

Non-selective proton multiple quantum spectrum of benzene oriented in the nematic phase of a liquid crystal solution. Only one half of the total spectrum, which is symmetric about its center, is shown. Multiple quantum transitions are separated according to ΔM by the time proportional phase incrementation technique. The central two and four quantum lines (at $2\Delta\omega$ and $4\Delta\omega$, respectively) have been truncated in height. The spectral width shown is 50 kHz.

The width of each order in Figure 3.1 is equivalent to the single quantum bandwidth and the one quantum region of that figure may be compared (except for intensities) with Figure 2.1. The expected reduction of transition density with higher orders is seen in Figure 3.1. For example, there is only a single pair of five quantum lines. The origins of these and other transitions are understood from the spin energy level diagram shown in Figure 3.2. The permutation symmetry of benzene proton spin functions is isomorphous with the D_6 point group leading to eight irreducible representations. (Benzene also has an inversion center making the full point group D_{6h}. Inversion symmetry only becomes important in the zero quantum spectrum.) The five quantum pair comes from the $(A_1)_3 \rightarrow (A_1)_{-2}$ and $(A_1)_2 \rightarrow (A_1)_{-3}$ transitions. An analysis of this spectrum becomes completely trivial if we assume the benzene ring has a perfectly hexagonal shape. The dipolar coupling constants are then geometrically related by

$$D_{ortho} = 3\sqrt{3}\, D_{meta} = 8\, D_{para}$$

The coupling D_{ortho} is uniquely determined by the five quantum splitting which can be shown to be independent of scalar couplings. Assuming anisotropic indirect spin-spin couplings to be negligible, the relation is then

$$\frac{1}{2}\,(D_{ortho}) = \frac{\text{Five Quantum Splitting}}{3.7649}\,.$$

If we assume the scalar couplings are equivalent to their isotropic values, then all couplings are completely determined except for the relative signs of D_{ij} and J_{ij}. An attempt to fit the spectrum with

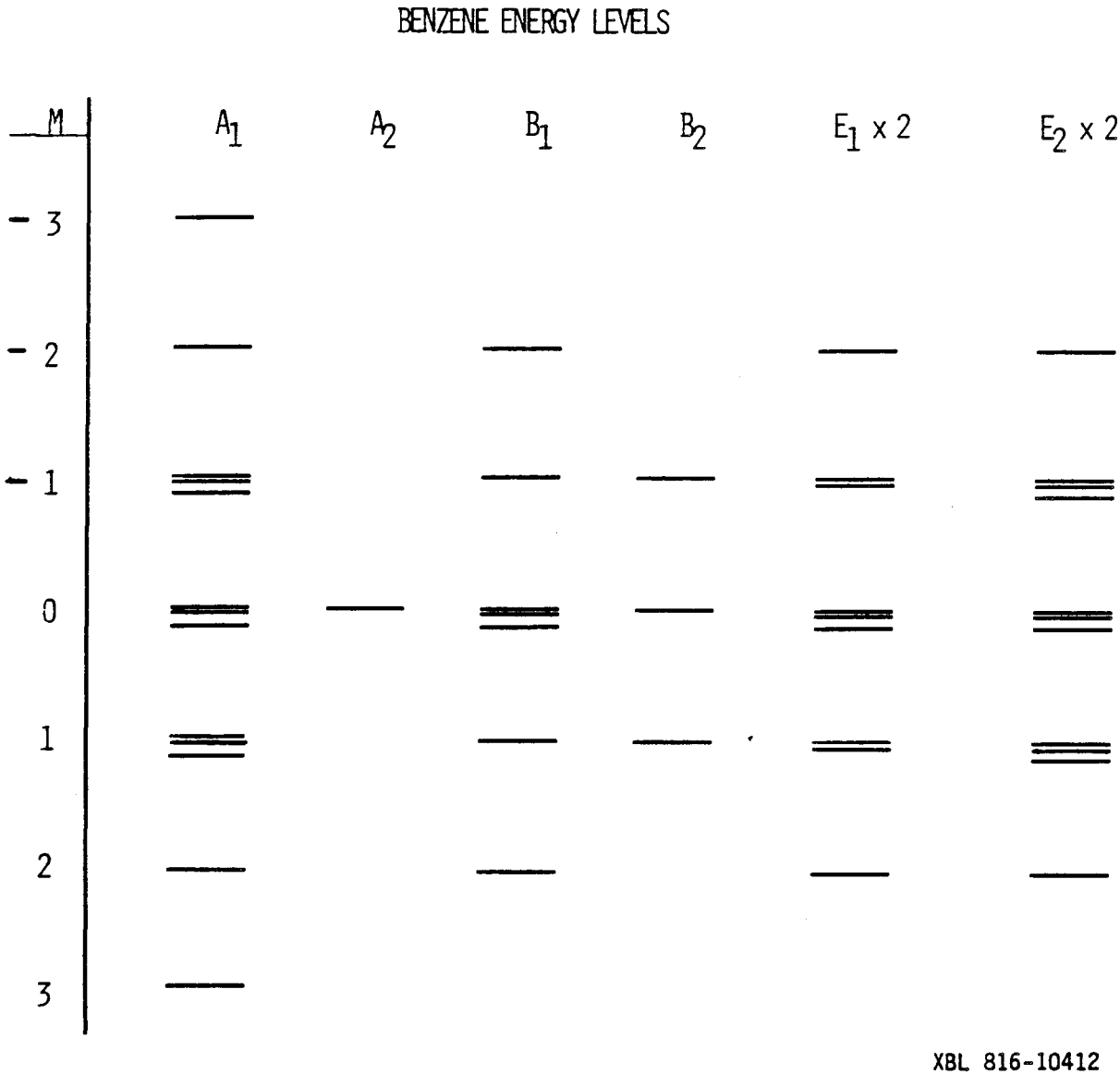

Figure 3.2

Benzene spin energy level diagram. The total magnetic quantum number for the six proton spins, M, is shown on the left hand edge. States are classified according to the eight irreducible representations of the D_6 point group. Multiple quantum transitions are only allowed between states in the same representation.

$D_{ortho} > 0$ was unsuccessful and so it is concluded that dipolar couplings are negative. If we choose a molecule fixed axis system with the z axis along the six-fold symmetry axis, and x, y axes in the ring plane, then by Equation (2.33)

$$D_{ortho} \propto \frac{1}{2} \frac{S_{zz}}{r^3_{ortho}}$$

The proportionality is entirely determined by nuclear properties (γ_{proton}) and the choice of units. If the usual value of $r_{ortho} = 2.482$ Å for benzene is assumed, then the five quantum spectrum gives us the (averaged) order parameter S_{zz}.

3.2 Theory

This section will cover the basic theory for non-selective multiple quantum NMR experiments. A brief review of the density matrix is first given and the most general multiple quantum pulse sequence described. The rotational properties of the multiple quantum propagator with even and odd quantum intensity dependence on pulse sequence parameters are discussed. Methods for separating orders based on properties of the multiple quantum propagator under radio frequency phase shifts are also reviewed. Experimental examples with benzene in a nematic liquid crystal demonstrate several outcomes of the theory.

3.2.1 The Density Matrix

It was mentioned in Chapter 1 that the finite number of states and bound energies of a coupled nuclear spin system make the density matrix approach [3,68] particularly useful in pulsed NMR theory. We review here the density matrix formalism as it applies in later calculations.

The wavefunctions $\{\psi\}$ which are solutions to the quantum mechanical Schrödinger equation may be expanded in a complete (orthonormal) basis $\{\phi\}$ as

$$|\psi_k\rangle = \sum_i C_{ki}|\phi_i\rangle, \tag{3.1}$$

$$\langle\psi_k| = |\psi_k\rangle^\dagger = \sum_i C_{ik}^*\langle\phi_i|.$$

In general, the expansion coefficients, $\{C\}$, are complex numbers (i.e., they may be written with a magnitude and phase). If we have an ensemble of systems all in the same state ψ_k, then the expectation value of some observable quantity is

$$\langle O\rangle = \langle\psi_k|O|\psi_k\rangle \tag{3.2}$$

$$= \sum_i \sum_j C_{ik}^* C_{kj} \langle\phi_i|O|\phi_j\rangle,$$

where O is a quantum mechanical operator. For a collection of states, each occurring with a probability p_k, the ensemble averaged expectation value is

$$\langle\bar{O}\rangle = \sum_k p_k \langle\psi_k|O|\psi_k\rangle, \tag{3.3}$$

$$= \sum_k \sum_i \sum_j p_k C_{ik}^* C_{kj} \langle\phi_i|O|\phi_j\rangle,$$

$$= \sum_i \sum_j \overline{C_i^* C_j} \langle\phi_i|O|\phi_j\rangle;$$

where the bars denote the ensemble average. The coefficients $\overline{C_i^* C_j}$ are the elements of an ensemble averaged "density matrix" given in the following equation:

$$(\underset{\approx}{\rho})_{ji} = \overline{c_i^* c_j}. \tag{3.4}$$

All of the theory in this chapter assumes an ensemble averaged density matrix and so the bar is left off $\underset{\approx}{\rho}$. Equation (3.3) may be rewritten as

$$\begin{aligned} \langle \vec{O} \rangle &= \sum_j \sum_i \rho_{ji} \langle \phi_i | O | \phi_j \rangle \\ &= \sum_j \sum_i \rho_{ji} O_{ij} = \mathrm{Tr}(\underset{\approx\approx}{O\rho}), \end{aligned} \tag{3.5}$$

where the definition of the trace of a matrix has been used. The "density matrix operator" is written

$$\hat{\rho} = \sum_k p_k |\psi_k\rangle\langle\psi_k|. \tag{3.6}$$

When the energy of a system is determined by a Hamiltonian H, the density matrix evolves in time according to its "equation of motion"

$$\hbar \frac{\partial}{\partial t} \rho(t) = -i[H, \rho(t)]. \tag{3.7a}$$

For our calculations, energies are expressed in frequency units and $\hbar$ is set to one in what follows. The general solution to Equation (3.7a) is

$$\rho(t) = e^{-iHt} \rho(0)\, e^{iHt}, \tag{3.7b}$$

for a time-independent Hamiltonian. When the Hamiltonian is time-dependent, a time-ordered integration over the duration t in the exponential will be required. This treatment is implicit in the rotating frame form of the radio frequency Hamiltonian, Equation (1.8). Evolution of a density matrix operator in the presence of a time-dependent Hamiltonian is handled mathematically with average hamiltonian theory [6].

For a system in thermal equilibrium with its surroundings, $\underset{\approx}{\rho}$ is diagonal. In this case, the coefficients $|\bar{C}_i|^2$ correspond to the probability of finding the ensemble in state ϕ_i, i.e., they are populations. In order for $\underset{\approx}{\rho}$ to have non-zero off-diagonal elements, the coefficients $C^*_{ik}C_{kj}$ must survive the ensemble average of Equation (3.3). This implies there exists a definite phase relation among states of the ensemble. Thus, off-diagonal elements of $\underset{\approx}{\rho}$ represent a coherent superposition of the states $\{\phi\}$. The off-diagonal elements are termed coherences.

The probabilities in Equation (3.6) are given by a statistical distribution of energies at equilibrium

$$p_i = \frac{\exp(-E_i/kT)}{\sum_i \exp(-E_i/kT)} , \tag{3.8}$$

where k is Boltzmann's constant and T the temperature. Thus, the thermal equilibrium density matrix operator is given by

$$\rho_{eq} = \frac{\exp(-H/kT)}{Tr(\exp(-H/kT))} \tag{3.9}$$

with the exponential defined by

$$\exp(-H/kT) = 1 - \frac{H}{kT} + \frac{1}{2}\frac{(H)(H)}{(kT)^2} \ldots . \tag{3.10}$$

In the high field approximation in which the Zeeman interaction is the largest contribution to H, the equilibrium density matrix operator is expanded

$$\rho_{eq} = 1 - \beta I_z + \ldots , \tag{3.11}$$

and the constant β is defined as

$$\beta = (\gamma H_0/kT)/Tr(\exp(-H/kT)).$$

Since the unit operator in Equation (3.11) commutes with all operators in H, it is often neglected to yield the reduced density matrix

$$\rho_{eq} = -\beta I_z$$

which has been truncated to the first term. In a high field and at most temperatures encountered in NMR, β is small and higher order terms are negligible (the high temperature approximation).

3.2.2 The Basic Multiple Quantum Experiment

The most general pulse sequence used for generating and observing multiple quantum coherence in proton NMR is shown in Figure 3.3. The basic three pulse sequence in Figure 3.3a consists of pulses with relative radio frequency phases ϕ_i and rotation angles $\theta_i (\theta_i = \omega_1 t_{p_i})$. The NMR signal $S(\tau;t_1,t_2)$ as a function of the time parameters τ, t_1, and t_2 is detected during t_2. Using phase sensitive detection (see Chapter 5), two contributions are separated into two spectrometer "channels" corresponding to detection of oscillating field components along the rotating frame x and y axes. These are related to the expectation values $\langle I_x \rangle$ and $\langle I_y \rangle$. The choices of values for parameters τ, t_1, t_2, θ_i, ϕ_i are determined by the spin system under investigation and which transitions are desired. The affect of each is discussed below.

Figure 3.3b shows a pulse sequence which is actually used in the theory below. The experiment is more symmetric from the standpoint of density matrix evolution if we imagine we observe a signal proportional to $\langle I_z \rangle$. This is effected by placing a fourth pulse, $P_4(\theta_4, \phi_4)$, to transfer magnetization back along the z axis. The experiments themselves

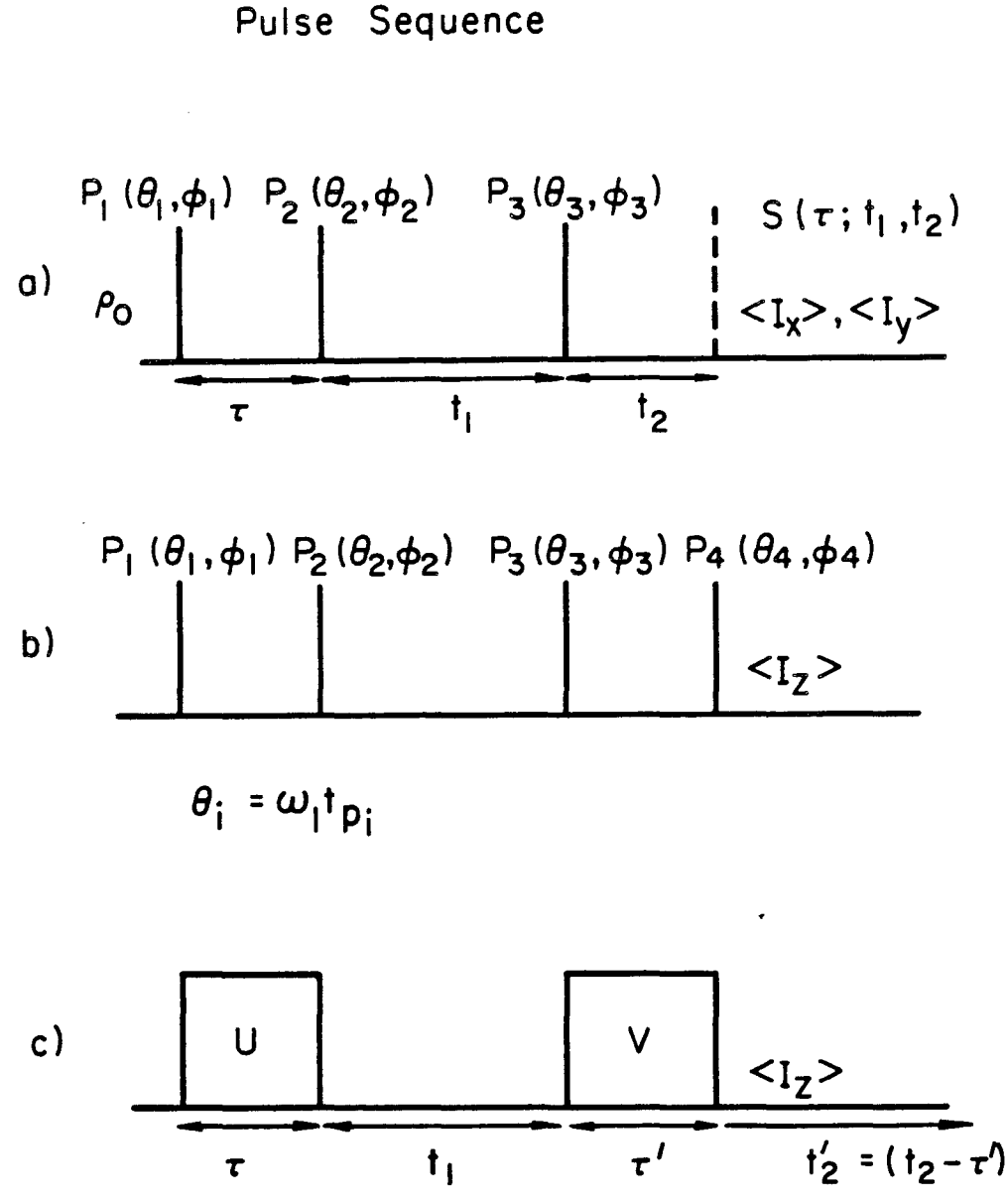

Figure 3.3 XBL818-4148

The simplest pulse sequence used for generating and detecting multiple quantum coherences in NMR. a) The first two pulses (P_1 and P_2) create coherences which evolve freely for time t_1. These "invisible" coherences are then detected during t_2 by the action of a third pulse (P_3, the "mixing" pulse). The two dimensional signal, $S(\tau;t_1,t_2)$, is a function of the parameter τ. b) A fourth pulse, P_4, is included in the theory and $\langle I_z\rangle$ calculated from the density matrix. c) A generalization of the sequence in b) in which the preparation propagator is $U(\tau)$ and the detection propagator is $V(\tau')$. In the experiment of a), only one point in t_2 at τ' is collected for each value of t_1.

do not contain this last pulse because of the requirement for observation of magnetization oscillating transverse to the main field.

Figure 3.3c illustrates a conceptualization of multiple quantum experiments which is used below. The signal written in terms of parameters in Figure 3.3a is familiar in the general field of two-dimensional Fourier transform spectroscopy [56]. We instead use parameters of Figure 3.3c in expressions for the signal $S(\tau;t_1,\tau')$ in equations below ($\tau' = t_2$). As we show below, this allows a convenient mathematical treatment of density matrix evolution.

The sequence of Figure 3.3c may be viewed as consisting of three parts. The multiple quantum coherences are generated during a "preparation" period labeled U. In terms of parameters in Figure 3.3, the propagator for this period is given by

$$U = e^{+i\theta_2 \vec{I}\cdot\hat{n}_2} e^{-iH\tau} e^{+i\theta_1 \vec{I}\cdot\hat{n}_1}. \qquad (3.12)$$

In Equation (3.12), $\vec{I}$ is the spin angular momentum operator and $\hat{n}_1$, $\hat{n}_2$ are unit vectors in the rotating frame x, y plane, defined by the relative r.f. phases ϕ_1, ϕ_2. The Hamiltonian is given by H. Multiple quantum coherences are then allowed to evolve freely during the "evolution" period of duration t_1. No NMR signal is detected from these coherences during t_1. This is because evolution of a coherent superposition of states involved in a multiple quantum transition does not correspond to magnetic dipole radiation. Because of this, it is necessary to transfer multiple quantum coherences back into single quantum coherences which we can detect. This is accomplished during the "detection" period labeled V in Figure 3.3c. The propagator for this period, of duration τ', may be written

$$V = e^{+i\theta_4 \vec{I}\cdot\hat{n}_4} e^{-iH\tau'} e^{+i\theta_3 \vec{I}\cdot\hat{n}_3} \qquad (3.13)$$

in analogy with Equation (3.12). In Figure 3.3c the parameter t_2 has been set equal to τ'. It has been shown that $t_2 = \tau' = \tau$ produces the maximum signal [66,67].

The signal is collected after the detection period and is a function of τ, t_1, and t_2: $S(\tau;t_1,t_2)$. The two-dimensional Fourier transform could then be applied to produce a two-dimensional spectrum $S(\tau;\omega_1,\omega_2)$. A single quantum spectrum results from a slice in the ω_2 direction and the multiple quantum spectrum is found from a projection along ω_1. For experiments in this work it is sufficient to collect just the single point at $t_2 = \tau'(t_2' = 0)$. This point represents the integral over the ω_2 spectrum. Although some signal will be lost in ω_1 due to phase differences among lines in ω_2, the technical convenience of single point detection must be compared to the effort required to compute the full 2-D spectrum. For constant values of τ, t_1, and $t_2 = \tau'$, application of the pulse sequence then yields a single data point. The entire sequence is then repeated with a new value of t_1, the evolution time. Proceeding in this manner, a multiple quantum "free induction decay" is mapped out. Fourier transformation of the result as a function of t_1 produces a multiple quantum spectrum such as Figure 3.1.

If we use Equation (3.7b) and (3.5), we can write the signal in terms of density matrix evolution as

$$S(\tau;t_1,\tau') \propto \langle I_z \rangle = \mathrm{Tr}(I_z\rho)$$

$$= \mathrm{Tr}[I_z V e^{-iHt_1} U\rho_0 U^\dagger e^{iHt_1} V^\dagger], \qquad (3.14a)$$

$$= \mathrm{Tr}[V^{\dagger} I_z V \, e^{-iHt_1} U \rho_0 U^{\dagger} e^{iHt_1}], \tag{3.14b}$$

$$= \sum_{jk} (U\rho_0 U^{\dagger})_{jk} (V^{\dagger} I_z V)_{kj} \, e^{i\omega_{kj} t_1}, \tag{3.14c}$$

with ω_{kj} the transition frequency $(2\pi(\nu_k - \nu_j))$. Fourier transformation with respect to t_1 gives

$$S(\tau;\omega_1,\tau') \propto \sum_{jk} (U\rho_0 U^{\dagger})_{jk} (V^{\dagger} I_z V)_{kj} \delta(\omega - \omega_{kj}) \tag{3.15a}$$

$$= \sum_{jk} (\underset{\approx}{P}(\tau))_{jk} (\underset{\approx}{Q}(\tau'))_{kj} \delta(\omega - \omega_{kj}) \tag{3.15b}$$

In the equations above, ρ_0 is the density matrix just prior to the first pulse. Often, but not always, we start the experiment with the equilibrium density matrix, $-\beta I_z$, and, setting $-\beta$ equal to one for now, $\rho_0 \equiv I_z$. The matrix $\underset{\approx}{P}$ is the preparation matrix and $\underset{\approx}{Q}$ is the detection matrix. When $\tau' = \tau$ and $\rho_0 = I_z$, then $\underset{\approx}{Q}(\tau') = \underset{\approx}{P}(-\tau)$.

3.2.3 Properties of the Preparation Matrix

We now consider the form of $\underset{\approx}{P}$ for specific values of θ_i and ϕ_i. For now we will assume that all chemical shifts are equal and so we can set $\sigma_i = 0$. In addition, quadrupolar and scalar couplings are excluded from the Hamiltonian below but may be treated in a straightforward manner. From the results of Chapters 1 and 2, the spin Hamiltonian may be written

$$H = -\Delta\omega I_z + \sum_{i<j} D_{ij} (3I_{zi} I_{zj} - \vec{I}_i \cdot \vec{I}_j), \tag{3.16a}$$

or, in terms of spherical tensor components.

$$H = -\Delta\omega \sum_k T_0^{1,k} + \sum_{i<j} A_0^{2,ij} \, T_0^{2,ij} \tag{3.16b}$$

where, from Equation (2.13-2.15),

$$A_0^{2,ij} = -\sqrt{6}\,\frac{\gamma_i\gamma_j}{r_{ij}^3}\,P_2(\cos\theta_{ijz}) \tag{3.17a}$$

$$T_0^{2,ij} = (6)^{-\frac{1}{2}}\,[I_{+1}^i I_{-1}^j + 2I_0^i I_0^j + I_{-1}^i I_{+1}^j] \tag{3.17b}$$

$$T_0^{1,j} = I_0^i = I_{zi}, I_{\pm 1}^i = \pm\frac{1}{\sqrt{2}}\,I_{\pm i} \tag{3.17c}$$

All of the experimental pulse sequences can be written so that the first two pulses are at opposite phase, i.e., $\phi \equiv \phi_1$; $\bar{\phi} \equiv \phi_2 = \phi + \pi$, and rotate I_z by the same angle $\theta_1 = \theta_2 \equiv \theta$. The propagator U may then be written

$$U(\theta,\phi,\tau) = e^{-i\theta\vec{I}\cdot\hat{n}}\,e^{-iH\tau}\,e^{i\theta\vec{I}\cdot\hat{n}} \tag{3.18a}$$

With ϕ the phase shift relative to the rotating frame y axis,

$$e^{i\theta\vec{I}\cdot\hat{n}} = e^{i\phi I_z}\,e^{i\theta I_y}\,e^{-i\phi I_z},$$

then,

$$U(\theta,\phi,\tau) = e^{i\phi I_z}\,U(\theta,\tau)\,e^{-i\phi I_z}, \tag{3.18b}$$

$$U(\theta,\tau) = e^{-i\theta I_y}\,e^{-iH\tau}\,e^{i\theta I_y}.$$

Likewise, for the detection propagator ($\theta_3 = \theta_4 \equiv \theta'$ and $\phi_3 = \phi$; $\phi_4 = \phi + \pi$),

$$V(\theta',\phi,\tau') = e^{i\phi I_z}\,V(\theta',\tau')\,e^{-i\phi I_z} \tag{3.19a}$$

$$V(\theta',\tau') = e^{-i\theta' I_y}\,e^{-iH\tau}\,e^{i\theta' I_y}. \tag{3.19b}$$

As an example of the affect of phase, we consider what happens when the first two pulses are at some phase relative to the final pulses. This causes an order-dependent phase shift of the preparation matrix relative to detection. From Equation (3.18), (3.19) and (3.14) we find

$$\sum_{jk} (U(\theta,\phi,\tau)I_z U^\dagger(\theta,\phi,\tau))_{jk} (V^\dagger(\theta',\phi,\tau')I_z V(\theta',\phi,\tau'))_{kj} \delta(\omega - \omega_{kj})$$

$$= \sum_{jk} (U(\theta,\tau)I_z U^\dagger(\theta,\tau))_{jk} (V^\dagger(\theta',\tau')I_z V(\theta',\tau'))_{kj}$$

$$\times e^{-i(M_j - M_k)\phi} \delta(\omega - \omega_{kj}) \qquad (3.20)$$

Equation (3.20) states that a shift in the phase of the radio frequency preparation pulses results in $\Delta M = M_j - M_k$ times the phase shift for a multiple quantum line in the spectrum. This will have implications for the separation of orders and phase Fourier transformation techniques as discussed below, but for now we take $\phi = 0$. We now look at specific cases for the parameters of Figure 3.3.

To calculate the affect of pulse angle θ, we make use of transformation properties for spin operators. Again, we write the preparation propagator

$$U(\theta,\tau) = e^{-i\theta I_y} e^{-iH\tau} e^{i\theta I_y}$$

$$= e^{-iH'\tau}$$

where

$$H' = e^{-i\theta I_y} H e^{i\theta I_y}. \qquad (3.21)$$

The effect of the rotation implied in Equation (3.21) can be calculated by a transformation with Euler angles $(\alpha,\beta,\gamma) = (0,\theta,0)$. From Equation (2.17) and a definition of the Wigner rotation matrix, the rotated Hamiltonian H' is $(H = H_z + H_D)$

$$H' = -\Delta\omega\cos\theta T_0^1 + \frac{\Delta\omega}{\sqrt{2}}\sin\theta[T_{+1}^1 - T_{-1}^1]$$

$$+ \sum_{i<j} A_0^{2,ij}\{\frac{1}{2}(3\cos^2\theta - 1)T_0^{2,ij}$$

$$+ (\frac{3}{8})^{\frac{1}{2}}\sin2\theta[T_{+1}^{2,ij} - T_{-1}^{2,ij}]$$

$$+ (\frac{3}{8})^{\frac{1}{2}}\sin^2\theta[T_{+2}^{2,ij} + T_{-2}^{2,ij}]\} \qquad (3.22a)$$

or, replacing the T_q^k spin operators with spin angular momentum operators,

$$H' = -\Delta\omega\cos\theta I_0 - \frac{\Delta\omega}{2}\sin\theta[I_{+1} + I_{-1}]$$

$$+ \sum_{i<j} D_{ij}\{\frac{1}{2}(3\cos^2\theta-1)(3I_0^iI_0^j - \vec{I}_i\cdot\vec{I}_j)$$

$$+ (\frac{3}{2})\sin2\theta[(I_{+1}^iI_0^j + I_0^iI_{+1}^j) - (I_{-1}^iI_0^j + I_0^iI_{-1}^j)]$$

$$+ (\frac{3}{2})\sin^2\theta[I_{+1}^iI_{+1}^j + I_{-1}^iI_{-1}^j]\}. \qquad (3.22b)$$

The affect of the preparation matrix $\underset{\approx}{P}$ may then be found by considering the expansion [3]

$$P(\tau) = \rho_0 + i\tau[\rho_0,H'] - \frac{\tau^2}{2}[[\rho_0,H'],H'] + \ldots \qquad (3.23)$$

In what follows, we introduce definitions for the preparation matrix using different initial density matrix operators $\rho_0 = I_z$, I_x, I_y:

$$P_\theta^z \equiv U(\theta,\tau)\ I_z\ U^\dagger(\theta,\tau) \tag{3.24a}$$

$$P_\theta^x \equiv U(\theta,\tau)\ I_x\ U^\dagger(\theta,\tau) \tag{3.24b}$$

$$P_\theta^y \equiv U(\theta,\tau)\ I_y\ U^\dagger(\theta,\tau) \tag{3.24c}$$

We now consider specific cases for $\underset{\approx}{P}$.

Case 1 $\theta = \frac{\pi}{2}$; $\Delta\omega = 0$; $\rho_0 = I_z$.

For this case, the preparation sequence is $\frac{\pi}{2}\ y,\tau,\ \frac{\pi}{2}\ \bar{y}$ ($\bar{y}$ means a pulse with phase 180° relative to y). Equation (3.22a) becomes

$$H_{xx} \equiv H' = \sum_{i<j} A_0^{2,ij} \{-\frac{1}{2}\ T_0^{2,ij} + (\frac{3}{8})^{\frac{1}{2}}\ [T_{+2}^{2,ij} + T_{-2}^{2,ij}]\} \tag{3.25}$$

$$H_{xx} = \sum_{i<j} D_{ij} \{+\frac{1}{2}\ (3I_{zi}I_{zj} - \vec{I}_i\cdot\vec{I}_j) + \frac{3}{2}\ (I_{+1}^i I_{+1}^j + I_{-1}^i I_{-1}^j)\}$$

$$H_{xx} = -\frac{1}{2}\ H_{zz} + (\frac{3}{4}) \sum_{i<j} D_{ij}(I_{+i}I_{+j} + I_{-i}I_{-j}).$$

In Equation (3.25), subscripts on H have been introduced which refer to rotation of the bilinear dipolar Hamiltonian, i.e., H_{xx} means H_{zz} rotated by a 90° y pulse.

Since H_{xx} only contains T_q^2 operators with q = 0, ± 2, it is a zero quantum and two quantum operator. This is a direct consequence of the bilinear nature of H_{zz}. Linear operators, such as those contained in the chemical shift Hamiltonian, cannot create multiple quantum coherences by themselves. If the commutators in Equation (3.23) are evaluated, using Equation (3.25) and setting $\rho_0 = I_z$, it is easily seen that $P_{\frac{\pi}{2}}^z$ will only contain operators connecting states separated by $\Delta M = 0$ or ΔM even. Thus, this preparation sequence creates only even quantum coherences.

The expansion (3.23) can be used to determine the dependence of each order on τ when this time is short [33,67]. Zero quantum operators do not appear until the τ^2 term. Other even n quantum operators first appear in the $\tau^{(n-1)}$ term. In most experiments, the higher quantum transitions are desired requiring the expansion to contain significant contributions from high order terms. This implies longer values of τ for which the expansion will not converge fast. The explicit short time τ power dependence approach is then replaced by the choice of a preparation time such that $\nu_D\tau \sim 1$ where ν_D is a measure of the "size" of H_D in Hertz. Experimental methods exist [69] for choosing values of τ which are best for creating transitions of a certain order.

Case 2 $\theta = \frac{\pi}{2}$; $\Delta\omega = 0$; $\rho_0 = I_y$.

For this case, the propagator U will contain the same rotated Hamiltonian as before (Eq. 3.25). The preparation propagator now becomes

$$P^y_{\frac{\pi}{2}} = e^{-iH_{xx}\tau} I_y e^{iH_{xx}\tau}.$$

Again, using the expansion of Equation (3.23) this propagator can be shown to contain only odd quantum operators. The operator I_y may be written as a combination of $T^1_{\pm 1}$ operators. Recalling the commutation relations in Equation (2.16b) we see that $P^y_{\frac{\pi}{2}}$ will contain products such as $T^{1,i}_{+1}T^{1,j}_{0}$, $T^{1,i}_{-1}T^{1,j}_{+1}T^{1,k}_{+1}$, ... etc. and so is entirely odd quantum in nature. The first term in Equation (3.23) with odd n quantum coherence is the τ^n term. The initial density matrix $\rho_0 = I_y$ may be prepared by proceeding the multiple quantum pulse sequence with an x phase pulse. With $\phi = 0$, the first y pulse then does nothing and may be omitted. An odd quantum preparation sequence is then $\frac{\pi}{2}$ x,τ, $\frac{\pi}{2}$ y.

Case 3 $\theta = \frac{\pi}{4}$; $\Delta\omega = 0$; $\rho_0 = I_z$

Now the added terms in H' are the first order operators $T^{2,ij}_{\pm 1}$. Once again, considering the commutators in Equation (3.23) we see that $P^z_{\frac{\pi}{4}}$ will contain all orders of multiple quantum operators, both even and odd. The τ power dependence of these is somewhat different than the previous cases. For example, the first term with three quantum operators is the τ^2 term. For very short preparation times, the three quantum transitions will appear faster than if the odd quantum sequence of case 2 is used.

If we use a $\frac{\pi}{2}$ pulse as the first pulse then the sequence may be written

$$\frac{\pi}{2}\, y, \tau, \frac{\pi}{4}\, \bar{y} = \frac{\pi}{4}\, y, \frac{\pi}{4}\, y, \tau, \frac{\pi}{4}\, \bar{y}.$$

In this case, the preparation matrix is

$$\underset{\approx}{P} = \frac{1}{\sqrt{2}}\, U(\tfrac{\pi}{4},\tau)[I_z + I_x]\, U^{\dagger}(\tfrac{\pi}{4},\tau) \equiv \frac{1}{\sqrt{2}}\, (P^z_{\frac{\pi}{4}} + P^x_{\frac{\pi}{4}}). \tag{3.26}$$

Both terms above contain even and odd quantum operators.

So far we have considered just the preparation portion of Figure 3.3c. As we said before, multiple quantum coherences evolving during t_1 are unobservable and we have to reconvert them to single quantum signal. The properties of the detection matrix in Equation (3.15) are essentially the same as the results above when $\tau' = \tau$. Equation (3.15) states that $\underset{\approx}{Q}$ will have to contain operators for the coherences of interest if they are to be observed. For example, if the detection sequence of Figure (3.3b) is $\frac{\pi}{2}\, y, \tau, \frac{\pi}{2}\, \bar{y}$ then only even quantum transitions can be observed. The signal ultimately depends on the product of $\underset{\approx}{P}$ and $\underset{\approx}{Q}$ and so we can

selectively prepare and detect either even quantum, odd quantum or both coherences in the experiment. This principle is demonstrated experimentally below.

In summary, we have shown that multiple quantum coherences can be prepared and detected by a number of simple sequences which are only selective in the sense that the rotated Hamiltonian (Eq. (3.22a)) and initial density matrix ρ_0 can be chosen to contain T_q^k terms where q is even, odd, or a mixture of both. The specific cases of $\underset{\approx}{P}$ and $\underset{\approx}{Q}$ considered above are summarized here.

$$P_{\frac{\pi}{2}}^{z},\ Q_{\frac{\pi}{2}}^{z} \text{ pure even quantum} \tag{3.27a}$$

$$P_{\frac{\pi}{2}}^{y},\ Q_{\frac{\pi}{2}}^{y} \text{ pure odd quantum} \tag{3.27b}$$

$$P_{\frac{\pi}{4}}^{z,x},\ Q_{\frac{\pi}{4}}^{z,x} \text{ both even and odd quantum} \tag{3.27c}$$

We have only considered the case when the resonance offset $\Delta\omega$ is zero. The affect of the offset term in a Hamiltonian can be included straightforwardly. Now the preparation matrix is given by

$$P = e^{-i\theta I_y} e^{+i(-\Delta\omega I_z + H_{zz})\tau} e^{i\theta I_y} \rho_0 e^{-i\theta I_y} e^{-i(-\Delta\omega I_z + H_{zz})\tau} e^{i\theta I_y}$$

$$P = e^{-iH'_{xx}\tau} \exp(-i\Delta\omega\tau\cos\theta I_z)\exp(-i\Delta\omega\tau\sin\theta I_x)\exp(\Delta\omega\tau\cos\theta\sin\theta I_y)$$

$$x\ \rho_0 \exp(-\Delta\omega\tau\cos\theta\sin\theta I_y)\exp(i\Delta\omega\tau\sin\theta I_x)\exp(i\Delta\omega\tau\cos\theta I_z)\ e^{+iH'_{xx}\tau}\ . \tag{3.28}$$

For a general rotation angle of θ, Equation (3.28) would be difficult to evaluate. From Equation (3.22a) it is obvious that an offset will result in the occurrence of both even and odd quantum coherences in $\underset{\approx}{P}$. For the trivial case of $\theta = \frac{\pi}{2}$, Equation (3.28) becomes (with $\rho_0 = I_z$)

$$P^z_{\frac{\pi}{2}}(\Delta\omega) = \cos\Delta\omega\tau\ P^z_{\frac{\pi}{2}} - \sin\Delta\omega\tau\ P^y_{\frac{\pi}{2}} . \qquad (3.29)$$

A similar expression obtains if $\rho_0 = I_y$ and for $Q^{z,y}_{\frac{\pi}{2}}(\Delta\omega)$. If there are no chemical shift differences, the spectrometer may be set so that $\Delta\omega = 0$. This condition cannot be met for all chemically shifted nuclei in a general spin system and so chemical shift differences will tend to mix even and odd coherences in the preparation. When chemical shifts are small compared to dipolar couplings, this affect will not be too severe.

3.2.4 The Effect of Static Field Inhomogeneities/TPPI

From a consideration of the energy level diagram for N coupled spin ½ nuclei in Figure 1.2 and the form of the rotating frame Zeeman Hamiltonian, it can be seen that the affect of a resonance offset $\Delta\omega$ is multiplicative in multiple quantum evolution. The n quantum coherences will evolve with an offset of $n\Delta\omega$ where $\Delta\omega$ is the single quantum offset. The static field that a sample experiences is not perfectly homogeneous and there will be a distribution of $\Delta\omega$'s over the sample volume. The result is a familiar broadening of resonances in the spectrum whenever the distribution of field offsets is wider than the natural linewidth - a situation which is often the case in proton liquid crystal spectroscopy. The n quantum coherence will be broadened by n times the single quantum inhomogeneity. Unless removed, this broadening would prohibit the

observation of high order multiple quantum spectra.

Spin echoes of the Hahn type [70] are used to circumvent this problem. Placing a π pulse in the center of t_1 will reverse evolution under linear terms in the Hamiltonian. Bilinear terms such as the dipolar Hamiltonian remain unaffected by this pulse. All evolution from terms with $\Delta\omega I_z$ is refocussed at the end of the evolution period, thus removing the field broadening. Each multiple quantum coherence then evolves with just the dipolar frequencies and all orders will overlap. In order to separate contributions to the spectrum from different orders, the method of time proportional phase incrementation (TPPI) [59,60,65] is used.

The TPPI experiment is shown in Figure 3.4b. The first two pulses are at some relative phase ϕ and $\phi + \pi$ with respect to the third and fourth. This phase is incremented each time t_1 is incremented by Δt_1, so that $\Delta\phi = (\Delta\omega)(\Delta t_1)$ where here $\Delta\omega$ is just a parameter. From Equation (3.20) we see that each multiple quantum line is phase shifted by $\exp(-i\Delta M\phi) = \exp(-i\Delta M\Delta\omega t_1)$. The result is that the n quantum coherences appear to evolve with an effective offset of $n\Delta\omega$. To ensure that all orders are contained in the frequency spectrum without fold back, the phase increment is set so that $\Delta\phi \leq \frac{\pi}{N}$. This phase shift is usually a fraction of $\pi/2$ so that the usual spectrometer quadrature phases are not adequate. A delay line phase shifter under digital control of the pulse programmer is used and is fully described in Chapter 5.

3.2.5 Phase Fourier Transform Averaging

Similar to TPPI, the method of phase Fourier transform (PFT) averaging may be used to separate multiple quantum orders [56,63]. Considering Equation (3.20) as a Fourier series in phase indicates that coherences can be separated in phase space according to $\Delta M\phi$. Coaddition of different

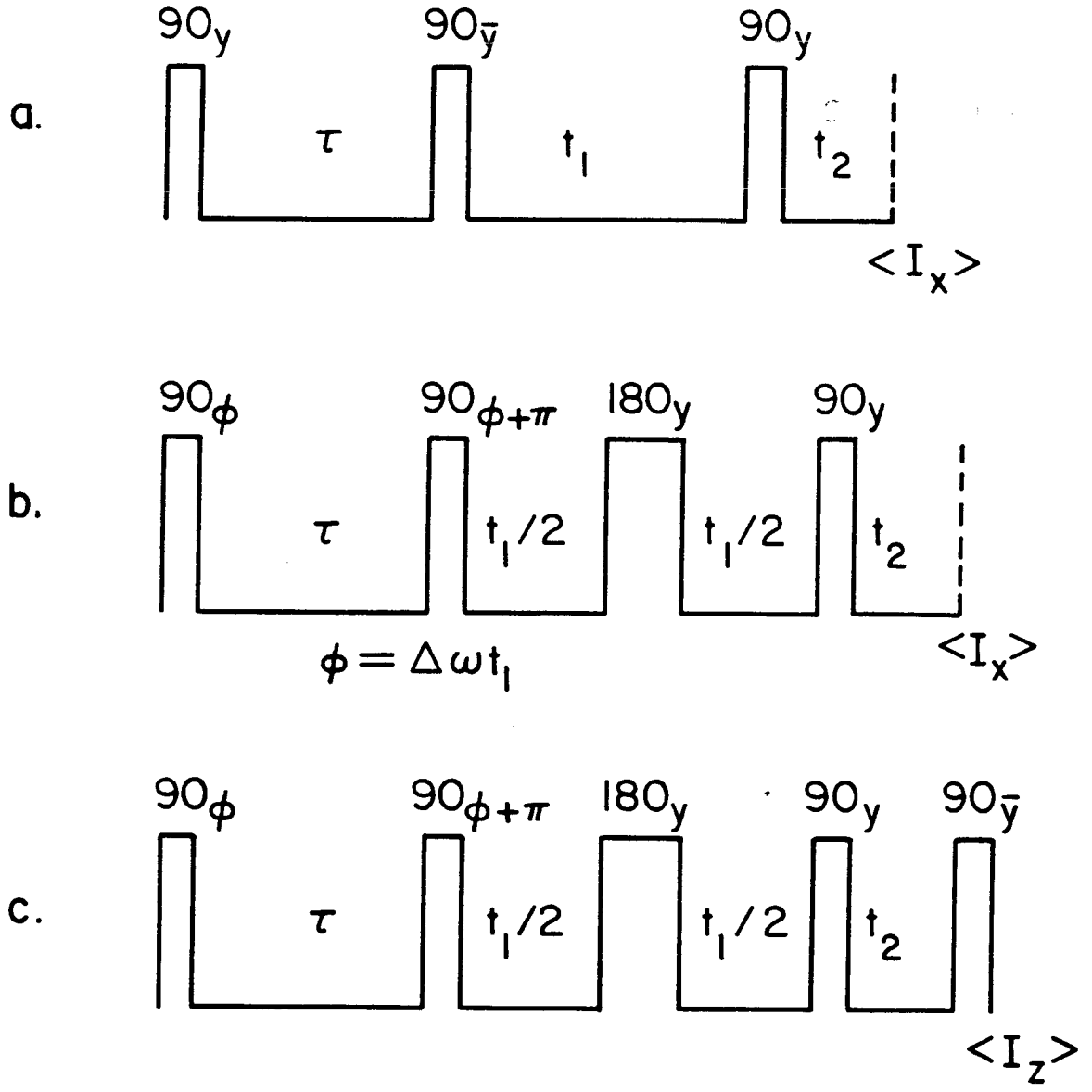

Figure 3.4 XBL 8010-12245

The time proportional phase incrementation pulse sequence. In a), the usual three pulse multiple quantum sequence is repeated with 90° pulses ($\nu_1 t_p = \frac{1}{4}$). b) TPPI pulse sequence. A spin echo pulse (180°) is placed in the middle of t_1 to remove inhomogeneous broadening in the evolution of multiple quantum coherences. The first two pulses are phase shifted by an angle ϕ which is a linear function of the evolution time: $\phi = \Delta\omega t_1$. c) As in Figure 3.3c, the density matrix evolution is more symmetric if we imagine that there is an additional final pulse and we detect $\langle I_z \rangle$.

spectra with properly chosen preparation phases will allow the cancellation of contributions to the total spectrum from all but a few orders. As an example, the even quantum orders may be selected over odd quantum by adding two spectra taken with preparation phases ϕ and $\phi + \pi$. The odd quantum signal changes sign whereas the even quantum shows a phase shift of zero and constructively adds. Extensions to other orders is straightforward.

3.2.6 Intensities

As we have seen, preparation and detection matrix elements, which determine the extent to which coherences appear in the multiple quantum signal, are a function of the times τ and t_2. Choosing $t_2 = \tau' = \tau$ has proved adequate for our analysis. From Equation (3.15) it can be shown that the phases of different multiple quantum lines will not be the same. This causes loss of intensity in those orders where lines overlap but is not a problem in resolved higher order spectra. In principle, all lines will have the same phase if a time reversal sequence [72] is used during detection so that $\underset{\approx}{Q}(\tau') = \underset{\approx}{Q}(-\tau)$. In practice, this is not necessary and magnitude spectra are usually calculated to avoid having to phase correct individual lines.

As discussed previously, for very short preparation times, not all coherences are created due to a strong power dependence on τ. This is demonstrated experimentally in Figure 3.5. For the shortest preparation times, only the one quantum transitions are observed. As soon as τ becomes on the order of .1 msec, all orders are observed to some intensity. As τ is further increased, individual lines are seen to oscillate as expected from the forms of $\underset{\approx}{P}$ and $\underset{\approx}{Q}$. We mentioned earlier that the sizes of couplings in H_D may be used as an estimate of an appropriate value of

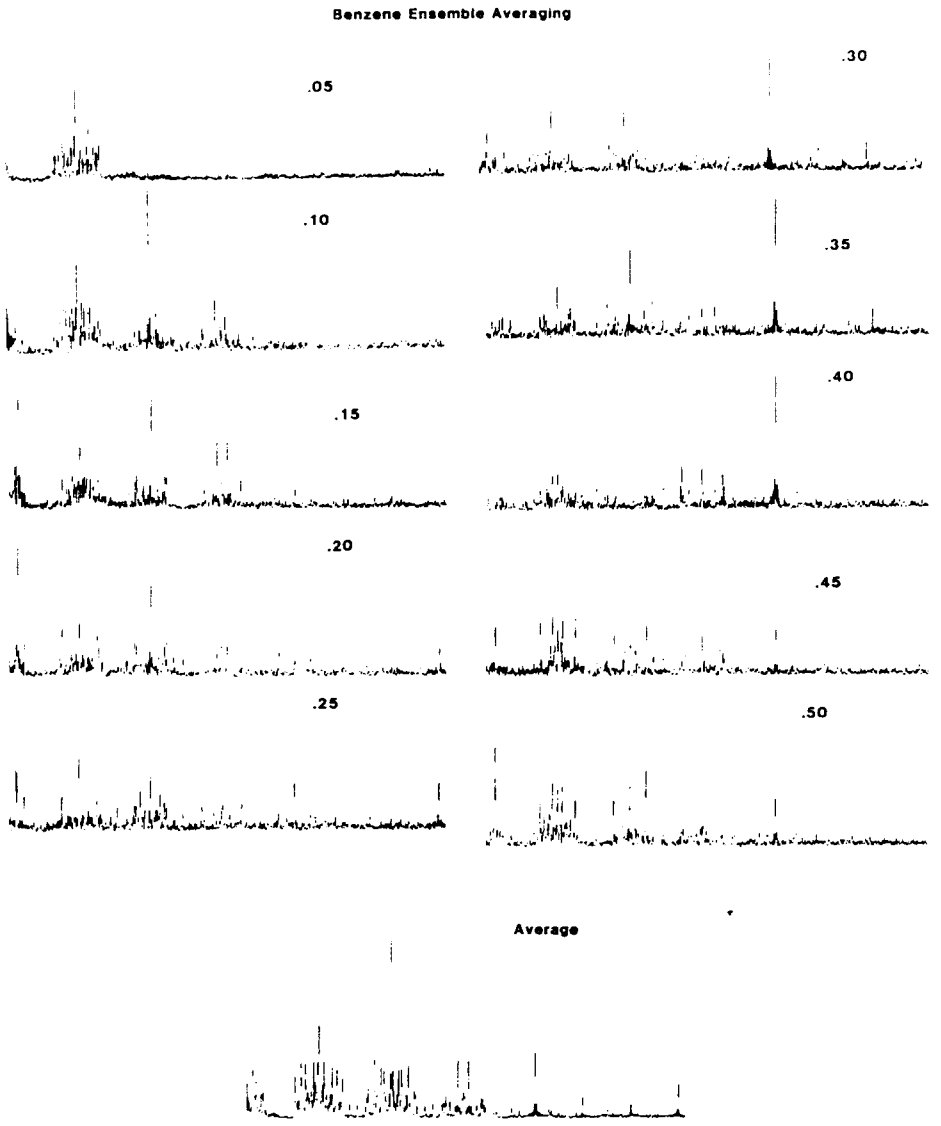

XBL 818-1772

Figure 3.5

Experimental demonstration of "ensemble" averaging used in multiple quantum NMR spectroscopy. The preparation time, τ, is varied for the ten magnitude spectra shown at the top. This time is given in milliseconds above each trace. For very short preparation times, only the lowest orders are observed. For longer values of τ, individual lines oscillate in magnitude. The average of these ten spectra is shown at the bottom.

τ for a general spin system. Actually, transitions for all orders are observed in a fraction of this time for benzene. This is a result of molecular symmetry and the precise nature of $\underset{\approx}{P}$ for benzene dipolar couplings [66]. It is possible to map out the τ dependence of $\underset{\approx}{P}$ experimentally for any order [73,69]. For small spin systems, this allows one to choose values of τ which produce greater average intensity in a particular order than an arbitrary choice of τ might.

To remove an intensity dependence on τ in the final spectrum, several magnitude spectra from experiments with different preparation times may be averaged together. This is referred to as "ensemble" averaging and is shown for benzene in Figure 3.5. If a sufficient number of τ values over a wide range are used then the average should approach some asymptotic intensity distribution. In a "statistical" limit one would assume that each transition occurs with equal probability in the averaged spectrum. As we have seen in Equation (1.29), for large spin systems, the number of transitions per order is in a Gaussian distribution. We then expect the statistical limit integrated intensity per order to fall off exponentially with n^2 for $n = |\Delta M|$. This is shown in Figure 3.6 and is qualitatively correct for the benzene experiment. Such a distribution implies that high order multiple quantum spectra will be difficult to observe for large spin systems by non-selective techniques. When the spin system is an undiluted liquid crystal, a practical limit of about ten coupled protons is tractable by non-selective means. Dilute samples, of course, present further complications.

It turns out that the statistical limit underestimates the intensity that will be found in some isolated high order transitions [66,67]. Figure 3.7 shows theoretical statistical and exact τ average stick spectra

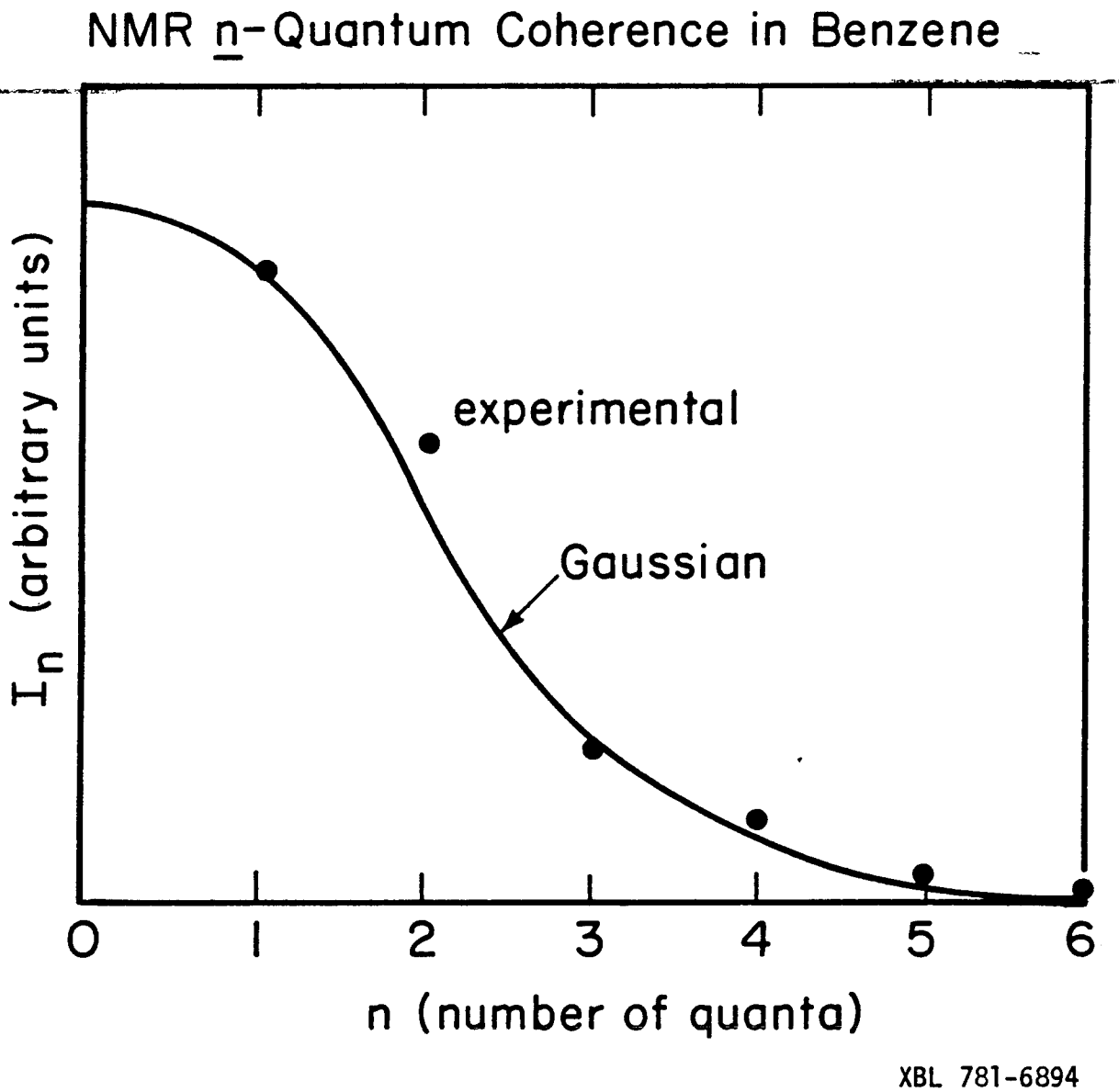

Figure 3.6

Integrated intensity per order for benzene ensemble averaged multiple quantum experiment. The solid curve is one half of a Gaussian distribution normalized for N = 6. The experimental points indicate that this distribution is qualitatively correct for a large spin system.

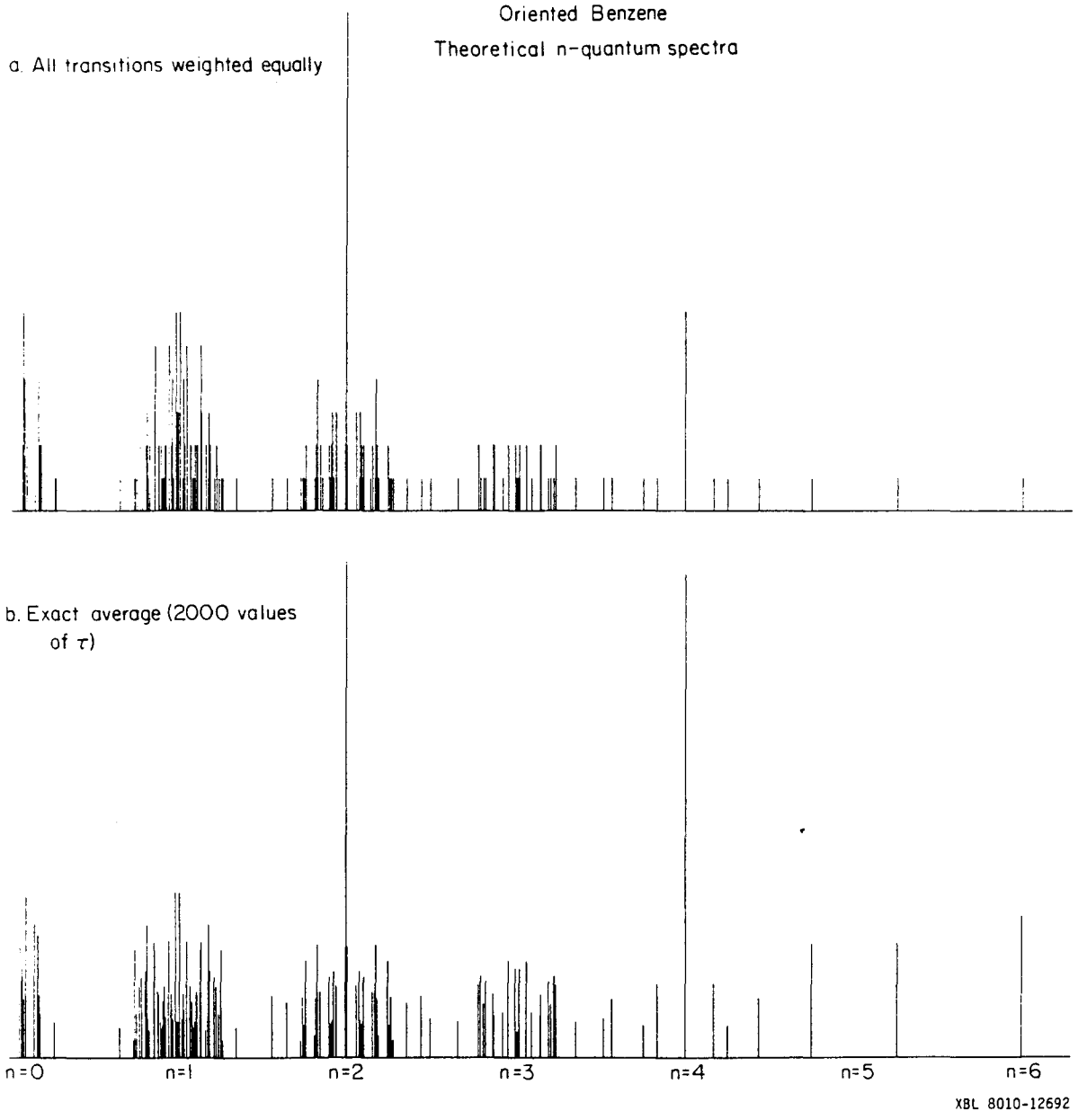

Figure 3.7

Theoretical n-quantum spectra for oriented benzene. a) In this "statistical" limit case, all transitions are assumed equally probable and so of equal intensity. b) The average of 2000 spectra calculated from exact values of preparation time, τ. The intensities here are the result of detailed calculation of density matrix evolution.

for benzene. The statistical spectrum was produced by weighting each allowed transition equally. Some degenerate transitions add to produce the largest lines. The exact τ average spectrum of Figure 3.7b results from a computer calculation by Murdoch, et al. [66,67] from Equation (3.15) using experimentally obtained benzene couplings. In this spectrum, the high order transitions are, on the average, more intense than one quantum transitions. The six quantum line is the most intense single transition. This exact average fits the experimental spectrum of Figure 3.1 more accurately in its intensity pattern than the statistical limit theory of Figure 3.7a.

For computational purposes, it is convenient to remove the time dependence of preparation and detection matrices in Equation (3.15). With $\tau' = \tau$, integrating over τ, the result for the intensity magnitude of a single transition $j \rightarrow k$, assuming an even quantum preparation matrix, may be written [66],

$$\langle |S_{jk}| \rangle_{\tau} = \sum_{\alpha} \sum_{\beta} B_{\alpha\beta}^2 + \begin{bmatrix} \text{terms involving} \\ \text{overlapping} \\ \text{transitions} \end{bmatrix} \tag{3.30}$$

The time independent elements $B_{\alpha\beta}$ are defined by

$$B_{\alpha\beta} = A_{\alpha j} X_{\alpha\beta} A_{\alpha k} = (\underset{\approx}{A}^{\dagger} \underset{\approx}{X} \underset{\approx}{A})_{jk} \tag{3.31a}$$

with

$$\underset{\approx}{A} = \underset{\approx}{S}^{\dagger} \exp(-i \frac{\pi}{2} \underset{\approx y}{I}) \underset{\approx}{S} \tag{3.31b}$$

$$\underset{\approx}{X} = \underset{\approx}{S}^{\dagger} \underset{\approx x}{I} \underset{\approx}{S} \tag{3.31c}$$

$$\underset{\approx}{H} = \underset{\approx}{S}^{\dagger} \underset{\approx}{\Lambda} \underset{\approx}{S} \tag{3.31d}$$

In the equations above, $\underset{\approx}{H}$ is the Hamiltonian matrix and $\underset{\approx}{\Lambda}$, $\underset{\approx}{S}$ are the eigenvalue and eigenvector matrices, respectively. For the high quantum orders where transitions are resolved (all orders for benzene), the second term in Equation (3.30) may be dropped and the "ultimate" τ averaged intensity is readily obtained. Equation (3.30) is easily modified to handle odd, or a mixture of even and odd, coherences. Programs have been written by Murdoch [67] which are capable of simulating the exact or ultimate τ averaged spectrum for molecules of up to eight protons. Theory spectra showing calculated intensities in this and the next chapter were obtained using these programs.

In addition to symmetry selection rules restricting allowed transitions to the irreducible representations of the molecular point group, there are further symmetry affects forbidding some zero quantum transitions. When the permutation group contains the inversion element (center of symmetry), some states will exhibit either gerade (even) or ungerade (odd) behavior under inversion. When the Hamiltonian is purely bilinear (chemical shifts and offset terms equal to zero) and the number of spins is even, states in the M = 0 Zeeman manifold may not be connected in zero quantum coherences by the preparation matrix in a multiple quantum experiment [66]. Similar to the inversion symmetry element, M = 0 states will be even or odd under the operator which flips all spins. If H is purely bilinear, this operator anticommutes with $P^{\phi}_{\pi/2}$ if the preparation sequence is $\frac{\pi}{2}\ \phi$, τ, $\frac{\pi}{2}\ \bar{\phi}$. The result is that only states of opposite parity under the spin-flip operator are connected in zero quantum coherences. When the preparation sequence involves other than $\frac{\pi}{2}$ pulses, so that P may be written as a combination of P^{z}_{θ} and P^{y}_{θ} as in Equation (3.26), then the spin-flip operator no longer anticommutes with coherence preparation and no inversion selection rules for zero quantum transitions are imposed.

Figure 3.8 shows an expanded trace of the zero quantum region of Figure 3.1. Ninety degree pulses were used in preparation and detection and so they may be written as $P^{\phi}_{\pi/2}$ and $Q^{\phi}_{\pi/2}$, respectively. The stick spectrum underneath the experimental trace contains line positions of all theoretical zero quantum resonances disregarding spin inversion symmetry. Markers beneath this stick spectrum show lines which should not appear by the spin inversion selection rule stated above. Although not all allowed transitions are resolved, most are observed to some intensity while the forbidden transitions are indeed missing.

Zero quantum transitions are unaffected by field inhomogeneity [63]. If the multiple quantum experiment is performed in strong field gradients and with no π pulses, then only zero quantum resonances will be narrow enough to be observed. This provides a convenient method for zero quantum selection. Selecting zero quantum transitions in this manner and using the sequence $\frac{\pi}{2}\ \phi,\ \tau,\ \frac{\pi}{4}\ \bar{\phi},\ t_1,\ \frac{\pi}{4}\ \phi,\ \tau$; sample, the spectrum of Figure 3.9 is obtained. The use of $\frac{\pi}{4}$ pulses has resulted in the appearance of almost all zero quantum lines. Although exact intensities are not shown in Figure 3.9, the missing B_1 transitions are normally only weakly allowed [71].

3.3 Even/Odd Quantum Experiments: Benzene

What follows are experimental examples demonstrating several outcomes of the theory in Section 3.2. Most of these experiments include π pulses at $\tau/2$ in the preparation and at $(t_2 = \tau')/2$ in detection periods to eliminate the effects of field inhomogeneities and to ensure the on-resonance condition. Linewidths are only a few hertz because of an additional echo π pulse in the evolution period. Transitions are separated according to order ΔM by using the TPPI technique. The TPPI phase

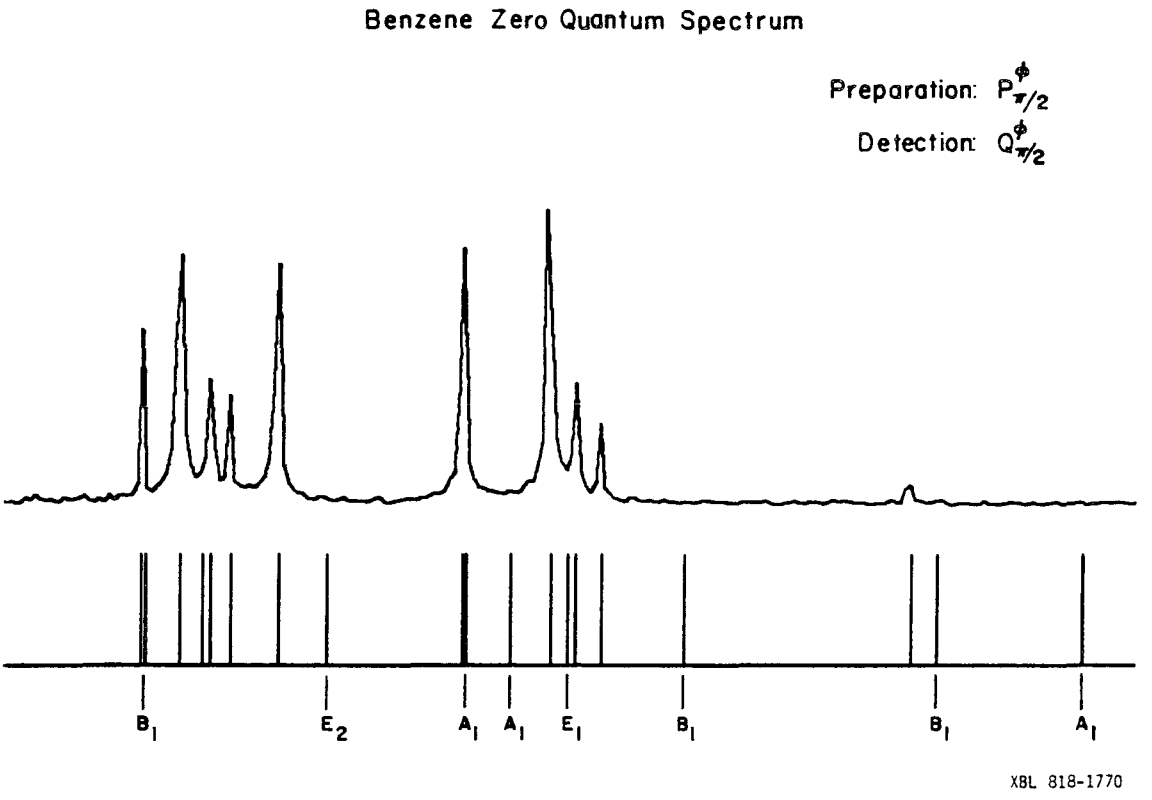

Figure 3.8

Benzene zero quantum spectrum. This is an expanded trace of the zero quantum region of Figure 3.1. The preparation and detection pulses are all $\pi/2$ pulses. In this case, spin inversion anti-commutes with P and Q and only transitions between states of opposite parity are allowed. Transitions forbidden by inversion symmetry and their representations are indicated beneath the theoretical stick spectrum.

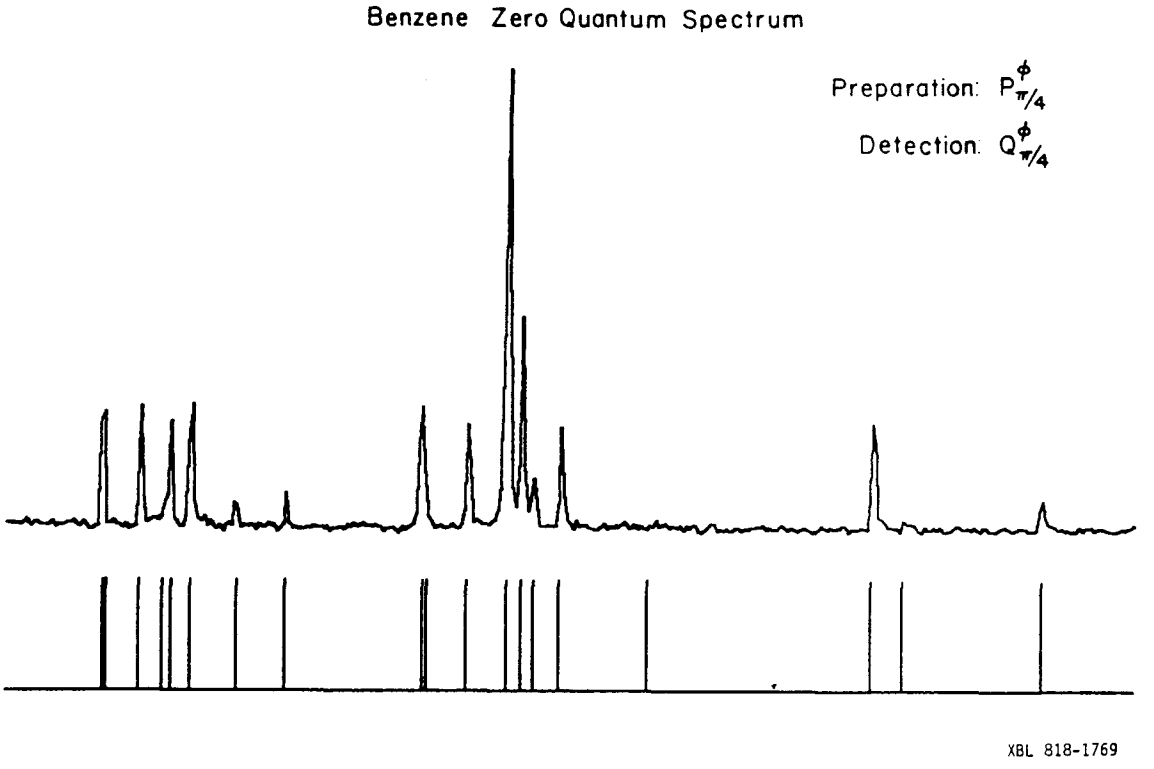

Figure 3.9

Benzene zero quantum spectrum. This spectrum was obtained using the sequence $\pi/2\phi$, τ, $\pi/4\bar{\phi}$, t_1, $\pi/4\phi$, τ. Spin inversion selection rules do not forbid any $M = 0$ transitions with this sequence. Missing transitions are of B_1 symmetry which are only weakly allowed. Only zero quantum transitions are observed in a field which was purposely made inhomogeneous.

shift used was 29.5°. This places the six quantum spectrum just below the Nyquist frequency. All spectra were taken from a single sample of ~30% (by mole) benzene in Eastman liquid crystal #15320. The solution was nematic at room temperature. Sample environment in the probe was temperature regulated to within $\pm$0.1°C (see Chapter 5 for a description of the probe). Generally, 8K words in the Fourier transform are sufficient to resolve most peaks, although, at the sampling rates used, the multiple quantum interferogram does not completely decay. Only one half of the frequency spectrum, which displays reflection symmetry about the DC component, is shown in each of the figures. The two halves of each spectrum were co-added in a manner which enhances the symmetry about the center of each order and improves signal-to-noise slightly. All spectra are magnitude plots. By Equation (3.20), the TPPI phase, $\phi(t_1)$, can be removed from $\underset{\approx}{P}$ and $\underset{\approx}{Q}$. The equations below are written with $\phi(t_1) = 0$ as though the preparation phase is coincident with the rotating frame y axis as in Figure 3.4a. This causes no loss of generality in the analysis.

3.3.1 Pure Even Quantum Spectrum

Figure 3.10 shows a benzene spectrum containing only the even quantum orders. The sequence of Figure 3.4b was used with the addition of π pulses midway in the preparation and detection periods. The signal $S(\tau;t_1,t_2)$ was polarized into one channel of the spectrometer quadruature (phase sensitive) detector. Observation in the other channel corresponds to the detection matrix $Q^y_{\frac{\pi}{2}}$ and a signal $\propto$ to

$$\langle I_+ \rangle(\omega) = \sum_{jk} (P^z_{\frac{\pi}{2}})_{jk} (Q^y_{\frac{\pi}{2}})_{kj} \delta(\omega - \omega_{kj}) = 0. \qquad (3.32)$$

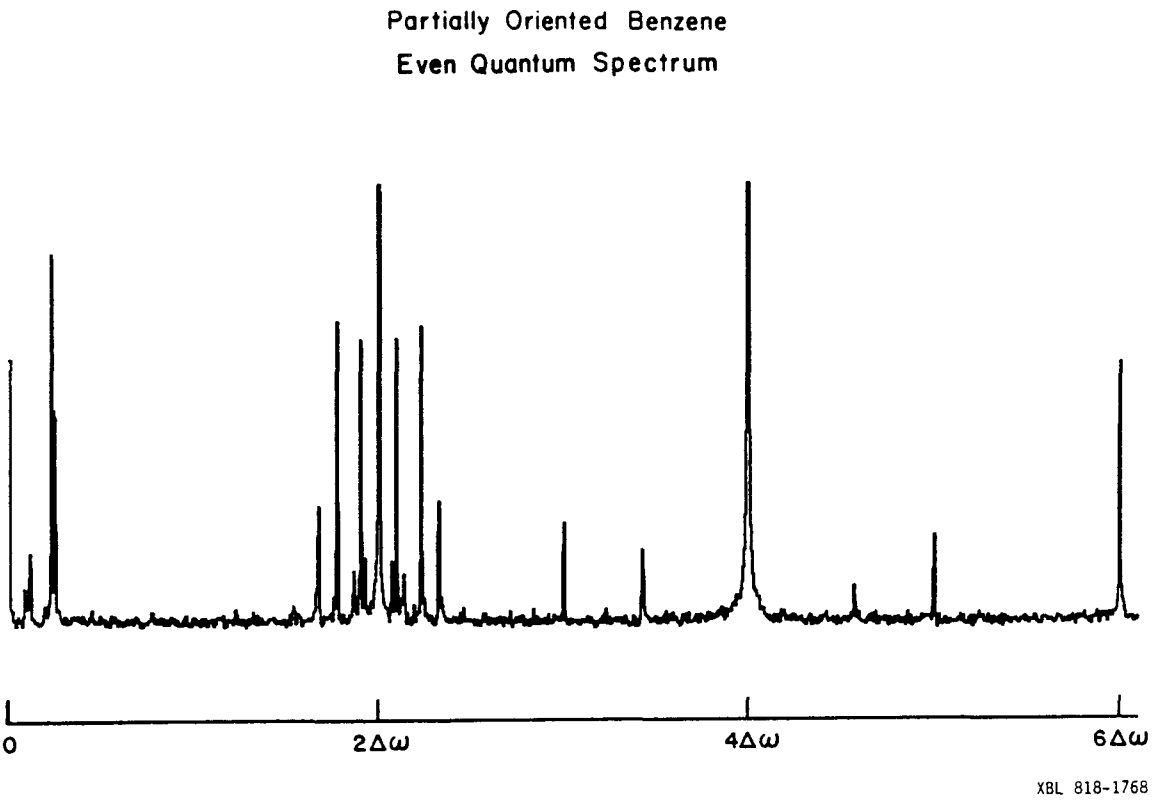

Figure 3.10

Benzene even quantum experiment. The pulse sequence used prepares only even quantum coherences. This is demonstrated by a complete lack of one, three, or five quantum lines. Orders are separated by the TPPI technique. The signal was polarized to one channel of the phase sensitive detector.

The odd quantum detection $Q^{y}_{\frac{\pi}{2}}$ does not connect states prepared by $P^{z}_{\frac{\pi}{2}}$ which is even quantum.

3.3.2 Pure Odd Quantum Spectrum

The benzene spectrum shown in Figure 3.11 demonstrates that, in analogy to a pure even quantum experiment, it is possible to detect only odd quantum orders. This is accomplished with the sequence (omitting pulses for clarity) $\frac{\pi}{2}\ \phi$, τ, $\frac{\pi}{2}\ (\phi+\frac{\pi}{2})$, t_1, $\frac{\pi}{2}\ y$, t_2; sample, where ϕ is the TPPI phase. As usual, $t_2 = \tau' = \tau$ in this experiment. The preparation and detection matrices are then $P^{y}_{\frac{\pi}{2}}$ and $Q^{y}_{\frac{\pi}{2}}$ for observation of signal $\propto \langle I_y \rangle$. As with the pure even quantum experiment, the signal can be entirely polarized in one spectrometer channel. The signal $\propto\langle I_x \rangle$ is then (with the TPPI $\phi(t_1) = 0$)

$$\langle I_x \rangle(\omega) = \sum_{jk} (P^{y}_{\frac{\pi}{2}})_{jk}\ (Q^{z}_{\frac{\pi}{2}})_{kj}\,\delta(\omega - \omega_{kj}) \tag{3.33}$$

and will be zero in analogy with the arguments for Equation (3.32).

3.3.3 Breaking Even/Odd Symmetry

It is quite often the case that both even and odd high order multiple quantum spectra are desired for spectral analysis. It then becomes necessary to remove the even or odd quantum nature of preparation and detection matrices to avoid repeating the experiment to get all orders. This may be accomplished in a number of ways.

A resonance offset is one approach which, from Equation (3.29), mixes even and odd quantum preparation (and detection) operators. Using the sequence $\frac{\pi}{2}\ y$, τ, $\frac{\pi}{2}\ \bar{y}$, t_1, $\frac{\pi}{2}\ y$, $t_2 = \tau$; sample, the complex signal becomes (dropping the subscript $\frac{\pi}{2}$ on P and Q terms)

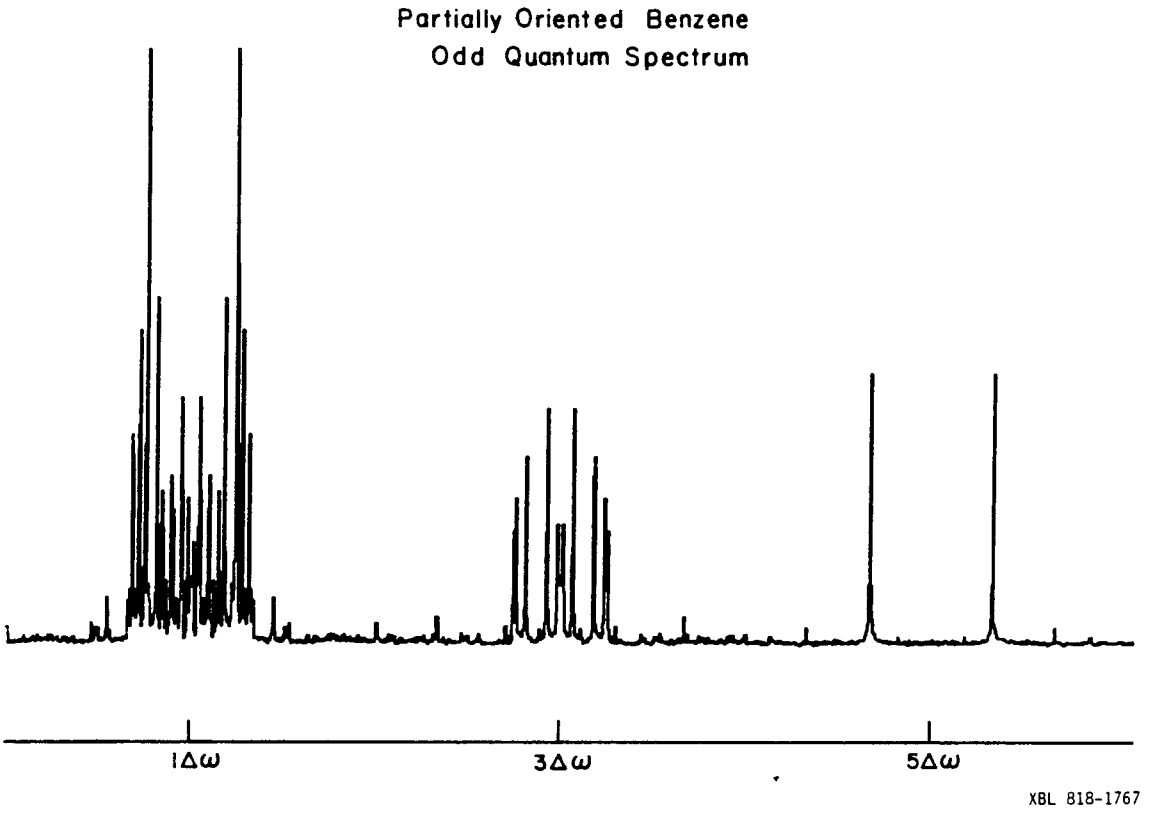

Figure 3.11

Benzene odd quantum experiment. The pulse sequence used prepared only odd quantum coherences. There is no intensity from zero, two, four, or six quantum transitions. The signal was polarized to one channel of the spectrometer detector and TPPI was used to separate orders.

$$\langle I_x\rangle(\omega) \equiv \langle I_x\rangle(\omega) + i\,\langle I_y\rangle(\omega)$$

$$\propto \sum_{jk} \{[\cos^2\Delta\omega\tau P^z_{jk}Q^z_{kj} + \sin^2\Delta\omega\tau P^y_{jk}Q^y_{kj} - \cos\Delta\omega\tau\sin\Delta\omega\tau(P^z_{jk}Q^y_{kj} + P^y_{jk}Q^z_{kj})]$$

$$+ i[\cos^2\Delta\omega\tau P^z_{jk}Q^y_{kj} - \sin^2\Delta\omega\tau P^y_{jk}Q^z_{kj} + \cos\Delta\omega\tau\sin\Delta\omega\tau(P^z_{jk}Q^z_{kj} - P^y_{jk}Q^y_{kj})]\} \tag{3.34}$$

The zy and yz cross terms have been included in Equation (3.34) for completeness but do not contribute to the signal. Thus, both channels contain signal from even and odd quantum coherences. For any arbitrary value of $\Delta\omega\tau$, the signal energy, $\propto|\langle I_+\rangle|^2$, will not necessarily be the same as pure even or odd quantum experiments yield but, when "ensemble" averaged over τ this energy partitions equally among even and odd orders, with the total the same as either of the pure coherence experiments. This method of removing even quantum selection was used to produce the spectrum of Figure 3.1.

Making use of Equation (3.26) we can also produce a spectrum with all orders by setting the second pulse in a standard preparation sequence to a $\frac{\pi}{4}$ pulse. The TPPI sequence is then (again, leaving out the π pulses which keep $\Delta\omega = 0$) $\frac{\pi}{2}\,\phi$, τ, $\frac{\pi}{4}\,\bar{\phi}$, $t_1/2$, π, $t_1/2$, $\frac{\pi}{4}\,y$, τ; sample. Now detection of signal from all coherences is possible. Once again, the τ dependence of intensities is different than the pure even or odd quantum experiments. An average of experiments for a sufficient range of values for τ will exhibit the total signal distributed among all orders.

We can combine two of the experiments above to both create all orders and simultaneously selectively polarize the signal into the quadrature channels. This is accomplished with the TPPI sequence $\frac{\pi}{2}\,\phi$, τ, $\frac{\pi}{4}\,\bar{\phi}$, $t_1/2$, π, $t_1/2$, $\frac{\pi}{2}\,y$, τ; sample, with $\Delta\omega = 0$. (In practice, π pulses are once again inserted in preparation and detection to ensure that $\Delta\omega = 0$). Now,

the two components of the complex signal become (with $\phi(t_1) = 0$ as usual)

$$\langle I_x \rangle = \frac{1}{\sqrt{2}} \sum_{jk} (P^z_{\frac{\pi}{4}} + P^x_{\frac{\pi}{4}})_{jk} (Q^z_{\frac{\pi}{2}})_{kj} \delta(\omega - \omega_{kj}) \tag{3.35a}$$

$$\langle I_y \rangle = \frac{1}{\sqrt{2}} \sum_{jk} (P^z_{\frac{\pi}{4}} + P^x_{\frac{\pi}{4}})_{jk} (Q^y_{\frac{\pi}{2}})_{kj} \delta(\omega - \omega_{kj}) \tag{3.35b}$$

The preparation sequence, as before, produces all orders of coherence. If all chemical shifts are equal, the detection matrices for $\langle I_x \rangle$ and $\langle I_y \rangle$ are solely even and odd quantum, respectively. Thus, the even quantum coherences will only be detectable in one channel and the odd quantum in the other, if the spectrometer reference phase is properly adjusted. In a spectrum averaged over values of τ, the intensity will once again be evenly distributed among even and odd channels, with the total the same as a pure even or odd quantum experiment.

Figure 3.12 shows the spectra that are obtained when the two channels of the above experiment are separately Fourier transformed. The spectrometer reference delay was carefully adjusted so that the two components of signal in Equation (3.35) correspond to the quadrature detection channels. The transform of one channel gives a spectrum with only even orders while the spectrum from the other channel exhibits only odd. This experiment combined even/odd selectivity with phase Fourier transform techniques. Two multiple quantum free induction decays with preparation sequences $\frac{\pi}{2}\ \phi,\ \tau,\ \frac{\pi}{4}\ \bar{\phi}$ and $\frac{\pi}{2}\ \bar{\phi},\ \tau,\ \frac{\pi}{4}\ \phi$ were acquired. The channels containing even orders were added and those containing odd were subtracted. In this way, small amounts of bleed-through signals were removed. The multiple quantum sampling rate (Δt_1) has been increased by about a factor of two without interference between orders.

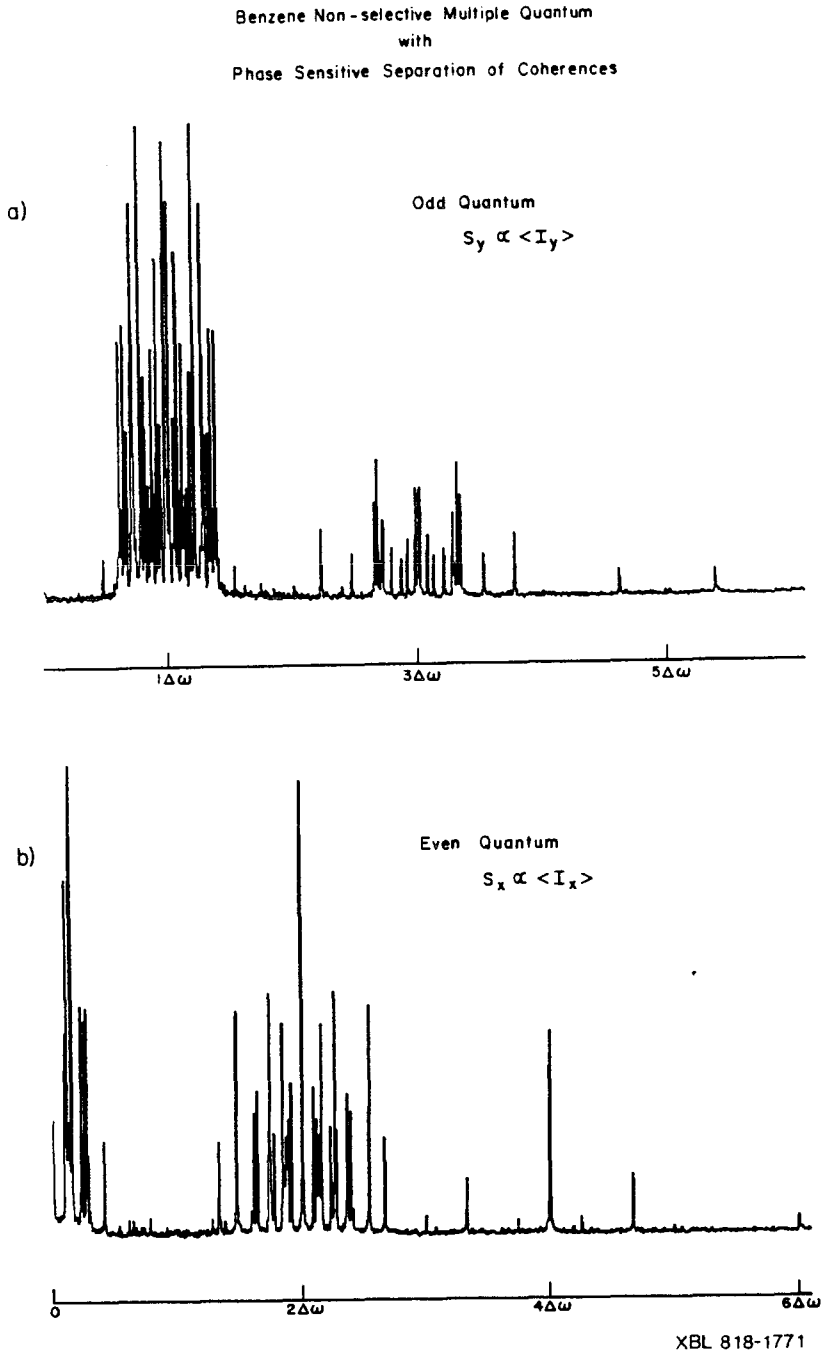

Figure 3.12

Benzene non-selective multiple quantum NMR spectra. This experiment combines the theoretical results leading to the spectra of Figures 3.10 and 3.11. All orders of coherence are prepared but odd orders are detected out of phase by 90° with respect to even orders. Fourier transformation of the y channel signal, S_y, leads to the odd quantum spectrum of a) while the even quantum orders are obtained from S_x in b).

3.4 The Effect of Chemical Shifts

Up till now, we have ignored the chemical shift Hamiltonian in our analysis of the multiple quantum density matrix. This proves adequate when considering molecules such as benzene in which all chemical shifts are equal. In this case, we can take the chemical shifts as zero by redefining the rotating frame frequency ω. Most molecules of interest will not have chemically equivalent spins and so for the density analysis matrix to be useful we must consider the effect of H_{cs}.

When coupled nuclei are chemically inequivalent, two effects will arise in a multiple quantum experiment. First, the preparation and detection matrices are different from the examples we have considered in the previous sections. The pure even or odd quantum preparation matrix is a consequence of the bilinear Hamiltonian $H_J + H_D$ when offset and chemical shift terms are absent. H_{cs} can be included in a straightforward manner in the expressions for $\underset{\approx}{P}$ and $\underset{\approx}{Q}$ [33]. The result is that even and odd coherences appear in the same preparation matrix. Thus chemical shifts remove selectivity of even or odd quantum orders in a manner similar to a resonance offset (the latter, however, is under control of the experimenter). As previously mentioned, if chemical shifts are small compared to the couplings then a preparation matrix may still contain predominantly even or odd quantum coherences.

As a second effect, the chemical shifts will cause multiple quantum coherences to evolve with relative frequency offsets during t_1. In principle, this evolution could remain unperturbed by r.f. pulses and chemical shifts measured in the final spectrum. A problem arises when TPPI is used to retain homogeneously broadened lines while removing inhomogeneous broadening with the formation of a spin echo. A π pulse

centered in the evolution period (Fig. 3.4c) is used to create the echo by refocusing linear terms in the Hamlitonian which commute with H_J and H_D. This pulse will also cause a transfer of coherence between multiple quantum transitions which produces additional lines in the final spectrum. The problem here is very similar to the measurement of relaxation parameters in strongly coupled isotropic systems [74]. The origin of additional lines and an estimation of their affect on spectral analysis is the subject of the remainder of this section.

Before going on to a determination of the signal when H_{cs} is present, we first review a simple AB spin-½ system as an example [77]. Normally, when chemical shifts are absent, the composite two-spin states may be classified as three triplets and one singlet under spin exchange. There are four allowed transitions among the triplet states all of which are degenerate when $H = H_J$ and D_{AB}, the dipolar coupling, is zero. When the Hamiltonian instead contains H_D and $J_{AB} = 0$, two degenerate transitions produce one line at $+(3/4)D$ and the other two appear at $-(3/4)D$. When a chemical shift is introduced, the $M = 0$ triplet and singlet states are mixed in the actual eigenstates. This partially removes the transition degeneracy to produce new lines in the spectrum. Whenever the coupling (J or D) is small compared to the shift difference $\delta = \frac{1}{2}(\sigma_A - \sigma_B)$ the Hamiltonian terms H_J and H_D can be truncated to that portion which commutes with H_{cs} and the spectrum is termed first order [79]. Figure 3.13 shows theoretical AB spectra when the total Hamiltonian is $H_{cs} + H_J$ or $H_{cs} + H_D$ and for varying ratios of the bilinear coupling to chemical shift difference. The left hand stick spectrum in part b represents the familiar isotropic first order spectrum in which $J << 2\delta$. In an anisotropically ordered sample such as a liquid crystal, the dipolar coupling D is usually much larger than 2δ. This situation is depicted on the

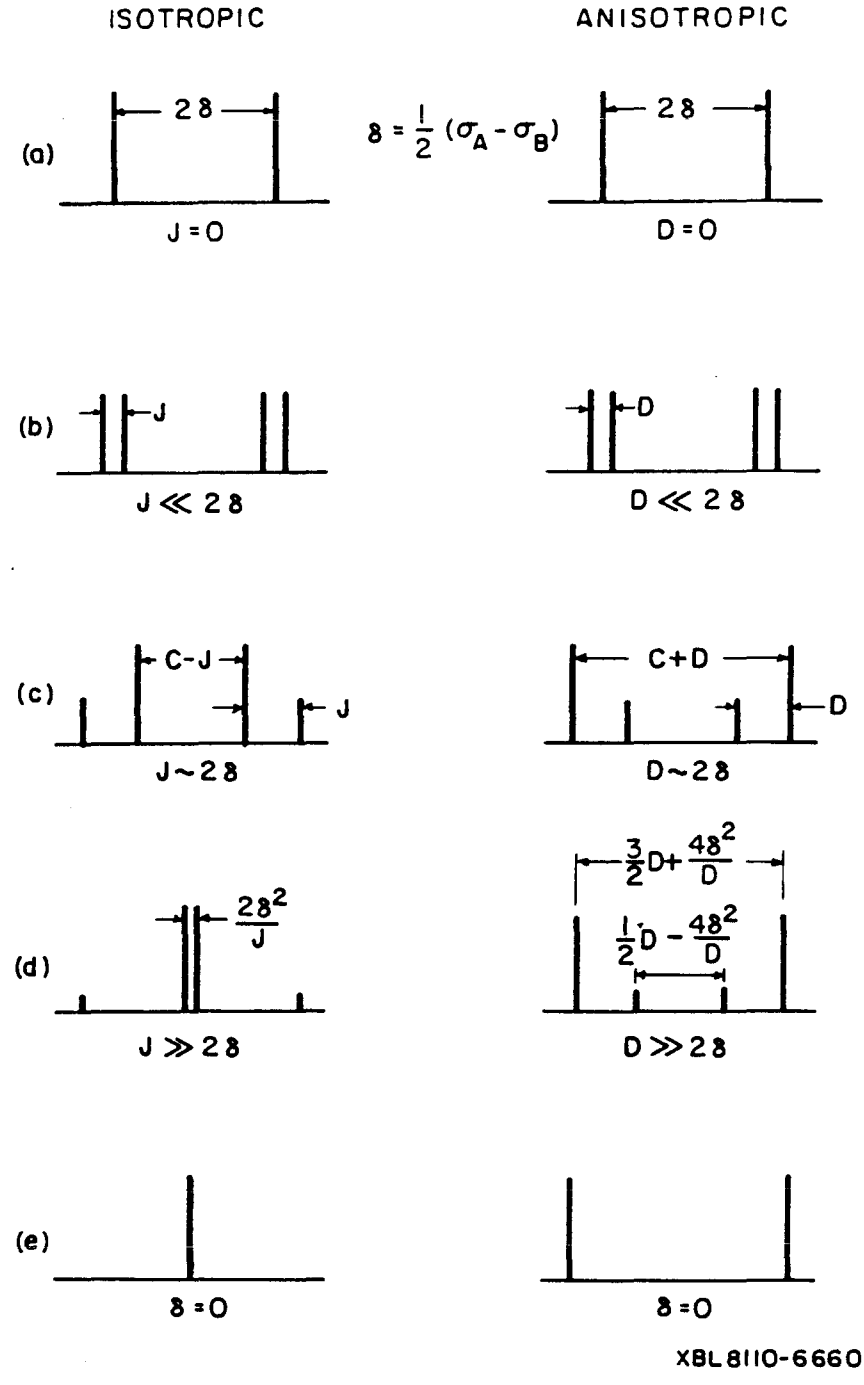

Figure 3.13

Theoretical stick spectra for an AB two spin-1/2 system. The case of an isotropic sample is shown at the left ($D_{AB} = 0$). The anisotropic case is on the right where, for convenience, $T_{AB} = 0$. Individual spectra in parts a through e are for varying ratios of the relevant coupling to $\delta = 1/2(\sigma_A - \sigma_B)$. The usual (first order) isotropic case is shown in b. The usual anisotropic spectrum is shown in d.

right hand side of part e. For purely structural analysis, we may wish to ignore or remove the chemical shift and reduce the number of parameters required to fit the spectrum. When chemical shifts differences are small compared to D_{ij}'s, we will see below that a single π pulse removes H_{cs} from single quantum and multiple quantum coherence evolution, to first order. Small additional lines appear in single quantum or multiple quantum spin echo spectra due to coherence transfers caused by the π pulse. It is our aim in this section to describe this phenomenon and estimate the magnitude of line shifts and intensities for simple spin systems. Analogies may then be drawn for more complicated systems.

We approach this problem by considering a simple two dimensional FT NMR experiment shown in Figure 3.14. This sequence is familiar in two dimensional spin echo spectroscopy [75] and is equivalent to that used to obtain the middle spectrum of Figure 2.1. The time domain is separated into two sections: t_1 is the usual evolution period after the density matrix is prepared by the first $\pi/2$ pulse and t_2 here corresponds to t_2' in Figure 3.3c. We wish to calculate the effect of the π pulse at $t_1/2$ when chemical shifts are present. The general two dimensional signal is then given by (assuming a y $\pi/2$ pulse and x π pulse)

$$\begin{aligned} S_x(t_1,t_2) \propto \mathrm{Tr}\{ & I_x \exp(-iH_3 t_2)\exp(-iH_2 t_1/2)\Pi \\ & \times \exp(-iH_1 t_1/2) I_x \exp(iH_1 t_1/2) \\ & \times \Pi^{\dagger} \exp(iH_2 t_1/2)\exp(iH_3 t_2)\}, \end{aligned} \tag{3.36}$$

where the propagator for a π x pulse is given by [75]

$$\Pi = \exp(+i\pi I_x) \tag{3.37a}$$

$$= (2i)^N \prod_{k=1}^{N} (I_x)_k. \tag{3.37b}$$

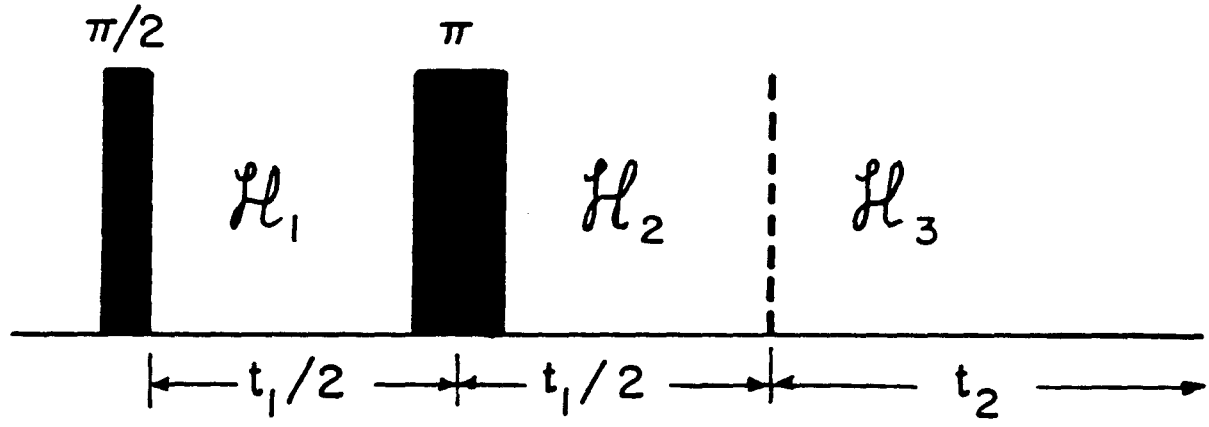

Figure 3.14

Pulse sequence used for two dimensional spin echo spectroscopy. The evolution period, t_1, contains a π pulse in its center. Hamiltonians in the three periods are denoted H_1, H_2, and H_3. In a strongly coupled system of chemically inequivalent spins, the π pulse will cause additional lines to appear in the ω_1 spectrum from coherence transfers.

Equation (3.37b) is obtained from an expansion of the exponent in Equation (3.37a) and using $I_x = \Sigma(I_x)_k$ where $(I_x)_k$ is an operator for a single nucleus [75]. We have assumed that the π pulse non-selectively excites all N nuclei.

For our purposes it is sufficient to consider only the case when all three Hamiltonians are equal: $H_1 = H_2 = H_3 \equiv H$. When H contains only the Zeeman offset and bilinear terms,

$$H = -\Delta\omega I_z + H_D + H_J \tag{3.38}$$

we may evaluate Equation (3.36) easily by inserting the identity operator

$$\Pi^\dagger\Pi = 1 \tag{3.39}$$

appropriately. The result is

$$\begin{aligned} S_x(t_1,t_2) \propto \mathrm{Tr}\{&I_x \exp(-iH_3t_2)\exp(-iHt_1/2) \\ &\times \exp(-iH^Rt_1/2)I_x\exp(iH^Rt_1/2) \\ &\times \exp(iHt_1/2)\exp(iH_3t_2)\} \end{aligned} \tag{3.40}$$

where

$$H^R \equiv \Pi H\Pi^\dagger = +\Delta\omega I_z + H_D + H_J \tag{3.41}$$

Bilinear terms in H are unaffected by the π pulse. Because all terms in H are mutually commuting, we find that the offset term is removed from the evolution, as expected in light of the discussion on TPPI.

The difficulties alluded to above arise when a chemical shift Hamiltonian is present and the total Hamiltonian is

$$H = -\Delta\omega I_z + \sum_i \sigma_i I_{zi} + H_D + H_J. \tag{3.42}$$

H_{cs} does not commute with H_D or H_J when not all σ_i are equal. When the sample is isotropic and J couplings small compared to relative chemical shift differences (a first order spectrum), H_J can be truncated to that part which commutes with H_{cs} and a π pulse will again remove chemical shift evolution from t_1. Molecules may sometimes contain large J couplings and when anisotropically ordered in a liquid crystal, D couplings are usually as large as or greater than chemical shift differences. The chemical shift Hamiltonian may be written as two terms

$$H_{cs} = \frac{1}{2(N-1)} \sum_{i<j} [(\sigma_i - \sigma_j)(I_{z_i} - I_{z_j}) + (\sigma_i + \sigma_j)(I_{z_i} + I_{z_j})] \quad (3.34a)$$

$$H_{cs} = \frac{1}{(N-1)} \sum_{i<j} [\delta_{ij}(I_{z_i} - I_{z_j}) + \tau_{ij}(I_{z_i} + I_{z_j})] \quad (3.43b)$$

where

$$\delta_{ij} \equiv \frac{1}{2} (\sigma_i - \sigma_j) \quad . \quad (3.44a)$$

$$\tau_{ij} \equiv \frac{1}{2} (\sigma_i + \sigma_j). \quad (3.44b)$$

As an example, the commutator of H_{cs} and H_D is evaluated as

$$[H_{cs}, H_D] = -\frac{1}{4} \sum_{i<j} \delta_{ij} D_{ij} (I_{+i} I_{-j} - I_{-i} I_{+j}). \quad (3.45)$$

As an approach to evaluating Equation (3.40) when chemical shifts are present, one may expand the exponentials containing H with the well-known Zassenhaus formula [3]

$$\exp(A+B) = \exp(A)\exp(B)\exp([A,B]/2)\exp([B,[A,B]]/3) + [A,[A,B]]/6)... \quad (3.46)$$

and use perturbation or average hamiltonian theory. However, products

such as $\delta_{ij}D_{ij}$, $\delta_{ij}^2 D_{ij}$, $D_{ij}^2\ \delta_{ij}$,..., etc. occur and the expansion will not converge unless $t_1/2$ is small. Multiple π pulses in t_1 may be used to scale or remove higher order terms in the average hamiltonian. [59] As another approach, Equation (3.40) may be evaluated directly in a basis set which diagonalizes the Hamiltonian. Evaluating the matrix elements directly yields [75]

$$S_x(t_1,t_2) \propto \sum_{ijk\ell} Z_{ijk\ell} \exp(i\omega_{ij}t_2) \exp[i(\omega_{ij} - \omega_{k\ell})t_1/2] \qquad (3.47)$$

where

$$Z_{ijk\ell} = (I_x)_{ij}(I_x)_{k\ell}(\Pi)_{jk}(\Pi^\dagger)_{\ell i}, \qquad (3.48)$$

and

$$\omega_{ij} = H_{ii} - H_{jj}.$$

The matrix elements of Π are easily evaluated. In the simple product basis set, from Equation (3.37b)

$$(\Pi)_{mn} = i^N \delta_{m(2^N-n+1)}, \qquad (3.49)$$

where the usual definition of the Kronecker delta is used:

$$\delta_{m(2^N-n+1)} = 1 \text{ for } m = 2^N-n+1$$
$$= 0 \text{ otherwise.}$$

In the eigenstate basis set, Π is given by

$$(S\Pi^\dagger S)_{ij} = \sum_{mn} S^\dagger_{im}\Pi_{mn}S_{nj} = (i^N) \sum_m S^*_{mi}S_{(2^N-m+1)j} \qquad (3.50)$$

where $\underset{\approx}{S}$ is the eigenvector matrix. Now, $\underset{\approx}{S}$ is block diagonalized by total Zeeman quantum number so that $\Delta M_{k\ell} \equiv M_k - M_\ell = 0$ for the element $S_{k\ell}$. We may then find the change in M for Π in this basis set as follows. The total Zeeman quantum number for state i is given by

$$M_i = k_i - \frac{N}{2} \tag{3.51}$$

where k_i is the number of spins "up" (i.e., number of α's). Thus, from Equation (3.50) and $\Delta M_{mi} = \Delta M_{(2^N-m+1)j} = 0$,

$$\Delta M_{ij} = M_i - M_{2^N-m+1}$$

$$= k_i - k_{2^N-m+1}$$

but

$$k_{2^N-n+1} = N - k_n,$$

so, finally

$$\Delta M_{ij} = 2k_i - N = 2M_i = -2M_j \tag{3.52}$$

for $(\Pi)_{ij}$ in system basis set. Equation (3.52) will prove useful when considering a TPPI multiple quantum experiment. It may be shown [75] that the intensity coefficients for the signal, Equation (3.48), obey the following index permutation properties.

$$Z_{ijk\ell} = Z_{k\ell ij} = Z^*_{\ell kji} = Z^*_{ji\ell k}. \tag{3.53}$$

Before going on to the multiple quantum case, we first consider an AB spin system as a simple example which illustrates the effect of the π

pulse in the two frequency domains. Two dimensional Fourier transformation of Equation (3.47) gives (neglecting relaxation effects)

$$S(\omega_1,\omega_2) \propto \sum_{ijk\ell} Z_{ijk\ell}\, \delta(\omega_2 - \omega_{ij})\delta(\omega_1 - \omega_{ijk\ell}) \qquad (3.54)$$

in which $\omega_{ijk\ell} = (\omega_{ij} - \omega_{k\ell})/2$. The ω_2 spectrum will contain the usually allowed single quantum spectrum with intensities different from those obtained from a single pulse experiment. The spectrum projected along the ω_1 axis will show new lines whose intensity depends on the extent to which simple product states are mixed by both the couplings and chemical shifts. A. Kumar, et al. have evaluated the intensities and frequencies for an AB system with J_{AB}, D_{AB} and δ_{AB} all non-zero [76]. The results are presented for convenience in Table 3.1. The quantities used in that table are defined as follows.

$$\delta_{AB} = \delta \equiv \frac{1}{2}(\sigma_A - \sigma_B)$$

$$\tau_{AB} = \tau \equiv \frac{1}{2}(\sigma_A + \sigma_B)$$

$$D = D_{AB}, J = J_{AB}$$

$$C = [(J - \tfrac{1}{2}D)^2 + 4\delta^2]^{\frac{1}{2}}$$

$$\cos 2\theta = 2\delta/C, \sin 2\theta = (J - \tfrac{1}{2}D)/C.$$

It should be noted that D_{AB} here is defined as twice the quantity used by Kumar, et al.

The intensities in Table 3.1 will vary depending on the ratio of couplings and of each coupling to the chemical shift difference, δ. For the case we are interested in - liquid crystal systems - D is usually

Table 3.1

Frequencies and Intensities for the 2D Spin Echo Spectrum of an AB System

	ω_2 (relative to τ)[a]	ω_1 (relative to 0)	Intensity
1.	$\frac{1}{2}(J+D) - \frac{1}{2}D$	$\frac{1}{2}(J+D) - \frac{1}{2}D$	$(1+\sin 2\theta)\sin 2\theta$
2.	$\frac{1}{2}(J+D) - \frac{1}{2}D$	$\frac{1}{2}(J+D)$	$\cos^2 2\theta$
3.	$\frac{1}{2}(J+D) + \frac{1}{2}D$	$\frac{1}{2}(J+D) + \frac{1}{2}C$	$-(1-\sin 2\theta)\sin 2\theta$
4.	$\frac{1}{2}(J+D) + \frac{1}{2}C$	$\frac{1}{2}(J+D)$	$\cos^2 2\theta$
5.	$-\frac{1}{2}(J+D) + \frac{1}{2}C$	$-\frac{1}{2}(J+D) + \frac{1}{2}D$	$(1+\sin 2\theta)\sin 2\theta$
6.	$-\frac{1}{2}(J+D) + \frac{1}{2}C$	$-\frac{1}{2}(J+D)$	$\cos^2 2\theta$
7.	$-\frac{1}{2}(J+D) - \frac{1}{2}C$	$-\frac{1}{2}(J+D) - \frac{1}{2}D$	$-(1-\sin 2\theta)\sin 2\theta$
8.	$-\frac{1}{2}(J+D) - \frac{1}{2}C$	$-\frac{1}{2}(J+D)$	$\cos^2 2\theta$

[a] $\tau = \frac{1}{2}(\sigma_A + \sigma_B)$.

much larger than both J and δ. Figure 3.15 shows the ω_1 spectra calculated from Table 3.1 for two extreme cases. The isotropic, first order case is characterized by D = 0 and J << 2δ and is shown in Figure 3.15a. The chemical shift is removed to first order and the major lines represent the symmetrical J splitting centered about $\omega_1 = 0$. Figure 3.15b gives the expected spectrum for the case when D >> 2δ and, for convenience, J has been taken as zero. Again, the chemical shift is removed to first order and the major lines appear where they would be expected in ω_2 had δ been rigorously zero. These lines are shifted from their position when $\delta = 0$ by approximately $\frac{2\delta^2}{D}$. The additional lines resulting from coherence transfers induced by the π pulse are found at $\pm \frac{1}{2}$ D and are of low intensity when D >> 2δ. The small lines at $\pm \frac{1}{4}$ D are from transitions which become allowed when the chemical shift mixes the triplet and singlet two-spin wavefunctions. They also appear in ω_2 centered about $\tau = \frac{1}{2}(\sigma_A + \sigma_B)$.

We now turn to the TPPI experiment of Figure 3.4c. We wish to determine the nature of any new lines which may result from a π pulse when the spin system has non-equivalent nuclei. For the experiments in this work, only the single point at $t_2' = 0$ ($\tau' = \tau$) is collected for each of t_1 and only a one dimensional transform is calculated. The signal may be written in a manner similar to Equation (3.47) and the transform with respect to t_1 calculated to give

$$S(\tau;\omega_1,\tau') \propto \sum_{ijk\ell} Z_{ijk\ell}\, \delta(\omega_1 - \omega_{ijk\ell}) \tag{3.55}$$

where

$$Z_{ijk\ell} = (P(\tau))_{ij}(Q(\tau'))_{k\ell}(\Pi)_{jk}(\Pi^{\dagger})_{\ell i} \tag{3.56}$$

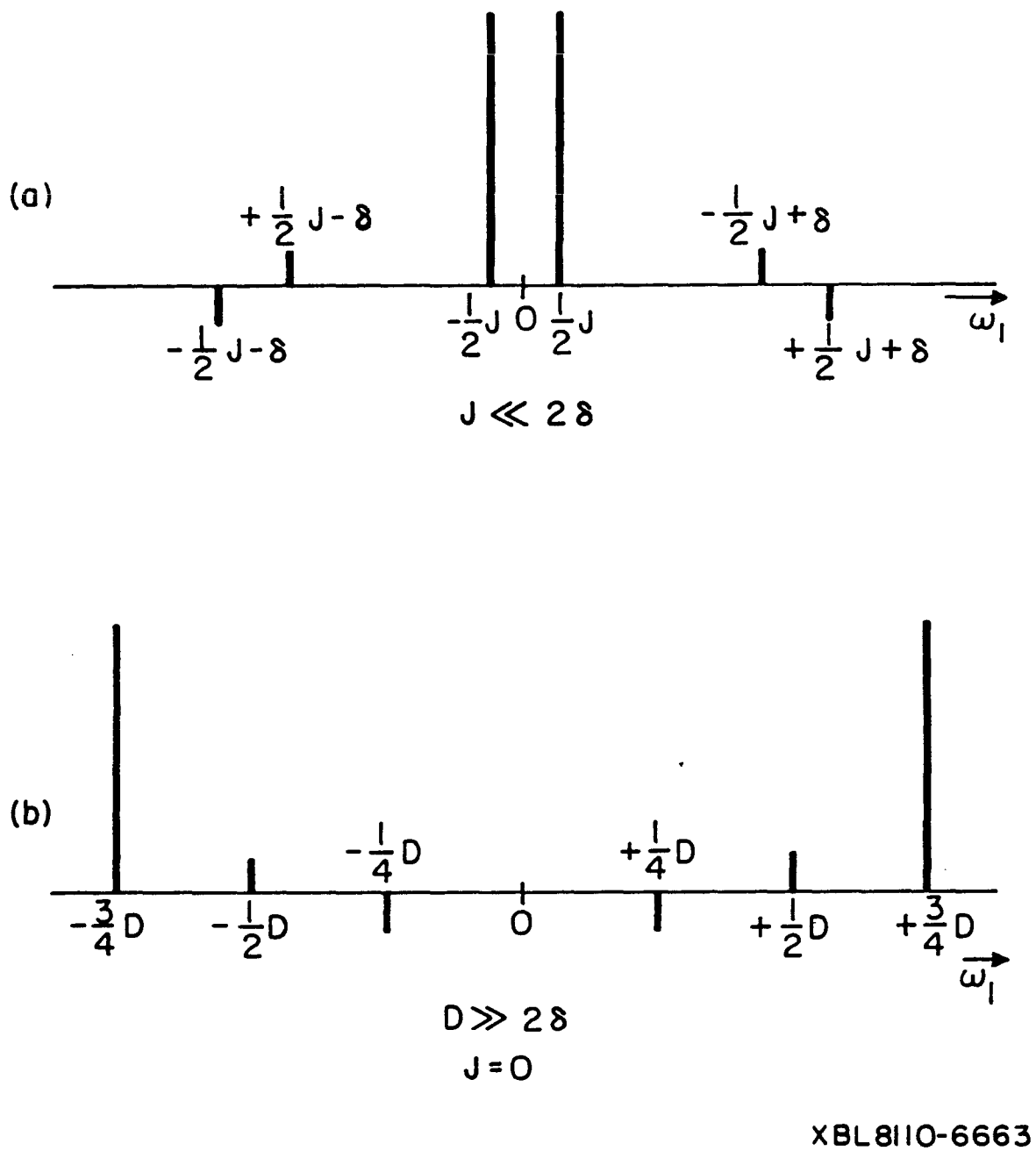

Figure 3.15

Spin echo spectra of an AB spin-1/2 system in the ω_1 direction from the two dimensional sequence of Figure 3.14. The chemical shift is removed to first order by the echo so that line positions are approximately those shown. a) The result for a first order isotropic system. b) A strongly coupled anisotropic system. T_{AB} has been set to zero for convenience.

As we have seen in previous sections, the preparation and detection matrices may contain all orders of coherence in a non-selective experiment, hence ΔM_{ij}, $\Delta M_{k\ell}$ = +N,+N-1,...,-N+1,-N. We may use Equation (3.52) to show that a π x pulse will only transfer coherence between pairs of states separated by the same ΔM. For $Z_{ijk\ell}$,

$$\Delta M_{ij} = \pm n, \qquad n = N, N-1, \ldots\ldots$$

$$\Delta M_{jk} = 2M_j,$$

$$\Delta M_{\ell i} = 2M_\ell = -2M_i,$$

hence

$$\Delta M_{k\ell} = \pm n.$$

Thus, the π pulse will not cause a transfer of coherence between multiple quantum orders. The intensity coefficient, $Z_{ijk\ell}$, is impossible to calculate without an exact knowledge of the system Hamiltonian. Even with model coupling constants and chemical shifts, $Z_{ijk\ell}$ may be difficult to estimate in a large spin system. A program has been written by J. Murdoch [67] capable of simulating the exact τ averaged intensities for a general system of up to eight spins when a π pulse is present during the evolution period. Model calculations using this program on AB, AB_2 and more complicated spin systems [78] indicate that relative intensities follow a pattern similar to the single quantum experiment described in this section. Additional lines caused by the π pulse are generally small when $2\bar{\delta}_{ij} << \bar{D}_{ij}$. Those transitions arising from states only weakly mixed by the chemical shift are, as expected, only weakly pumped by the non-selective two pulse preparation. Absolute intensities, averaged over

τ, relative to an identical spin system but with chemical shifts zero, are somewhat different.

3.5 Conclusion

In this chapter we have outlined the theory of the simplest, non-selective multiple quantum experiments including the time proportional phase incrementation technique for retaining homogeneous linewidths with complete separation of orders. We have indicated the nature of increased resolution in the higher orders and have also argued the limitations due to a Gaussian distribution of integrated intensities. A brief presentation of the inherent even quantum transition nature arising from a bilinear spin pumping operator in multiple quantum preparation and detection has also been given. Several methods for observing even, odd or all transitions are demonstrated with experimental examples in benzene. Finally, the extent of distortions in the spectrum caused by a π pulse in the evolution period of a TPPI sequence when chemical shift differences are present has been discussed. Selective preparation and detection for enhanced signal intensities in high quantum spectra have not been discussed.

Chapter 4

Experimental Studies of Molecules with Internal Motion: Biphenyl

4.1 Introduction

We have stated several times so far that the aim of acquiring NMR spectra of oriented molecules in a liquid crystal phase is to learn something about molecular structure, conformational statistics, and anisotropic ordering. In Chapter 1 we saw that part of this information comes from couplings in the dipolar Hamiltonian. The object is then to determine D_{ij}'s from frequency measurements taken from the spectrum. If the molecule is rigid (or vibrational effects can be accounted for) and contains a small number of coupled spins or sufficiently high symmetry, this task may be simple. Analytical expressions may exist relating transition frequencies to parameters of interest and line assignments may possibly be made unambiguously. We have seen, however, that as the number of spins is increased, or when the molecule exhibits less simplifying symmetry elements, the single quantum spectrum rapidly becomes intractable. Each transition frequency is a complicated linear combination of parameters of the Hamiltonian and transition density becomes so high that individual lines are no longer resolved. Even if sufficient independent and resolved lines exist to determine the problem, the sheer number of possible initial line assignments which each produce an acceptable fit, may make an analysis difficult.

The approach of multiple quantum NMR then appears to offer a significant advantage by producing high order subspectra which contain considerably fewer transitions then the single quantum spectrum. Often, these transition frequencies are simply related to dipolar couplings

making the whole process of analysis more straightforward. When there are few well resolved transitions, only a few line assignment possibilities will need to be considered.

Once couplings are uniquely determined from either a single quantum or multiple quantum spectrum, it remains to interpret these in terms of one or several possible molecular models. For dipolar couplings, the model must include both the geometric parameters and order parameters. If it is assumed that the molecule is completely rigid, then a classical model of geometry will allow us to interpret the results in terms of bond angles and lengths. Vibrations and perhaps other motions will always be present, however, and strictly speaking, must be included in our model. We will, in general, distinguish between two types of motion, although this does not imply they should always be treated independently. The first includes small amplitude vibrations which are usually treated as harmonic and cause slight corrections to each D_{ij}. Harmonic vibrations are handled through a normal mode analysis which has been developed for the case of anisotropically ordered molecules by Lucas [87]. The theoretical and computational approaches have been reviewed by Sykora, et al. [88].

The second type of internal motion which we identify is so-called "large amplitude" vibrations or torsions. Examples have already been cited and Emsley and Lindon devote an entire chapter to the subject [18]. Included in this are free rotor-like motions of a subunit of a large molecule, a molecule which jumps or tunnels between conformations, and pseudo-rotation such as that occurring in many cyclic compounds. This chapter reports results for a simple case of large amplitude internal motion which occurs in the biphenyl moiety. The phenyl rings are able to

rotate about the axis which contains the C-C inter-ring linkage. The angle between two planes, each of which is defined by the carbon atoms of one ring, is referred to as the dihedral angle and is denoted as ϕ. If the potential contains a minimum, the angle at that minimum is defined as ϕ_m. Biphenyl was chosen because it represents a very simple type of motion in a potential which is periodic and one dimensional. Molecules studied in this work which contain the biphenyl unit are shown in Figure 4.1. The biphenyls para-substituted (4, 4' locations) with halogen or deuterium atoms were studied as solutes dissolved in a liquid crystal. The cyano and alkyl chain substituted biphenyl, 4-cyano-4'-n-pentyl-d_{11}-biphenyl (5CB-d_{11}) is a pure liquid crystal which was studied in its nematic phase. We also present the single quantum deuterium spectrum of the alkyl chain of this molecule in the following sections.

4.1.1 Background: Structural Studies of Biphenyls

The biphenyl unit is quite prevalent in organic molecules and naturally serves as a choice for theoretical and experimental studies. Theoretical work has centered on the use of molecular orbital calculations to model the internal geometry and potential as a function of dihedral angle [80-84]. Early experiments were conducted on X-ray analysis of solid biphenyl [86] and electron diffraction measurements in the gas phase [85]. Unsubstituted biphenyl is believed to be planar in the solid and to occur with a dihedral angle of about 42° in the gas phase. Theoretical calculations confirm these measurements and attempt to model the potential to rotation of the rings by the inclusion of several contributions. These contributions are either of two types: conjugation and non-bonded interactions. Conjugation includes all electronic effects which tend to bring the ring planes together and reduce ϕ. Non-bonded

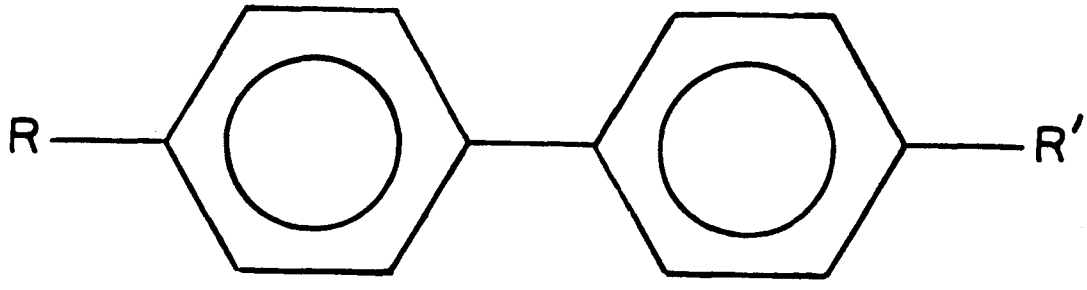

$R = R' = Cl, Br, D, H$

$R = C_5D_{11}, \quad R' = CN$

XBL 8110-6661

Figure 4.1

Molecules studied by single and multiple quantum NMR. The symmetrically substituted biphenyls (4,4'-dichloro-,4,4'-dibromo-, and 4,4'-d_2-biphenyl) and unsubstituted biphenyl were studied as salutes in liquid crystal solutions. The alkyl cyanobiphenyl, 5CB-d_{11}, is a pure liquid crystal studied in the nematic phase.

interactions include steric hindrance, bond deformation, and intermolecular interactions which may raise the total potential at either $\phi = 0$ or $\phi = 90°$. The combination of these two general types of interactions make up the total potential which determines the preferred dihedral angle ϕ_m. Thus, it is reasonable that biphenyl should be planar in the solid where intermolecular interactions dominate, and at some angle $\leq 90°$ when they are absent, as in the gas phase. The theoretical form of the potential varies depending on whether bond deformations, which are a function of ϕ are allowed [81-83].

Although the value of ϕ at the potential minimum arrived at by several authors closely agree, relative heights of the barrier to rotation at $\phi = 0$ and $\phi = 90°$ vary depending on the calculation approach. Dewar, et al. [83] and Fischer-Hjalmars [81] calculate a slightly lower barrier for ϕ at 90° while Casalone, et al. [82], who include bond deformation in their model, find that the barrier is lower at $\phi = 0°$. The magnitude of both barriers, at $\phi = 0°$ and 90°, generally falls between 2 and 5 kcal/mole.

Since these early investigations, biphenyl has been studied in a number of varied forms and conditions. Recent studies include Penning ionization from pure biphenyl adsorbed onto a clean metal surface [89] and a wealth of magnetic resonance results [95-99] on substituted biphenyls. A brief review of the current magnetic resonance results for halogenated biphenyls in liquid crystals is given in the next section.

4.1.2 Substituted Biphenyls in Liquid Crystals

The literature contains many examples of molecules dissolved in liquid crystals which exhibit a simple 4-fold periodic potential characterized by a single "dihedral" angle. Examples include studies of the

bipyridyls and bithiophenes [90-94] and substituted biphenyls [95-99]. The bipyridyl [93] and bipyrimidine [94] studies are quite similar to the biphenyl problem. For 2,2'-bithiophene, one can imagine an internal rotational barrier sufficiently large to cause slow interconversion between true cis and trans isomers. In the models used to analyze the spectra, an attempt is made to deduce population ratios for these two isomers [91,92]. The problem is somewhat underdetermined unless enough assumptions are made to determine the ratio.

There have been a number of studies published on biphenyl solutes in liquid crystals. These all involve some substitution; pure ($C_{12}H_{10}$) biphenyl spectra have not been published. Substitution patterns are almost invariably symmetric with respect to the C_2 operation along the para axis linking the two phenyl rings. This choice of symmetry is convenient because, as we shall show, only three of the possible five independent order parameters are necessary in the analysis. Further symmetry reduces this number to two.

In all of the biphenyl studies, a value for the dihedral angle is found. This result varies depending on the nature of the substitutions and method of analysis. For highly substituted molecules, there are not enough couplings to simultaneously determine all order parameters, bond lengths and angles, and all terms in the inter-ring potential. Thus, it is desirable to limit the number of substituents, an approach which, of course, increases the number of single quantum transitions. The least substituted molecules studied have two para-substituents such as in the case of 4,4'-dichlorobiphenyl [96]. This pattern of substitution does not reduce the sensitivity in the spectrum to the dihedral angle since a coupling involving nuclei in the 4,4' (para) positions will not depend on

ϕ. Perhaps the most extensive study of the internal rotational degree of freedom has been carried out by Field, et al. [97,98]. This group has studied the dihedral angle obtained from NMR measurements in liquid crystals as a function of substituents which are ortho to the inter-ring linkage. Although many assumptions are made, a clear correlation is demonstrated between ϕ and the van der Waals radii of these substituents suggesting that the major contribution in the non-bonded interaction portion of the potential is from steric hindrance.

The primary example of a biphenyl group studied in this work is that found in 5CB-d_{11} (see Fig. 4.1), which is a pure nematic liquid crystal. The cyanobiphenyls have received considerable attention in a variety of studies which are briefly reviewed below.

4.1.3 Alkylcyanobiphenyls

The homologous series of 4-cyano-4'-n-alkyl-biphenyls have been studied by a number of spectroscopic techniques including X-ray [100], deuterium [101-102] and proton [103,104] NMR, infrared [105] and, more recently, dielectric relaxation [106,107]. This series contains alkyl chains ranging from butyl to octyl and exhibits many of the non-chiral, thermotropic mesophases among its members. The shorter length molecules (e.g., 5CB) exhibit only a nematic phase between crystalline and isotropic, while longer chain members of the series can be induced to form smectic phases. For practical applications, the alkyl cyanobiphenyls have a remarkable stability and high dielectric anisotropy making some of them ideal for electric field display devices.

In large part due to the cyano group, each molecule has a large dipole moment. The X-ray studies [100] have indicated an antiparallel head-to-tail arrangement in the nematic and isotropic phases of

pentylcyanobiphenyl (5CB) and heptylcyanobiphenyl (7CB). In this arrangement, molecular dipole moments alternate in direction between molecules over a large domain, thus giving the most energetically favorable situation. It has been suggested from the results for 5CB that local end-to-end structure between opposing molecules occurs with a spacing of 1.4 times the molecular length [100].

Deuterium NMR studies of 5CB, 7CB and 8CB have focussed on the ordering of the deuterated alkyl chain. Results indicate a variety of conformational possibilities exist for the chain. In this Chapter, the deuterium spectrum of the chain of 5CB-d_{11} will be compared with previous studies. The proton single quantum spectrum of the unsubstituted nematic liquid crystal might be expected to be completely unresolved because of the large number of spins and high degree of ordering. As a result, proton spectra have only been analyzed for 5CB [103,104] when one section of the molecule is substituted with deuterium. An analysis of the single quantum, deuterium decoupled proton spectrum of 4-cyano-4'-pentyl-d_{11}-2',3',5',6'-d_4-biphenyl [103] yielded a partial estimate of the order tensor elements for the aromatic core and the structure of the cyano substituted ring. A multiple quantum NMR study by Sinton and Pines [104] has yielded a preliminary analysis of the biphenyl group structure. The experimental results of the latter work and a more thorough analysis of the spectrum will be presented in this chapter.

To gain an appreciation of the complexity present in the proton spin system of 5CB-d_{11}, consider Figure 4.2. This figure shows the single quantum proton spectrum of the liquid crystal in the nematic phase and under conditions of moderate field homogeneity. With the degree of

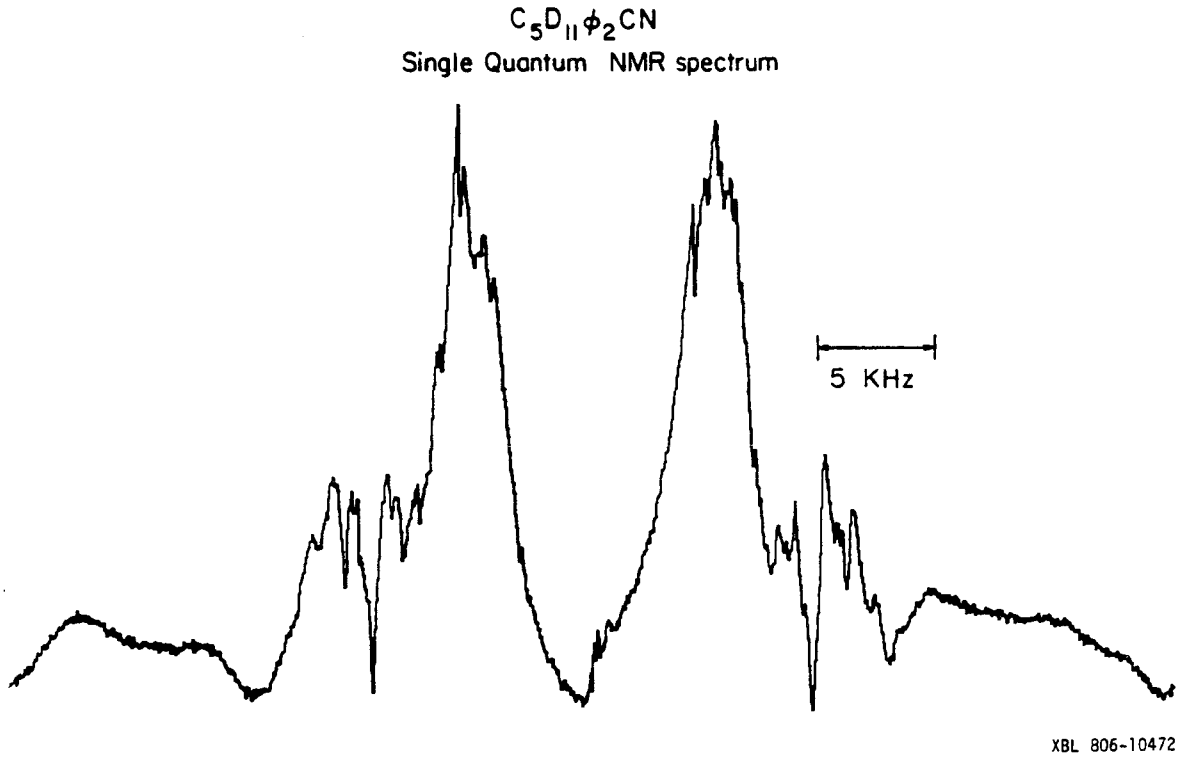

Figure 4.2

Single quantum proton spectrum of 5CB-d_{11}. Double quantum deuterium decoupling was used to remove couplings to the alkyl deuterons. The separately measured inhomogeneous proton H_2O line width was ~.05 ppm. Temperature of the sample was regulated at 26.0°C. The total width shown is 50 kHz.

resolution in this spectrum, very little useful structure exists. Although a higher resolution experiment, such as a two dimensional spin echo experiment, should yield some improvement, the spectrum would remain difficult to analyze. Because of slow molecular fluctuations and the high degree of ordering in the room temperature nematic phase, each transition is fairly broad ($\gtrsim$200 Hz). Symmetry considerations alone predict over 3000 allowed single quantum transitions in a band width of ~50 kHz. (Of course, the actual number of observable transitions will be less due to degeneracies and to low intensity for some.) The single quantum spectrum obviously contains many overlapping transitions.

The proton multiple quantum spectrum of the same liquid crystal is shown in Figure 4.3. The reduction in transition density with increasing multiple quantum order, as for benzene in Chapter 3, is apparent. All orders are present with sufficient signal-to-noise to allow an analysis. Each order is contained in a width about that of the single quantum spectrum of Figure 4.2 for a total width shown of 500 kHz. Before going on to detail an analysis of this spectrum, in the next section we will describe the symmetry properties of a biphenyl group and indicate how the high order multiple quantum transitions reflect this symmetry.

4.2 Biphenyl Symmetry Models

In determining the point group of para-substituted biphenyl, four basic models must be considered. 1) Free rotation of the rings where the potential as a function of ϕ is a constant. 2) Only one static conformation with angle ϕ between the rings is allowed, or the molecule interconverts between conformations with angles $\pm\phi$. This model may be considered for the cases when the two rings are either equivalent (identical substituents and geometries) or inequivalent. 3) The rings are

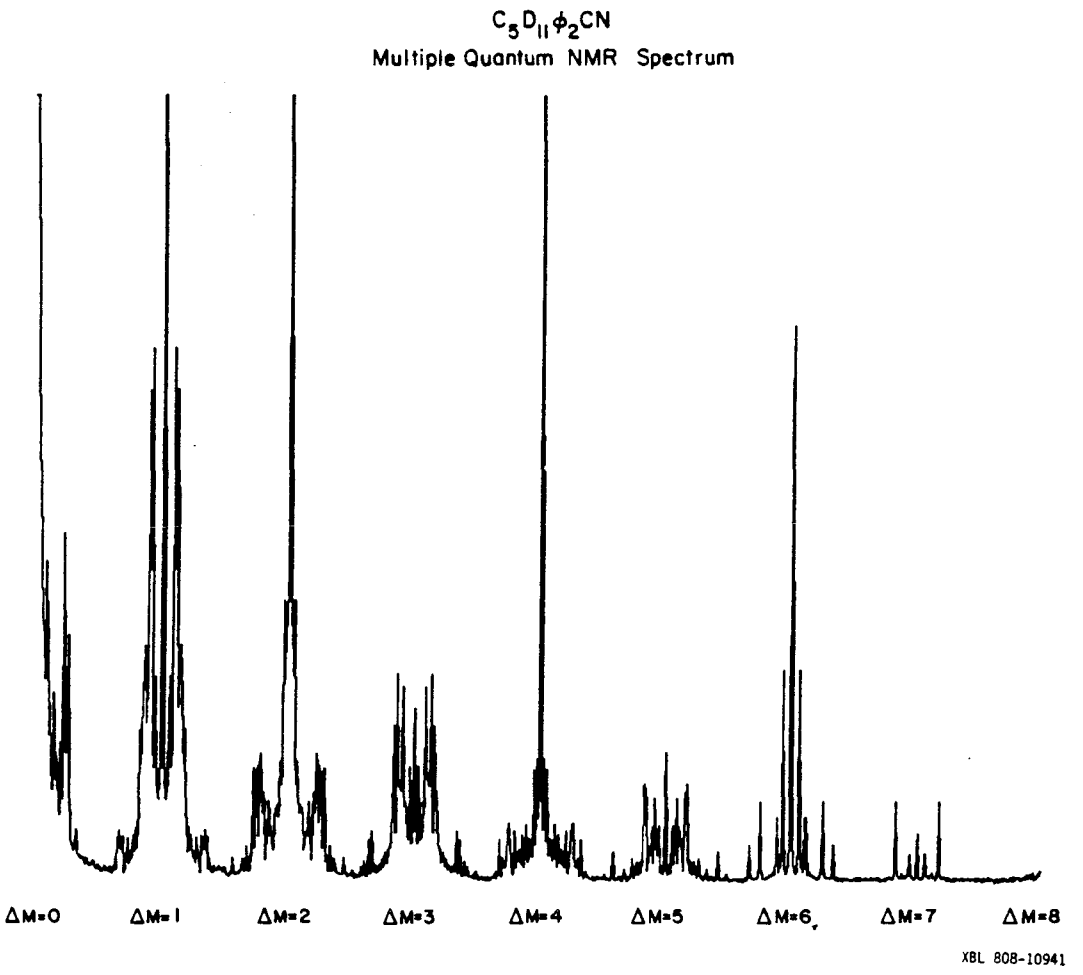

Figure 4.3

Proton multiple quantum NMR spectrum of 5CB-d_{11}. The multiple quantum subspectra are separated according to the order of the transitions. The change in magnetic quantum number, ΔM, is indicated beneath the subspectra. Only one half of the symmetric zero and eight quantum regions are shown. The full width shown in 500 kHz. No deuterium decoupling irradiation was used.

entirely equivalent and the molecule interconverts between the four equally probable conformations at dihedral angles $\pm\phi$ and $\pi \pm \phi$ (see Fig. 4.4). 4) The rings are inequivalent but the four conformations of case 3) are present. Each of these models may be modified in the manner in which dipolar couplings are averaged over internal motions. Harmonic vibrational corrections may be added by a normal mode analysis and couplings may also be averaged over the torsional motion about ϕ.

The first model - that of free rotation - is generally ruled out by experimental results. The permutation group of the proton spins for a single conformation of a para-substituted biphenyl with equivalent rings is isomorphous with D_2. Free rotation effectively increases the symmetry to D_{2h}. The resulting reduction in allowed transitions is not commensurate with experimental results [94]. This appears reasonable since a finite barrier is predicted by theory. This barrier, however, is not expected to be large enough as ϕ goes through 90° to prevent interconversion to the other two symmetry related conformations. All four conformations are depicted in Figure 4.4. If the biphenyl group changes between these four conformations fast compared to the inverse of the couplings which are a function of ϕ - a reasonable assumption again considering the magnitude of the barriers - then this motion will effectively create two new reflection planes. In all examples found in the literature to date, only models which include an average of all four symmetry related conformations of Figure 4.4 adequately fit the oriented NMR data. Thus, we will focus on models 3) and 4) above. The difference between these concerns whether the phenyl rings are equivalent or not. If they are, implying that the para-substituents are either the same or do not perturb ring structure or motion differently, then there must exist a

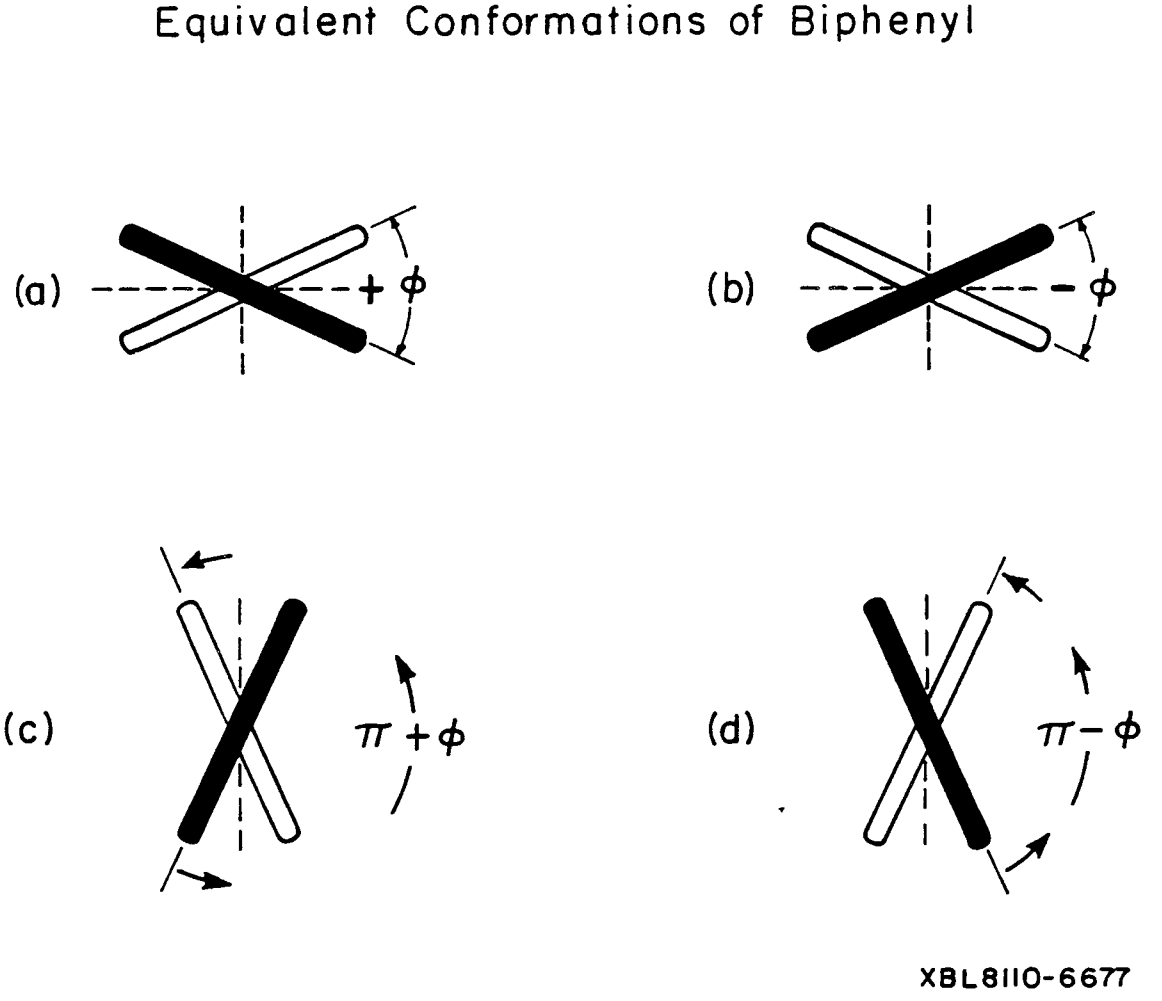

Figure 4.4

Four equivalent conformations of biphenyl for dihedral angles $\pm\phi$ and $\pi \pm \phi$. The molecule is assumed to change between these conformations at a rate which is fast compared to the inverse of couplings which are a function of ϕ. This motion creates two effective mirror planes perpendicular to the page and containing the dotted lines.

symmetry element which exchanges them. Otherwise there will be fewer irreducible representations in the molecular point group.

These two possible symmetries are shown in Figure 4.5 along with the numbering of protons which will be adopted for the rest of this chapter and coordinate systems chosen for calculating the D_{ij}'s. The higher symmetry case, in which para-substituents are the same (X) and the rings are equivalent, is shown on the left. When the rings are inequivalent as in the case of different substituents (X,Y), the right hand side of Figure 4.5 is applicable.

4.2.1 Equivalent Rings: D_4 Point Group

When determining the point group applicable to a spin Hamiltonian, it is the permutation symmetry of nuclear spins which defines the group symmetry elements [34]. The permutation symmetry group of a symmetrically para-substituted biphenyl (exchanging between the four conformations of Figure 4.4) is isomorphous with the D_4 point group. The character table for this group, along with a definition of the symmetry elements is given in Table 4.1. Each ring has an effective C_2 axis of its own (flip ring about molecular long axis without flipping other ring) due to equal conformational probabilities. These are denoted C_2^A and C_2^B in Table 4.1. In addition, both rings may simultaneously flip - a C_2 operation for the whole molecule, C_2^{AB}. For the space coordinates, there are two C_2 axes perpendicular to the axis containing the inter-ring linkage. These operations combined with the ring C_2 elements result in spin symmetry elements denoted as R. This element means effectively "exchange the rings". Two elements in one class, R_2^A and R_2^B, refer to operation by C_2^A or C_2^B before the exchange, respectively. The other class (R_2^{AB}, R) is simply an exchange of rings.

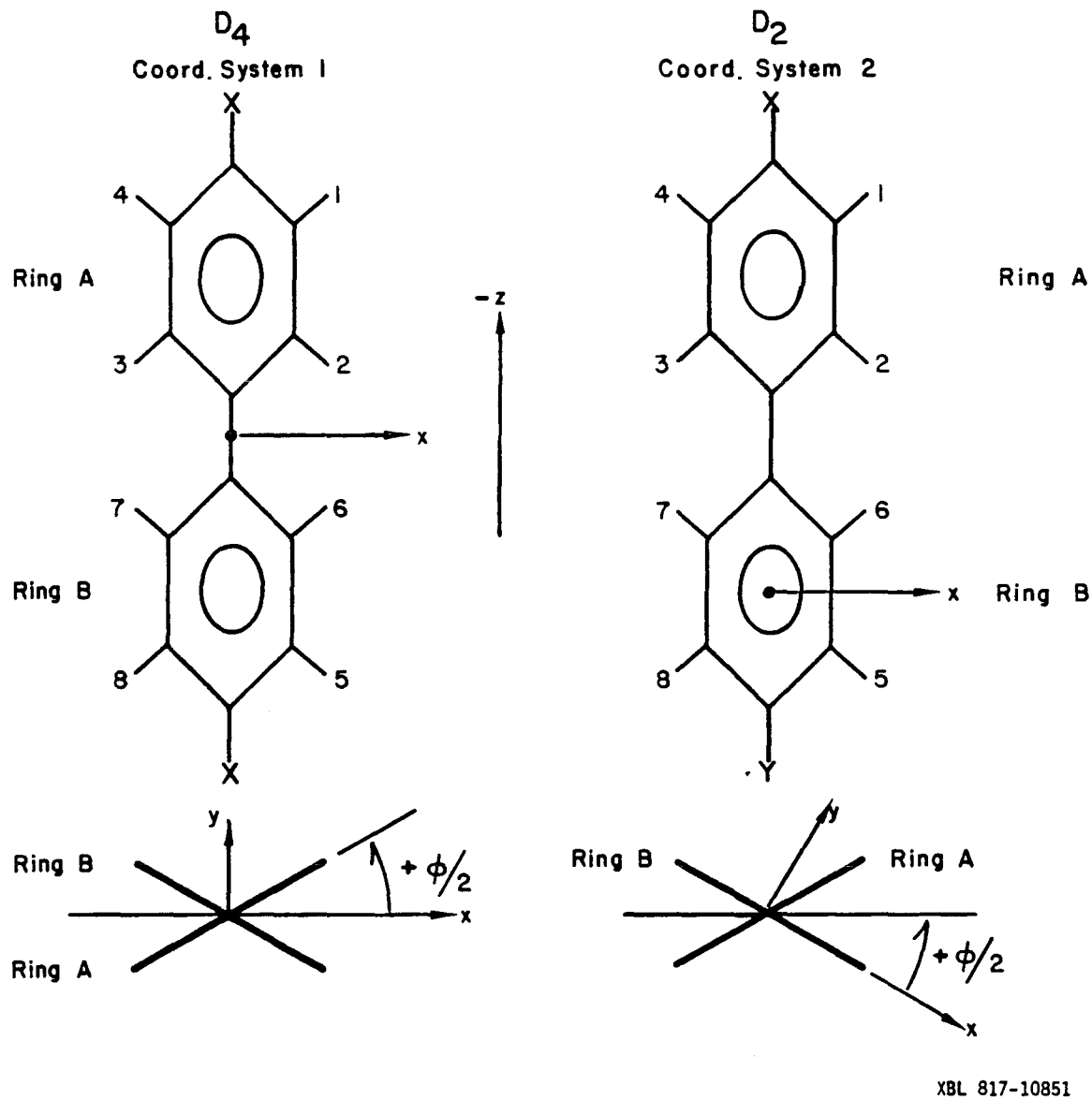

Figure 4.5

Two possible symmetries for a para-substituted biphenyl. On the left, the para-substituents are equivalent (X) and the effective average permutation symmetry for the numbered protons is D_4. With different substituents (X and Y), the point group is D_2. Coordinate system #1 for D_4 lies between the rings with x and y axes bisecting the inter-ring angles. Coordinate system #2 for D_2 lies in ring B with the x axis in the ring plane for all ϕ. The projections defining the direction of positive ϕ are seen looking down the z axis onto the xy plane.

Table 4.1

D_4 Point Group Character Table for Symmetry Elements of Symmetrically Para-substituted Biphenyl

a)	E	$2C_4$	$C_2 = C_4^2$	$2C_2'$	$2C_2''$
b)	E	(R_2^A, R_2^B)	C_2^{AB}	(R, R_2^{AB})	(C_2^A, C_2^B)
c)	(12345678)	(56784321) (87651234)	(43218765)	(56781234) (87654321)	(43215678) (12348765)
A_1	1	1	1	1	1
A_2	1	1	1	-1	-1
B_1	1	-1	1	1	-1
B_2	1	-1	1	-1	1
E	2	0	-2	0	0

a) D_4 symmetry elements for space variables for an object of this point group.

b) D_4 permutation elements for symmetric para-substituted biphenyl (see text).

c) Permutation elements according to numbering of Figure 4.5.

The resulting energy level diagram for D_4 symmetry is shown in Figure 4.6. From this, the predicted number of transitions for each multiple quantum order is given in Table 4.2. These predictions take into account the double degeneracy of the E symmetry transitions but not of other possible degeneracies for the lower orders. It has been shown that the number of symmetry allowed transitions in the high order spectra may be predicted without a complete reduction of the entire Hamiltonian [33]. Since the Hamiltonian matrix only has nonzero elements H_{ik} for $\Delta M_{ik} = 0$ (i.e., it is block diagonal by Zeeman quantum number), we only have to consider blocks for the highest value of M when predicting the high order transitions. In particular, the N-1 transitions only connect totally symmetric (A_1) states. A familiar property of this representation is that the "symmetrized" basis states (linear combinations of product states) are invariant to all group symmetry operations. We can write down the A_1 symmetrized states for the $M = \pm(\frac{N}{2} - 1)$ manifold easily by noting that they must be linear combinations of those simple product states which convert into one another under group operations. The $M = \pm(\frac{N}{2} - 1)$ simple product states are those for which all but one of the spins are in a single orientation (α or β for spins-1/2). By identifying the number of these states which are not related by any of the symmetry operations, we can determine dimensions of the A_1, $M = \pm(\frac{N}{2} - 1)$ manifolds.

Returning to the specific example of a D_4 symmetry biphenyl group, we see that there are only two proton sites, those ortho and meta to the substituents, which cannot be exchanged by any of the operations in the character table (Table 4.1). We immediately predict that there will be only four symmetry allowed transitions in the seven quantum spectrum, consisting of two doublets. If we ignore chemical shifts (they are

Symmetrically Para-substituted Biphenyl
D_4 Point Group Energy Level Diagram

M	A_1	A_2	B_1	B_2	E
-4	1				
-3	2			2	2X2
-2	7	1	3	5	2X6
-1	10	4	4	10	2X14
0	15	5	7	11	2X16
1	10	4	4	10	2X14
2	7	1	3	5	2X6
3	2			2	2X2
4	1				

XBL 8110-7191

Figure 4.6

Spin energy level diagram for a symmetrically para-substituted biphenyl (D_4 symmetry). The six irreducible representations are given at the top. The E representation is doubly degenerate. Values for the total magnetic quantum number, M, are shown along the left hand side. Numbers inside the table are dimensions of Zeeman submatrices occurring in each representation.

Table 4.2

Predicted Number of Transitions in the Multiple Quantum Spectrum of a Symmetrically Para-substituted Biphenyl

n-Quantum Order	# Transitions[a]	Symmetry
8	1	A_1
7	4	A_1 (2 doublets)
6	14	A_1 (7 doublets)
	4	A_1 (triplet)
	4	B_2 (triplet)
	2 x 4	E (triplet)
	21 total unique transitions	
5	68	A_1 (34 doublets)
	20	B_2 (10 doublets)
	2 x 24	E (12 doublets)
	92 total unique transitions	
4	286 total	
3	628 total	
2	1142 total	
1	1580 total	

[a] For 8, 7, 6, 5 quantum a breakdown by symmetry is given and only the number of unique transitions given in totals (ignoring accidental degeneracies). The double degeneracy of the E representation is not counted in any of the totals.

removed by a TPPI π pulse) then each doublet will appear centered about $7\Delta\omega$ in a non-selective spectrum of all orders. We may also write down the $M = \pm 3$ A_1 symmetrized states. They are schematically represented in Figure 4.7. One consists of a combination of simple product states with the unique spin ortho to substituents and the other contains the meta unique spin.

One can proceed in this manner for the N-2 quantum spectrum by identifying unique combinations of two "labeled" spins. Now representations other than A_1 must be considered. Counting schemes have been proposed [33] which unify this approach and are applicable to a variety of cases when molecules exhibit internal motion. For the lower order spectra, Hamiltonian submatrix dimensions are large and this approach becomes difficult. However, a rigorous group theory application will allow transition number predictions to be made.

4.2.2 Inequivalent Rings: D_2 Point Group

The character table defining symmetry elements for the case when the biphenyl rings are inequivalent (right side of Fig. 4.5) is given in Table 4.3. The permutation elements are similar to the D_4 case except for the lack of a ring exchange (R) operation. The resulting energy level diagram is shown in Figure 4.8. Numbers of transitions may be predicted in the manner of the last section with the results given in Table 4.4. There are now four unique proton sites and twice as many high order transitions compared with the D_4 symmetry model.

From this analysis, the symmetry of the molecule should be evident from the seven and six quantum spectra. If we see more than two doublets in the seven quantum spectrum, we know immediately that the rings cannot be equivalent. If more than four doublets should appear then some

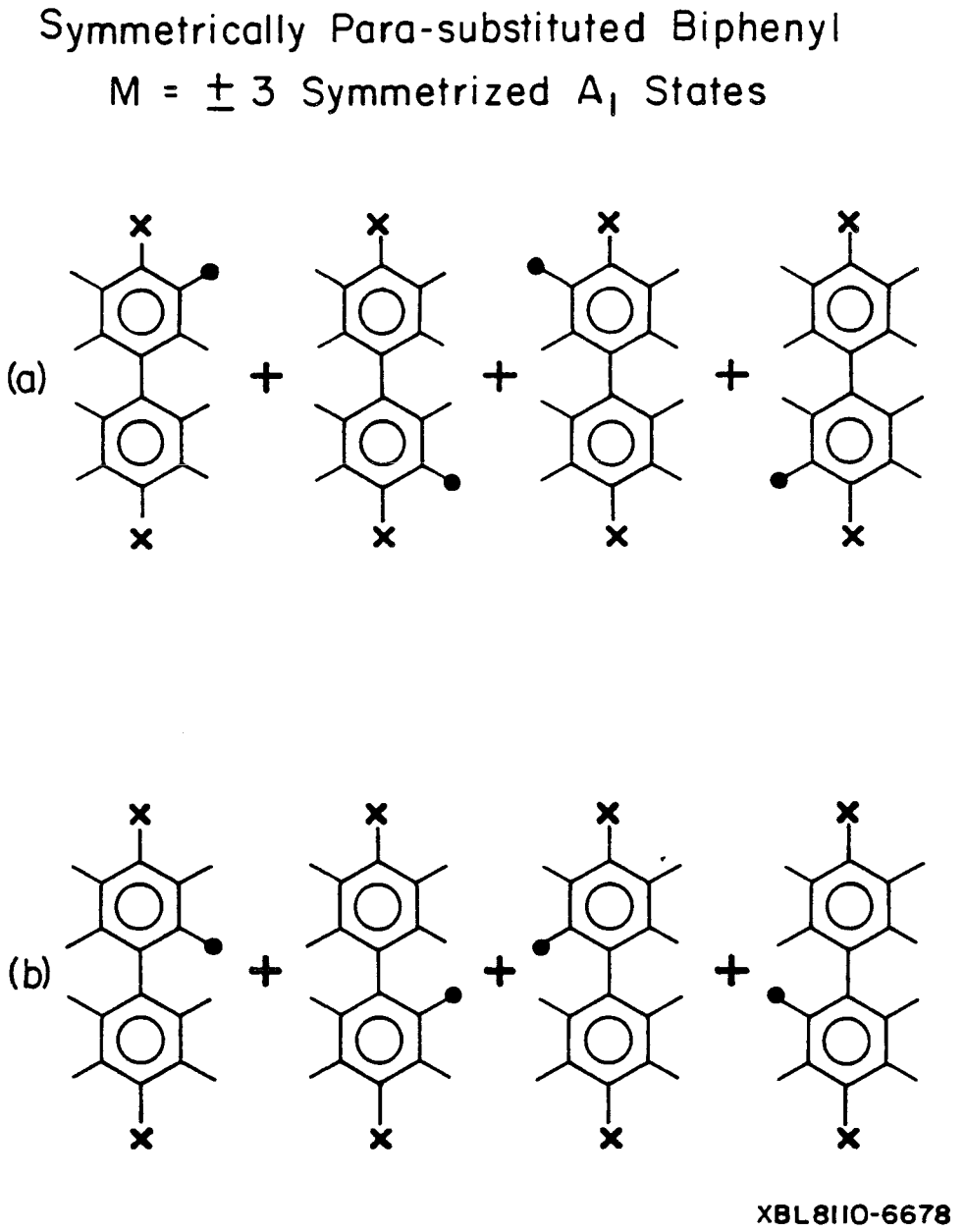

Figure 4.7

Schematic representation of symmetrized M = ± 3 A_1 states for a biphenyl having D_4 symmetry. The proton spin labeled with a dot is in a quantum state (α or β) opposite to that of the other seven spins. Each symmetrized state a) and b) is a linear combination of simple product states for the proton spins. These two symmetrized states make up a 2 x 2 matrix which must be diagonalized to yield true eigenstates of the Hamiltonian.

Table 4.3

D_2 Point Group Character Table for Symmetry Elements of Asymmetrically Para-Substituted Biphenyl

a)	E	C_2^Z	C_2^Y	C_2^X
b)	E	C_2^{AB}	C_2^A	C_2^B
c)	(12345678)	(43218765)	(43215678)	(12348765)
A_1	1	1	1	1
B_1	1	1	-1	-1
B_2	1	-1	1	-1
B_3	1	-1	-1	1

a) D_2 symmetry elements for space variables of an object of this point group.

b) D_2 permutation elements for asymmetrically para-substituted biphenyl.

c) Permutation elements according to numbering of Figure 4.5.

Asymmetrically Para-substituted Biphenyl

D_2 Point Group Energy Level Diagram

M	A_1	B_1	B_2	B_3
-4	1			
-3	4		2	2
-2	12	4	6	6
-1	20	8	14	14
0	26	12	16	16
1	20	8	14	14
2	12	4	6	6
3	4		2	2
4	1			

XBL 8110-7192

Figure 4.8

Spin energy level diagram for an asymmetrically para-substituted biphenyl (D_2 symmetry). The four irreducible representations are shown along the top and values of the total magnetic quantum number are given on the left hand side. Numbers within the table are submatrix dimensions for each representation and different values of M.

Table 4.4

Predicted Number of Transitions in the Multiple Quantum Spectrum of an Asymmetrically Para-substituted Biphenyl

n Quantum Order	# Transitions[a]	Symmetry
8	1	A_1
7	8	A_1 (4 doublets)
6	24	A_1 (12 doublets)
	24	A_1 (6 triplets)
	4	B_2 (triplet)
	4	B_3 (triplet)
	41 total unique transitions	
5	136	A_1 (68 doublets)
	24	B_2 (12 doublets)
	24	B_3 (12 doublets)
	184 total unique transitions	
4	556 total	
3	1256 total	
2	2256 total	
1	3160 total	

[a] For 8, 7, 6, 5 quantum, a breakdown by symmetry is shown and only the number of unique transitions given in totals (ignoring accidental degeneracies).

assumption, e.g., about the phase or purity of the liquid crystal, must be invalid. Without exact knowledge of the couplings, we cannot predict where all of the additional lines from a symmetry lower than D_4 should appear. However, if the rings are only slightly different, then E symmetry lines of the D_4 point group are expected to split into two closely spaced lines. Roughly speaking, this is a reflection of the doubly degenerate E representation of the D_4 point group "splitting" into the B_2 and B_3 representations of D_2. In a similar sense, the A_1 representation of D_2 can be viewed as a combination of the states in A_1 and B_2 of D_4. The states of A_2 and B_1 in the D_4 group condense to form B_1 of D_2. Unlike the E representation however, this situation cannot necessarily be expected to produce a simple splitting of D_4 lines. Thus, if the distortions breaking the symmetry are only slight, we can expect a number of overlapping, unresolved transitions due to near degeneracies and perhaps a few additional resolved lines.

4.2.3 Order Parameters

We determine the number of order parameters necessary to describe a spectrum by considering effects of molecular symmetry on the definitions in Equation (2.32). We find it convenient to use Equation (2.33) for the dipolar couplings requiring the Saupe cartesian order parameters. We demonstrated in Chapter 2 that, in general, we require five order parameters for each allowed conformation of molecules oriented in a uniaxial phase. The C_2 operation about the long axis of the biphenyl group implies that the orientational distribution function describing a transformation from a molecule fixed axis system to director frame must also have C_2 symmetry about this axis. We chose the z molecular axis to be along this C_2 axis for both D_2 and D_4 cases and find that S_{xz} and S_{yz} must be zero.

At this point the two symmetry cases differ. The additional ring exchange symmetry of the D_4 model implies that there should only be two independent order parameters. Thus, we should be able to easily find the molecular fixed axis system in which the order tensor is diagonal. Such an axis set is conveniently chosen with its origin along the C-C inter-ring bridge as depicted on the left hand side of Figure 4.5. The x axis then bisects the dihedral angle for all values of ϕ. The y axis is then perpendicular to the effective reflection plane containing z and caused by the rapid interconversion between conformations. We will refer to this set of axes as coordinate system #1 here and in the Appendix. The independent order parameters are then the diagonal elements S_{zz} and $(S_{xx}-S_{yy})$. Because these are insensitive to the conformational state of the molecule, a single order tensor suffices to calculate D_{ij}'s and an average over the four conformations implies averaging just the geometric quantities according to Equation (2.36).

The less symmetric D_2 case requires one independent off-diagonal element in $\underset{\approx}{S}$. We define the molecular fixed axis system for this case to have its origin in one of the rings (see Fig. 4.5). The x axis lies in the plane of this ring and the y axis is perpendicular to it. The non-zero order parameters in this axis system - coordinate system #2 are then S_{zz}, $(S_{xx} - S_{yy})$ and S_{xy}. We see from Equation (2.32c) that the S_{xy} for different conformations are related by a sign. Thus,

$$S_{xy}^{\phi} = S_{xy}^{\pi+\phi} = -S_{xy}^{-\phi} = -S_{xy}^{\pi-\phi}. \tag{4.1}$$

Averaged dipolar couplings can then be calculated for this case from three independent numbers and a relative sign in the order tensor and again we find that biphenyl does not present complications in the analysis due to its internal motion as described in Chapter 2.

4.2.4 Parameters

Assuming J couplings do not change when a molecule is dissolved in liquid crystals, we may use values obtained from isotropic measurements when analyzing a spectrum from an oriented phase. This is common practice reported in the literature and, with the small values of J_{ij} compared to D_{ij}, seems justified in most cases. Since the spectra are usually obtained by the TPPI technique, we also assume that the chemical shifts are removed and set them to zero. We will have to consider the extent to which lines are shifted by this technique in the manner described in Chapter 3. Fortunately, computer programs have been written in this laboratory [67] which allow modeling of spectra when chemical shifts are non-zero and so estimates to be made of line shift magnitudes.

If we assume the biphenyl has D_4 symmetry, then there are seven unique dipolar couplings to determine from the spectrum. Four of these are intra-ring couplings which are the same for both rings. The remaining three are sensitive to the dihedral angle and inter-ring distances. Assuming nothing about the structures of the molecule, then there are seven molecular parameters which must be determined from these couplings:

$$\begin{aligned} & r_{12} = r_{34} = r_{56} = r_{78}, \\ & r_{14} = r_{58}, \\ & r_{23} = r_{67}, \\ & r_{260}, \\ & \phi, \\ & S_{zz}, (S_{xx} - S_{yy}) \end{aligned} \tag{4.2}$$

where r_{260} is the distance between protons two and six when $\phi = 0$.

To determine something about the potential, some of the quantities in Equation (4.2) will have to be fixed. In an analysis of a single quantum spectrum of 4,4'-dichlorobiphenyl, Niederberger, et al. [96] fixed r_{14}. The four intra-ring couplings then determine ring structure and order parameters. The remaining three couplings were used to find r_{260}, ϕ and one piece of information about the potential. This analysis initially assumed an average only over the four static conformations of Figure 4.4. A more sophisticated average over vibrational or torsional motions requires further structural and order parameter assumptions. The inclusion of an average over the torsional motion in which ϕ changes cause only a slight improvement in the overall fit for the case of 4,4'-dichlorobiphenyl [96].

When the para-substituents on a biphenyl unit are not the same, the D_2 symmetry means there are 12 unique dipolar couplings. The 11 molecular parameters to determine from these are

$$
\begin{aligned}
& r_{12} \neq r_{56}, \\
& r_{14} \neq r_{58}, \\
& r_{23} \neq r_{67}, \\
& r_{260}, \\
& \phi, \\
& S_{zz},\ (S_{xx} - S_{yy}),\ S_{xy}.
\end{aligned}
\tag{4.3}
$$

All of these, plus something about the potential, may be determined from experimental couplings. Further reasonable assumptions may be made to simplify the complexity of the problem.

Clearly we cannot simultaneously vary all of these parameters to obtain a fit without some sort of iterative approach. The details of the least squares approach used in this work are found in the Appendix. We can, however, vary only one parameter while all others are fixed to get some idea of the sensitivity splittings in the spectrum have to this parameter. This can be done in a systematic manner to determine which lines will direct convergence and to help identify possible line assignment difficulties. Program BIPH4PARA (see appendix) was written to accomplish this for the six and seven quantum A_1 symmetry transitions from input parameters of Equation (4.2) and (4.3). When D_4 symmetry is assumed, a standard set of geometric parameters, based on a phenyl skeleton identical to that of benzene and with $r_{260} = 1.818$ Å, is used. This corresponds to a C-C inter-ring bridge length of 1.50 Å, $r_{CH} = 1.082$ Å, $r_{CC} = 1.400$ Å, and a C-C-H angle of 120°. This standard set of parameters is given in Table 4.5.

Figure 4.9 shows the variation of six quantum A_1 symmetry transition frequencies with dihedral angle ϕ. Only one half of the symmetrical spectrum which would appear at $6\Delta\omega$ in a non-selective multiple quantum experiment is shown. The order parameters found for 5CB-d_{11} from an analysis of the spectrum in Figure 4.2 and assuming D_4 symmetry [104] were used. This analysis yielded a value for the dihedral angle (see below) which is labeled in Figure 4.9. Two features to note in this figure are the high sensitivity of some transitions to ϕ in the region of best fit and that some transitions pass through near degeneracy for some values of ϕ. Figure 4.10 shows a similar dependence on ϕ for two members of the four seven-quantum transitions.

Table 4.5

Standard Geometry for D_4 Symmetry Biphenyl

$$r_{12} = r_{34} = r_{56} = r_{78} = 2.482 \text{ Å}$$

$$r_{14} = r_{23} = r_{58} = r_{67} = 4.299 \text{ Å}$$

$$r_{260} = 1.818 \text{ Å}$$

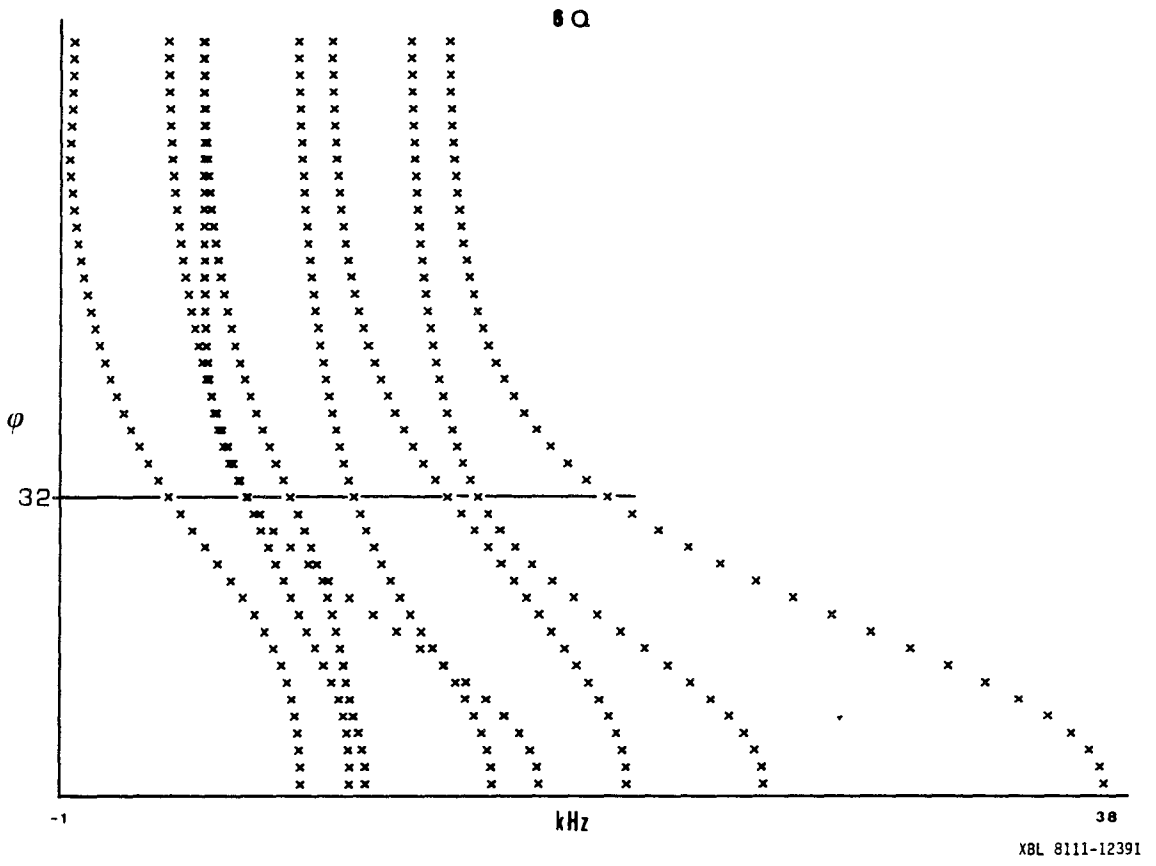

Figure 4.9

Variation of six quantum A_1 symmetry transition frequencies for a symmetrically substituted biphenyl with dihedral angle ϕ. One half of the symmetric spectrum calculated from D_4 dipolar couplings for each of 45 values of ϕ from 0 to 88° is shown. The frequency scale shown is relative to the center of the six quantum spectrum. Structure and order parameters used in the calculation are those in Table 4.5 and $S_{zz} = 0.568, (S_{xx} - S_{yy}) = 0.057$.

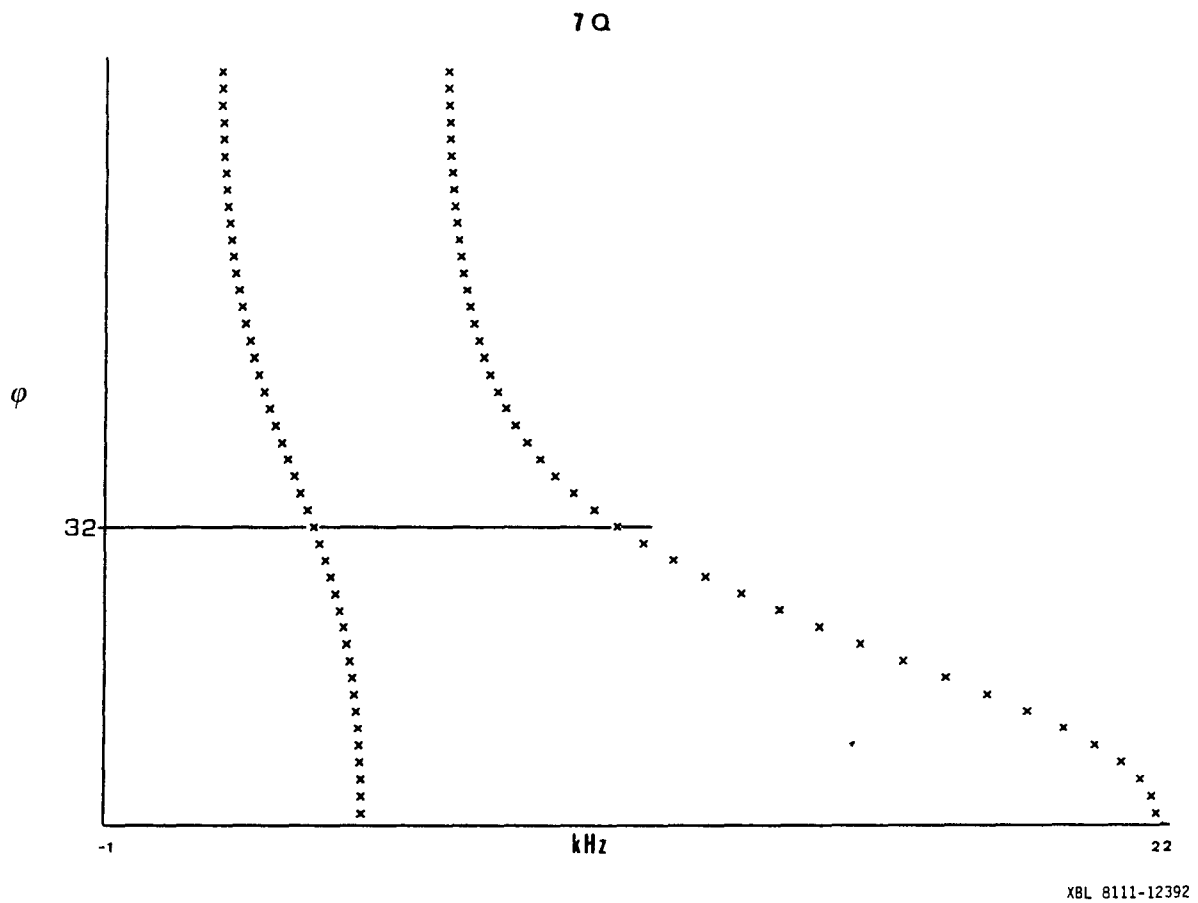

Figure 4.10

Variation of seven quantum transition intensities with ϕ from 0 to 88° for a symmetrically para-substituted biphenyl. Only one half of the symmetric spectrum for each value of ϕ is shown. Structure and order parameters are the same as for Figure 4.9.

With the long axis of the molecule chosen as the z axis, one would expect S_{zz} to be the dominant order parameter and transitions to exhibit a linear dependence on this parameter when all others are held constant. This is found for six quantum lines as shown in Figure 4.11. Here S_{zz} is varied from -0.5 to +0.95. The transition frequency dependence on $(S_{xx} - S_{yy})$ over the same range with S_{zz} held constant is shown in Figure 4.12. The dependence is weaker as expected. However, all lines but one vary in a positive sense with a pair of transitions crossing at $(S_{xx} - S_{yy}) = +0.15$. Clearly, this order parameter may not be neglected in any model calculation. Similar trends for the seven quantum lines are found.

We can also look at the sensitivity of a spectrum to changes in internuclear distances. Single couplings should be strongly affected due to the $(r_{ij})^{-3}$ dependence. However, the high order transition frequencies are actually the results of linear combinations of couplings and so will be less sensitive to changes in particular distances. As examples, the seven quantum D_4 transitions are shown as functions of r_{12}, r_{260}, and r_{14} in Figures 4.13, 4.14, and 4.15, respectively. All other parameters are fixed as these distances vary. Strong dependences are shown on r_{12} and r_{260} but not on r_{14}. This last distance affects intra-ring geometry significantly but inter-ring parameters only slightly.

The program is also capable of producing A_1 representation transition frequencies for a D_2 biphenyl symmetry. The six and seven quantum transitions as a function of ϕ are shown in Figure 4.16 and 4.17 respectively. For these plots, the ring B geometry was fixed to the benzene parameters of Table 4.5. For the other ring (A), r_{23} was set to 4.100 Å and r_{14} to 4.299 Å. The order parameters were chosen to be

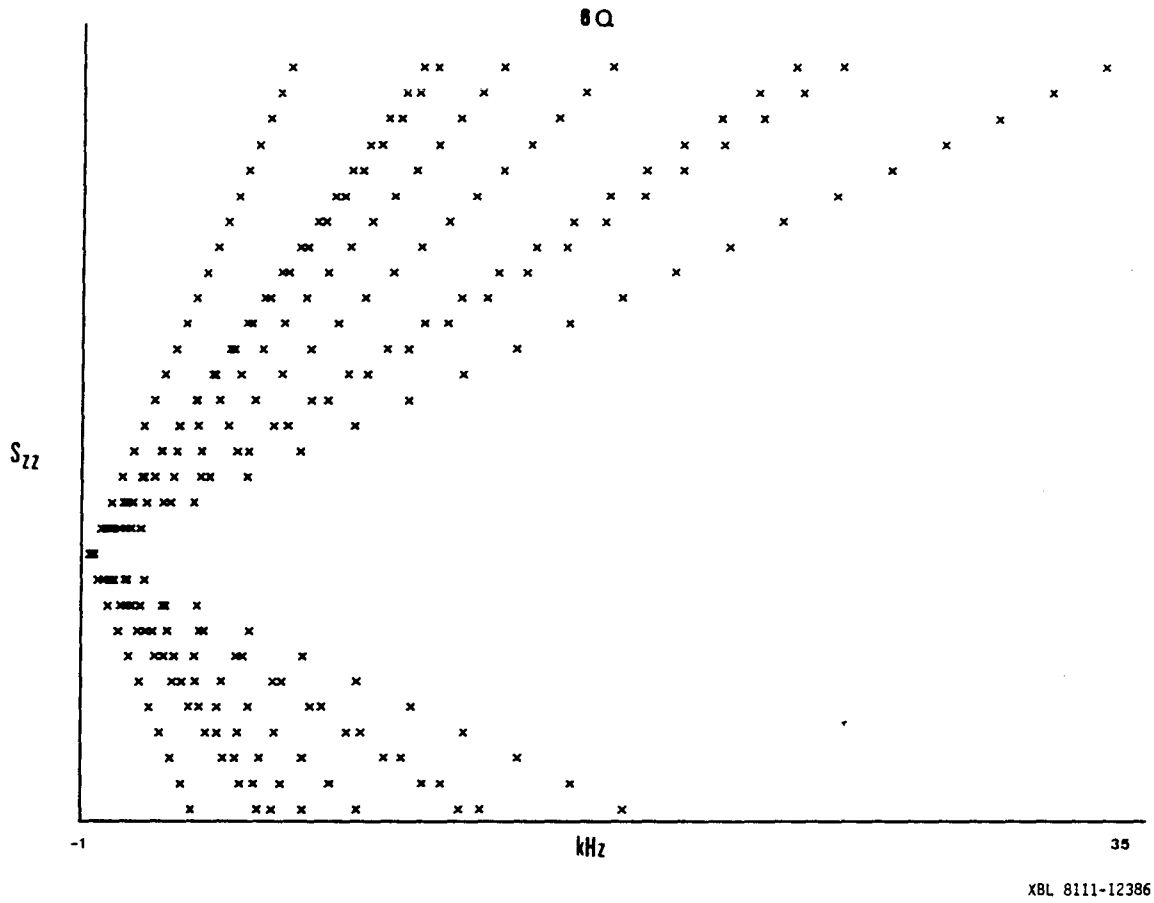

Figure 4.11

Variation of six quantum A_1 symmetry transition frequencies with the order parameter S_{zz} and assuming D_4 symmetry for an eight spin-1/2 substituted biphenyl. S_{zz} ranges from -0.5 to 1.0. Other parameters are the same as for Figure 4.9 and with $\phi = 32°$. Only one half a spectrum symmetric about the center of the order for each value of S_{zz} is shown.

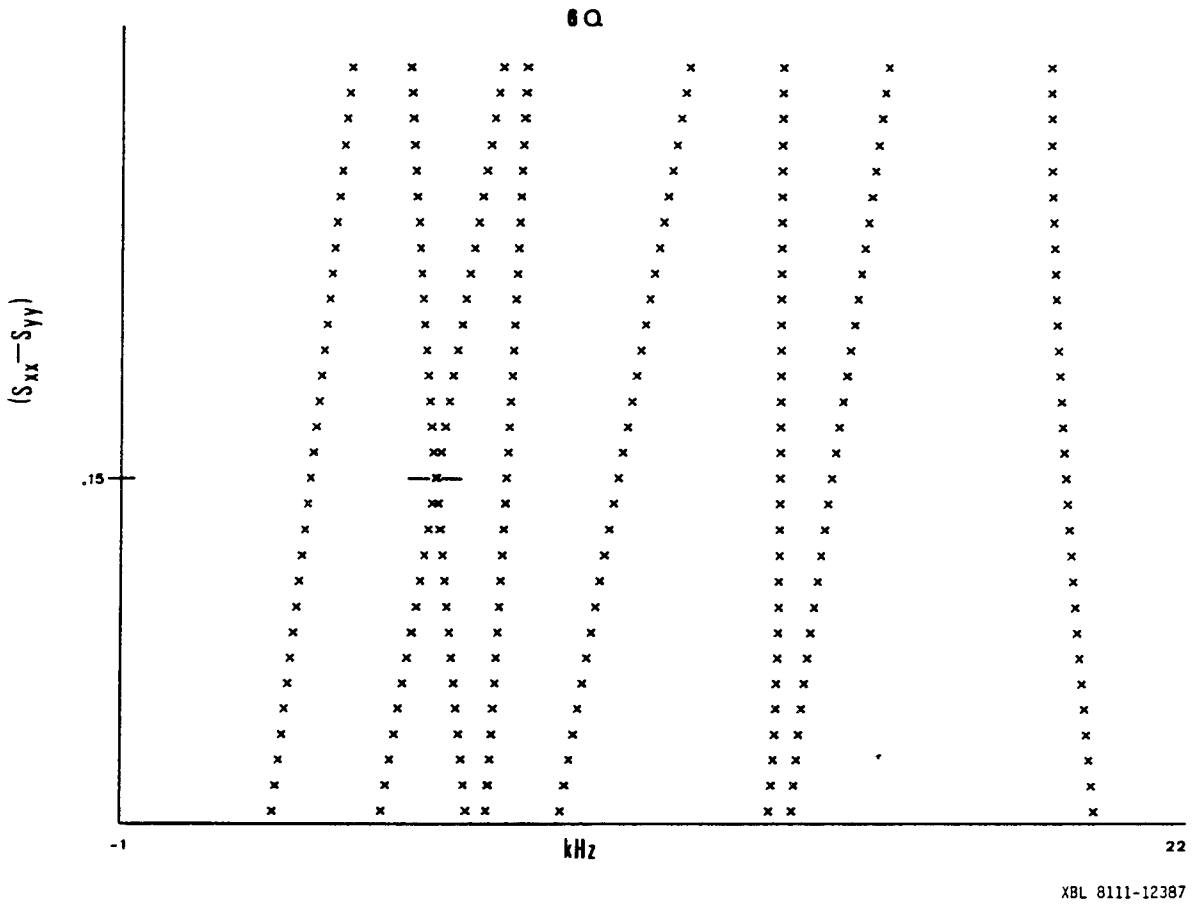

Figure 4.12

Variation of six quantum A_1 symmetry transition frequencies with the order parameter $(S_{xx} - S_{yy})$ which ranges from -0.5 to 1.0. Other parameters are the same as Figure 4.11 with $S_{zz} = 0.6$. Only one half of the spectrum for each value of $(S_{xx} - S_{yy})$ is shown.

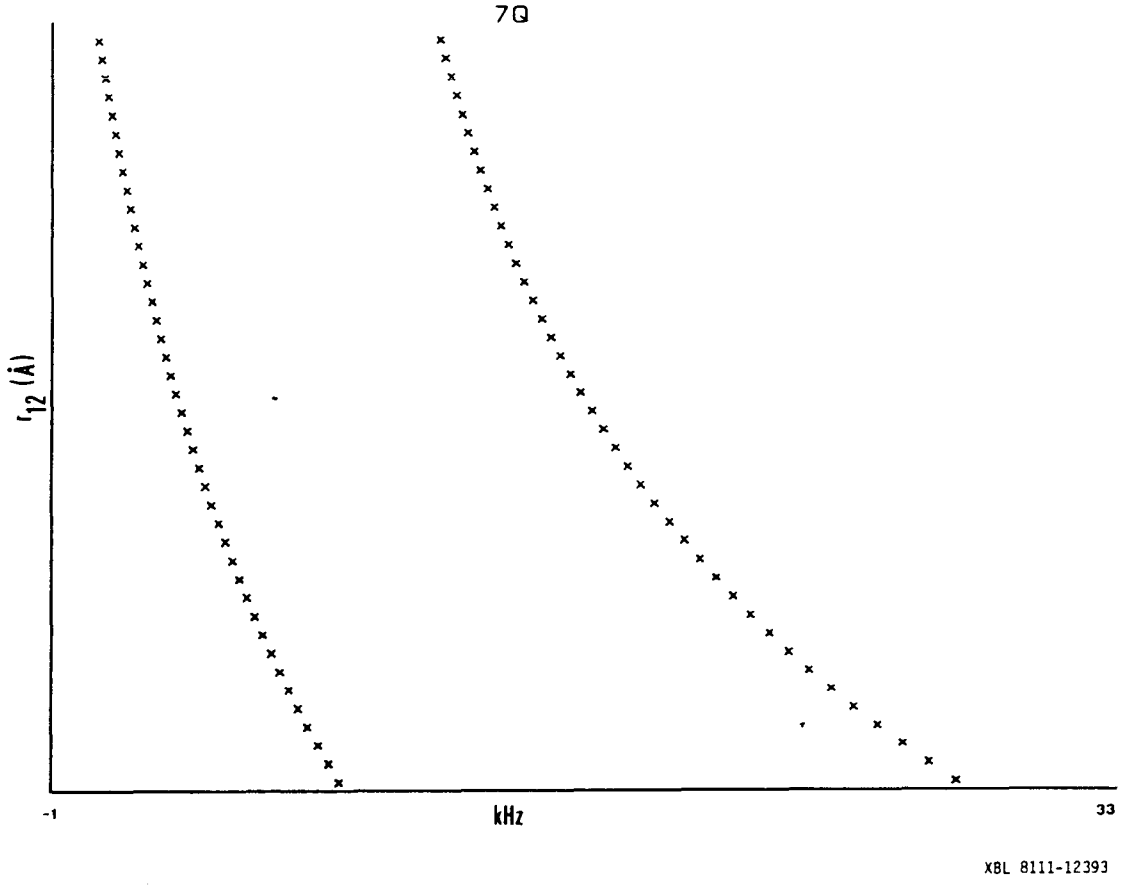

Figure 4.13

Variation of seven quantum transition frequencies of a symmetrically para-substituted biphenyl with internuclear distance r_{12}. The range of r_{12} is 2.0 to 3.0 Å in steps of 0.025 Å. Other parameters are the same as Figure 4.9 with $S_{zz} = 0.568$, $(S_{xx} - S_{yy}) = 0.057$ and $\phi = 32°$. Only one half of the spectrum at each value of r_{12} is shown.

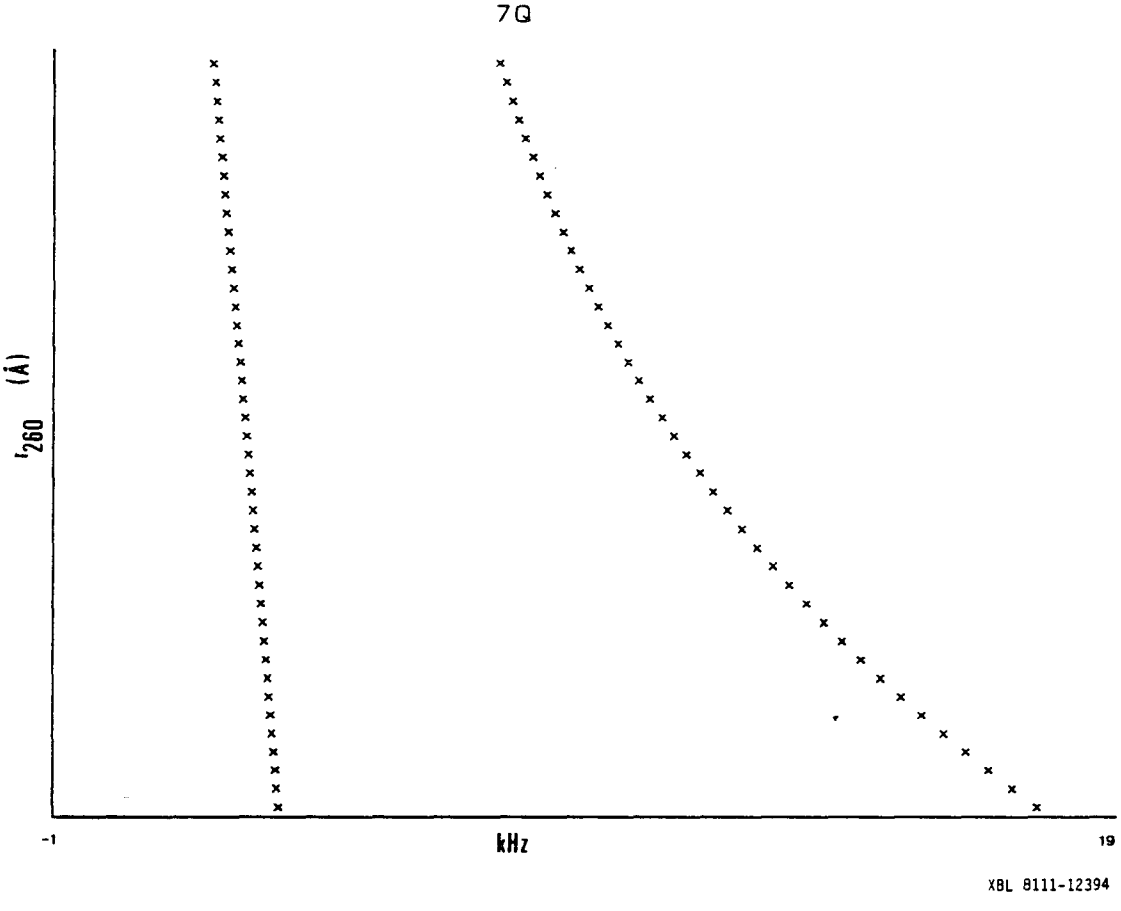

Figure 4.14

Variation of seven quantum transition frequencies with r_{260} for a D_4 symmetry para-substituted biphenyl. The distance r_{260} ranges from 1.5 to 2.0 Å in steps of 0.025 Å. Other parameters are the same as Figure 4.13 with r_{12} = 2.482 Å. Only one half of the spectrum at each value of r_{260} is shown.

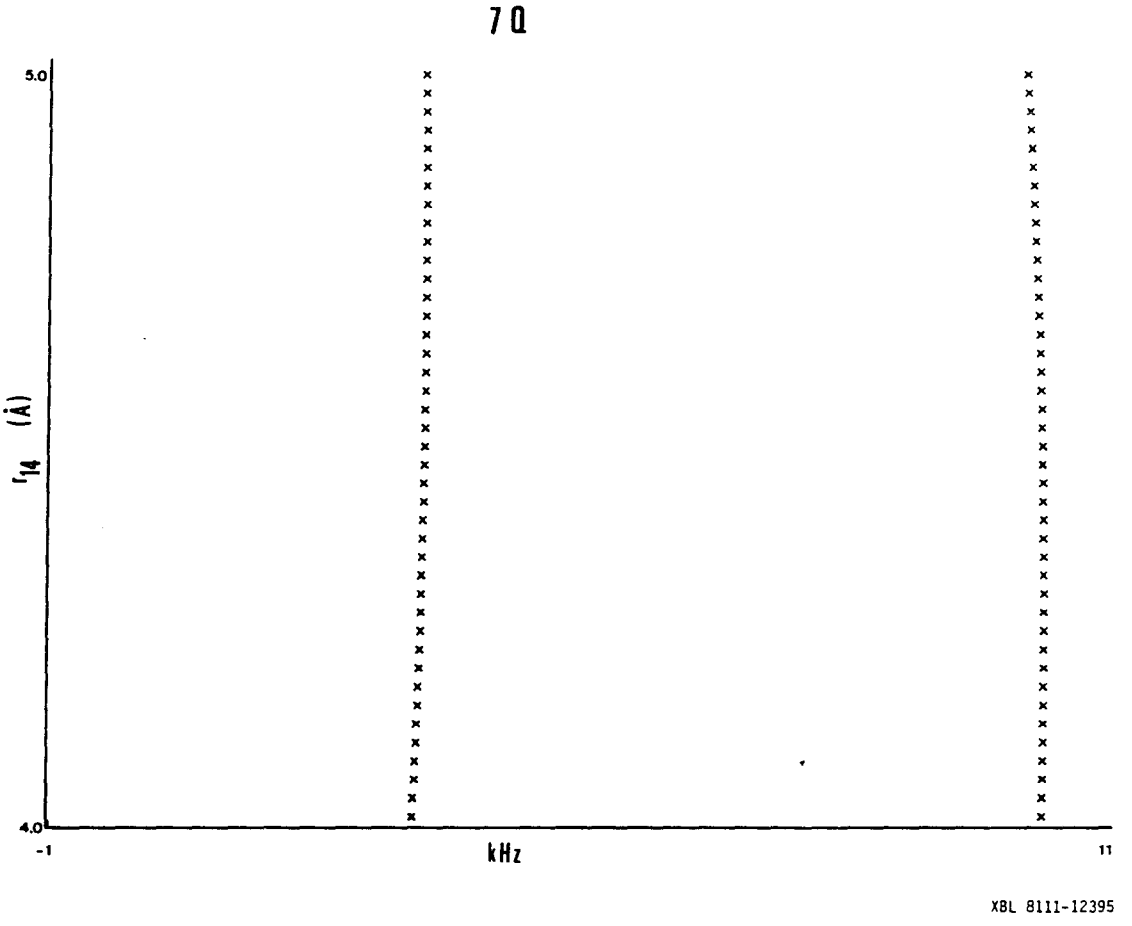

Figure 4.15

Variation of seven quantum transition frequencies with internuclear distance r_{14}. This parameter ranges from 4.0 to 5.0 Å in steps of 0.025 Å. Other parameters are the same as for the previous two figures with r_{260} = 1.818 Å and r_{12} = 2.482 Å. D_4 symmetry for the biphenyl is assumed. Only one half of each spectrum is shown.

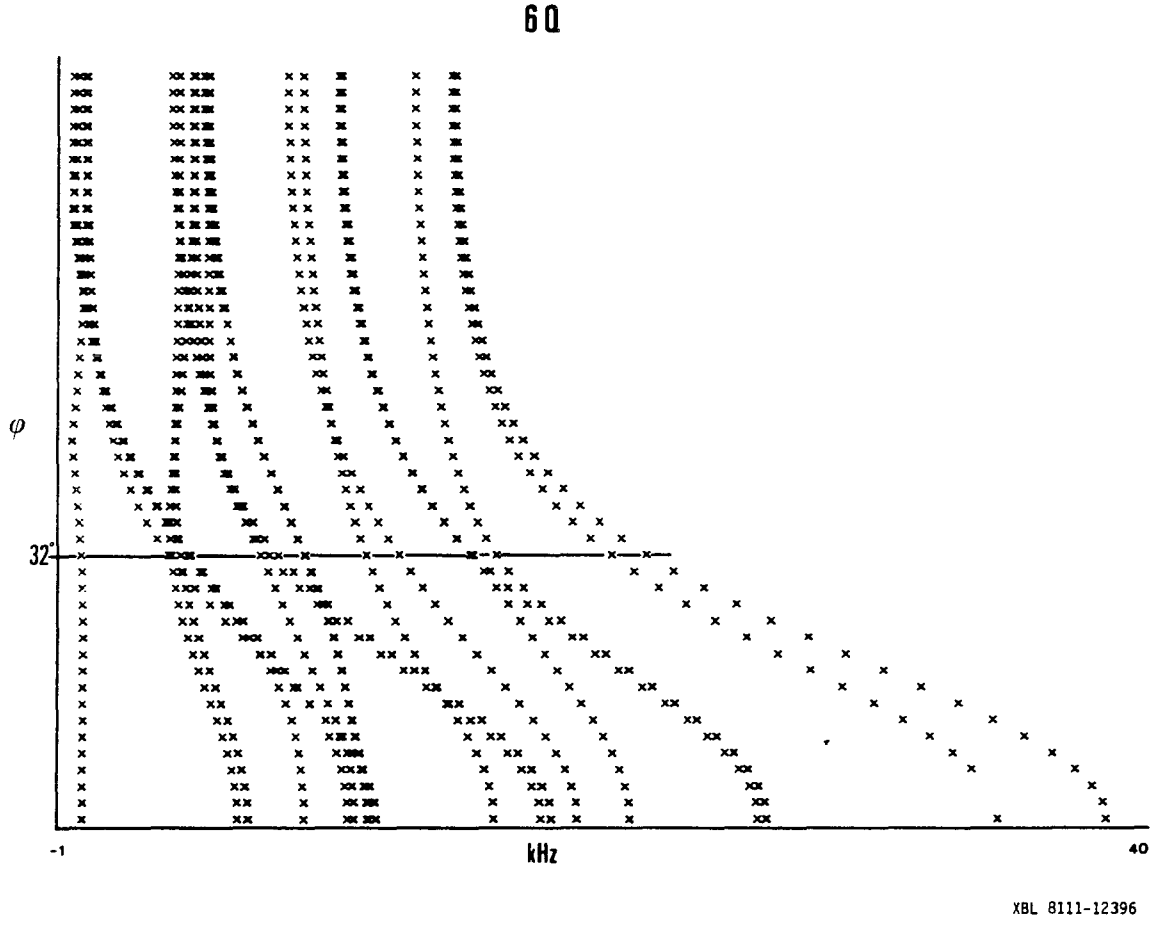

Figure 4.16

Variation of six quantum A_1 symmetry transition frequencies of an asymmetrically para-substituted biphenyl with dihedral angle ϕ from 0 to 90°. The same structural parameters for the D_4 symmetry calculations of the preceding figures were used with a slight distortion of r_{23} = 4.100 Å which changes the symmetry to D_2. The order parameters were set at S_{zz} = 0.6, $(S_{xx} - S_{yy})$ = 0.03, and S_{xy} = 0.03. Only one half of each spectrum is shown.

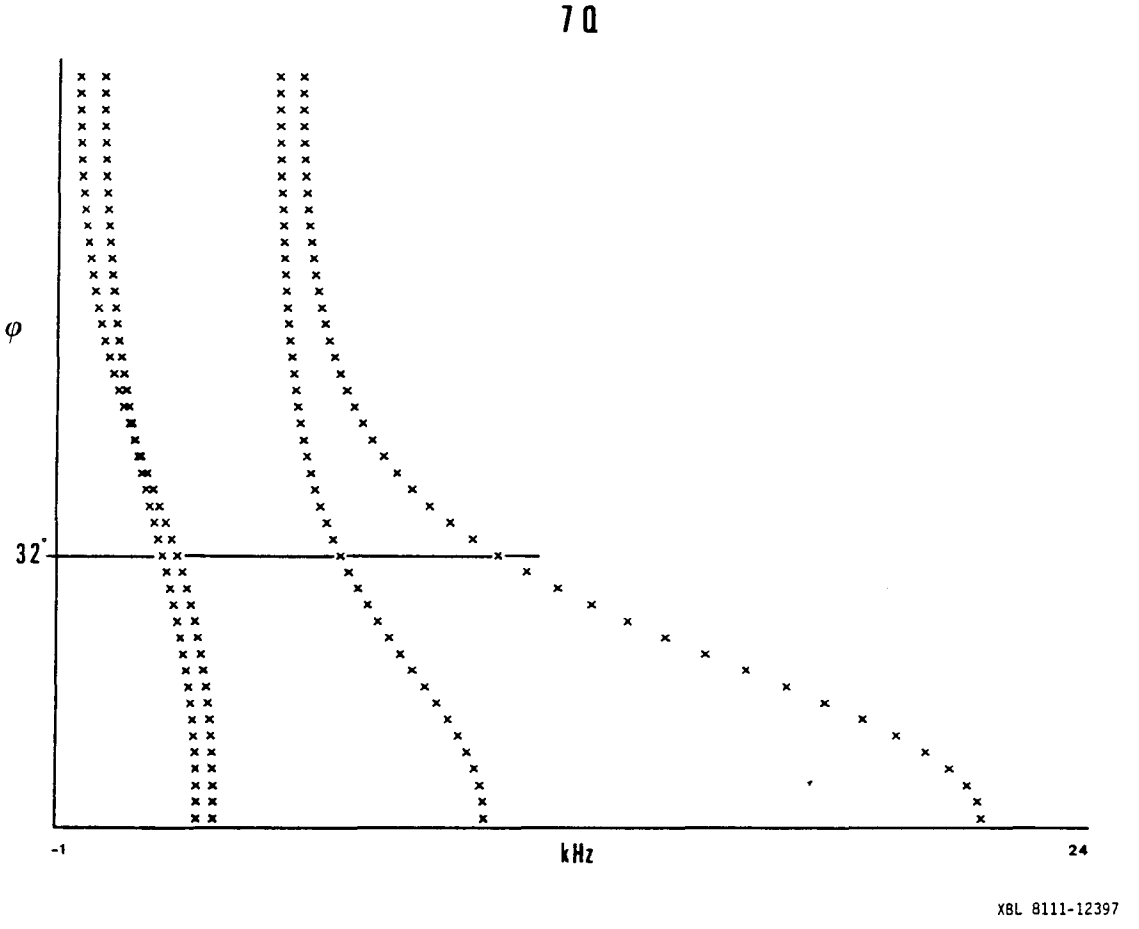

Figure 4.17

Variation of seven quantum transition frequencies for an asymmetrically substituted biphenyl (D_2 point group) with dihedral angle ϕ. Other parameters are the same as in Figure 4.16. Only one half of the spectrum at each value of ϕ is shown.

$S_{zz} = 0.6$, $(S_{xx} - S_{yy}) = 0.03$ and $S_{xy} = 0.03$ and, as before, $r_{260} = 1.818$ Å. The overall picture is similar to that for the D_4 case except now several sets of transitions collapse to near degeneracy in the six quantum spectrum (see Fig. 4.16). This occurs close to a value of ϕ obtained for 5CB-d_{11} [104] (see below).

Next, we investigate the behavior of six and seven quantum transitions as molecular symmetry moves from D_2 through D_4 and back to D_2. If one ring is distorted relative to the other and this distortion is changed so that the rings eventually become equivalent, we should see the number of transitions change. This is shown for one half of the six and seven quantum spectra in Figure 4.18 and 4.19, respectively. The distortion chosen was in r_{23} for ring A. This distance ranges from 4.275 to 4.325 Å in steps of 0.001 Å for the plots of Figures 4.18 and 4.19. The order tensor for coordinate system #2 was calculated so that it becomes diagonal if transformed to coordinate system #1 ($\phi = 32°$). Thus, when $r_{23} = 4.300$ Å, it is equal to r_{14}, r_{67}, and r_{58}, so the symmetry is D_4. As seen in Figures 4.18 and 4.19, line frequencies do not vary much but transitions unique to D_2 symmetry simply disappear on either side of the D_4 region. Because there are effectively only two independent order parameters used, this particular distortion only mildly perturbs the couplings from a D_4 symmetry. Ultimate τ averages (see Chapt. 3) confirm that lines unique to D_2 symmetry in Figures 4.18 and 4.19 are of very low intensity relative to those in the D_4 symmetry region.

As a final example, we consider a case when there are three truly independent order parameters. For this calculation, the rings had equivalently distorted geometries with $r_{14} = r_{58} = 4.500$ Å, $r_{23} = r_{67} = 4.000$ Å, $\phi = 32°$ and with the rest of the parameters as in Table 4.5.

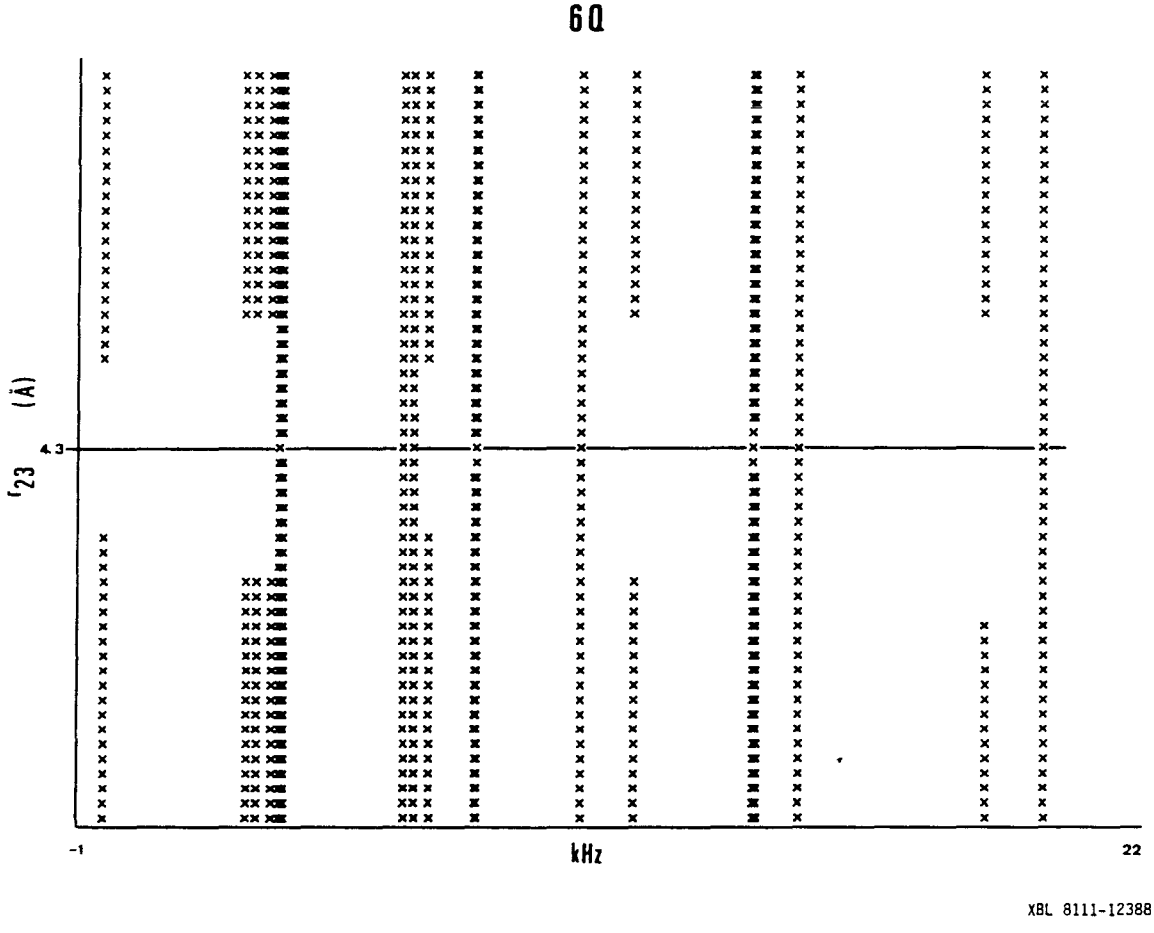

Figure 4.18

Variation of six quantum A_1 symmetry transition frequencies with internuclear distance r_{23}. This parameter ranges from 4.275 to 4.325 Å in steps of 0.001 Å. When r_{23} = 4.300 Å the effective symmetry is D_4. On either side of this point the effective symmetry is D_2 as evidenced by the increased number of transitions. Ultimate τ averaged intensities for those lines unique to the D_2 symmetry cases are small relative to other lines for this particular symmetry-changing distortion.

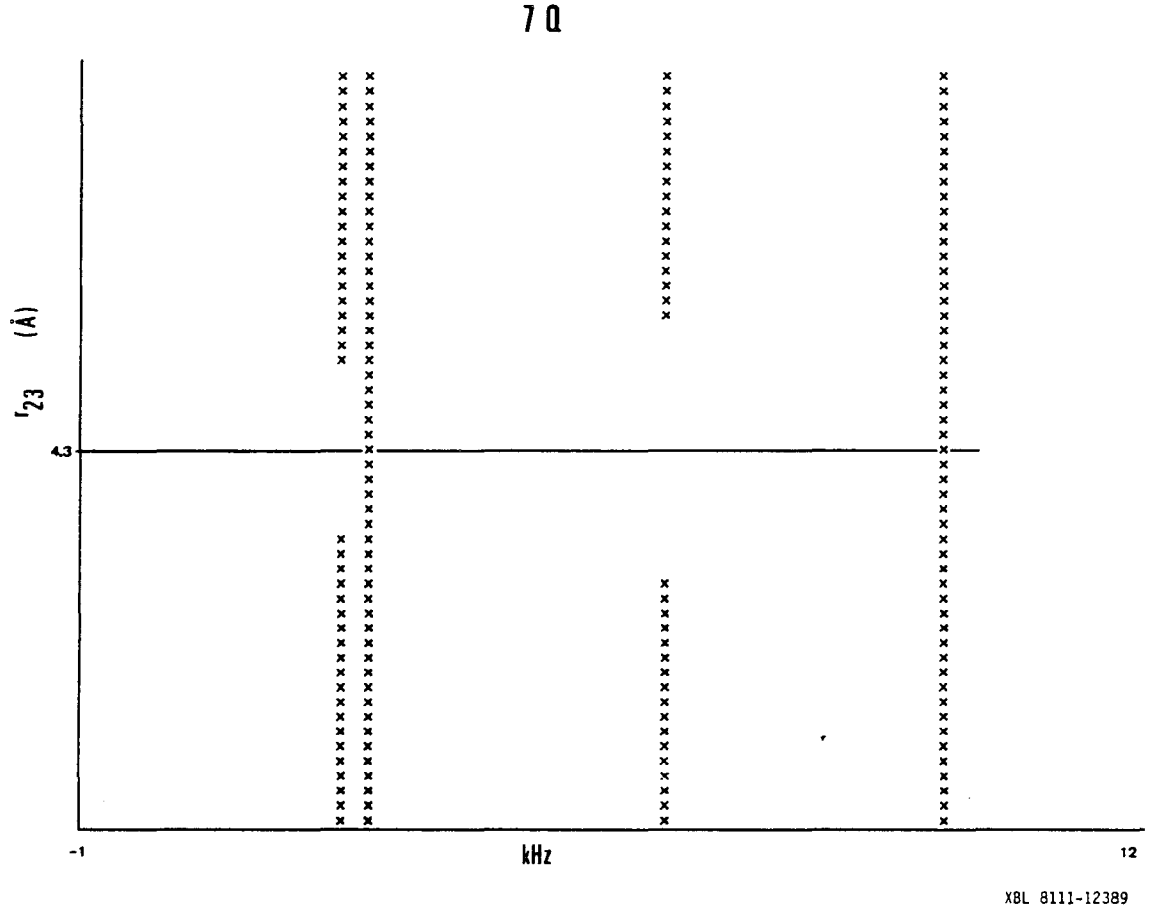

Figure 4.19

Variation of seven quantum transition frequencies with internuclear distances r_{23}. The range of this parameter is from 4.275 to 4.325 Å in steps of 0.001 Å. Other parameters are the same as in Figure 4.18. There are four pairs of transitions when the effective symmetry is D_2 and only two pairs when the symmetry is D_4. Only one half of the spectrum at each value of r_{23} is shown.

Figure 4.20 shows the six quantum transition frequencies as a function of S_{xy} which ranges from -0.20 to +0.20 in steps of 0.01. The variation of S_{xy} was designed so that a D_4 symmetry became effective where labeled in the figure. Now transition frequencies do indeed change significantly and some lines merge to a degenerate frequency at the point where D_4 symmetry is effective.

We could proceed in this manner to determine the many different parameter dependences high order transitions exhibit. We have already seen some general trends and discussed symmetry changes above. Small symmetry breaking distortions cause some additional lines of low intensity and splittings from near degeneracy at the expected D_4 symmetry frequencies. This approach of single parameter variation is limited, however, and an iterative technique which simultaneously varies several parameters is required to fit a spectrum.

4.3 Results: 4-Cyano-4'-n-pentyl-d_{11}-biphenyl

The procedure of Gray and Mosley [108] with a slight modification reported elsewhere [104] was used to synthesize 5CB-d_{11}. Transition temperatures were measured with a polarizing microscope and found to be T_{C-N} = 23°C and T_{N-I} = 31°C. Isotopic purity was estimated at 98%. A sample of about 400 mg was sealed under vacuum in a 6 mm o.d. glass tube. A double tuned NMR probe was used for double resonance experiments while a single tuned probe was used when heteronuclear decoupling was absent. Probe circuits are described in Chapter 5.

The single quantum proton spectrum has already been presented in Figure 4.2. Deuterium double quantum decoupling [109] removed deuterium-proton dipolar couplings. With its lack of resolution, no analysis of the spectrum was attempted. Deuterium single quantum and proton multiple quantum spectra are presented below.

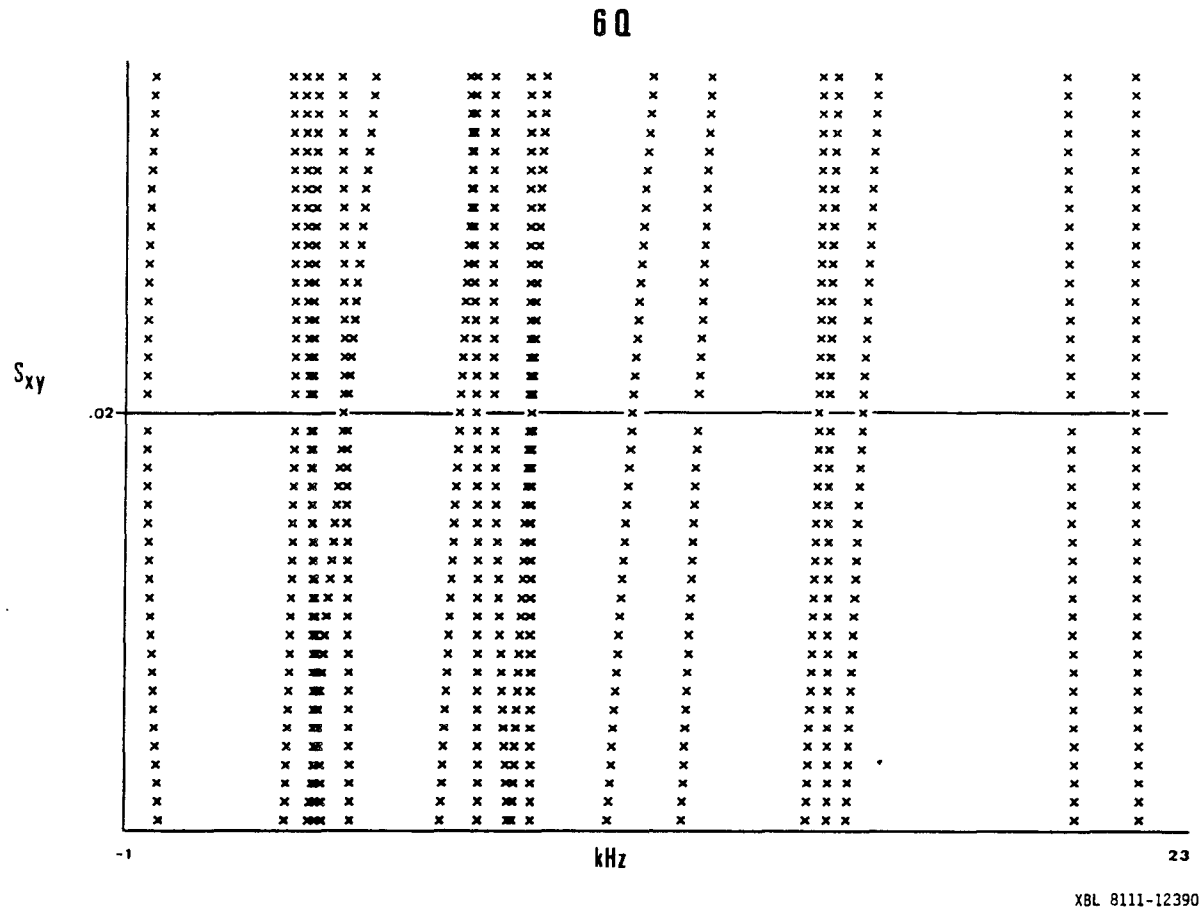

Figure 4.20

Variation of six quantum A_1 symmetry transitions of para-substituted biphenyl with order parameter S_{xy} ranging from -0.2 to +0.2. Other parameters are set at their values for D_4 symmetry at the point labeled in Figure 4.18. The off-diagonal order parameter causes an effective D_2 symmetry for the biphenyl couplings except at the one point labeled for $S_{xy} = 0.02$. At this point, the order tensor is diagonalized by transforming from coordinate system #2 to #1 (see Fig. 4.5).

4.3.1 Deuterated Chain Spectrum

A single quantum, proton decoupled deuterium spectrum of 5CB-d_{11} in the nematic phase at 25.1°C is shown in Figure 4.21. The total width shown in 75 kHz. Five major doublets with line widths between 300 and 700 Hz are observed. Each doublet is symmetrically centered about the resonance offset. This doublet structure is expected from anisotropically ordered spin-1 nuclei and arises from the quadrupole coupling of each chain segment, scaled by the order tensor [39]. Smaller splittings of some of the lines are from dipolar couplings between deuterons on the same carbon.

An expanded trace of the right hand half of Figure 4.21 is shown in Figure 4.22. Each member of a quadrupolar doublet is numbered for identification below. We wish to assign peaks in this spectrum to specific chain segments. The quadrupolar doublet splitting for a single segment may be written as [102]

$$\Delta\nu_q^i = \frac{3}{2} q_{CD}^i \{S_{zz} \langle (\frac{3}{2} \ell_{azi}^2 - \frac{1}{2}) + \frac{\eta^i}{2} (\ell_{azi}^2 - \ell_{bzi}^2) \rangle + \frac{1}{2} (S_{xx} - S_{yy}) \langle (\ell_{cxi}^2 - \ell_{cyi}^2) + \frac{\eta^i}{3} (\ell_{axi}^2 - \ell_{ayi}^2 + \ell_{byi}^2 - \ell_{bxi}^2) \rangle \}. \quad (4.4)$$

This equation implicitly assumes that a single order tensor, independent of the conformational state of the molecule, describes the spectral transitions. Here q_{CD}^i and η^i are the characteristic quadrupolar coupling constant and asymmetry parameter defined in Chapter 1 for a C-D bond in segment i of the chain. The ℓ_{abi} are direction cosines between a C-D bond fixed axis system (abc) and the molecular fixed axis system in which the order tensor is diagonal. For C-D bonds, η is generally small (~0.01) and q_{CD}^i is about 168 kHz for most CD_2 and CD_3 groups. Neglecting

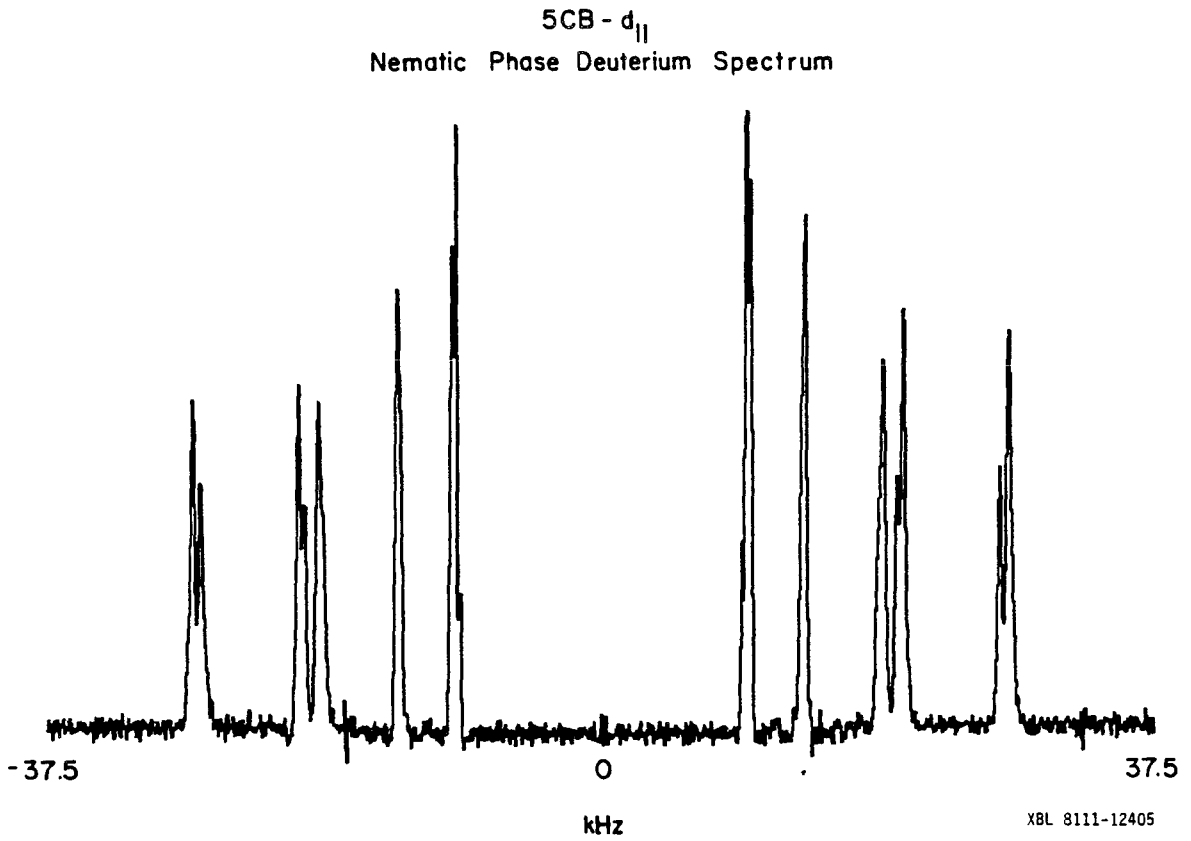

Figure 4.21

Deuterium NMR spectrum of 5CB-d_{11} in the nematic phase at 25.1°C. Each pair of lines centered on 0 Hz results from the quadrupolar interaction tensor for the deuterons on one of the chain carbons. Smaller splittings of each line arise from dipolar interactions between spins on the same carbon. Couplings to the aromatic portion of the molecule have been removed by high power proton decoupling.

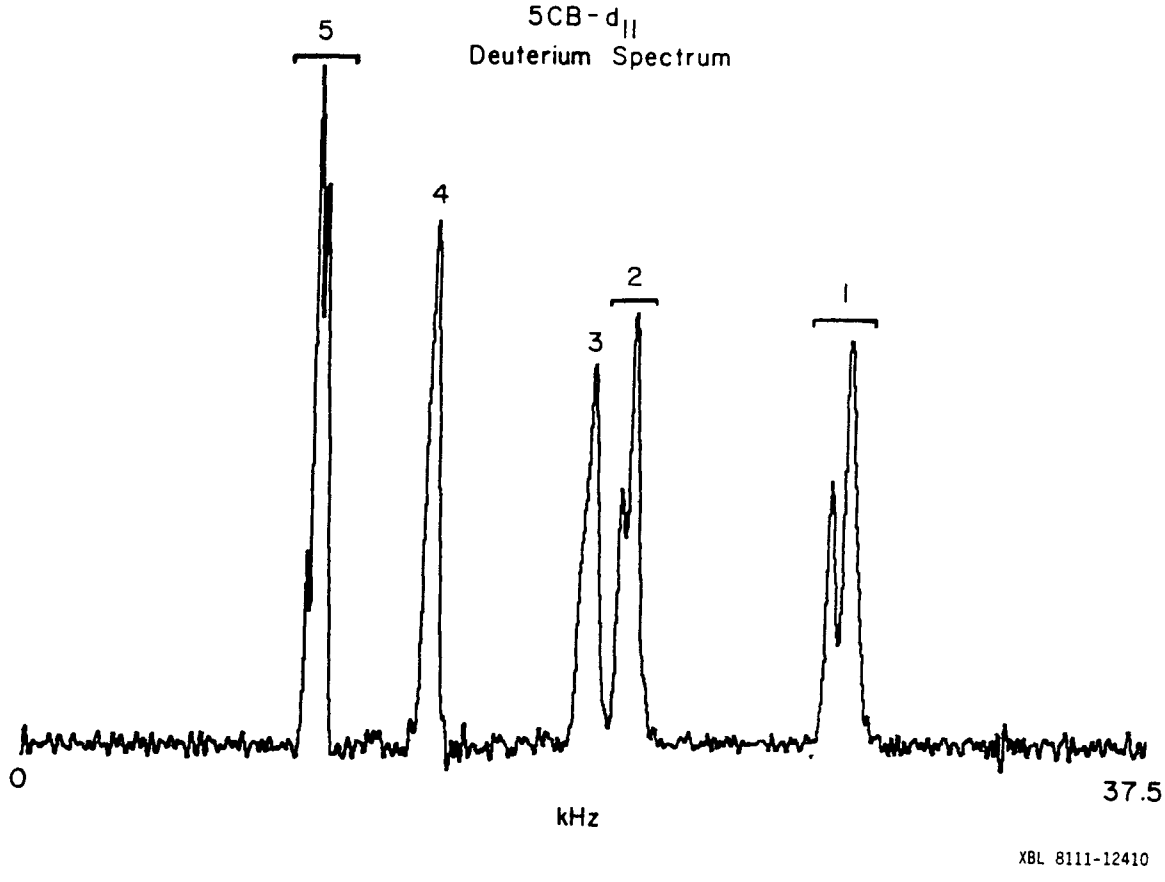

Figure 4.22

Expanded trace of the upper half of Figure 4.21 for the deuterium NMR spectrum of 5CB-d_{11} in the nematic phase. Quadrupolar satellite lines are numbered for reference in the text.

terms with η and assuming that $(S_{xx} - S_{yy})$ is small, we define an effective order parameter for each segment and the doublet splitting from segment i is given simply as

$$\Delta\nu_q^i = \frac{3}{2} q_{CD} S_{CD}^i \tag{4.5}$$

where

$$S_{CD}^i \equiv S_{zz} \langle \frac{3}{2} \ell_{azi}^2 - \frac{1}{2} \rangle . \tag{4.6}$$

Some peaks in Figure 4.22 may be assigned easily. The CD_3 group should give the most intense signal and, because of its position in the chain, experience the greatest amount of motion from the many conformational possibilities of the chain. Hence the largest peak with the smallest $\Delta\nu_q$, peak #5, is assigned to the methyl group. Likewise, the peak with the largest splitting and, thus, greatest order parameter by Equation (4.5), is assigned to the CD_2 group attached to the phenyl ring. This is #1 in Figure 4.22. Other assignments are more tentative, but it is expected that segment order parameters and so $\Delta\nu_q^i$ will vary monotonically with segment position. From recent T_1 measurements, Emsley, et al. [110] have proposed that this is indeed true except for peaks #2 and #3 which they assign to methylenes 3 and 2, respectively, counting out from the ring. The cause of this unexpected behavior is quadrupolar splittings has not been explained.

We can determine the dipolar couplings within several segments from the additional structure of some lines of Figure 4.22. Luz, et al. [43, 44] have worked out the transition frequencies and intensities expected from isolated groups of two and three equivalent deuterons. They have shown that the relative signs of dipolar (D) and quadrupolar couplings and the magnitude of D may be determined from CD_2 and CD_3 resonances.

The theory predicts that each component of a quadrupolar doublet from a CD_2 group will be split into a triplet of intensities 2:3:1 and frequencies $\frac{3}{2}$ D, $-\frac{1}{2}$ D, $-\frac{3}{2}$ D relative to ν_q, the quadrupole frequency relative to the Zeeman offset ($\Delta\nu_q = 2\nu_q$).

Figure 4.23 shows an expanded trace of line #1 of Figure 4.22. If we assume the triplet frequencies are not shifted significantly by homogeneous broadening, then the experimental spectrum gives a value for 2D. In previous studies of deuterated nematogen alkyl chains in which a methylene triplet was resolved it was found that a fit to experiment could only be made when quadrupolar and dipolar couplings were assumed to be of opposite sign [44]. Taking q^i_{CD} as positive, a value of -281 Hz is obtained for the CD_2 dipolar coupling of the first segment in 5CB-d_{11}. This agrees favorably with values obtained by Boden, et al. [102] for 8CB deuterated in the alkyl chain. The trace of part B in Figure 4.23 shows the theory stick spectrum broadened by a Gaussian function to match the linewidth of experiment. This confirms that the major transition frequencies of the triplet shift very little with broadening. The homogeneous linewidth is a result of small random fluctuations in the director and small couplings to deuterons on adjacent segments. In a similar manner, the dipolar coupling for the methylene of line #2 in Figure 4.22 is determined to be approximately -201 Hz.

The theory for an isolated methyl group predicts that each member of the quadrupolar doublet will be further split into a septet of intensities 3:8:3:1:7:3:2 and frequencies 3D, 1D, $\frac{1}{2}$ D, $-\frac{1}{2}$ D, -1D, -2D, $-\frac{5}{2}$ D relative to ν_q. Again, a fit to experiment is obtained when the couplings are of opposite sign. An expanded trace of the methyl resonance of Figure 4.22 is shown in Figure 4.24 along with theoretical stick and

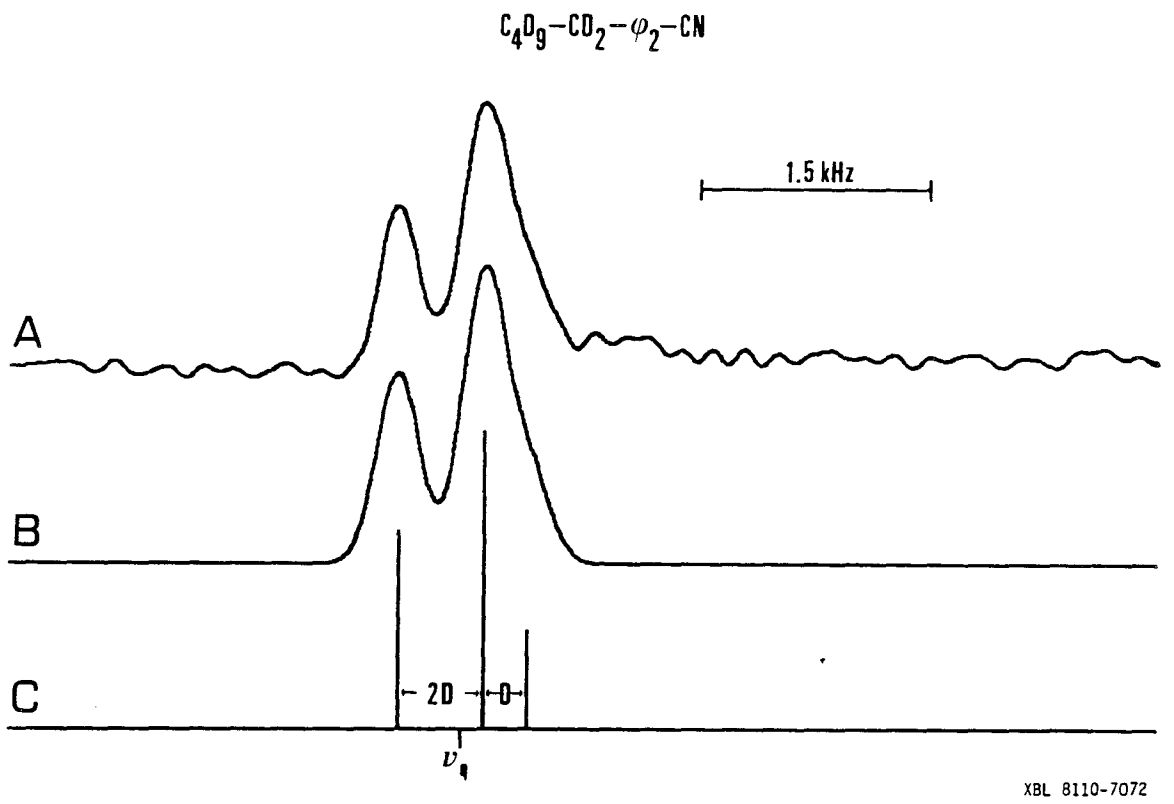

Figure 4.23

Part A shows an expanded trace of peak #1 of Figure 4.22 which is assigned to the first methylene unit of the alkyl chain in 5CB-d_{11}. B and C are a theoretical fit to the experiment with the deuterium dipolar coupling reported in the text. C shows the stick spectrum for two equivalent deuterons while B shows the theoretical spectrum broadened with a Gaussian function to match the experiment in A.

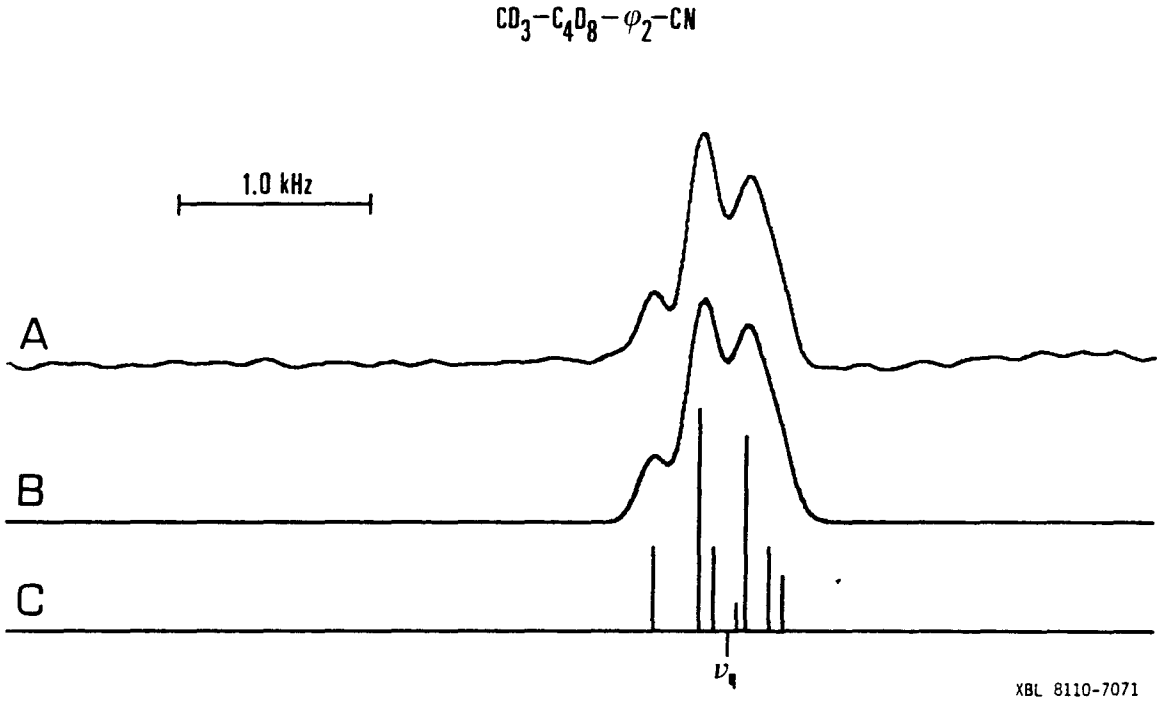

Figure 4.24

Expanded trace of peak #5 in Figure 4.22. A is the experimental line which is assigned to the chain methyl group deuterons of 5CB-d_{11}. B and C are a theoretical fit using the dipolar coupling reported in the text. C is the stick spectrum predicted for three equivalent deuterons and B has been broadened by a Gaussian function to match the linewidth of A.

Gaussian broadened spectra. The major peaks in the stick spectrum are separated by 2D and, again assuming homogeneous broadening shifts these only slightly, a value for the methyl dipolar coupling of -128 Hz is determined.

We now estimate the order parameters for each segment from Equation (4.5). For those lines of Figure 4.21 with unresolved dipolar structure, $\Delta\nu_q^i$ was estimated from peak positions alone. Where some resolved dipolar structure exists, $\Delta\nu_q^i$ was calculated from the position of ν_q^i in the multiplet structure. The results are given in Table 4.6 along with a comparison with results obtained at a higher temperature by Emsley, et al. [101] for the same liquid crystal. The ratio of order parameters is nearly independent of segment number for these two sets of data. This would seem to indicate that the assumption of a single, conformationally independent order parameter for each chain segment is qualitatively correct. However, an extensive temperature dependence study of deuterium spectra from similar liquid crystals by Boden, et al. [102] indicated that, for the models chosen, individual methylene order parameters could not be simply related to a single molecular order tensor. Furthermore, the temperature dependence of the ratios $\Delta\nu_q^i/\Delta\nu_q^k$ could not be explained by assuming different conformations order equivalently and that the order tensor may be averaged independent of conformation.

As a final point, we note that a crude estimate of S_{zz} is possible from the order parameter for the first chain segment. From Equation (4.6), we have

$$|S_{zz}| = 2|S^1_{C-D}|\langle 3\ell^2_{azi} - 1\rangle^{-1}. \qquad (4.7)$$

Table 4.6

Chain Segment Order Parameters from the Deuterium NMR Spectrum of 5CB-d_{11}

Line #[a]	$\Delta\nu_q$[b]	$\lvert S_{CD}\rvert$[c] This work[d]	$\lvert S_{CD}\rvert$[c] Ref [101][e]	Ratio
1	55.0	0.218	0.185	0.848
2	40.8	0.162	0.134	0.829
3	38.3	0.152	0.125	0.823
4	27.7	0.110	0.090	0.820
5	20.0	0.080	0.065	0.818

[a] See Figure 4.22.

[b] Quadrupolar splitting in kHz. Calculated relative to dipolar structure peaks when resolved.

[c] Only the magnitude of the order parameter can be determined.

[d] Spectrum taken at 25.1°C.

[e] Spectrum taken at 31°C.

We assume the order tensor is diagonal in a frame whose z axis coincides with that of Figure 4.5. With a value of 109.5° for the C-C-D bond angle from the phenyl ring to methylene deuteron, and S^1_{CD} from Table 4.6, we find $|S_{zz}| \approx 0.66$.

4.3.2 Proton Multiple Quantum Spectrum

Figure 4.3 shows the proton multiple quantum spectrum of 5CB-d_{11} in the nematic phase at a regulated temperature of 26.0°C. A non-selective TPPI pulse sequence was used with the signal intensity distributed among all orders due to a resonance offset and field inhomogeneity during the preparation and detection periods. The TPPI phase increment used was 22.5° and Δt_1 was 1.0 μsec. No deuterium decoupling irradiation was applied. A total of six multiple quantum interferograms were collected for values of τ ranging from 0.4 to 1.4 msec and varying by 0.2 msec. Each had 16384 data points in both phase sensitive channels. For each τ, the channels were separately Fourier transformed (32 K points), and the magnitude spectra averaged together. The spectra from different values of τ were then averaged together to give the result shown in Figure 4.3. With this choice of parameters, the frequency resolution is 30.5 Hz/point. Linewidths are not the same for all lines with values ranging from about 150 to 210 Hz.

4.3.3 Analysis of the Proton Multiple Quantum Spectrum Assuming D_4 Point Group Symmetry

In a preliminary analysis [104], a set of couplings were derived from this spectrum assuming D_4 symmetry for the biphenyl group and using only selected five, six, and seven quantum lines. A total of 24 unique line assignments were made among these orders and an iterative fit performed by the least squares program MQITER described in the Appendix.

The final RMS error of the fit was 26.4 Hz. The resulting seven dipolar couplings are reported in Table 4.7. It should be noted that the definition of the dipolar coupling used in this thesis differs by a factor of two from that used in Table 1 of Sinton, et al. [104]. Also, the numbering in Table 4.7 is consistent with Figure 4.5. The theoretical line positions obtained for the six and seven quantum spectra are shown in Figure 4.25 along with expanded traces of these regions from Figure 4.3.

As a first attempt to analyze these couplings in terms of order parameters and structure, it was assumed that each ring has perfect hexagonal structure defined by the parameters of Table 4.5 [104]. Using coordinate system #1 of Figure 4.5, we see from Equation (B.4a) in the Appendix that D_{12} is given simply as

$$D_{12} = -\left(\frac{\gamma^2 h}{2\pi}\right) \frac{S_{zz}}{r_{12}^3} \quad .$$

and we obtain a value of 0.568 ± 0.001 for S_{zz}. The only two remaining parameters to determine are $(S_{xx} - S_{yy})$ and ϕ. In the original analysis [104], each of these was varied while holding the other constant to find a local minimum at $(S_{xx} - S_{yy}) = 0.057 \pm 0.002$ and $\phi = 32 \pm 1°$. The reported errors were estimated from the shape of the RMS deviation curve for the computed couplings close to this minimum and may not be entirely realistic. The order parameters agree well with those reported by Emsley, et al. [103] for 5CB-d_{15}, considering the difference in temperature at which their values were obtained.

We can use a least squares treatment to fit calculated to experimental couplings when several of the parameters of Equation (4.2) are

Table 4.7

Experimental Coupling Constants for 4-Cyano-4'-n-pentyl-d_{11}-biphenyl Assuming D_4 Biphenyl Symmetry

Proton Dipolar Couplings[a] (Hz)		Proton Scalar Couplings[b] (Hz)	
D_{12}	-8956 ± 3	J_{12}	8.0
D_{13}	94 ± 4	J_{13}	0.0
D_{14}	760 ± 6	J_{14}	2.0
D_{15}	-294 ± 4	J_{15}	0.0
D_{16}	-729 ± 4	J_{16}	0.0
D_{23}	780 ± 5	J_{23}	2.0
D_{26}	-3481 ± 5	J_{26}	0.0

[a] Errors have been estimated from RMS fit of the iteration and procedure given in Appendix A.

[b] Assumed values.

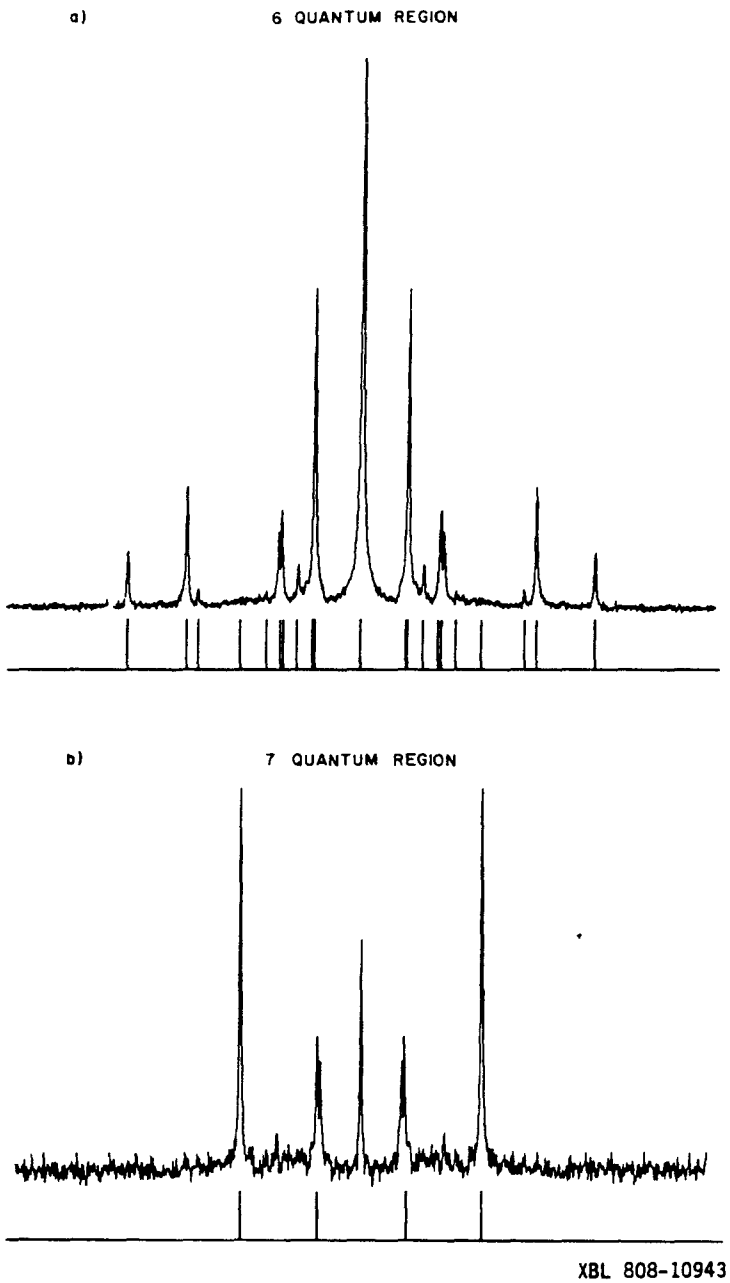

Figure 4.25

Six and seven quantum regions of the proton multiple quantum spectrum of 5CB-d_{11} (see Fig. 4.3). Each trace shows a total width of 62.5 kHz. The frequency markers below each experimental trace show the best fit calculated spectrum assuming a D_4 symmetry for the biphenyl group and resulting in the couplings of Table 4.7. The central line in the center of the seven quantum spectrum is a result of pulse imperfections and lack of decoupling in the experiment.

allowed to vary independently. Program BIPH5PARA was written for this purpose and is described fully in the Appendix. Iterations in which all seven parameters of Equation (4.2) were varied independently failed to converge to a final fit. Several couplings depend strongly on a number of these parameters and so may cause an early divergence unless the initial parameters are fairly close to a minimum RMS deviation from experimental couplings. We have seen in Figure 4.15 that six quantum transitions vary little with r_{14} and so this distance was fixed at 4.299 Å. BIPH5PARA was used to fit the remaining parameters with a final RMS deviation for the calculated couplings of 10.1 Hz, somewhat lower than the original two parameter fit [104]. The results are listed in Table 4.8.

The most striking aspect of this fit is the large increase of r_{260} and decrease in ϕ from the values for the benzene ring geometry fit reported using Table 4.5. Allowing r_{260} to increase would be expected to cause ϕ to decrease as the steric hindrance between protons ortho to the ring bridge is lessened. The distance r_{260} has been determined in the solid and gas phases by X-ray and electron diffraction measurements [80, 85-86]. Typically, a value of about 1.8 Å was found with a spread of about 10%. The value in Table 4.8 is then somewhat larger than might be expected.

In considering the possible causes for this unusually large ring separation, we might suspect the lack of vibrational averaging of calculated couplings. The parameters of Table 4.8 were derived from a model which does not include an average of couplings over small amplitude vibrational excursions of the nuclei. Thus, the distances reported are not necessarily their equilibrium values. In their analysis of the proton spectrum of 5CB-d_{15} (alkyl chain and adjacent ring deuterated), Emsley

Table 4.8

Biphenyl Structure and Order Parameters for 5CB-d_{11} Determined with Assumption of D_4 Symmetry[a]

Internuclear Distances (Å)		Order Parameters[c]	
r_{12}	2.47 ± 0.02	S_{zz}	0.565 ± 0.010
r_{14}	4.299[b]	$(S_{xx}-S_{yy})$	0.071 ± 0.007
r_{23}	4.27 ± 0.03		
r_{260}	1.98 ± 0.03		
Dihedral Angle (degrees)			
ϕ_m	30.4 ± 0.2		

[a] Errors estimated by methods described in Appendix A.

[b] Fixed at assumed value.

[c] For coordinate system #1 of Figure 4.5.

and co-workers found that the inclusion of vibrational averaging significantly affected their results [103]. To model the vibrations of the liquid crystal rings, this group used the normal mode analysis of 4,4'-bipyridyl as an approximation. Only three independent numbers could be determined from this spectrum and so it was not possible to derive values for all the parameters required to describe the ring structure. Infrared spectra of 5CB-d_{11} have been reported [105], but no normal mode analysis has been carried out. Thus, no vibrational averaging has been included in any analysis reported here.

In addition to averaging the couplings over small amplitude vibrations, the effect of a continuous torsional motion of the rings about ϕ might be required. Rigorously, this would require a solution to the quantum mechanical Schrodinger equation. The potential for the motion can be approximated as an expansion in a Fourier series by [112]

$$V(\phi) = \sum_{k=1}^{\infty} \frac{V_{2k}}{2} (1 - \cos 2k\phi) \qquad (4.8)$$

Obviously, there are not enough couplings to determine all of the parameters of Equation (4.3) and more than a few of the coefficients of Equation (4.8). Assumptions about the structure or reasonable values for the first few coefficients in $V(\phi)$ and neglect of higher order terms is required. The Schrodinger equation could then be written in a form having solutions in terms of Mathieu functions [112]. In a much simpler approach used for 4,4'-bipyridyl [93] and 4,4'-dichlorobiphenyl [96], the probability distribution function for ϕ was assumed to be a Boltzmann distribution. In both studies, only small changes in the averaged couplings were found. The magnitude of the corrections for 5CB-d_{11}

estimated from these results would be below the level of precision in the couplings determined from the available resolution in the spectrum. In the studies cited above, it was assumed that the order tensor is independent of ϕ and so may be removed from the averaging of couplings as discussed in Chapter 2. This assumption might affect the final value obtained for $\underset{\approx}{S}$ and so be invalid for 5CB-d_{11}. Without a knowledge of a possible dependence on ϕ for $\underset{\approx}{S}$, not averaging the couplings over the internal rotation can not be eliminated as a possible source of error in any final fit.

Figure 4.25 shows the resulting theoretical line frequencies for the six and seven quantum transitions. We also calculated the magnitude of exact τ averaged signal intensities for the five, six, and seven quantum spectra. The computer program mentioned in Chapter 3 and written by J. Murdoch was used with the couplings of Table 4.7. The results are shown in Figures 4.26, 4.27 and 4.28. The fits of intensity patterns to the experimental spectra are fairly close but differences do exist. These differences are most likely due to the exclusion of chemical shifts and heteronuclear couplings with the chain deuterons from the calculation. As we saw in Chapter 3, when chemical shifts are present in a strongly coupled spin system, the π pulse used for a 2D spin echo experiment will change the intensity coefficient for each line in the spectrum relative to its free evolution intensity coefficient. The extent of the change is determined by the relative sizes of the linear chemical shift Hamiltonian, which is partially refocussed by the action of the π pulse, and the bilinear coupling Hamiltonian, which is unaffected by it. In the absence of deuterium Larmor frequency r.f. pulses, the Hamiltonian for proton-deuteron couplings causes a density matrix evolution for the proton spins

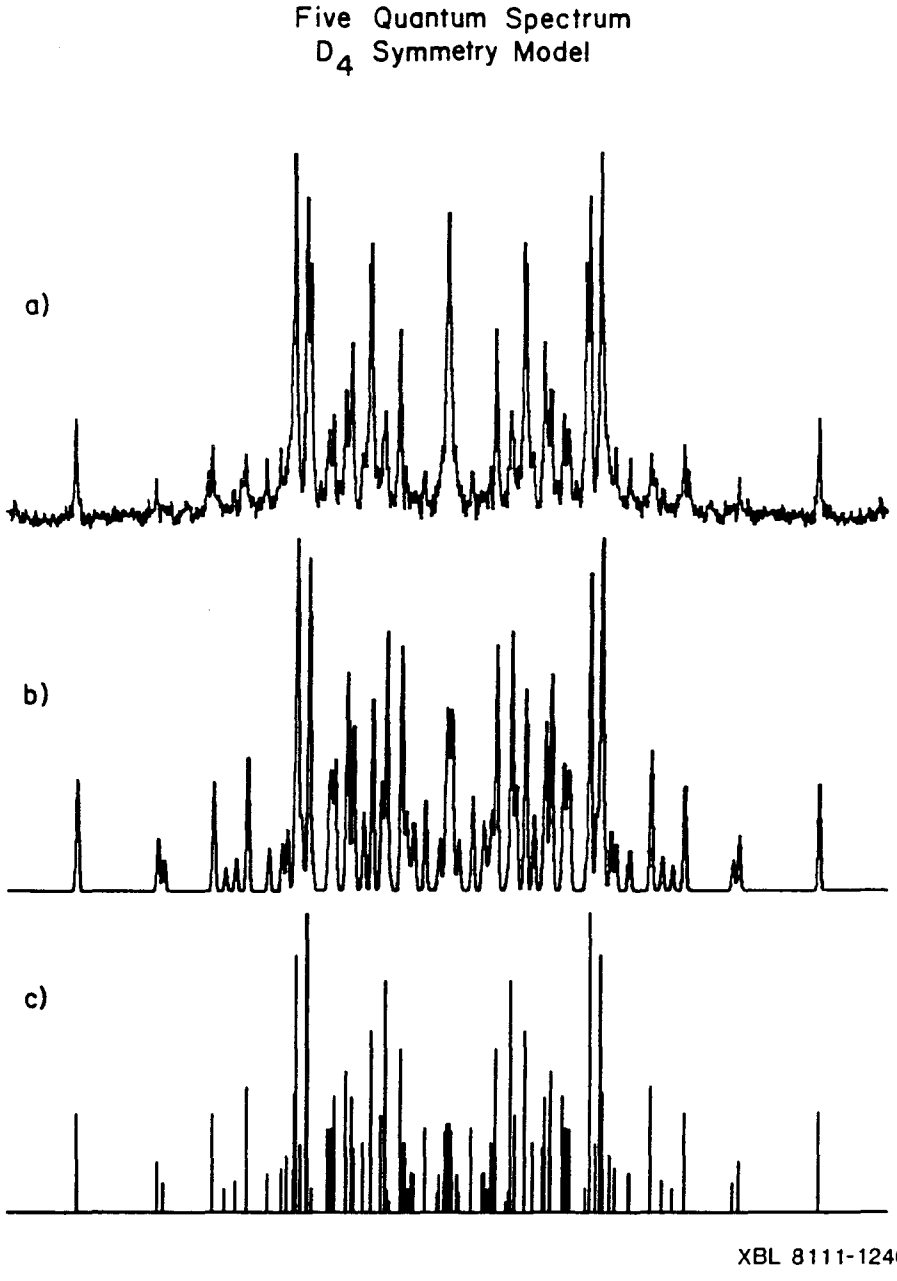

Figure 4.26

Five quantum spectral fit assuming D_4 symmetry for the biphenyl group in 5CB-d_{11}. In a) the experimental spectrum for the five quantum region of Figure 4.3 is shown on an expanded scale. Total frequency width shown is 62.5 kHz. b) and c) show the theoretical spectra calculated from the best fit couplings of Table 4.7 with intensities from exact dynamical calculations of the density matrix using values of the preparation time from the experiment. In b) the spectrum has been broadened to match the linewidth of the experimental transitions.

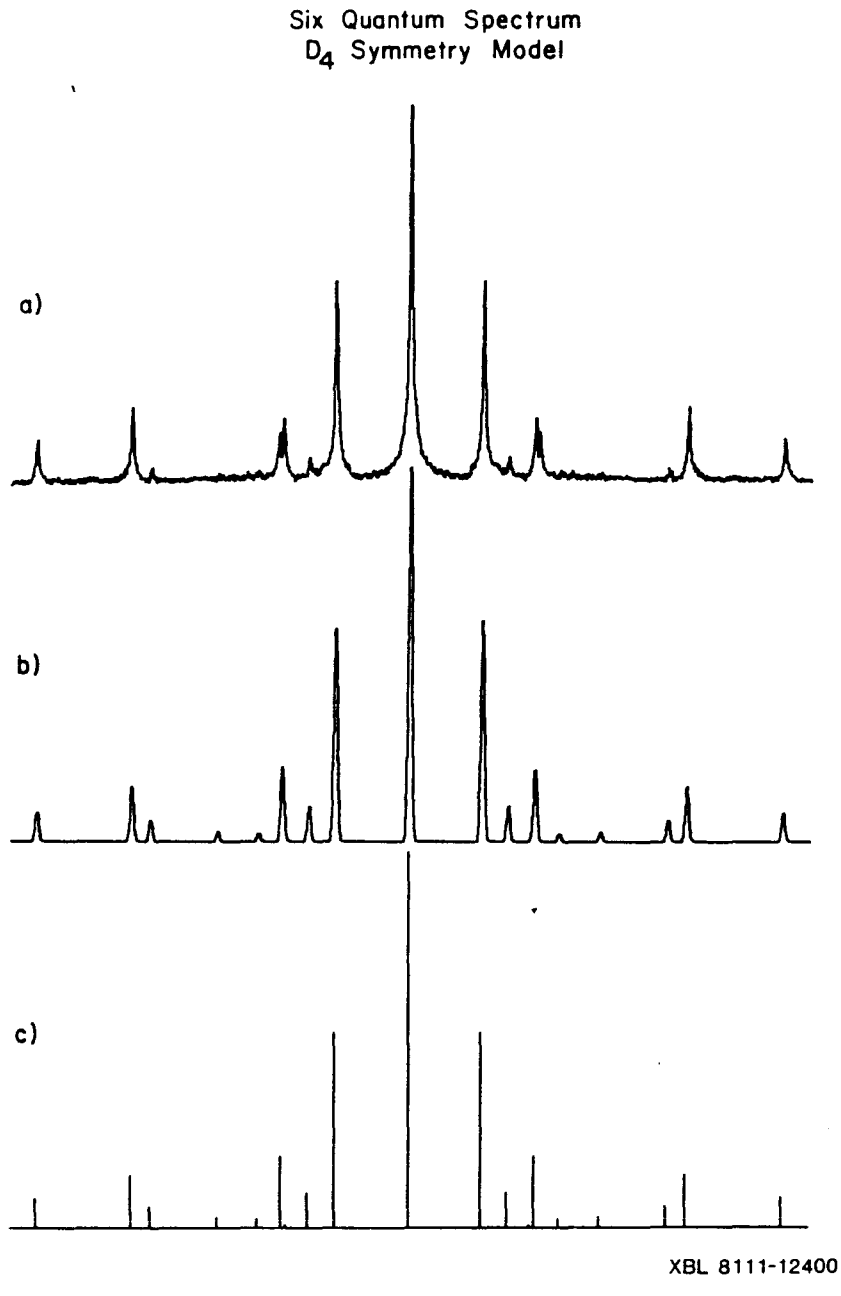

Figure 4.27

Six quantum spectral fit assuming D_4 symmetry for the biphenyl group in 5CB-d_{11}. a) Expanded trace from Figure 4.3. Total width shown is 44189 Hz. b) and c) show the theoretical fit with intensities calculated from exact dynamics of the density matrix using values for the preparation time from the experiment. The broadened linewidth in b) matches that of the experimental lines in a).

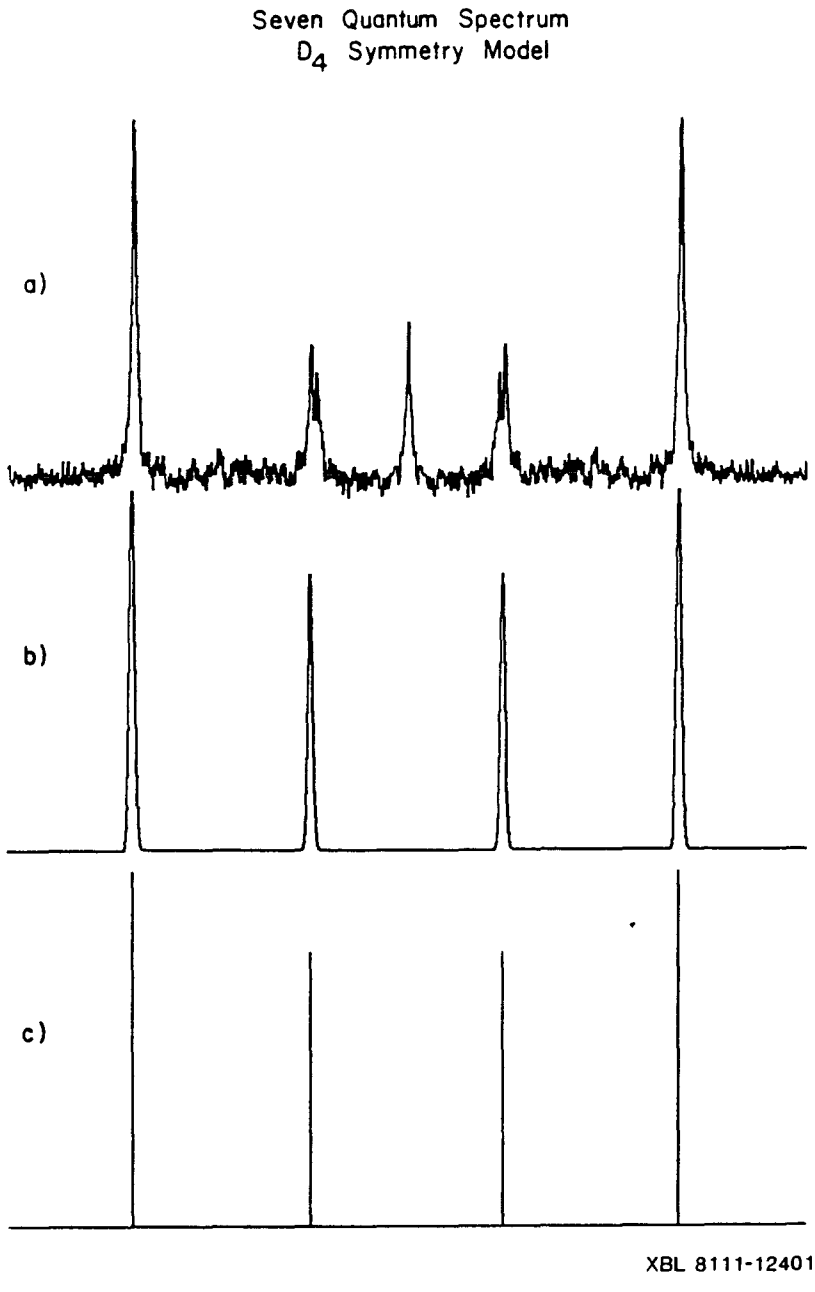

Figure 4.28

Seven quantum spectral fit assuming D_4 symmetry for the biphenyl group in 5CB-d_{11}. a) Expanded trace of experimental seven quantum region with a total width of 31982 Hz. The central line is due to pulse imperfections in the experiment. The intensities of b) and c) are from exact dynamical density matrix calculations. The broadening in b) matches the linewidths of the outer transitions in a).

similar to their chemical shift Hamiltonian. The evolution from these heteronuclear couplings is not entirely refocussed by a single proton π pulse and will cause intensity distortions in the same manner as the chemical shifts. Thus, because no deuterium decoupling was used in this experiment and with the presence of proton chemical shifts, intensities calculated from just proton homonuclear couplings are not expected to match the experimental spectrum exactly. However, these homonuclear couplings certainly dominate the spin Hamiltonian for 5CB-d_{11} and so a qualitative fit is found in Figures 4.26, 4.27, and 4.28. The extent to which couplings are precisely determined in the theoretical model also affects the quality of the intensity fit.

4.3.4 Additional Structure in the Proton Multiple Quantum Spectrum of 5CB-d_{11}

It has been noted that some of the splittings in the high order proton spectra of 5CB-d_{11} cannot be explained on the basis of this simple D_4 symmetry approach [104]. For example, close inspection of the seven quantum spectrum in Figure 4.25b indicates that the inner pair of lines is split into two pairs. Also, only one of the lines in a closely spaced doublet of the six quantum spectrum fits the theoretical transitions. These lines were not assigned in the simulation and so are not reflected in the RMS error reported above.

There are several possible sources of this added structure to consider. For example, we demonstrated in Chapter 3 that the presence of chemical shifts in a two-dimensional spin echo experiment will cause additional lines to appear in the ω_1 spectrum. In a similar manner, heteronuclear couplings may cause splittings of transitions or new lines to appear when a π pulse is used. Finally, since the pentyl and cyano groups are certainly not equivalent, a D_2 symmetry model may be required to explain the high order spectra of 5CB-d_{11}.

4.3.4.1 Estimation of the Effect of Chemical Shifts

We can confidently ignore chemical shifts as the cause of a closely spaced pair of lines in the seven quantum spectrum. To see how this is so, we consider a much simpler spin system for convenience in computation. If the permutation group for the couplings of a three spin system has C_2 symmetry, then the inclusion of a chemical shift difference between the two spins exchanged by the C_2 operation and the third spin does not change this permutation group [79]. Such a spin system is classified as AB_2. For a three spin-1/2 AB_2 system, the eigenstates are classified as either symmetric or antisymmetric under exchange of the B spins. The dimensions of the Zeeman manifolds of the symmetric states for M = -3/2, -1/2, 1/2, 3/2 are 1, 2, 2, 1, respectively. There are only two antisymmetric states, one each for M = -1/2 and 1/2. The six symmetric states form a system similar to the M = $\pm$4 and M = $\pm$3 manifolds of the D_4 symmetrized energy level diagram of Figure 4.6. Like an AB_2 system, inclusion of the chemical shift Hamiltonian for a para-substituted biphenyl does not change the symmetry from D_4 or D_2. The D_4 point group M = $\pm$3 spin functions, schematically represented in Figure 4.7, are symmetric under exchange of the labeled ortho or para sites, similar to the AB_2 system states described above. For an AB_2 oriented system, we predict two transitions in the two quantum spectrum obtained without an evolution period π pulse. This is analogous to the seven quantum predictions for the D_4 point group eight spin system given in Table 4.2. Thus, along with the results of Section 3.4, we can use a simple AB_2 system to model the behavior of a seven quantum spin echo spectrum of a D_4 symmetry biphenyl. Analytical expressions for the oriented AB_2 energy levels can be obtained from the solution for the single quantum spectrum givey by Emsley, et al. [111].

Figure 4.29 shows theoretical two quantum spectra for an AB_2 system in which the chemical shift difference, δ_{AB}, is small compared to the dipolar couplings. The intensities are an average for 2000 values of τ from 0.05 to 100 msec. Figure 4.29a shows the four line spectrum expected when no spin echo π pulse is used during the evolution period. Figure 4.29b shows the resulting two quantum spectrum when a π pulse is used to refocus the chemical shift and inhomogeneous evolution. The equations of Section 3.4 and the computer program described there were used to calculate both the frequencies and intensities for Figure 4.29. The chemical shift is removed by the π pulse and small new lines appear centered between transitions on either side of the two quantum resonance offset (0 Hz in Fig. 4.29). The largest transitions, at frequencies shifted only slightly from those predicted when $\delta_{AB} = 0$, are not split by the action of the π pulse (see Fig. 4.29b).

A similar situation is found in the seven quantum spectrum of 5CB-d_{11}. Computer calculations using the couplings of Table 4.7 and a reasonable range of values for the chemical shift difference between ortho and meta protons confirm this behavior. Additional lines from coherence transfers caused by the π pulse are indeed centered at the average of the transition frequencies on either side of $7\Delta\omega$. The exact τ averaged relative intensities of these additional lines is small and they cannot be observed in the seven quantum spectrum of Figure 4.25b. This trend is also found in the lower order spectra. We conclude that a non-zero chemical shift difference is not the cause of lines that cannot be explained by a D_4 symmetry model in the six and seven quantum spectra. The calculations also support the neglect of a chemical shift parameter in the analysis of transition frequencies in the TPPI echo spectrum. A single π pulse should

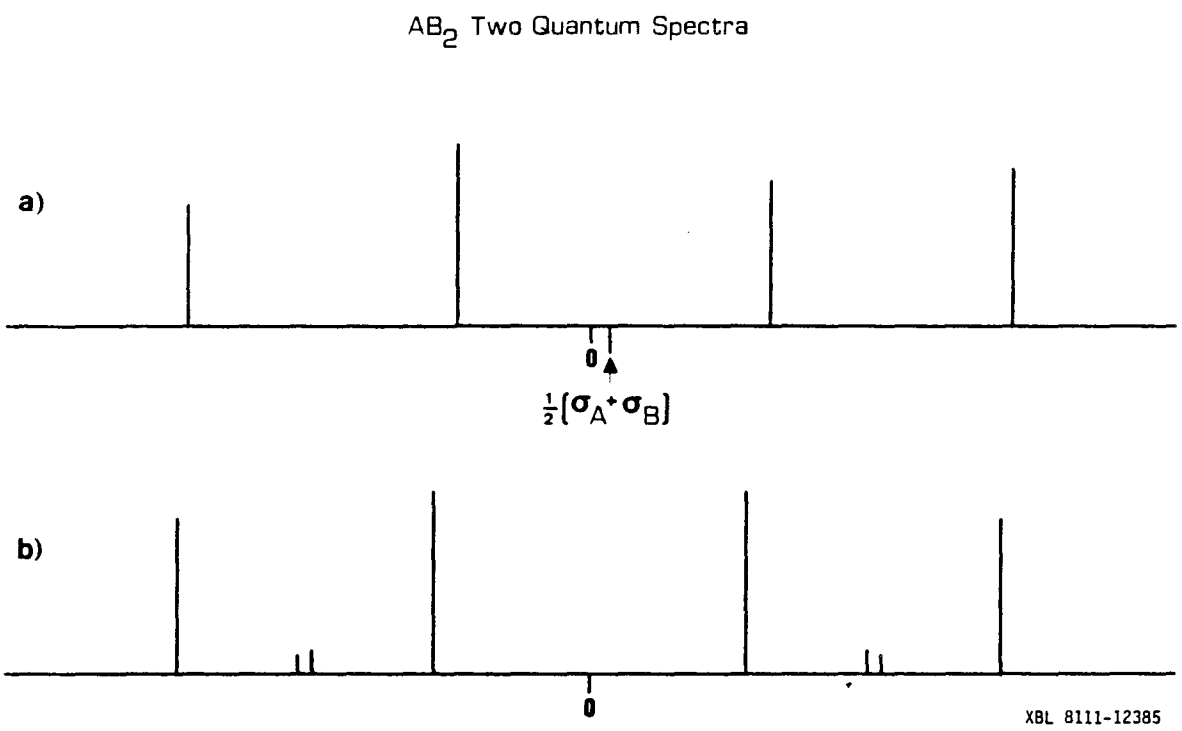

Figure 4.29

Calculated two quantum spectra for an anisotropically ordered AB_2 spin-1/2 system. Each spectrum is an average for 2000 values of the multiple quantum preparation time τ. a) Predicted spectrum when the chemical shift difference is not refocused by the application of a π pulse. b) When a π pulse is used, the frequency shifts relative to 0 caused by the chemical shift are removed and new lines with low intensities are predicted centered about the average of the major lines. Parameters used in the calculation are (in Hz) $D_{AB} = 1000$, $D_{BB} = 250$, $J_{AB} = 10$, $\delta_A = 100$, and $\delta_B = 0$.

be adequate to remove the chemical shift evolution unless the shift differences for ring protons in 5CB-d_{11} are inordinately large.

4.3.4.2 The Effects of Heteronuclear Couplings

Heteronuclear couplings between the ring and chain spins may also complicate the spectrum when a single π pulse is used during multiple quantum evolution. For certain special symmetries, a π pulse can be shown to decouple a single deuteron from several strongly coupled protons in the ω_1 spectrum of a two-dimensional experiment with an oriented sample [110]. A partial decoupling of the chain deuterons will occur for the proton TPPI experiment of 5CB-d_{11} but remaining heteronuclear dipolar structure could possibly exist on the proton transition lineshapes. The π pulse may reduce this structure to the point that it cannot be resolved in the fairly wide lines of Figure 4.3. An estimate of the exact line shape is difficult without a knowledge of the couplings involved. Using standard bond lengths and angles we can estimate the largest possible static dipolar coupling between a deuteron on the first chain methylene and a proton ortho to the chain-ring bond to be on the order of a few kilohertz. The actual coupling will be greatly reduced by $S_{zz} < 1.0$ and internal molecular motions. In fact, the power requirements for deuterium double quantum decoupling of the single quantum proton spectrum imply that this coupling is on the order of a few hundred hertz (see below). The seven quantum transitions of 5CB-d_{11} at 26°C occur at about 4 and 10 kHz relative to the center of the order and are sensitive to sums of a number of the proton-proton couplings. Thus, the magnitude of the heteronuclear coupling partially refocused by the π pulse is much smaller than the characteristic evolution frequencies in this order and a lack of deuterium decoupling in the experiment may not

be responsible for the added structure not explained by a simple D_4 symmetry model. However, these crude estimates do not allow us to unequivocally adopt this conclusion. Heteronuclear couplings can be scaled even further by the use of multiple π pulses during t_1 [59] or eliminated completely by a number of decoupling schemes. An attempt to decouple the chain deuterons from the proton multiple quantum spectrum of 5CB-d_{11} by using deuterium double quantum transitions is described below.

4.3.4.3 D_2 Symmetry Model

Finally, the effects of inequivalently distorted rings and a non-zero, off-diagonal element in the order tensor, which cause an effective D_2 symmetry for the protons in 5CB-d_{11}, were considered. Several sets of initial parameters were used for iterations in which the twelve unique dipolar couplings were allowed to vary independently. The final RMS error reported above for the D_4 symmetry iteration (26.4 Hz) is already below the digital resolution in the spectrum of Figure 4.3. Several attempts using initial D_2 couplings produced final fits somewhat better than this. However, the limited precision from the spectrum makes it difficult to judge which of these represents a better model for the biphenyl group in 5CB-d_{11} than the one discussed above. We saw earlier that if the distortions from D_4 symmetry are not too severe, in addition to some new transitions, there will be many near degeneracies which would not be resolved in the linewidths of a spectrum such as that of Figure 4.3. Thus the amount of new information in the high order spectra available to distinguish D_2 from D_4 couplings may not be sufficient. The number of parameters to obtain from nearly the same amount of information has increased significantly.

Many different sets of initial couplings modeled by assuming slight distortions in the rings and a finite value for S_{xy} were used in attempts to fit the five, six, and seven quantum spectra of 5CB-d_{11}. These D_2 symmetry iterations exhibit general trends in the final parameters derived. The r_{14}, r_{23}, r_{58}, and r_{67} parameters usually change significantly from those found in the D_4 symmetry fit. As an example, the best fit couplings for an iteration using the same 24 line assignments as the D_4 calculation described above, but allowing the 12 sets of couplings which are unique for D_2 symmetry to vary independently, are given in Table 4.9. The final RMS error of the fit from this iteration is 13.5 Hz. All the couplings have changed significantly from the D_4 couplings in Table 4.7. In particular, the couplings with the largest errors, D_{14}, D_{23}, D_{67}, D_{58}, are considerably different. Theoretical stick spectra for the five, six, and seven quantum regions, along with the experimental traces, are shown in Figures 4.30, 4.31, and 4.32.

Least squares iterations using program BIPH5PARA and varying all eleven of the D_2 molecular parameters of Equation (4.3) independently failed to converge to a final fit. We then assumed the value of one of these parameters. Two cases are considered here, with the results given in Table 4.10. The final RMS deviations of calculated from experimental couplings was 6 Hz for both cases. In case A, r_{260} was fixed at the value found for biphenyl from X-ray studies, i.e., $r_{260} = 1.818$ Å. All the parameters have changed significantly from those found with a D_4 model. The largest errors among the r_{ij}'s occur for those pairs of nuclei whose dipolar couplings are poorly determined (cf. Table 4.9). The distortions from a benzene geometry for the phenyl rings implied by these results are quite severe and do not seem realistic. Typical

Table 4.9

Experimental Coupling Constants for 5CB-d_{11} Assuming D_2 Symmetry

Proton Dipolar Couplings[a] (Hz)		Proton Scalar Couplings[b] (Hz)	
D_{12}	-8920 ± 6	J_{12}	8.0
D_{13}	144 ± 8	J_{13}	0.0
D_{14}	926 ± 9	J_{14}	2.0
D_{15}	-299 ± 4	J_{15}	0.0
D_{16}	-817 ± 6	J_{16}	0.0
D_{23}	581 ± 14	J_{23}	2.0
D_{25}	-719 ± 5	J_{25}	0.0
D_{26}	-3441 ± 4	J_{26}	0.0
D_{56}	-9000 ± 4	J_{56}	8.0
D_{57}	139 ± 4	J_{57}	0.0
D_{58}	635 ± 9	J_{58}	2.0
D_{67}	915 ± 10	J_{67}	2.0

[a] From iteration of 5, 6, 7 quantum lines. Errors estimated by method given in Appendix.

[b] Assumed values.

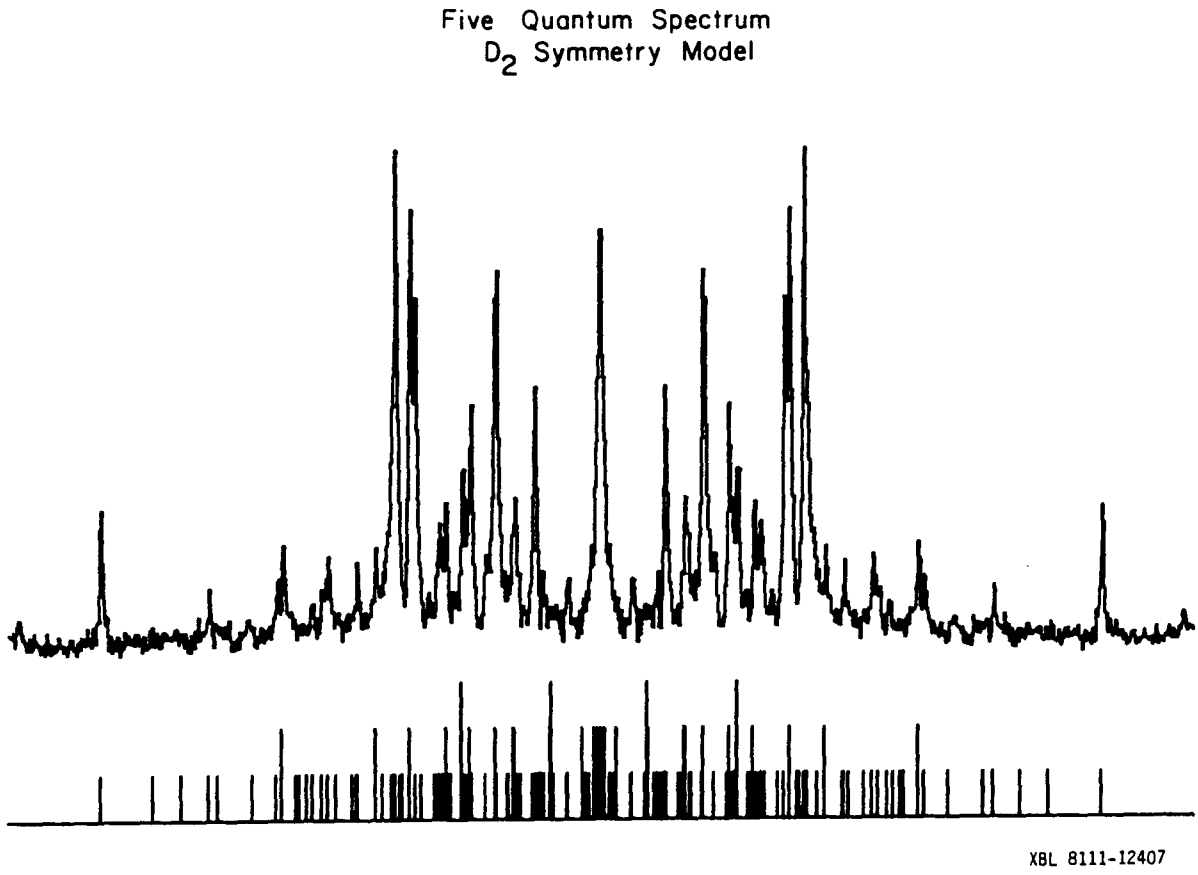

Figure 4.30

Five quantum spectrum of 5CB-d_{11} plotted with a total width of 62.5 kHz. Beneath the experimental trace is shown a stick spectrum calculated from the best fit couplings of Table 4.9, assuming a D_2 symmetry for the biphenyl group. Line heights for the theory are based on frequency degeneracies only.

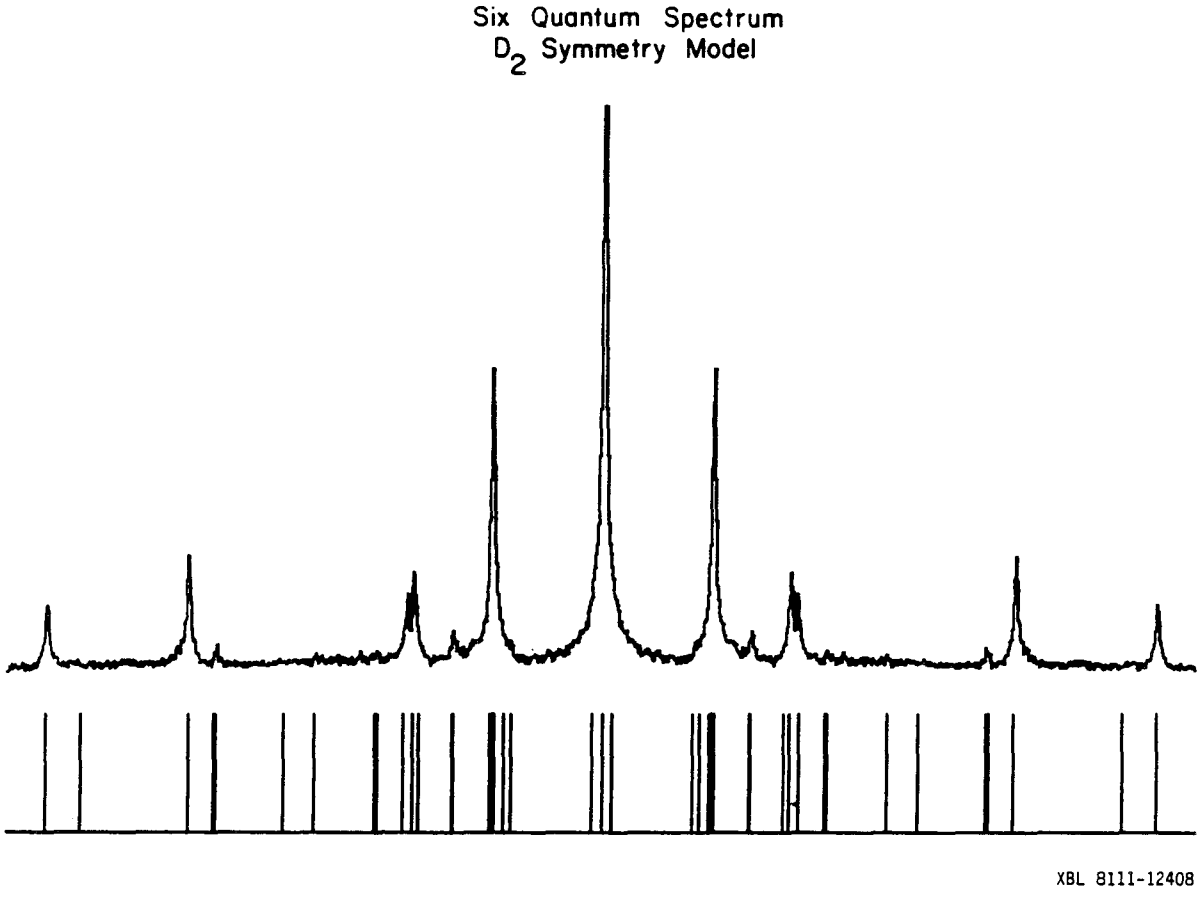

Figure 4.31

Six quantum spectrum of 5CB-d_{11} plotted with a total width of 44189 Hz. Beneath the experimental trace is shown a stick spectrum calculated from the best fit couplings of Table 4.9 assuming a D_2 symmetry for the biphenyl group. All theoretical lines are of unit height.

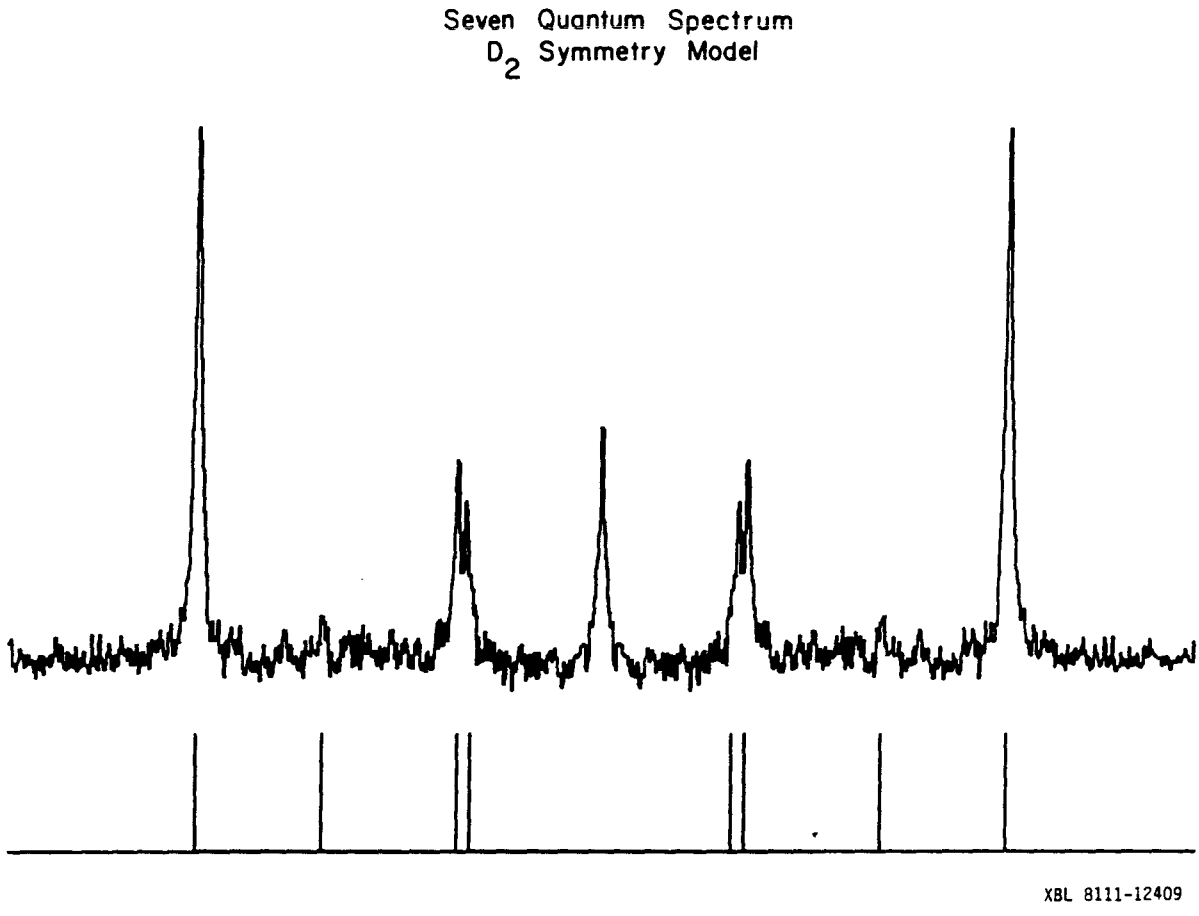

Figure 4.32

Seven quantum spectrum of 5CB-d_{11} plotted with a total width of 31982 Hz. Beneath the experimental trace is shown a stick spectrum calculated from the best fit couplings of Table 4.9 assuming a D_2 symmetry for the biphenyl group. The theoretical lines are all given unit height. The central line in the experimental spectrum is a result of pulse imperfections and the use of a π pulse without deuterium decoupling during multiple quantum evolution.

Table 4.10

Best Fit Structures and Order Parameters for 5CB-d_{11} Determined from Couplings of Table 4.9[a]

	CASE A	CASE B
	Internuclear Distances (Å)	
r_{12}	2.32 ± 0.05	2.453 ± 0.003
r_{14}	3.88 ± 0.09	4.11 ± 0.03
r_{23}	4.54 ± 0.09	4.81 ± 0.03
r_{56}	2.32 ± 0.04	2.456 ± 0.003
r_{58}	4.41 ± 0.17	4.67 ± 0.10
r_{67}	3.90 ± 0.13	4.14 ± 0.06
r_{260}	1.818[c]	1.93 ± 0.04
	Order Parameters[b]	
S_{zz}	0.48 ± 0.03	0.565[c]
$(S_{xx}-S_{yy})$	0.02 ± 0.02	0.03 ± 0.02
S_{xy}	0.007±0.007	0.008 ± 0.008
	Dihedral Angle (degrees)	
ϕ_m	28.9 ± 0.5	28.9 ± 0.5

[a] Errors estimated by methods in Appendix A.

[b] For coordinate system #2 of Figure 4.5.

[c] Fixed at assumed value.

distortions in internuclear distances found from NMR studies of solutes in liquid crystals are on the order of a few percent. The largest distortion from the benzene values in Table 4.10 for case A occurs for r_{14} and is nearly 10 percent.

The value of S_{zz} for case A in Table 4.10, using coordinate system #2, has changed significantly from that obtained using the D_4 symmetry model given in Table 4.8. Since the z axes of the two axis systems for D_2 and D_4 symmetries are parallel, these are expected to be the same. Thus, for case B, S_{zz} was fixed at the value obtain for the D_4 model while the other parameters were varied to obtain the best fit values given in Table 4.10. Several of the r_{ij} values are reasonably close to those obtained using the D_4 model and have smaller error limits than for case A. However, the distortions implied by values for r_{14}, r_{23}, r_{58}, and r_{67} still seem unreasonable. The remaining parameters are found to be essentially the same as for case A. Whether the results in Table 4.10 for case A or case B more accurately fits the actual parameters for 5CB-d_{11} cannot be determined from our analysis.

We have computed exact τ averaged theoretical intensities from the D_2 symmetry couplings of Table 4.9. The results for the six and seven quantum spectra are shown in Figures 4.33 and 4.34, respectively. The intensity patterns do not seem to reproduce the general features of the experimental spectra as well as the D_4 model intensities of Figures 4.27 and 4.28.

The closeness of the fit for lines shown in Figures 4.30, 4.31, and 4.32, and the RMS error for the spectral simulation reported above may be somewhat misleading. Only transitions which are predicted from a D_4 model were used in the initial assignment. Additional lines in the experimental six and seven quantum spectra, which are assumed here to be

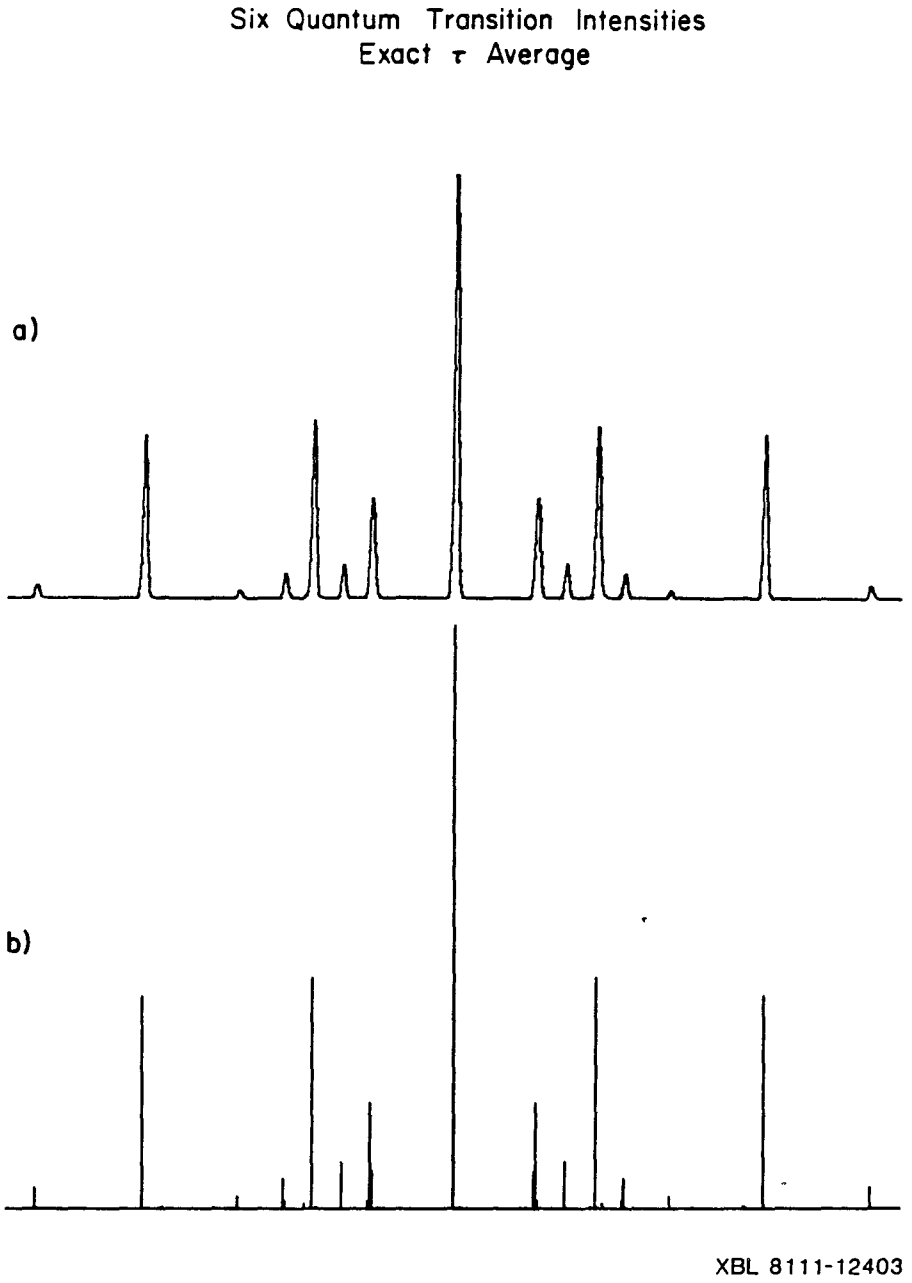

Figure 4.33

Theoretical six quantum spectra calculated from the D_2 symmetry couplings of Table 4.9. The intensities here are the result of an exact calculation of the multiple quantum signal averaged from the same values of the preparation time τ as those used in the experiment producing the spectrum of 5CB-d_{11} in Figure 4.3. Both a) and b) are plotted with the same width as Figure 4.31 and the broadening in a) is designed to match the experimental linewidth in that figure.

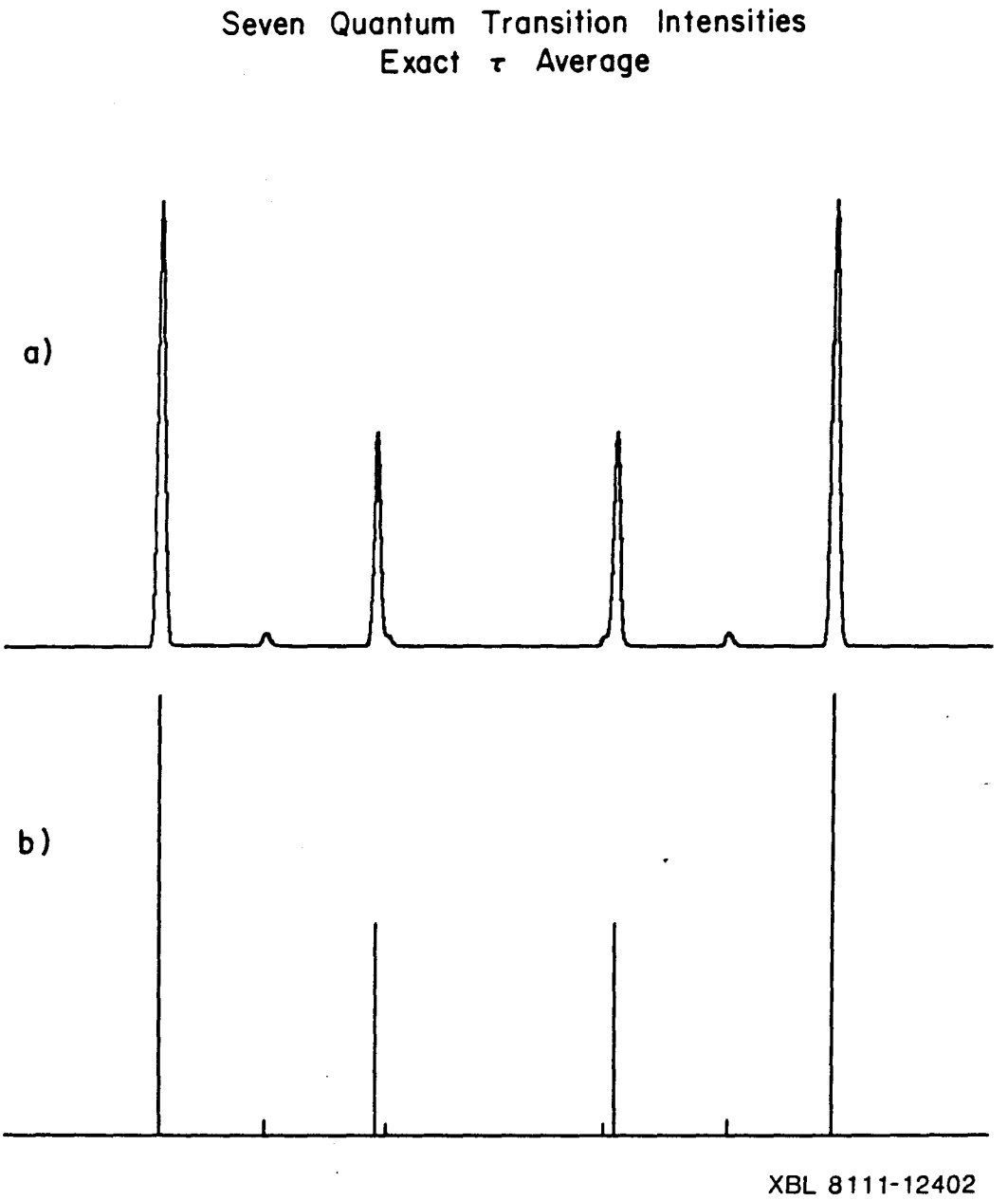

Figure 4.34

Theoretical seven quantum spectra calculated from the D_2 symmetry couplings of Table 4.9. As for Figure 4.33 the intensities are the result of an exact calculations using the same values of τ as for the experimental spectrum in Figure 4.3. Both a) and b) are plotted with the same width as Figure 4.32 and the broadening in a) is designed to match the experimental linewidth in that figure.

the result of symmetry lowering distortions, do not fit the theory spectrum as well as other transitions. When the two previously unassigned transitions of the six and seven quantum regions are included in the iteration, a final fit is obtained but with a significantly larger RMS error of about 60 Hz. The largest contributions to this error come from assignments for these additional lines. When the resulting couplings are interpreted for order parameters and structural quantities, distortions similar to those of Table 4.10 are found but with larger error limits.

In addition to real structural distortions as an explanation for an effective D_2 symmetry in the biphenyl group of 5CB-d_{11}, we investigated the possibility that the rings move inequivalently. This seems to be not entirely unreasonable as one ring has attached to it the light, unrestricting cyano group while the other moves relative to the bulky alkyl chain which presents steric hindrance due to the adjacent methylene group. A fit to the spectrum was obtained starting with the ring parameters from the D_4 symmetry analysis (Table 4.8) and varying all 12 D_2 couplings. The iteration was then repeated, allowing only the ring A (see Fig. 4.5) and inter-ring couplings to vary. Both models achieved adequate fits to the experimental five, six, and seven quantum spectra with the final RMS errors (~20 Hz) within the digital resolution of the Fourier transformed spectrum. When the resulting couplings were interpreted in terms of a model in which the rings are equivalently distorted but move inequivalently, only moderately close fits for the calculated couplings could be obtained. A fairly close fit (RMS = 18 Hz) was obtained from the set of 12 independent experimental couplings but then only when ring distortions were re-introduced. The resulting values for the internuclear distances resembled those of Table 4.10.

Several such models were tried, all with similar results. Adequate final fits for calculated couplings could only be obtained when inequivalent ring distortions were allowed. These results do not entirely preclude the possibility that the effective D_2 symmetry is due primarily to inequivalent ring motions as only the product of the order tensor with molecular parameters is obtained from the dipolar couplings. In addition, the probability distribution for the chain conformations will certainly affect the way the whole molecule orders and the proton spectrum from the biphenyl group is indirectly affected in a complicated manner that can not be entirely determined from the available spectral information in Figure 4.3. As a final note we point out that, in their analysis of the proton spectrum of 5CB-d_{15}, Emsley and co-workers also found exceptional distortions in r_{14} and r_{23} [103]. Due to the limited number of couplings which could be obtained from their spectrum, independent values for both parameters could not be found.

4.3.5 Deuterium Decoupling Experiments

There are many possible schemes available for decoupling of the proton spectrum of Figure 4.3. The choice is directed primarily by the same considerations as a normal single quantum spectrum. Double quantum deuterium decoupling was chosen because the r.f. power requirements are significantly less than for decopuling via single quantum transitions [109]. It was found that only a few kHz of deuterium r.f. field was required to decouple the single quantum spectrum with the result shown in Figure 4.2. This seems reasonable based on estimates for the largest heteronuclear coupling between ring protons and the first chain methylene deuterons. The deuterium r.f. field, ω_1, required to decouple a deuteron

with quadrupolar splitting ω_Q from a heteronucleus via double quantum transitions is given by [109]

$$\omega_1 \sim (\omega_Q \omega_D)^{\frac{1}{2}}$$

where ω_D is the dipolar coupling expressed in angular frequency units. The decoupling requirements cited above are then consistent with an ν_D of a few hundred hertz.

The multiple quantum spectrum was decoupled by applying deuterium irradiation at the center of the quadrupolar spectrum of Figure 4.21. The result is shown in Figure 4.35. There is a significant loss in signal-to-noise for this spectrum compared with Figure 4.3 which may be a result of two factors. First, the long deuterium pulse required to obtain each point in the multiple quantum signal may cause significant temperature gradients in the sample. This was reflected in the spectrum by a larger linewidth for transitions further from the centers of each order. This effect was partially circumvented by the use of smaller samples and longer delays between shots, as described in Chapter 5. The second cause for a lower signal-to-noise was the finite isolation of the spectrometer receiver from the high power deuterium transmitter. Even with good isolation of the probe circuits and the use of a narrow band filter before the receiver, several millivolts of deuterium r.f. at the receiver was difficult to avoid. This partially saturated the broadband preamp of the receiver causing the observed loss in signal-to-noise. This effect was most critical in the higher order regions of the spectrum where the integrated signal intensity is lower as we saw in Chapter 3. These problems complicated obtaining a spectrum with adequate signal-to-noise in the high quantum regions in a reasonable

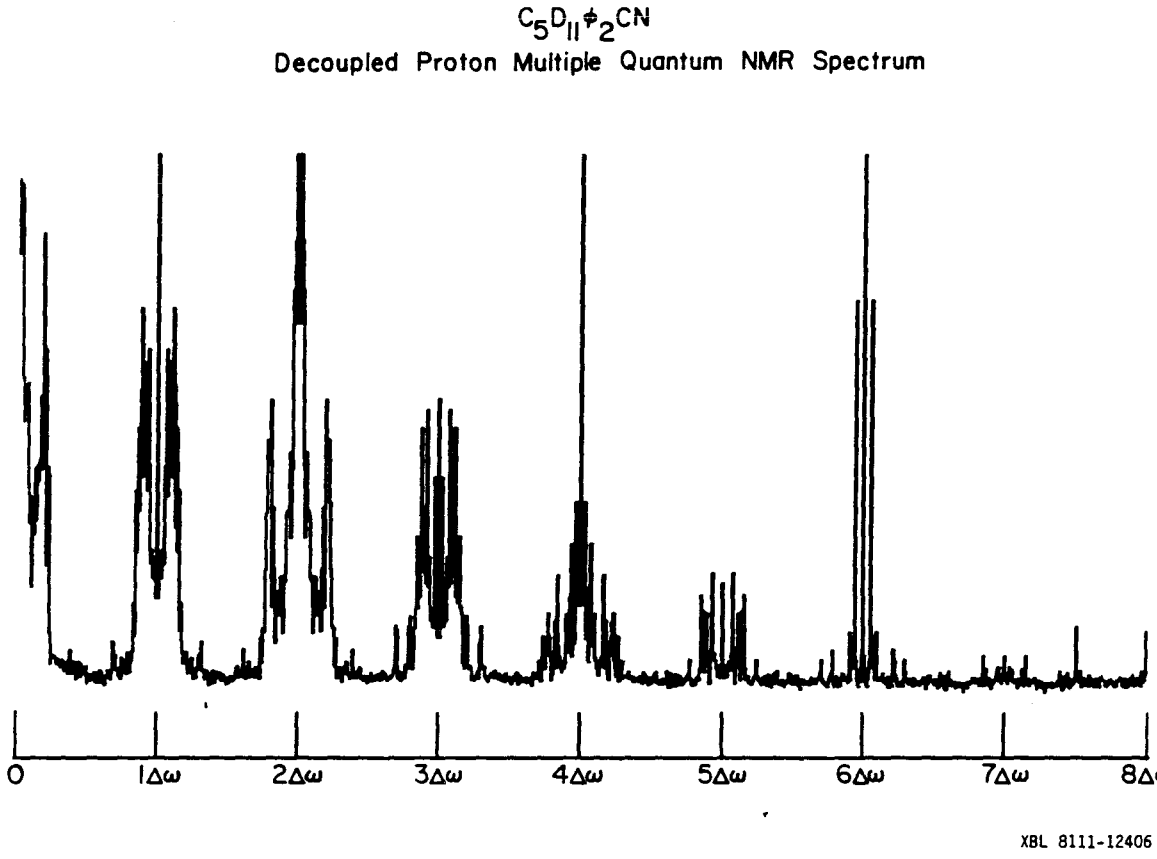

Figure 4.35

Deuterium decoupled proton multiple quantum spectrum of 5CB-d_{11} at 28.9°C. The spectrum is an average of six spectra obtained for six different values of τ from 0.2 to 1.2 msec with the same non-selective pulse sequence used to obtain the spectrum of Figure 4.3. Lines in the five, six, and seven quantum regions were used to obtain the couplings of Table 4.11. The total width shown is 500 kHz.

amount of overall acquisition time. Instrumental instabilities during decoupling experiments may also increase the two-dimensional "t_1 noise" present as a result of fluctuations in the prepared density matrix [69].

The spectrum of Figure 4.35 is the result of an average from six values of τ ranging from 0.2 to 1.2 msec in increments of 0.2 msec. Most of the experimental parameters were the same as for the undecoupled spectrum of Figure 4.3 except that the temperature was regulated at a slightly higher value of 28.9°C. The length of the multiple quantum t_1 signal was 16 K points in both phase sensitive channels for each τ and 32 K complex Fourier transforms were calculated. Figure 4.35 shows the resulting averaged magnitude spectrum. Linewidths are somewhat narrower than in the undecoupled spectrum with a typical value being 120 Hz.

4.3.5.1 D_4 Symmetry Model Analysis of Decoupled Multiple Quantum Spectrum

The poor signal-to-noise of the higher order spectral regions of Figure 4.35 makes an analysis more difficult than for an undecoupled spectrum. Nonetheless, a total of 13 lines were assigned in the five, six, and seven quantum regions for an iterative fit assuming D_4 symmetry couplings. The results are given in Table 4.11. The final RMS error of the fit for these lines was 21.2 Hz. The small number of lines which could be assigned in these orders leads to large error limits on the couplings in Table 4.11. As with the undecoupled spectrum, chemical shifts have been ignored in the analysis of this spin echo spectrum. The computed exact τ averaged line intensities for the six quantum transitions are shown along with an expanded trace of the six quantum region in Figure 4.36. Obviously, the fit is only marginally adequate. Broadening due to temperature gradients may be the cause of the lines with the greatest predicted intensity appearing with in fact the lowest intensity in the experimental spectrum.

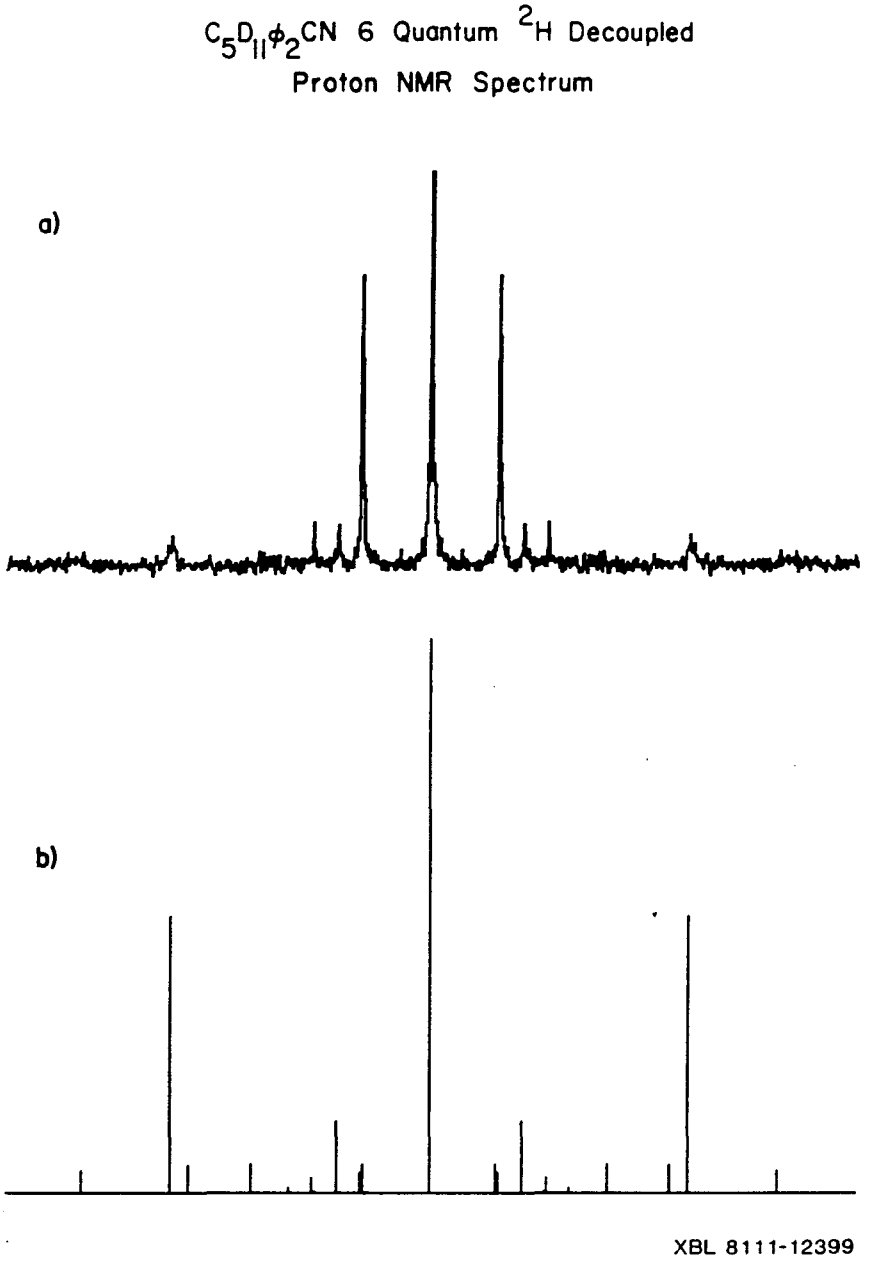

Figure 4.36

a) Expanded trace of the six quantum region of Figure 4.35. Total width shown is 44189 Hz. The central line is truncated in height. b) Theoretical spectrum calculated from the couplings of Table 4.11. Intensities are from an exact calculation using the same values of τ as in the experiment.

Table 4.11

Experimental Coupling Constants from the Deuterium Decoupled Proton Multiple Quantum Spectrum of 5CB-d_{11} Assuming D_4 Symmetry

Proton Dipolar Couplings[a] (Hz)		Proton Scalar Couplings[b] (Hz)	
D_{12}	-7818 ± 7	J_{12}	8.0
D_{13}	88 ± 8	J_{13}	0.0
D_{14}	577 ± 20	J_{14}	2.0
D_{15}	-226 ± 10	J_{15}	0.0
D_{16}	-653 ± 6	J_{16}	0.0
D_{23}	719 ± 12	J_{23}	2.0
D_{26}	-3057 ± 11	J_{26}	0.0

[a] Errors have been estimated from the RMS error of the iteration and the procedure given in Appendix A.

[b] Assumed values.

Despite the large error limits for the couplings of Table 4.11, a least squares analysis in terms of the parameters of Equation (4.2) for D_4 symmetry converged to a close fit. The final RMS deviation of calculated to observed dipolar couplings was only 3 Hz. The results are reported in Table 4.12. As with the D_4 model fit for the undecoupled spectrum of Figure 4.3, r_{14} was held constant at the value 4.299 Å for this calculation. Although the value of r_{260} is more in line with the value for biphenyl (1.818 Å) than the analysis of the undecoupled spectrum, ring distortion implied by r_{12} and r_{23} is quite severe. In addition, the value of ϕ_m has increased. It is not expected that a temperature increase of only 3° alone should cause such a change in ϕ_m. Perhaps the inclusion of vibrational or torsional averaging in the model would bring the two results more in line.

4.3.5.2 D_2 Symmetry Model Analysis for Decoupled Spectrum

Attempts to derive twelve unique D_2 symmetry dipolar couplings from just the 13 lines assigned in the higher order regions failed. The problem is only barely determined and so convergence may depend strongly on the closeness of the initially guessed couplings. If the iteration is started with the D_4 couplings of Table 4.11 then the RMS fit is already below the resolution in the Fourier transform spectrum, and so further improvement is unlikely. A more complete analysis may be possible when transition assignments in orders below the five quantum are included. For example, the decoupled spectrum shows a number of nearly resolved lines in the three and four quantum regions (see Fig. 4.35) which could be used. Such an analysis was not attempted in this work.

Table 4.12

Biphenyl Structure and Order Parameters for 5CB-d_{11} Determined from Couplings of Table 4.11 and Assuming D_4 Symmetry[a]

Internuclear Distances (Å)		Order Parameters[c]	
r_{12}	2.36 ± 0.03	S_{zz}	0.43 ± 0.01
r_{14}	4.299[b]	$(S_{xx}-S_{yy})$	0.06 ± 0.02
r_{23}	4.00 ± 0.10		
r_{260}	1.82 ± 0.05		
Dihedral Angle			
ϕ_m	$31.6 \pm 0.2°$		

[a] Errors estimated by methods of Appendix A.

[b] Fixed at assumed value.

[c] For coordinate system #1 of Figure 4.5.

4.3.6 Conclusions on Results for 5CB-d_{11}

As an example of the use of multiple quantum NMR, the spectra of 5CB-d_{11} demonstrate the utility of the approach. The higher order regions of the spectrum clearly show a greater simplicity than the single quantum spectrum. Line assignments can be made unambiguously when these orders are compared with spectra simulated from physically reasonable parameters. The symmetry characteristics of the biphenyl group are very simply related to the number of transitions which occur in the six and seven quantum spectra.

On the other hand, 5CB-d_{11} as an example demonstrates some of the limitations in the analysis of NMR spectra of oriented molecules. These limitations are present in both single quantum and multiple quantum NMR and are a result of the complexity of relationships between molecular structure and transition frequencies and not on the particular technique used to obtain the spectrum. For 5CB-d_{11}, the linewidths ultimately limit the level of precision available for couplings. Deuterium decoupling seems to reduce linewidths by at most only a factor of about two from the spin echo linewidths. This limit on the precision of couplings prevents an analysis refined beyond those presented in this work.

Of all the models which were used to explain the undecoupled five, six and seven quantum spectra of 5CB-d_{11}, the one which approximates the biphenyl proton symmetry as a D_4 point group system seems the most reasonable. The order parameters derived from the proton spectrum are in line with estimates from the single quantum deuterium spectrum of the alkyl chain and those obtained for 5CB-d_{15} [103]. The best fit molecular parameters of Table 4.8 for this model agree closely with

-ray and electron diffraction data for the internuclear distances of biphenyl, considering that no vibrational corrections have been applied. Theoretical transition frequencies calculated from this model fit most of the lines resolved in the higher orders with the RMS deviation well within the resolution of the Fourier transform. The calculated exact τ averaged transition intensities yield a qualitative fit to the experiment as shown in Figures 4.26, 4.27, and 4.28.

In contrast to this D_4 symmetry model, several models assuming an effective D_2 permutation symmetry for the biphenyl spins in 5CB-d_{11} yield molecular parameters which reflect large distortions in the phenyl rings. Because the transitions which are predicted by the D_4 model already fit the simulated spectrum within the available resolution, further slight improvements from the use of D_2 symmetry models do not allow an unequivocal choice for the best model. We have also seen that very slight symmetry breaking distortions perturb the spectrum in a manner resulting in a paucity of additional information with which we must determine the increased number of parameters of the lower symmetry model. Transitions in the high order spectra which are not predicted by a D_4 symmetry model are not as closely fit by the D_2 symmetry models considered here as other transitions.

We have tried to model the high order spectra of 5CB-d_{11} by considering cases where there are real structural differences between the rings or the rings experience inequivalent mobilities while undergoing internal motions. The data do not allow us to exclude the latter possibility, but seem to require real structural deformations of the rings to achieve the closest fits. In addition, we have considered the effects of proton chemical shifts and heteronuclear couplings on the multiple quantum spin

echo spectrum. We have presented arguments which demonstrate that chemical shifts are not responsible for the additional structure in the six and seven quantum regions. However, we are unable to do the same with absolute certainty for heteronuclear couplings between ring protons and chain deuterons. Deuterium decoupling experiments were not entirely conclusive in resolving this issue because of the lower signal-to-noise of the high order decoupled spectra.

Finally, we comment on the reliability of results from the various models used. At first, it may seem disturbing that several models achieved close fits with the spectrum but yielded internuclear distances which differ by amounts greater than their error limits. This, in part, reflects the fact that the errors are propagated directly from the degree of fit only for those lines assigned in the spectrum. Resolved lines in lower order spectra may also be assigned and perhaps would change the overall fit obtained. Particular care must be taken to consider those experimental lines which are poorly matched by the theory, such as in the six and seven quantum spectra of 5CB-d_{11}. In addition, systematic errors caused by the neglect of vibrational and torsional averaging of calculated couplings is not included in the error limits reported in this chapter. Inclusion of these contributions to the errors would tend to bring the results of the various models into closer agreement.

The best results in terms of reasonable values for bond angles and distances appears to be found in the D_4 symmetry model. For the value of the dihedral angle derived, almost all models closely agree. This is understandable considering the strong dependence on ϕ for the six and seven quantum transitions in the neighborhood where the best fit values are found. From our results, we can confidently give a value of $30 \pm 2°$ to the dihedral angle of the biphenyl group of 5CB-d_{11}.

4.4 Experimental Examples of Biphenyl Solutes

Of the other molecules shown in Figure 4.1 we will briefly present the results for 4,4'-dibromobiphenyl, 4,4'-d_2-biphenyl and pure biphenyl dissolved in liquid crystal nematic phases.

4.4.1 4,4'-d_2-biphenyl and 4,4'-dibromobiphenyl

The single quantum echo spectra of 4,4'-d_2-biphenyl dissolved in Eastman Kodak L.C. #15320 and 4,4'-dibromobiphenyl in 4-ethoxybenzylidene-4'-n-butylaniline (EBBA) are shown in Figures 4.37 and 4.38, respectively. Linewidths are narrower in both cases than for 5CB-d_{11} as a result of more reorientational freedom for the solutes. As a result, there should be adequate resolution in a well averaged single quantum spectrum to allow an analysis without resorting to a multiple quantum experiment, although the latter would of course, allow unambiguous line assignments to be made in higher orders. Deuterium decoupling for 4,4'-d_2-biphenyl could be easily achieved by frequency modulated irradiation or double quantum decoupling. The deuterium spectrum should yield an independent measure of one of the order parameters for comparison with the results of the proton spectrum. A TPPI multiple quantum spectrum of 4,4'-d_2-biphenyl is shown in Figure 4.39 and demonstrates the expected loss of signal-to-noise for a solute compared to a pure liquid crystal.

4.4.2 Unsubstituted Biphenyl

An analysis of the NMR spectrum of unsubstituted biphenyl dissolved in a liquid crystal has not been published before. Additional couplings to the para hydrogens, which are absent when these positions are substituted, are insensitive to the dihedral angle and the potential determining it. They will, however, add many more parameters from which the

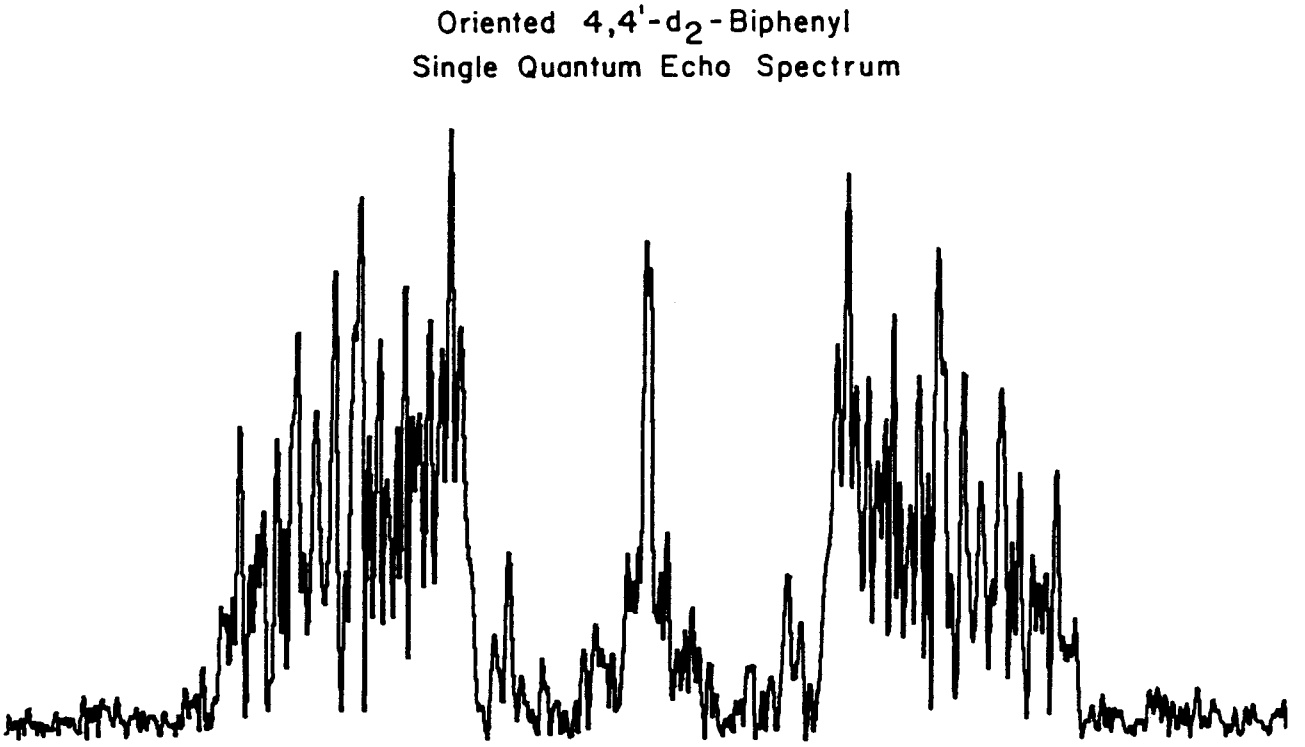

Figure 4.37

Single quantum proton spin echo spectrum of 4,4'-d_2-biphenyl dissolved in the nematic phase of a liquid crystal at 30°C. The total width shown is 16.67 kHz. No deuterium decoupling irradiation was used.

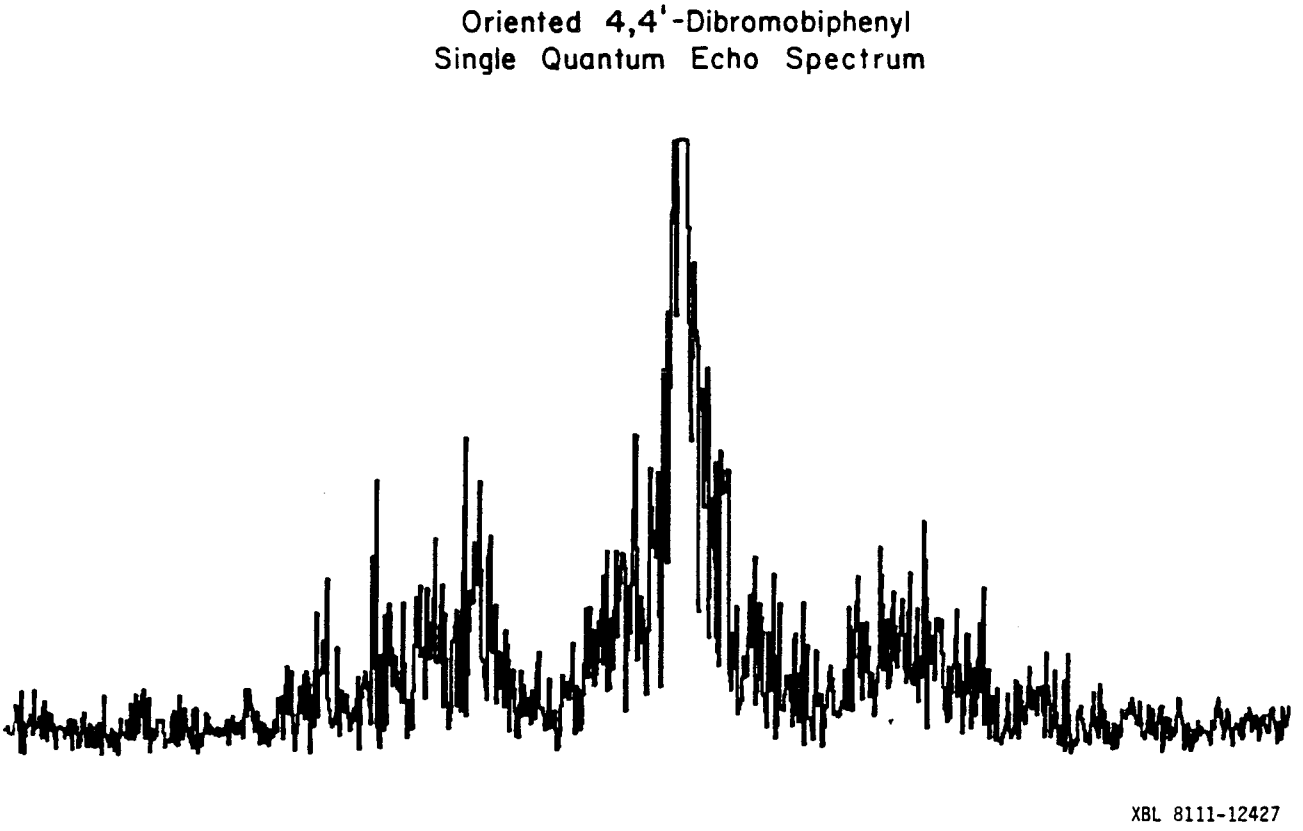

Figure 4.38

Single quantum proton spin echo spectrum of 4,4'-Br_2-biphenyl dissolved in the nematic phase of a liquid crystal at 65°C. The total width shown is 31.5 kHz. The central portion of the spectrum has been truncated in height.

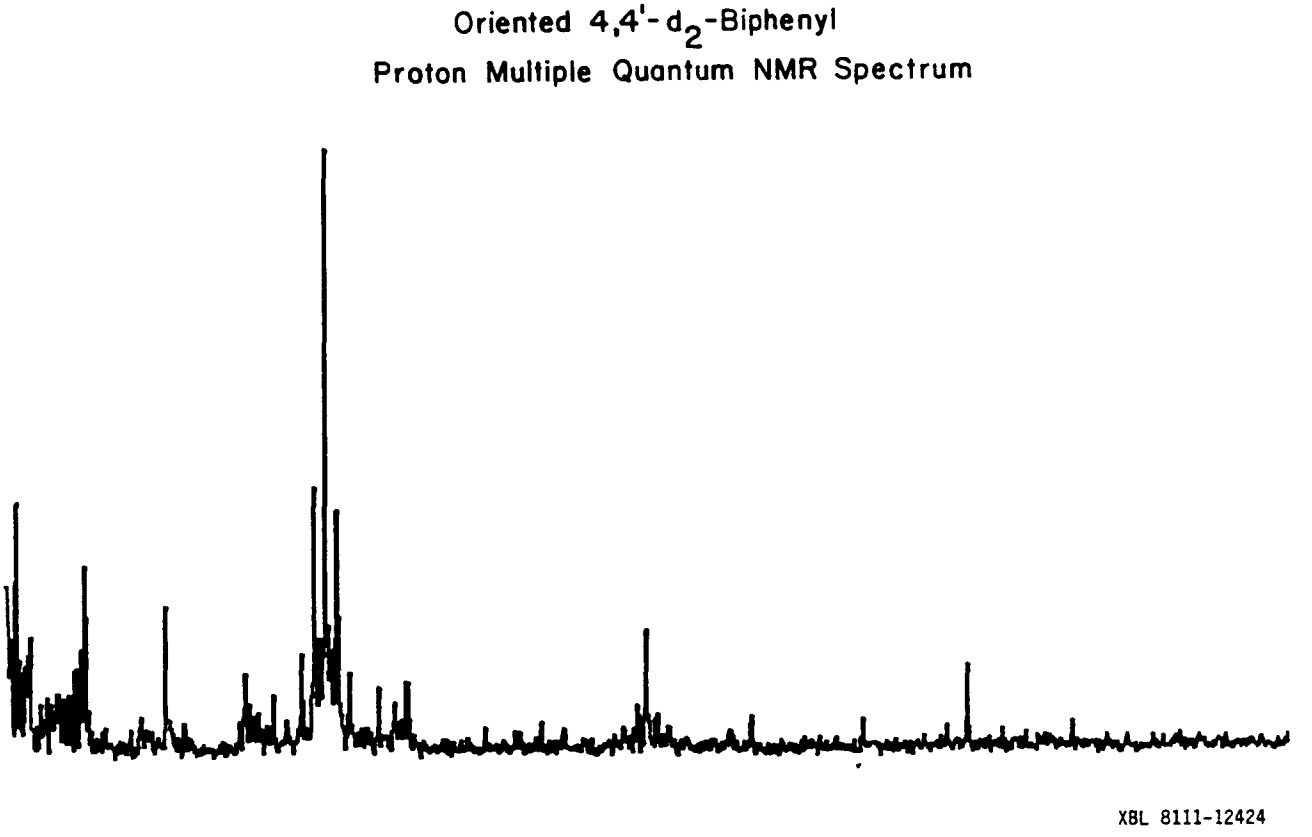

Figure 4.39

Proton multiple quantum TPPI spectrum of 4,4'-d_2-biphenyl at 30°C. An even quantum pulse sequence was used with preparation and detection times of 6 msec. Total width shown is 125 kHz. Most of the intensity is found in the zero and two quantum regions. No deuterium decoupling irradiation was used.

order tensor and ring structure may be obtained. Also, the resulting structure would be determined in the absence of perturbing affects of substituents.

The single quantum spectrum is tremendously complex even though some resolved structure exists. An even quantum TPPI echo spectrum is shown in Figure 4.40. There is little intensity in the highest orders as would be expected on the basis of the approximate statistical arguments for the intensity distribution given in Chapter 3. Extensive averaging would be required to produce sufficient signal-to-noise in, say, the six and eight quantum regions to allow an analysis. Alternately, this molecule is a reasonable candidate for the selective excitation techniques briefly mentioned at the start of Chapter 3.

4.5 Conclusion

Clearly, we have achieved some of our goals in this chapter. We have given examples with various substituted biphenyl molecules which illucidate the strengths and limitations of non-selective multiple quantum NMR. The case of 5CB-d_{11} shows how both deuterium single quantum and proton multiple quantum spectroscopy can be used in liquid crystals and compares the nature of information obtained from quadrupolar and dipolar interactions. Proton spectra are particularly desirable because of the higher precision for structural information and greater sensitivity available as a result of the larger gyromagnetic ratio. We have seen that a very simple model is capable of simulating most of the features of the high order spectra of 5CB-d_{11}. Transition frequencies in these spectra are only indirectly sensitive to the true order parameters for the entire molecule with its myriad of conformational

possibilities. Additional couplings to the alkyl chain, perhaps with a ^{13}C spin-1/2, would prove useful by adding features in the spectrum sensitive to the chain motions. Techniques which are extensions of the basic, non-selective multiple quantum experiments described here, such as heteronuclear multiple quantum NMR [113], could be used to increase the amount and variety of information available to determine molecular parameters.

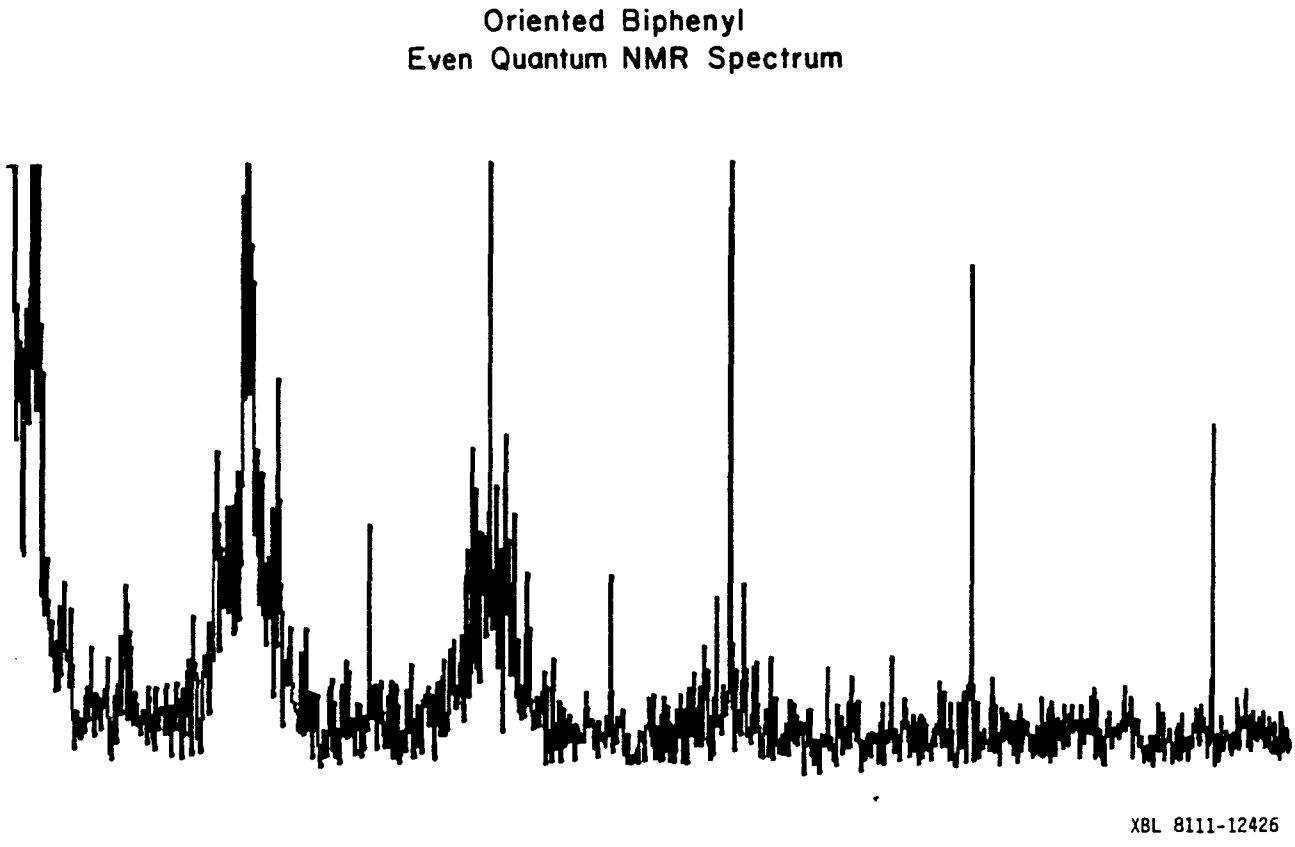

Figure 4.40

Proton even quantum TPPI spectrum of unsubstituted biphenyl dissolved in the nematic phase of a liquid crystal at 44°C. A total of four shots were averaged and the preparation time used was 4.0 msec. Total width plotted is 100 kHz. The single ten quantum transition is visible at the right hand side of the spectrum.

Chapter 5

Spectrometer

The experimental work described here was performed on two high field NMR spectrometers which are largely equivalent in their design and operation. Both are home-built, 180 MHz, pulsed Fourier Transform spectrometers capable of a variety of experiments in solids and liquids using ^{1}H, ^{13}C and ^{2}H resonance. Because most of the work was done on one of the two and this spectrometer has been modified during the course of experiments, a thorough description of its design follows.

5.1 Magnet

The magnet is a persistent superconducting solenoid made by Bruker Instruments and operating at a field of approximately 42.5 kG. The room temperature bore of its dewar has a diameter of 3.5 inches. The Larmor frequencies for the nuclei commonly observed at this field are:

^{1}H	185.04 MHz
^{13}C	46.52 MHz
^{2}H	28.40 MHz

In addition to the main solenoid there are three superconducting, linear gradient coils for shimming the field homogeneity. One is along the main field axis and the other two are orthogonal and in the transverse plane. These are normally left in a persistent mode during experiments. Within the bore there is a set of home-built, room temperature coils producing ten linear and higher order gradients. Using these coils and the superconducting coils field homogeneities less than 1 PPM over a

1 cm^3 region are easily obtained. The resulting field is extremely stable so that no field/frequency lock is necessary.

5.2 Low Power R.F. Section

A schematic diagram of the radio frequency electronics is shown in Figure 5.1. This figure shows the arrangement on the low frequency side for ^{13}C resonance; removal of the doubler and changing the X synthesizer setting converts this channel to ^{2}H resonance. All frequencies are supplied by two synthesizers: a Hewlett-Packard Model 3320A for the low frequency side (set at 3.26 MHz for ^{13}C and 8.40 MHz for ^{2}H), and a PTS Model 160 for the proton side. The rear panel output of the PTS synthesizer internal reference (10 MHz) is used to lock the HP synthesizer, generate the intermediate frequency (i.f.), and drive the pulse programmer clock.

Frequency generation for each channel is detailed more in Figure 5.2. The output of the HP synthesizer (front panel setting plus 20 MHz) is used directly for ^{2}H or doubled for ^{13}C. Switching and phase control for routing to the low frequency transmitter is done at this frequency. A local oscillator (ℓ.o.) frequency is generated by combination of this r.f. with the i.f. frequency. This ℓ.o. is used in the low frequency receiver when ^{13}C or ^{2}H observation is required. The 30 MHz i.f. frequency for both channels is generated by tripling the 10 MHz reference of the PTS synthesizer. Besides being used in the low frequency ℓ.o. generation, this i.f. is routed to the phase sensitive detectors and the r.f. generation for the high frequency (proton) channel.

Unlike the low frequency channel, pulse and phase control for the proton channel is done at the i.f. frequency. The front panel output of the PTS synthesizer at 155 MHz is used directly as the ℓ.o. frequency for

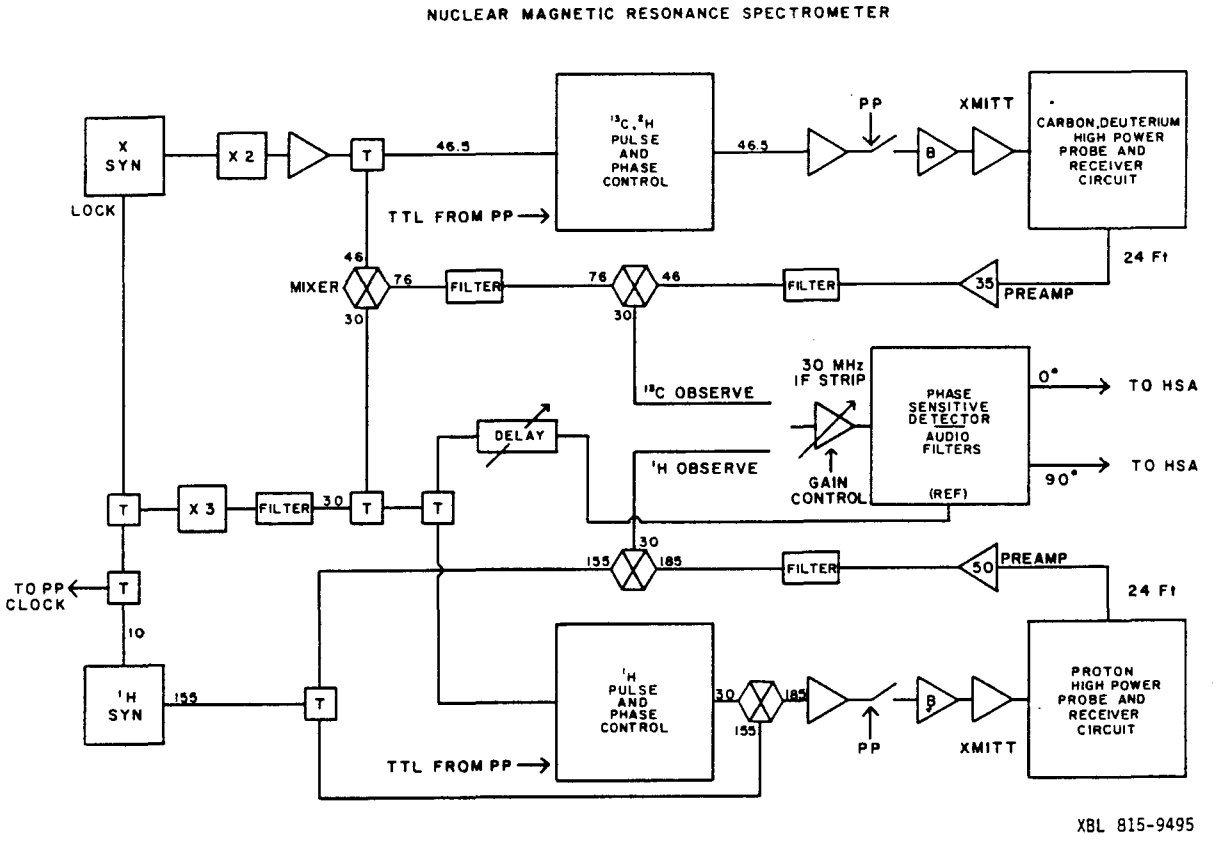

Figure 5.1

Block diagram of 180 MHz pulsed FT NMR spectrometer. Two nuclear frequency channels are shown. The proton frequency generation is based on a 155 MHz ℓ.o. synthesizer output. The X frequency generation, shown here for carbon, is based on the r.f. output of the X synthesizer. Both channels make use of the 30 MHz i.f. reference which is also used in the phase sensitive detector. See text for a complete description.

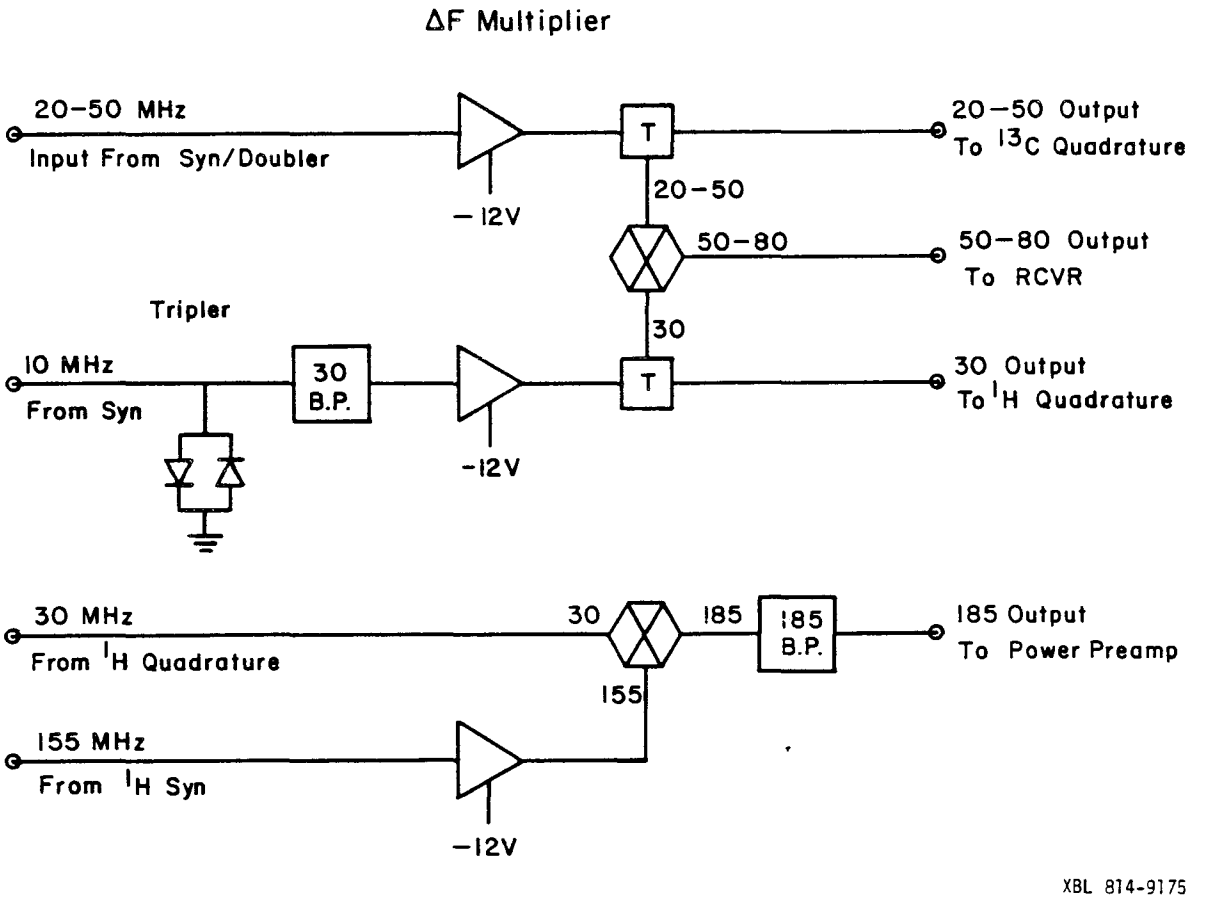

Figure 5.2

Block diagram of 180 MHz NMR spectrometer ΔF Multiplier. The X channel r.f. is used directly in quadrature pulse generation and is mixed with the 30 MHz i.f. to produce the receiver ℓ.o. frequency. This i.f. is produced by clipping the 10 MHz reference with shorting crossed diodes and filtering for the third harmonic. The generation of the proton r.f. pulses from ℓ.o. signal and i.f. pulses is also shown.

the proton channel. The 30 MHz pulse output is mixed up to the nuclear frequency by combination with this ℓ.0. frequency. This is then amplified and routed to the high power transmitters and probe. The 155 MHz ℓ.0. is also directed to the proton receiver where it is combined with the nuclear signal.

The pulse and phase generation (quadrature detection) for the low frequency channel is detailed in Figure 5.3. Switching is done at the r.f. used for sample irradiation. Two orthogonal phases are generated as the r.f. is passed through a hybrid. One phase is selected and a pulse is generated by a TTL controlled r.f. switch. A variable attenuator with 1 db increments is used to trim the pulse amplitude. For improved isolation, another r.f. switch in series is used before final amplification and transmission to the probe. The design of the r.f. switches used here and in the proton quadrature is shown in Figure 5.4. A TTL trigger is received and used to drive two Summit 571 r.f. gates in series. This circuit generally provides 30 to 40 db of isolation.

Although the experiments in this work require only one phase at the low frequency for decoupling, four quadrature phases (X, $\bar{X}$, Y, and $\bar{Y}$) are generally required at the proton frequency. In addition, techniques such as time proportional phase incrementation (TPPI) require finer control of some of the phases and an ability to rapidly and reproducibly change between them under TTL control from the pulse programmer. A schematic diagram of the proton quadrature generation is shown in Figure 5.5.

The 30 MHz i.f. signal is first split to two lines. One line is passed through a delay line phase shifter (Daico Model 100D0898) under TTL control of the pulse programmer. This is then further split and

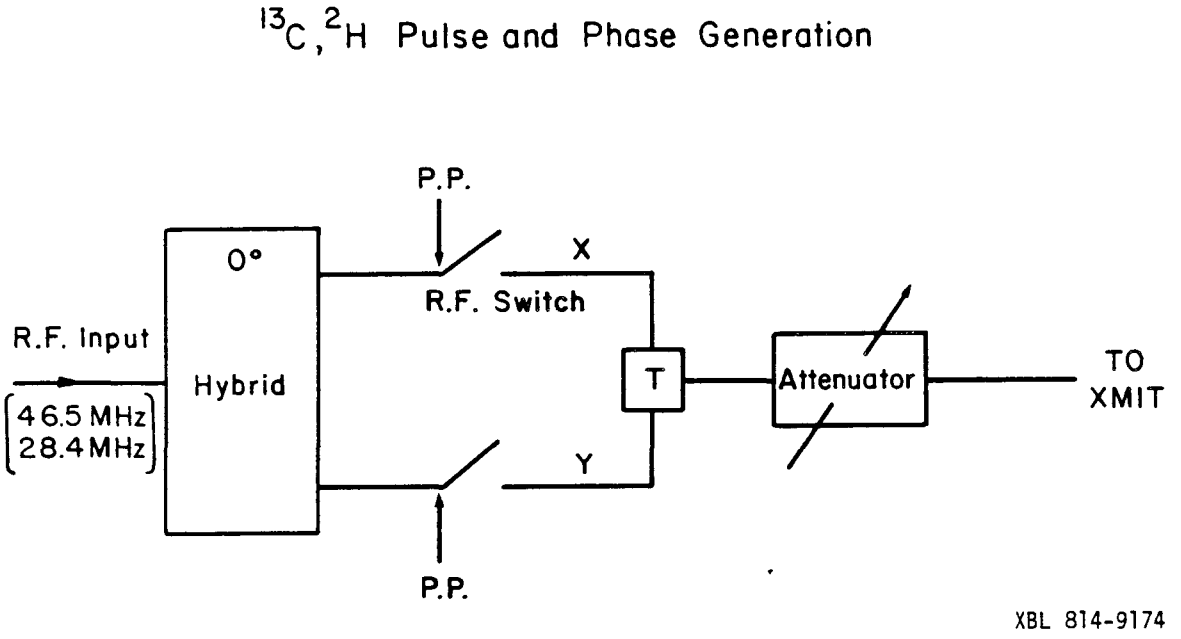

Figure 5.3

Block diagram of X channel quadrature pulse generation for 180 MHz NMR spectrometer. Switching is done directly at the nuclear frequency to avoid possible leak through of an ℓ.o. frequency. The attenuator is settable in 1 db steps.

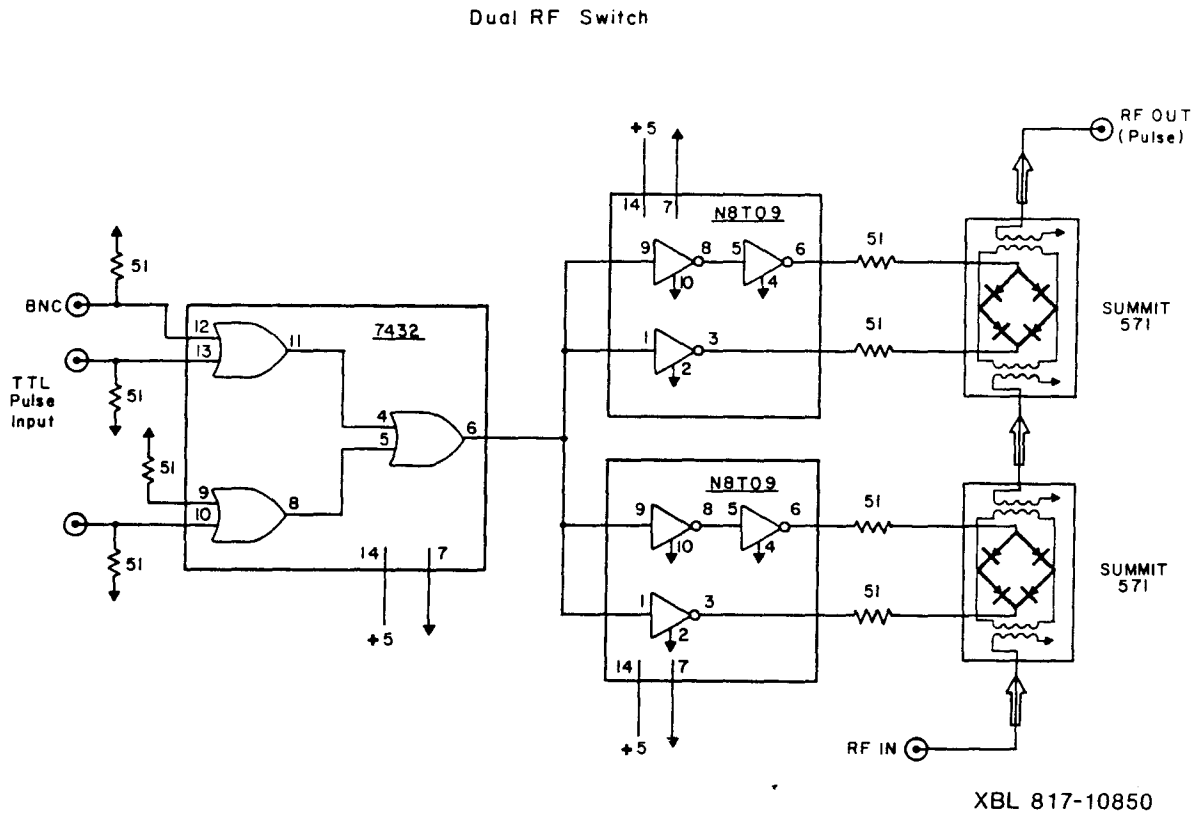

Figure 5.4

Dual r.f. switch for 180 MHz NMR spectrometer. TTL control pulses are input at the BNC connections and received by a quad OR buffer. The high and low outputs of the N8T09 drivers are used to bias a diode bridge which opens the r.f. gates. Two gates in series are used to produce $\gtrsim$80 db of isolation when the switch is "off".

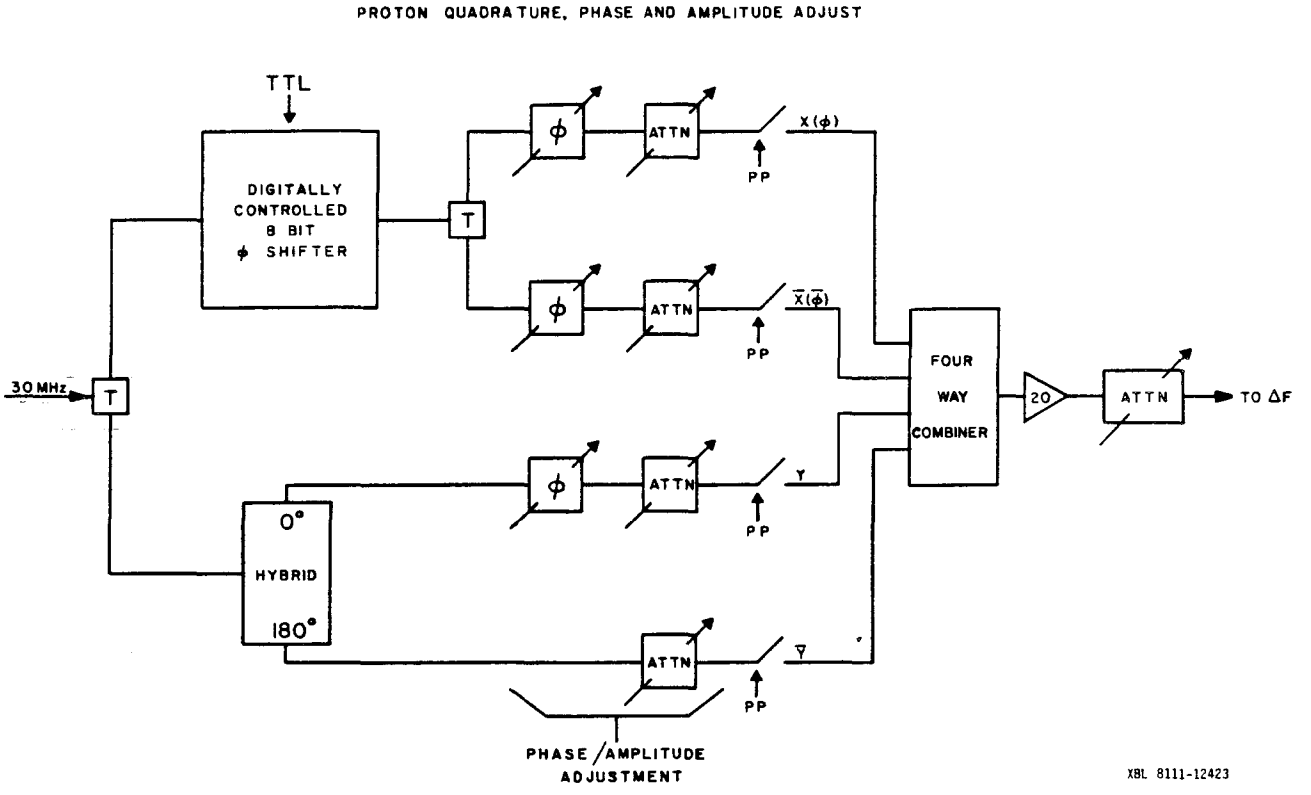

Figure 5.5

Block diagram of proton quadrature pulse generation for 180 MHz NMR spectrometer. With no delay chosen for the 8 bit phase shifter, the four lines are mutually orthogonal (X, $\bar{X}$, Y, $\bar{Y}$). For arbitrary delay, the first two lines are still 180° relative to one another (ϕ, $\bar{\phi}$) but at some other phase relative to the second two lines. The adjustment attenuators are continuously variable from 0 to 20 db and the phase delay adjusters vary from 0° to 90°.

passed through phase delay adjusters (Merrimac Model PSS-2-30) and variable attenuators (Merrimac Model ARS-1, 0-20 db). The result is two r.f. lines 180° in phase with respect to one another but at an arbitrary phase relative to the second line of the initial power splitter. This second line is passed through a hybrid to give two more lines (Y and $\bar{Y}$) with a 180° relative phase. Only amplitude control of the $\bar{Y}$ line is required for complete fine tuning of the four lines. After switching (dual r.f. switch, Figure 5.4) the outputs are recombined, amplified, and adjusted by a final attenuator with 1 db increments before conversion to the nuclear frequency and final transmission.

The 8 bit phase shifter is schematically represented in Figure 5.6. This unit consists of a series of delay lines which are switched in and out of line by TTL controlled gates. The total phase shift produced is the sum of the delays chosen. The precision of this phase shifter is $2\pi/256$ and the accuracy of phase shifts checked with a vector impedance meter is within $\pm 2°$ for an arbitrary phase shift. The VSWR of the unit is dependent on the phase setting and this results in an amplitude variation on the order of a few percent. This generally is not a problem if there is saturation of some amplification element down path of the phase shifter. Because of narrow band filtering in the r.f. circuitry, a phase shift is not effective until about 2 μsec after a change has been made in the 8 bit control word. This control word is generated by a digital controller shown in Figure 5.7. The 8 bit word sent to the Daico phase shifter is chosen from a number of sources input to a set of parallel multiplexers. The data sources include a front panel setting, a single latched byte from a computer interface or a FIFO output loaded from the computer, and a wrap around adding circuit used for phase incrementing as in the TPPI experiments.

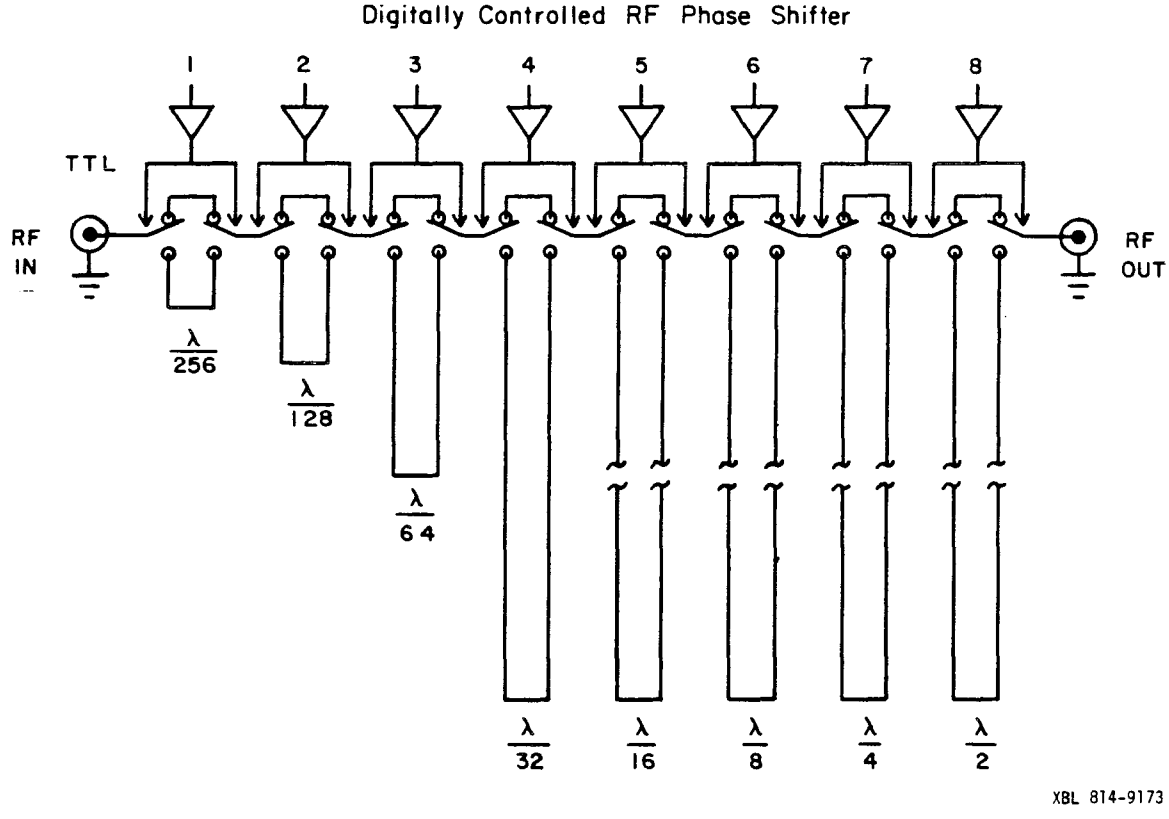

Figure 5.6

Schematic diagram of r.f. phase shifter. Phase shifts which are a multiple of $2\pi/256$ are caused by switching the various delay lines in the path of the i.f. signal. The eight bit TTL control word is supplied by the circuit shown in Figure 5.7.

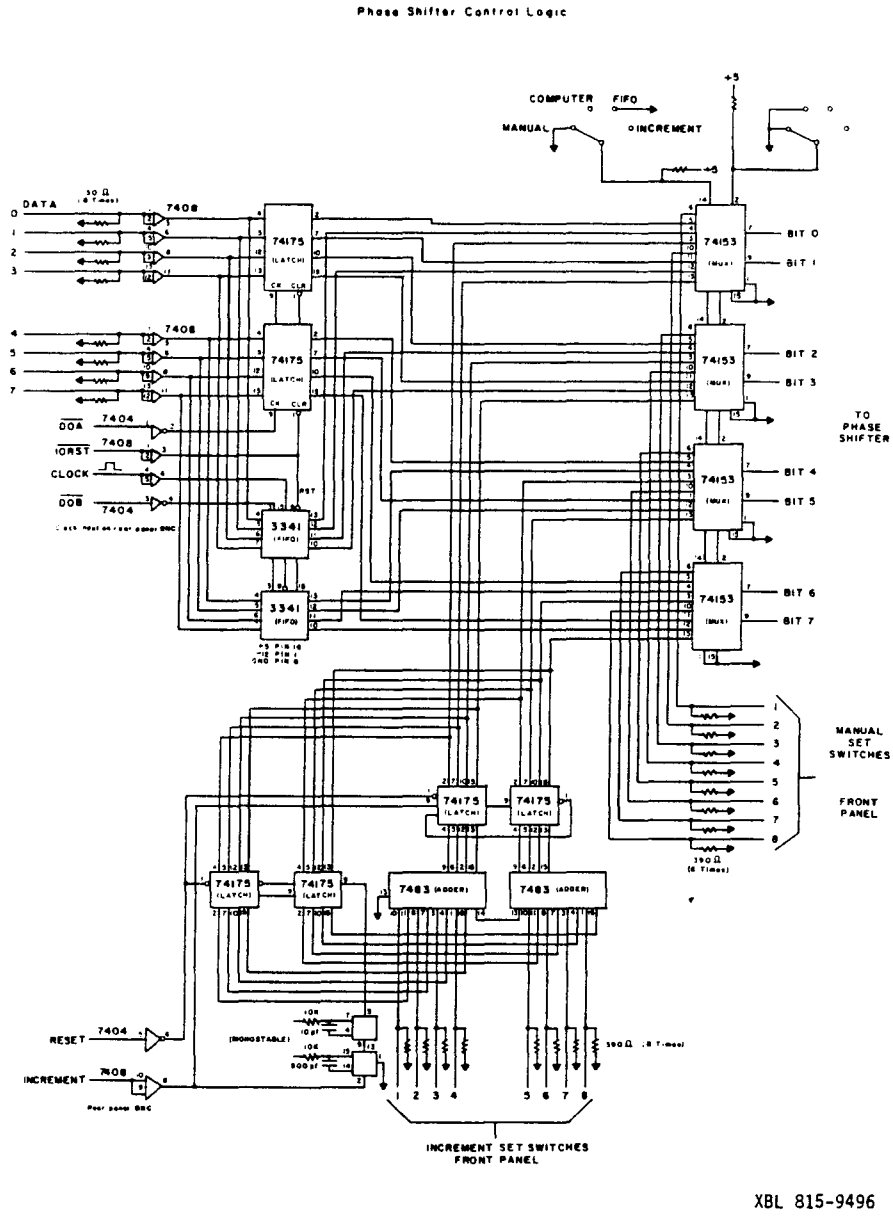

Figure 5.7

Circuit diagram for control logic supplying the eight bit word for the r.f. pulse shifter shown in Figure 5.6.

All mixers used in the low power r.f. section are high level, double balanced Anzac Model MD-143, Mini-Circuits ZAD-2, ZAD-1-1 or Hewlett Packard Model 10514A. All power dividers and combiners are either Anzac Model DV-50, Mini-Circuits ZSC-2-1, Anzac Model DS-312 (Four-Way), or Merrimac PD-20-50. Hybrids are Merrimac Model QH-1-30, Anzac Model JH-126, Anzac Model JH-125, or Mini-Circuits ZSCQ-2. Low power amplifiers are Anzac Model AM102 (~10 db) and Anzac Model AM105 (~20 db). All voltages (+5V, ±12V, +24V) are supplied by regulated power supplies and are further regulated by i.c. circuits at each component box.

5.3 High Power R.F. Section

Once the switching and r.f. generation has been accomplished, pulses are routed to the power preamp for amplification, secondary switching for isolation, and filtering before transmitting to the probe. This is shown in Figure 5.8. The 24, 25 and 53 db amplifiers are, respectively, Radiation Devices Models BBA-1-PB, BBA-1-PBM, and BBA-1-PM. The buffer amplifier for the proton channel is a 5 watt power amp from RF Power Labs Model M305-5.

A variety of power transmitters are available. For decoupling or pulses, the proton frequency is delivered as is to a cavity tuned Class C [114] transmitter with a 4CX250-B tetrode tube (2.5 kV plate, 130 V bias, and 500 V screen). Alternately, the buffer amplifier is bypassed and an Amplifier Research Model 100L Class A amplifier is used. Both arrangements are capable of producing 100 to 200 watts depending on input amplitude, tuning parameters, input attenuation, etc.

Similarly, several transmitters are available for ^{13}C and ^{2}H. Two Class C Millen type transmitters employing RCA 3E829 tubes are used,

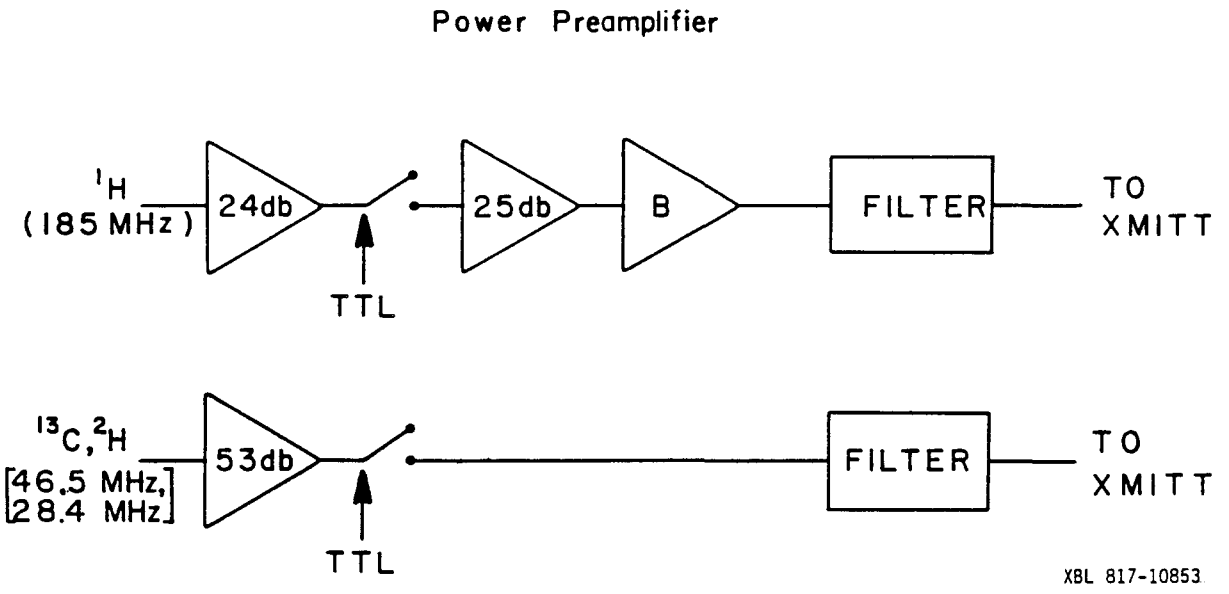

Figure 5.8

Block diagram showing final amplification, switching, and filtering before r.f. pulses are sent to high power transmitters. The output of this section is designed to provide enough power to drive and saturate the Class C transmitters described in the text. For use with the Class A transmitter for protons, the final buffer amplifier is removed and the output trimmed to ~1 V.

one tuned for ^{13}C and one for ^{2}H. Typically, 200 watts can be produced. In addition for higher power applications, a Drake Model L-7 driven by a ENI 350L will provide on the order of a kilowatt.

With a single coil probe design, care must be taken to protect the receiver preamplifier from the high power pulses. The circuit generally used is shown in Figure 5.9. Crossed diode pairs are used to block transmitter noise at levels $\lesssim$0.6 V. A quarter wave line at the observation wavelength with crossed diodes to ground protects the receiver. Occasionally, an additional quarter wave line and diodes are used for further protection. Typically, there is less than 1 V (peak to peak) of a distorted wave form leaking to the preamp during a pulse. A band pass filter is used between the probe and quarter wave line to improve rejection of the decoupling frequency when present.

5.4 Probes

Several home built probes were used in this work. Each probe used was chosen for particular characteristics which optimize signal-to-noise, high power decoupling and minimum sample heating.

The general resonance circuits used are shown in Figure 5.10. For experiments requiring only observation of the proton frequency with no decoupling, a simple, tunable resonance circuit was used. The tuning capacitor is a home-built unit consisting of an inner cylindrical conductor and an outer bell separated by a teflon dielectric. Matching capacitance of several silver mica or ceramic capacitors are placed in parallel. The sample coil is made from 18 or 20 gauge copper wire wrapped to form a solenoid of 5-7 turns with a diameter of 6 mm and about 1 cm long. With 200 watts of r.f. power and a probe Q ~ 100, rotating fields of 10-20 G can be generated.

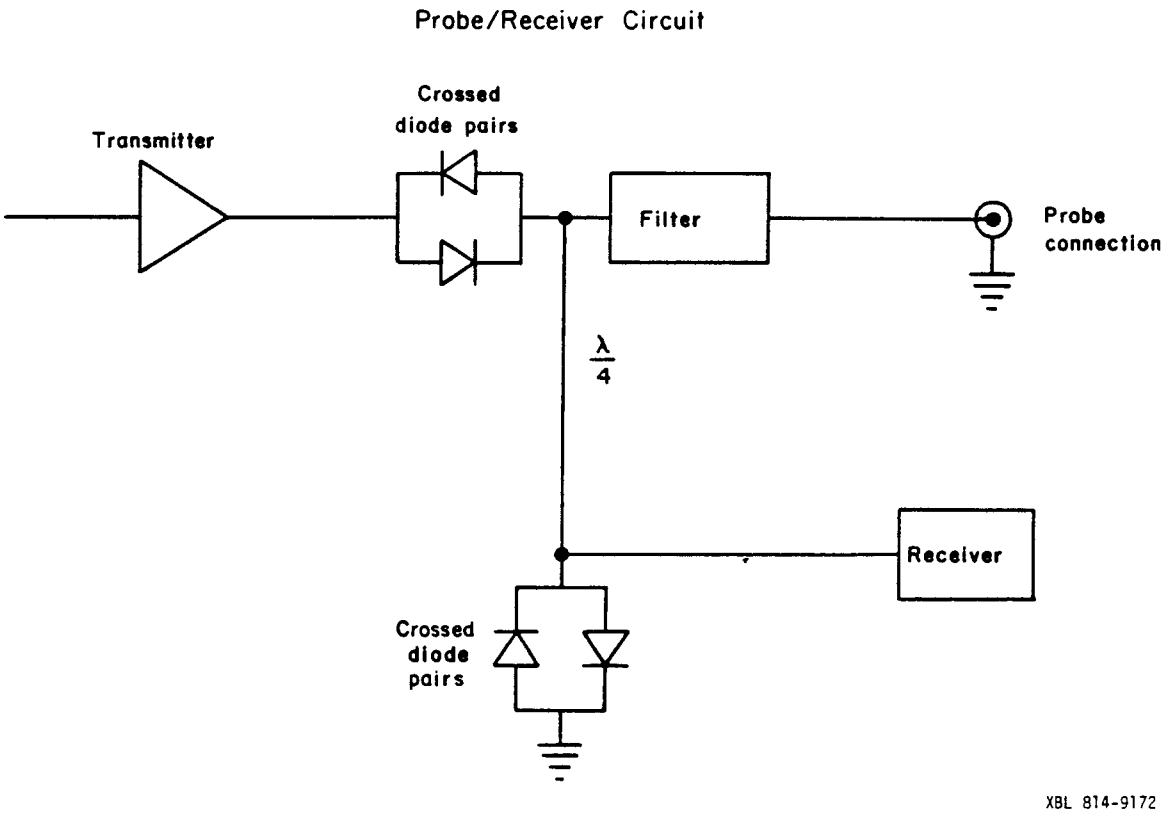

Figure 5.9

Probe and receiver connection to high power transmitter. Transmission diode pairs (IN 914) are used to block transmitter noise and protect the receiver preamp from high power pulses. The λ/4 line is a quarter of the wavelength being observed.

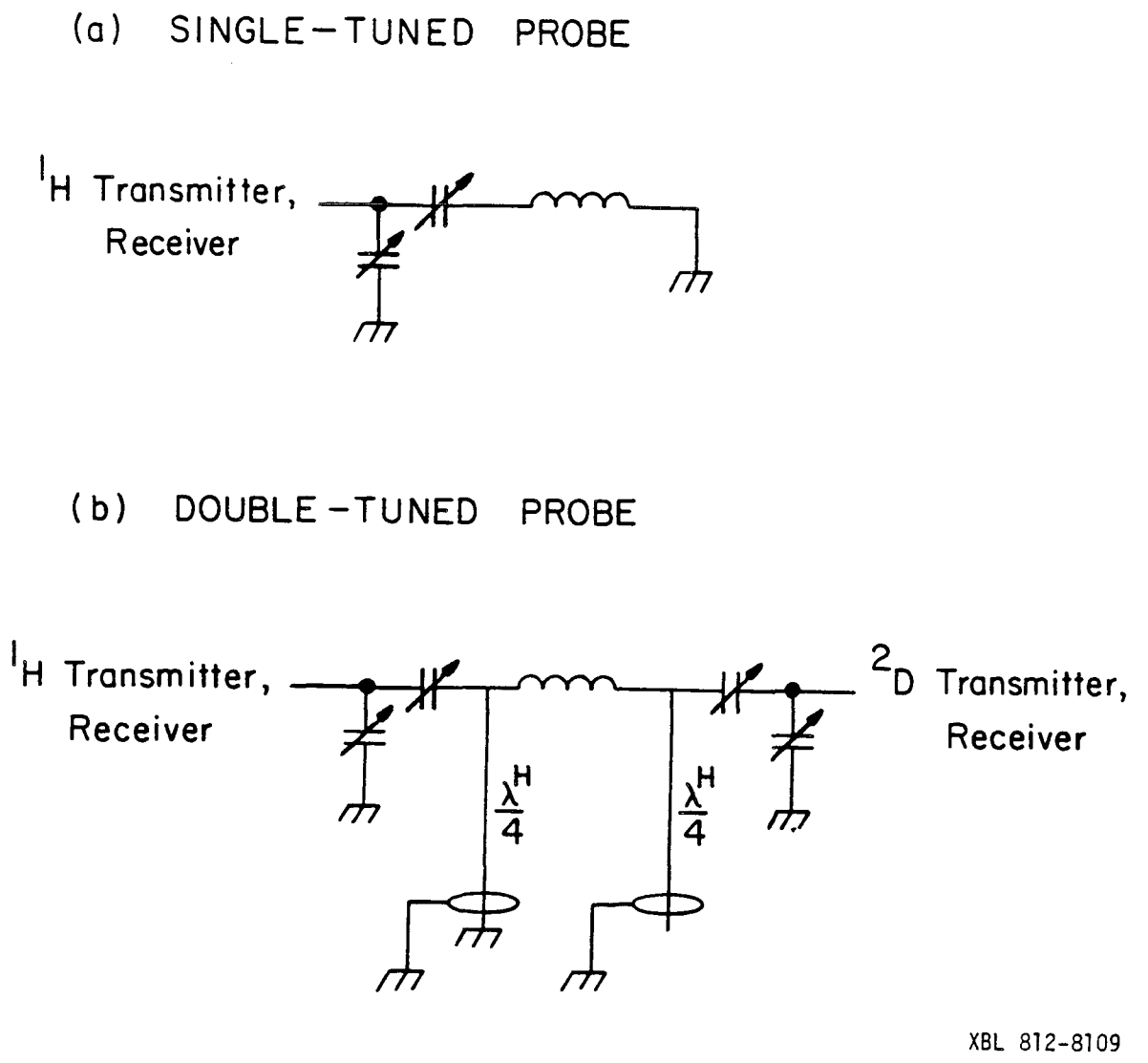

Figure 5.10

Probe circuits for NMR spectroscopy.

a) Single tuned circuit. Tuning is done with the variable cap in series with the sample coil. The second capacitor is adjusted to achieve impedance matching with the transmitter and receiver.

b) Double tuned circuit. Both low and high frequencies tune with the same coil. The proton wavelength is λ^H.

For double resonance experiments, an additional tuned circuit at the decoupler frequency is present. The double resonance probe must be capable of producing large r.f. fields at both frequencies, while detecting the microvolt-sized nuclear signal during decoupling. This implies good isolation between the two circuits. In addition, sample heating due to resistive losses in the coil are a problem when working with an ordered sample such as a liquid crystal.

Some of the double resonance experiments were performed on a two-coil probe. In this design, the deuterium resonance circuit is similar to the proton (Fig. 5.10a) except for capacitative values and a coil of saddle Helmholtz geometry. The saddle-shaped deuterium Helmholtz coil is mounted orthogonal to the proton solenoid and outside of the latter. This arrangement provides good isolation (30-40 db) and the distance of the decoupler coil from the sample avoids thermal contact. Dielectric losses in the sample itself can still be a problem. Typically, 20 G of rotating field can be achieved for ^{2}H decoupling, the main limitation being arcing at some point in the probe. This was found to be adequate for some of the experiments in this work.

When more decoupling field is required, a double-tuned, single coil arrangement (Fig. 5.10b) is necessary [115]. Most of the elements in this probe are similar to the single resonance circuit. High and low impedance points for the proton frequency are present on either side of the sample coil and are effected with the use of quarter wave lines: one grounded and one open. The use of a single solenoid coil for both high and low frequency improves decoupling by allowing for greater ^{2}H fields (40-50 G) and equivalent r.f. homogeneity over the sample for both channels. It was found, however, that sample heating during

decoupling was more problematic than with the Helmholtz coil due to the closer proximity of the coil to the sample. This was avoided by using a smaller sample with teflon spacers to hold it along the axis of the solenoid. The resulting reduction of the filling factor lowered the signal-to-noise somewhat. Although it has been claimed [116] that the efficiency, defined as the fraction of transmitter power that is delivered to the sample coil, will be significantly less for the high frequency side of a double-tuned probe of this design compared with a signal resonance circuit, it was found that, in general, 90° pulse times were nearly equivalent for the probes used in this work.

Because the anisotropic ordering of a thermotropic liquid crystal is dependent on temperature, careful control of the temperature of the sample environment is required. The probes used in this work are equipped with an evacuated glass dewar which surrounds the immediate region of the sample coil. Radio frequency power is passed into this region by leads through the KEL-F or teflon support on which tuning elements are mounted. The temperature is measured by a single copper-constantin thermocouple junction ~1 cm from the sample coil. The temperature is read by a Noric digital thermometer. Rough temperature regulation is achieved by passing air or N_2 through the sample region via an evacuated transfer line which is also the support rod for the probe. For temperatures above the ambient gas temperature, the gas is first heated by passing it through an element with up to 100 watts of regulated power. Colder temperatures are achieved by first bubbling house N_2 through liquid N_2, or passing air through a copper tube immersed in ice water. The temperature read by the digital thermometer is sampled periodically and compared against a preset value. If the temperature drops below this value, a small auxiliary heater (~30 watts)

in the probe transfer line is turned on. This heater is disabled during a pulse sequence and data acquisition to avoid noise pick-up. With this arrangement, the temperature sample of the environment can be regulated to $\pm$0.1°C over a range from -120° to +150°C.

5.5 Receiver Section

A high sensitivity NMR spectrometer must be able to detect the microvolt-level nuclear signals typically present and be designed so that the noise figure of the preamplifier determines receiver noise contributions. In addition, quadrature phase sensitive detection is employed to provide maximum signal-to-noise and for those experiments where the signal is not linearly polarized.

5.5.1 Preamplifier and IF Gain

The preamplifier sections of both the high and low frequency channels operate in a similar manner. For carbon and deuterium detection, the preamplifier (Miteg Model AU-IB-005M) provides about 35 db gain of the nuclear signal. After filtering, this is mixed with the ℓ.O. using a Hewlett-Packard model 10514A mixer to produce the 30 MHz receiver i.f. signal. The major difference in the proton receiver is the use of a preamplifier with ~50 db of gain and a Mini Circuits Model ZAD-1-1 mixer. Typically full receiver recovery follows 20 μsec after an r.f. pulse at the observation frequency.

Either receiver i.f. is routed to an i.f. strip amplifier (RHG Model EVT3010) with a band pass of 10 MHz. This unit provides 20 db of fixed plus 50 db of variable gain. This amplifier is nominally linear but must be calibrated when relaxation measurements are taken.

5.5.2 Phase Sensitive Detector/Audio Filters

Phase sensitive detection of the receiver i.f. signal is accomplished as follows (see Fig. 5.11). The 30 MHz spectrometer reference is first passed through a variable delay line and then split by a quadrature hybrid. Both channels are passed through mixers along with the i.f. strip output which has been divided with no phase difference. The audio output is filtered by variable low pass filters (see Fig. 5.12) and sent to the digitizers. The relative phase of the spectrometer and signal is adjusted by the reference delay line.

5.6 Digitizers

The $\pm$1 V phase detected signal channels are sent to the High Speed Acquisition system for digitizing and memory storage (see Fig. 5.13). The signals are first gained to $\pm$10 V by a small audio amplifier (AM101A). On a "START" pulse the signal is sampled by a Datel Model SHM-2 sample-and-hold and converted to 10 bits of data by a Datel Model ADC-G10B4C analog-to-digital converter. Total conversion time is 1 μsec. There is an equivalent circuit for each phase channel. The START pulse is generated and the data read by an interface attached to the spectrometer computer (Data General Nova 820). Successive data points (complex) are placed directly into the computer's memory as they are converted via the DMA. The interface can acquire up to 2048 complex data points with a dwell time of $\gtrsim$3 μsec. This provides adequate spectral breadth for all experiments in this work. The acquisition interface was built by Spectrometer Data Systems and has been modified to allow data collection from a single trigger pulse for an entire FID or from trigger pulses for each point in a FID. All data collection is synchronous with the pulse programmer clock.

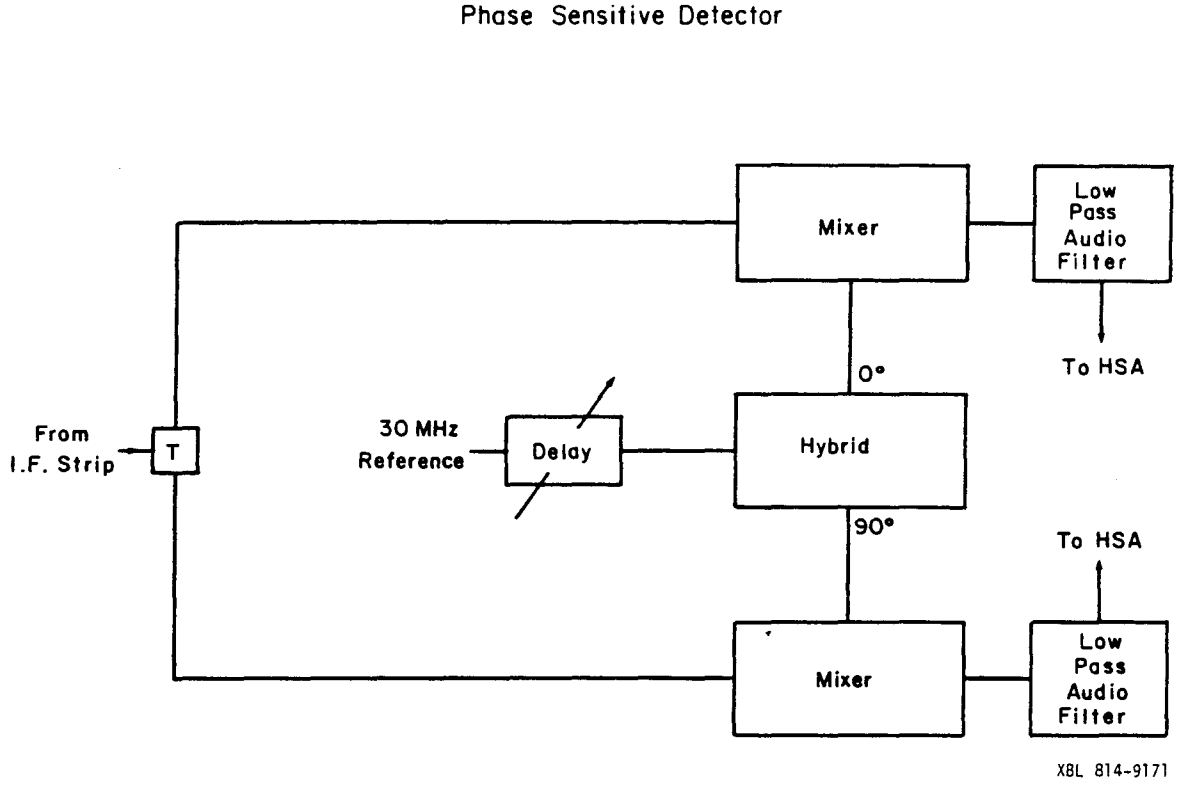

Figure 5.11

Phase sensitive detector. Heterodyne detection method is employed. The i.f. signal is divided with no phase difference and the reference is split into 0° and 90° lines. These are mixed to give two audio channels. HSA means High Speed Acquisition.

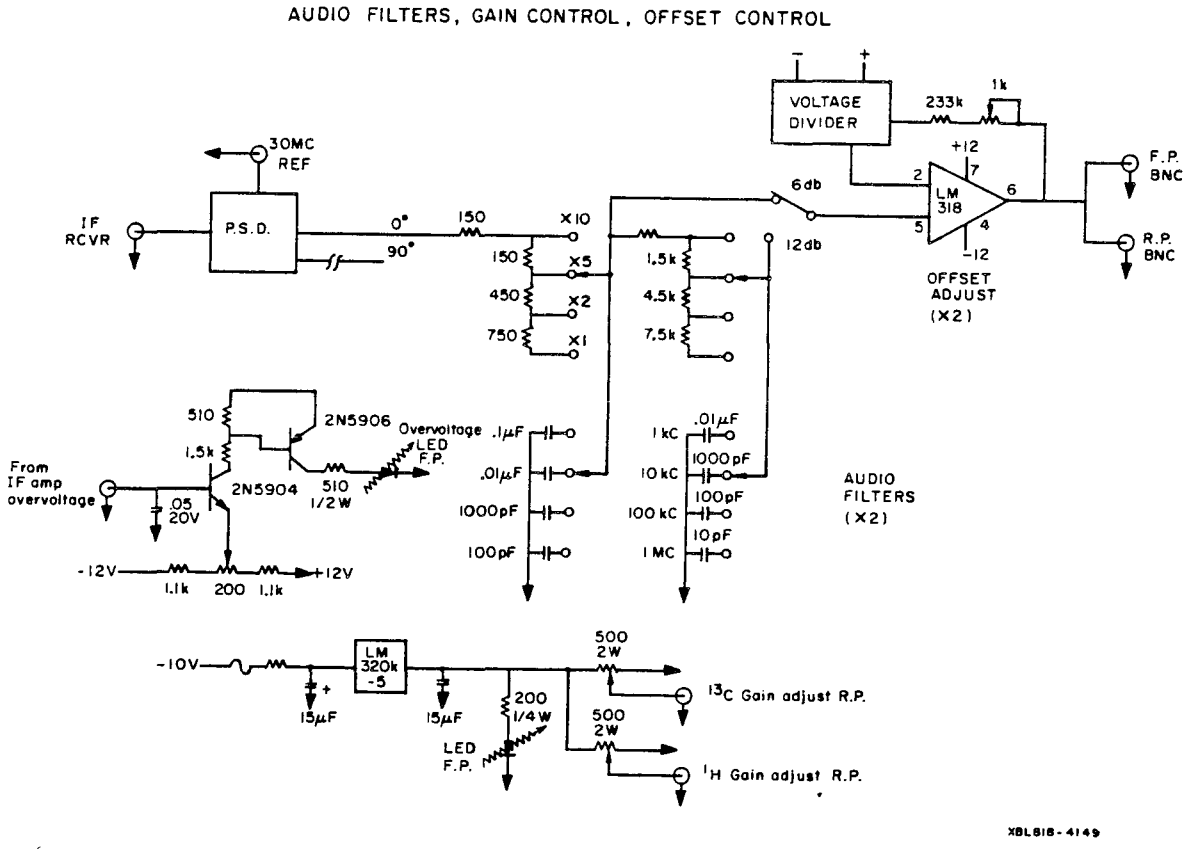

Figure 5.12

Audio filter circuits and miscellaneous circuitry for offset adjustment, IF gain control voltage and IF strip overvoltage detection. Each channel of the Phase Sensitive Detector output is passed through identical filters and offset op-amps. The 6 and 12 db selection affects filter roll-off characteristics.

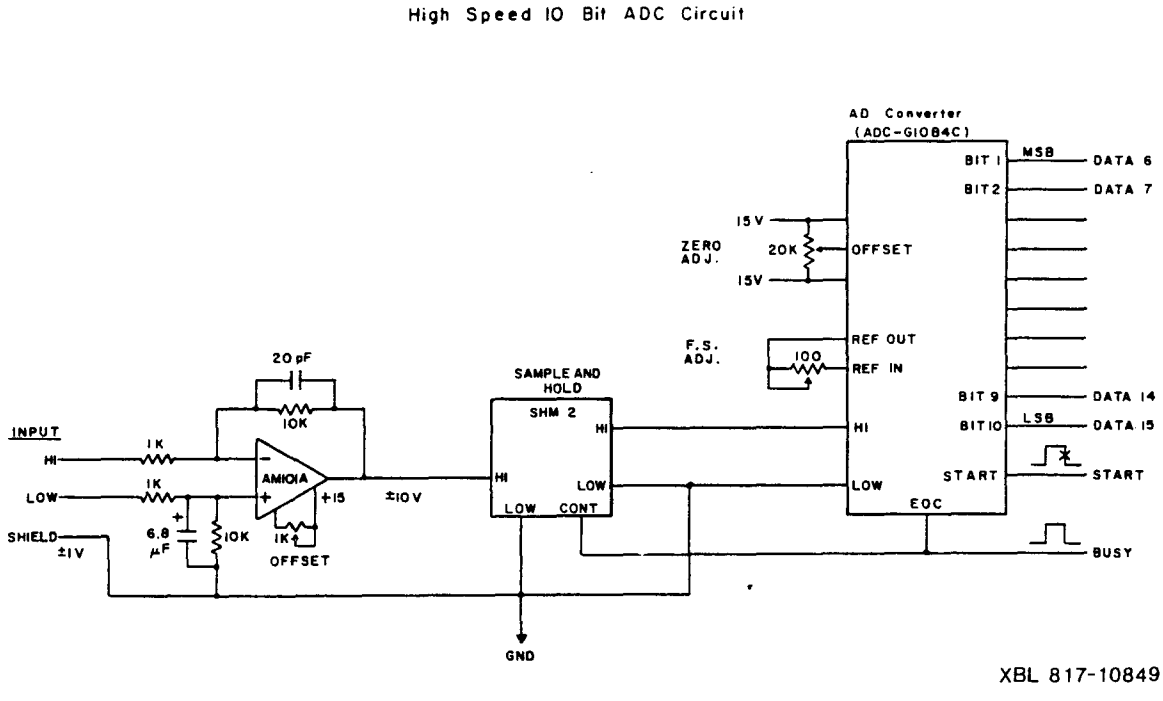

Figure 5.13

Data Acquisition circuit for 185 MHz NMR Spectrometer. Each channel of phase detected signal is converted to 10 bits of data. Conversion time is 1 μsec.

5.7 Pulse Programmer

The nature of the pulsed NMR experiments described in this work require a programmable unit to generate pulse gating and delays for the sequences used. The pulse programmer employed in this spectrometer is microprocessor based and contains its own memory and home-written software. This software (micro-code) allows pulse programs of up to 64 simple steps to be entered and executed. Each step can be an operation such as variable definition and incrementing, comparison of variables and branching, etc. Based on the pulse program instructions, the microprocessor outputs a sequence of timing words to either a RAM or FIFO memory. These timing words are clocked out by gating hardware which is based on the 10 MHz reference output of the proton synthesizer. Thus pulses and delays are settable in 0.1 μsec units and quite complicated sequences can be programmed. The microprocessor communicates with the spectrometer computer via the EIA interface of the system console. The design and operation of this pulse programmer are described in more detail elsewhere [45].

5.8 Computer

A dedicated minicomputer is used to direct the operations of the spectrometer. Data acquisition, data manipulation and peripheral control are all handled by specialized hardware and software.

5.8.1 Hardware

The spectrometer minicomputer is a Data General Nova 820 with a 16 bit word length and 32 K words of core memory. Mass storage is on a Data General 6045 hard disk subsystem with 10 Mbyte capacity. Data back up and storage is aided by a Data General 6030 single density floppy drive with 315 kbytes of storage capacity. Besides CPU, TTY, I/O,

Disk I/O and memory boards, several interfaces handling data display and x-y plotting, data acquisition and miscellaneous peripheral control reside in the main frame.

5.8.2 Software

To handle the many different operations of the spectrometer which are under computer control, a large program was written [117] mostly in FORTRAN with some subroutines in assembly language. This program comprises an independent, stand-alone operating system. Computer memory is partitioned by the software into well defined regions as shown in Figure 5.14. Most of the memory is devoted to data, allowing rapid acquisition and manipulation of digitized signals. The entire program cannot fit into the remaining memory and so is divided into a series of overlays which are swapped to memory from disk as needed.

This operating system consists of 60 commands which direct data acquisition and display, Fourier transformation, phase correction, and a variety of other operations. Commands are given simple names and accept parameters when executed. Commands may either be executed individually from the console or as a sequence from a previously defined string stored on disk (known as a MACRO). MACRO command strings except variables which are passed to the commands at execution time and MACRO's may be nested in almost any way desired. This arrangement allows unattended direction of a complicated experiment which is defined beforehand. Data is stored in a large archive on the hard disk system and later moved to floppy disk for long term storage.

In addition to the spectrometer operating program, several routines were written for specialized data manipulations. Among these is a series of programs which facilitate the calculation of a large, floating-point disk Fourier transform. These are described in Appendix C. This was

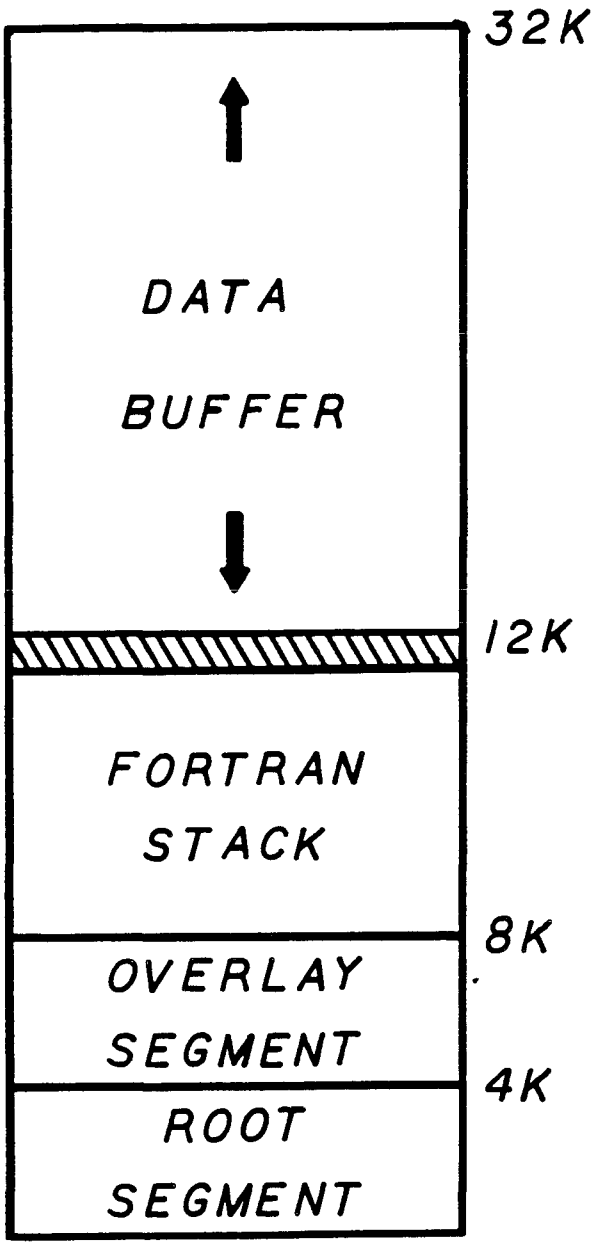

Figure 5.14

Software partitioning of 32768 words of Nova 820 memory for spectrometer operating system. Most of the memory is devoted to data with programs swapped into the overlay segment as needed. The hatched region is used for communications with the pulse programmer.

required in the work on liquid crystals because the computer word size (16 bit) and core memory size (32 K) limits the length of a Fourier transform that can be calculated by the spectrometer software to 8192 complex points. The disk based programs allow a spectrum of up to 64 K words (complex) to be calculated with no overflow.

5.9 Conclusion

In this chapter one of the two NMR spectrometers used in all experiments reported in this work has been described. The basic circuitry of the spectrometer consists of a low power r.f. section in which pulses are generated with well defined phases relative to the spectrometer reference. All pulse and delay timing is choreographed by a sophisticated, microprocessor-based pulse programmer. Pulses are amplified, converted to the nuclear frequency of interest, and transmitted to the sample probe. Two designs of tuned resonance circuits are used in the probes: a single coil for each resonance used or a single coil, double tuned probe. Each design offers some advantages over the other; the choice of probe was dictated by the considerations of signal-to-noise, sample heating and decoupling power requirements.

The dedicated minicomputer system with specialized software used with the spectrometer is also described in this chapter. This arrangement offers a great deal of flexibility in the types of experiments that can be performed. The ability to construct chains of simple commands as MACRO strings allows for automation of experiments once initial parameters are set. The High Speed Acquisition system employed is sufficiently fast for solid state experiments and adaptable to high resolution for liquid crystal and liquid samples. Magnetic field homogeneity is

obtained with a set of room temperature shim coils in addition to superconducting gradient coils. Finally, a low noise figure pre-amplifier followed by variable gain i.f. stage and phase sensitive detection yield the best arrangement from the standpoint of signal-to-noise.

APPENDIX A

Spectral Simulation and Iteration Programs

This appendix describes the simulation and iteration programs (MQITSET and MQITER) used to fit the multiple quantum spectra discussed in Chapters 3 and 4. Both programs and their subroutines are written in FORTRAN IV and execute on a DEC VAX/VMS 11/780 computer. All the file I/O statements are specific for that computer but may be modified to run on virtually any medium or large scale computer. The VAX system has 1.5 Mbytes of virtual memory and so program MQITER dimensions large arrays which allow it to handle up to 10 coupled spins.

In the following sections, the theory of linear least squares parameter adjustment is briefly reviewed and its application to NMR spectral fitting discussed. In Section A.2.3, a description of program flow for MQITER is given. Finally an example, partially oriented benzene, is presented to demonstrate the basic operation of MQITER.

A.1 MQITSET

MQITSET is a program used to collect data required for the execution of MQITER. The latter program is non-interactive and acquires all of its necessary data from file MQITER.DAT. MQITSET asks a series of questions and, based on the responses, collects coupling constants and creates the data file. In this manner, several data files can be created while the actual simulations and iterations are done in the background without interaction from a terminal.

A.2 MQITER

MQITER is the basic simulation and iteration program used for spectral fitting. For spectral simulation, input consists of the dipolar and scalar couplings. From these couplings the homonuclear, spin-1/2 Hamiltonian matrix is set up in a single product basis set. Chemical shifts and rotating frame offset are assumed to be zero. This is then subjected to a diagonalization routine employing the Jacobi rotation technique. Finally, the transition frequencies expected in the multiple quantum spectrum are calculated. This is done by first classifying eigenstate vectors by symmetry representation and then choosing all possible transitions within each representation.

Once an initial simulation has been done, experimental frequencies can be assigned to those calculated. The calculated frequencies are identified by a number given them in the simulation. With these as input, the program is run again and a linear least squares variation is used to refine the couplings and produce a new spectrum with a minimum RMS deviation from the experimental lines. The method of least squares variation is essentially the same as that used by Castellano and Bothner-By in their program LAOCN3 (see Ref. [118,119] and references therein). The next section will discuss the theory of these iterative calculations.

A.2.1 Least Squares Spectral Analysis

If a set of experimental measurements have been made, $\{m_i\}$, corresponding to a set of theoretical quantities, $\{M_k\}$ and it is necessary to find the parameters, $\{p_q\}$, which determine the M_k's from known quantities, i.e.,

$$M_k = f_k(p_1,\ldots,p_q), \tag{A.1}$$

then the method of least squares is appropriate. In this method, it is desired to minimize the quantity

$$\sum_{k=1}^{\ell} (\Delta M_k)^2, \tag{A.2}$$

where $\Delta M_k = m_k - M_k$. In matrix notation we require

$$\frac{\partial}{\partial p_j} (\Delta \underset{\approx}{m}^T \Delta \underset{\approx}{m}) = 0, \tag{A.3}$$

for all the parameters $j = 1, \ldots, q$. In order to obtain a solution for Equation (A.3), $\underset{\approx}{M}$ is expanded in a Taylor series about some initial parameters $\underset{\approx}{p}^{(0)}$.

$$\begin{aligned} \underset{\approx}{M} &= \underset{\approx}{M}^{(0)} + \sum_{j=1}^{q} \frac{\partial}{\partial p_j} (\underset{\approx}{M})_{p^{(0)}} (p_j - p_j^{(0)}), \\ &= \underset{\approx}{M}^{(0)} + \underset{\approx}{V} \Delta \underset{\approx}{p}. \end{aligned} \tag{A.4}$$

In Equation (A.4) it has been assumed that only small changes in parameters are to be considered and so terms with higher derivatives of $\underset{\approx}{M}$ are insignificant. If we use as the vector of residuals the difference between the measured quantities and the zero order term of Equation (A.4),

$$\Delta \underset{\approx}{M} = \underset{\approx}{m} - \underset{\approx}{M}^{(0)}, \tag{A.5}$$

then the minimization problem becomes,

$$\frac{\partial}{\partial p_j} (\underset{\approx}{V} \Delta \underset{\approx}{p} - \Delta \underset{\approx}{M})^T (\underset{\approx}{V} \Delta \underset{\approx}{p} - \Delta \underset{\approx}{M}) = 0, \tag{A.6}$$

which may be rewritten as

$$\underset{\approx}{V}^T \underset{\approx}{V} \Delta \underset{\approx}{p} = \underset{\approx}{V}^T \Delta \underset{\approx}{M}. \tag{A.7}$$

If $\underset{\approx}{M}$ is a linear function of the parameters, then Equation (A.7) is the solution which gives the form of the function in Equation (A.1). This is what has been assumed in going from Equation (A.6) to Equation (A.7), i.e., that $\underset{\approx}{V}$ is not a function of the parameters. For the case of spectral fitting in NMR where the measured quantities are transition frequencies, their dependence on coupling constants is, in general, not linear [118]. Thus, the parameters will have to be varied to approach the situation stated by Equation (A.7). The usual procedure is to solve the "normal equations,"

$$\Delta\underset{\approx}{p} = (\underset{\approx}{V}^T\underset{\approx}{V})^{-1}\ \underset{\approx}{V}^T\Delta\underset{\approx}{m}, \tag{A.8}$$

to give corrections to the parameters which are used to calculate a new $\underset{\approx}{M}^{(i)}$. It can be shown that, as long as the changes to the parameters are kept small so that the "linearization" approximation is valid, this method may converge to some set of final parameters $\underset{\approx}{p}^{(f)}$ representing a local minimum of residuals [120].

The question of uniqueness of the solution $\underset{\approx}{p}^{(f)}$ must then be taken up. It is possible that the convergence will be to a local minimum on the surface of parameter space which is one among several or even an infinite locus of solutions. Where the convergence ends up will be determined by the "closeness" of the initial parameters (i.e., the magnitude of the initial RMS error) and the assignments of the measured quantities, $\{m_i\}$. The Castellano/Bothner-By method requires a reasonably good choice of initial parameters and line assignments [119]. Generally, when the number of lines assigned does not greatly exceed the number of parameters varied, an improper line assignment will result in no convergence at all. Several different line assignments may be tried to isolate

those which do converge. For single quantum NMR spectra of a molecule with a large number of interacting nuclei, the number of different line assignments possible which fit within some range of the initial simulation becomes too great to allow a full least squares iteration of each. With the increased resolution and spectral simplicity inherent in high quantum spectra, the number of reasonable line assignments is greatly reduced. In a similar sense a variety of initial parameters may be used to probe the space of possible solutions. The advantages of using multiple quantum spectra in choosing initial parameters arise when a choice can be made between several different coupling constant models which predict different multiple quantum spectra.

For either a multiple quantum or a single quantum case, the uniqueness of a solution may depend on molecular symmetry. For example, it has been shown that two and three spin systems analyzed from line frequencies alone yield several or even an infinite number of solutions [121]. Unique solutions only become possible when intensity information is included. For a general spin system without symmetry, the direct and indirect couplings and the chemical shifts may all be determined uniquely except for the relative sign of the couplings with respect to shifts and for a permutation of the nuclei [122]. The ambiguity in numbering of nuclei is removed with the addition of molecular symmetry which also reduces the number of parameters required to solve for. In addition, when some of the parameters are assumed, the number of possible solutions is reduced. Thus, the uniqueness of a solution derived from the Castellano/Borthner-By method depends on how well the initial model fits an experiment and how many parameters in the model may be kept stationary.

Returning to Equation (A.8), it may now be seen what is required in the program MQITER. The measured quantities from a multiple quantum spectrum are the line frequencies,

$$\Delta \underset{\approx}{M} = \underset{\approx}{f} - \underset{\approx}{F}^{(0)}, \tag{A.9}$$

the parameters are the direct and indirect coupling constants (chemical shifts are assumed to be equal) and the derivative matrix is

$$(\underset{\approx}{V})_{ij} = \frac{\partial F_i}{\partial p_j} . \tag{A.10}$$

Equation (A.9) is evaluated by considering the eigenstates of the Hamiltonian for the initial parameters and the line assignments made from the spectrum. The derivatives of Equation (A.10) are found by differentiating the Hamiltonian in the simple product basis set:

$$\frac{\partial F_i}{\partial p_j} = \left[\frac{\partial \lambda_n}{\partial p_j} - \frac{\partial \lambda_m}{\partial p_j} \right] \tag{A.11a}$$

$$\frac{\partial \underset{\approx}{\Lambda}}{\partial p_j} = \frac{\partial}{\partial p_j} [\underset{\approx}{S}^{\dagger} \underset{\approx}{H} \underset{\approx}{S}]$$

$$= \frac{\partial \underset{\approx}{S}^{\dagger}}{\partial p_j} \underset{\approx}{H} \underset{\approx}{S} + \underset{\approx}{S}^{\dagger} \frac{\partial \underset{\approx}{H}}{\partial p_j} \underset{\approx}{S}$$

$$+ \underset{\approx}{S}^{\dagger} \underset{\approx}{H} \frac{\partial \underset{\approx}{S}}{\partial p_j}$$

$$= \frac{\partial \underset{\approx}{S}^{\dagger}}{\partial p_j} \underset{\approx}{S} \underset{\approx}{\Lambda} + \underset{\approx}{S}^{\dagger} \frac{\partial \underset{\approx}{H}}{\partial p_j} \underset{\approx}{S} + \underset{\approx}{\Lambda} \underset{\approx}{S}^{\dagger} \frac{\partial \underset{\approx}{S}}{\partial p_j}$$

$$\frac{\partial \underset{\approx}{\Lambda}}{\partial p_j} = \underset{\approx}{S}^{\dagger} \frac{\partial \underset{\approx}{H}}{\partial p_j} \underset{\approx}{S} + \underset{\approx}{\Lambda} \underset{\approx}{S}^{\dagger} \frac{\partial \underset{\approx}{S}}{\partial p_j} - \underset{\approx}{S}^{\dagger} \frac{\partial \underset{\approx}{S}}{\partial p_j} \underset{\approx}{\Lambda} \tag{A.11b}$$

In reaching Equation (A.11b), the orthonormality of the eigenvectors has been used. The left hand derivative matrix in Equation (A.11b) is diagonal and so we need only consider the diagonal elements of the right hand matrices. Those elements cancel in the last two terms and so

$$\left(\frac{\partial \underset{\approx}{\Lambda}}{\partial p_j}\right)_{mm} = \left(\underset{\approx}{S}^{\dagger} \frac{\partial \underset{\approx}{H}}{\partial p_j} \underset{\approx}{S}\right)_{mm} \tag{A.12}$$

Equation (A.12) states that the derivatives for $\underset{\approx}{V}$ in the normal equations can be found by differentiating the Hamiltonian and then applying the same transformation used to diagonalize it to yield the eigenstate derivatives. The differentiation of the Hamiltonian in the simple product basis is trivial since $H_{ik} = \Sigma c_i p_j$ and the eigenvectors required by Equation (A.12) are found at each cycle of the iteration.

Once the derivatives in Equation (A.12) are calculated, the normal equations may be solved according to Equation (A.8) to yield corrections to the parameters. The initial parameters are adjusted by these amounts and the next cycle of the iteration is started. In each cycle, the RMS deviation of the calculated lines and assigned frequencies is computed (Eq. (A.3)). If this RMS deviation does not change by more than one percent on going from one cycle to the next, then the definition of convergence has been reached and the final parameters used in a spectral simulation. Figure A.1 shows the overall procedure used in multiple quantum spectral fitting.

A.2.2 Error Analysis

The errors present in the digital resolution of a multiple quantum spectrum can be propagated to parameter errors by the usual techniques. It can be shown [118] that for the case where the standard deviations of

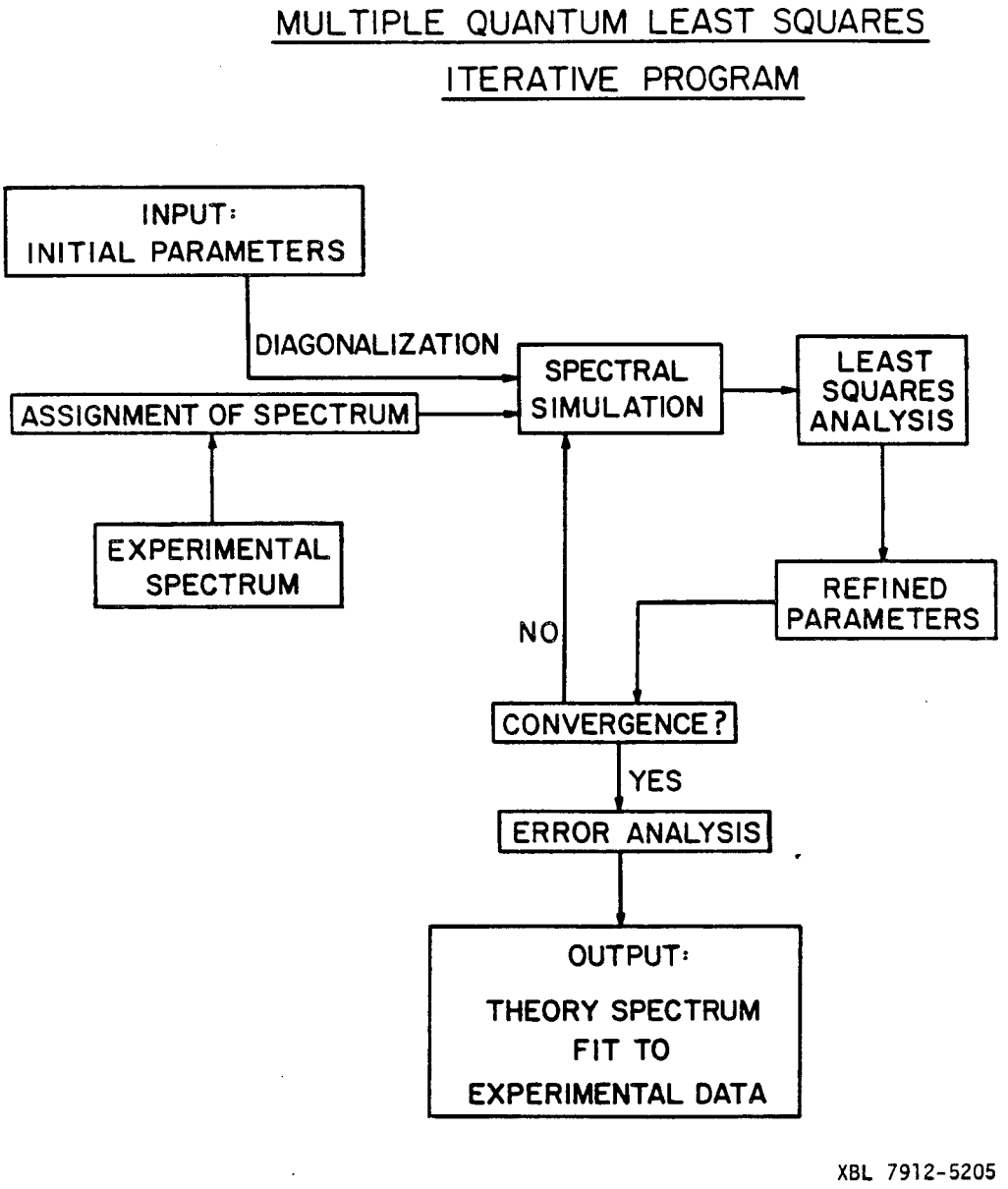

Figure A.1

Flow diagram for least squares iterative program used to fit and simulate multiple quantum NMR spectra.

each frequency measurement are the same, the variance-covariance matrix for the parameters derived from Equation (A.8) is given by the coefficients of the normal equations:

$$\underset{\approx}{C}_p = \sigma^2 (\underset{\approx}{V}^\dagger \underset{\approx}{V})^{-1} \tag{A.13}$$

Diagonal elements of $\underset{\approx}{C}_p$ give individual errors in each parameter (σ_i^2) and off-diagonal elements give the covariances defined by

$$C_{ik} = \langle (p_i - p_i^{(0)}) \rangle \langle (p_k - p_k^{(0)}) \rangle \tag{A.14}$$

where the angle brackets define an expectation value. In general, the parameters used for iteration are not independent and so the covariances are expected to be significant. As in the original program LAOCN3, the matrix in Equation (A.13) is diagonalized to give parameter errors for linear combinations of parameters forming a principle axis system in "error space". This may be of use in identifying those linearly independent combinations of parameters which define the system better. In addition, this locates the maximum and minimum errors possible for the parameters. In Equation (A.13) the variance σ^2, assumed equal for all lines used in the fitting, may be assumed from the final fit as [118]

$$\sigma^2 = (\Delta \underset{\approx}{M}^\dagger \Delta \underset{\approx}{M})/(k - q) \tag{A.15}$$

where k is the number of assigned lines and q is the number of parameters.

The propagation of errors from the refined parameters determined from MQITER to quantities such as bond angles and distances must also be considered. If the derivatives defining the relationship of the desired quantities, $\underset{\approx}{y}$, with respect to the variables $\underset{\approx}{x}$ are known, then the propagation of errors is expressed as

$$\underset{\approx}{C}_y = \underset{\approx}{D}\ \underset{\approx}{C}_x\ \underset{\approx}{D}^{\dagger}. \qquad (A.16)$$

$\underset{\approx}{D}$ is the matrix of derivatives, $\partial y_i/\partial x_k$, and $\underset{\approx}{C}_y$, $\underset{\approx}{C}_x$ are the variance-covariance matrices. Such a propagation of parameter errors will become important in the discussion of the program BIPH5PARA (Appendix B).

A.2.3 Program Description/MQITER

The listing for the iteration program MQITER is given in Appendix D. What follows is a brief description of the programs operations and subroutines. Table A.I gives a listing of the subroutines used and Table A.II a listing of the major matrices required. This listing is of a version designed to handle up to ten spins. Not all multiple quantum spectra may need to be calculated since line assignments may only be taken from the highest quantum transitions. If this is the case, the program allows for the exclusion of those parts of the Hamiltonian not necessary. The Hamiltonian is first set up in the simple product basis set in block diagonal form [118]. If a complete zero quantum or one quantum spectrum is desired then every submatrix must be set up in this basis set and then diagonalized. If this is the case, then the largest spin system possible with the array dimensions given in Table A.II is eight spins-½. MQITER is capable of calculating higher multiple quantum orders for greater than eight spins. As an example, if the five quantum is desired, none of the transitions involve the submatrix with M = 0 and its diagonalization may be omitted. This eliminates the need to diagonalize a 70 x 70 matrix and so computational time is decreased considerably. Some multiple quantum transitions for orders lower than five may still be found but those spectra will be incomplete. Variable MAXMAT holds the dimension of the largest Zeeman submatrix which is allowed. In this manner, part of the total multiple quantum spectrum can be

Table A.I

Subroutines and Functions Used by MQITER

Subroutine or Function Name	Called From	Purpose
1) LINORD	MQITER	Orders line assignments
2) CNTOUT	MQITER	Outputs coupling constants
3) HAMIL5	MQITER	Sets up Hamiltonian
4) CONDIT	MQITER	Sets up equations of condition
5) ERRIT	MQITER	Calculates RMS error
6) NORMAL	MQITER	Sets up normal equations
7) MINV	MQITER	Inverts a matrix
8) CORREC	MQITER	Corrects initial parameters
9) GENSYM	MQITER	Rearranges symmetric matrix
10) EIG2	MQITER HAMIL5	Diagonalizes a real symmetric matrix
11) EOUT	MQITER HAMIL5	Outputs energies
12) MQ2DIFF	MQITER	Calculates allowed MQ spectra
13) NUMSRT	HAMIL5	Calculates SP states
14) UNTRANS	HAMIL5 USWAP	Performs a unitary transformation
15) READMS	MQITER HAMIL5 SYMSET USWAP	File I/O
16) WRITMS	USWAP	File I/O
17) USWAP	HAMIL5	Rearranges Eigenvectors
18) SYMSET	MQ2DIFF	Calculates symmetry representations
19) FRQOUT	MQ2DIFF	Outputs frequencies
20) MAT	All routines	Array index functions
21) MATVEC	All routines	Array index functions

Table A.II

Major Arrays Used in MQITER

Array Name	Size	Purpose
D	(28)	Dipolar coupling constants
CJ	(28)	Scalar coupling constants
LST	(2,1024)	SP states and quantum numbers
NO	(11)	Binomial coefficients
NSP	(11)	Sum of binomial coefficients
NSM	(11)	Sum of allowed sub-matrix dimensions
EN	(256)	Energies
IPARAM	(28,15)	Parameters
DLMB	(256,28)	Derivatives of eigenvalues
MQIT	(2,10)	Multiple quantum orders
LASS	(230)	Experimental line assignments
EXPER	(230)	Experimental frequencies
DC	(230,28)	Matrix of derivatives
B	(230)	Miscellaneous work matrices
V	(784)	
BV	(28)	
WORK	(4900)	

calculated for nine and ten protons. The lowest orders for which all allowed transitions may be found are zero quantum for eight protons or less, seven quantum for nine protons and eight quantum when the molecule contains ten protons.

The program starts by opening three files; two are scratch files which will contain eigenvector matrices and one is the data file MQITER.DAT produced by MQITSET. The initial data is read in and certain array elements are determined. Variable N is the number of spins, LOWORD the lowest order transitions for which a complete spectrum is desired and ITER is the iteration control variable. Next, the couplings are read in (either from a previous data file with the same name as CASE or from MQITER.DAT) and output by subroutine CNTOUT. If this is an iterative calculation, the line assignments are also read in. Subroutine LINORD arranges them by order and line number for later calculation. Next, the parameters to be varied are read. A total of 28 parameter sets are allowed. With most molecules of interest, symmetry dictates that some parameters must be kept equal during the iteration [118]. As an example, for benzene, all the ortho couplings are equal and this forms one parameter set. A total of 15 parameters are allowed per parameter set. The method of specifying which dipolar or scalar coupling is meant by each parameter is described in the output of program MQITSET.

The iteration loop takes up the next eleven statements. Subroutine HAMIL5, described below, is called to set up and diagonalize the Hamiltonian matrix and find the derivative of this matrix with respect to each of the parameters. If ITER is zero, then the program just skips to the part which simulates the multiple quantum spectrum. Otherwise, subroutine CONDIT is used to calculate the equations of condition. ERRIT finds the current RMS error and returns variable NEXIT which determines

if convergence has been reached. Subroutine NORMAL sets up the normal equations according to Equation (A.8). MINV, a routine similar to a subroutine from an IBM subroutine package [123], inverts the normal equations coefficient matrix. Finally, CORREC applies the computed corrections to the parameters. ITER is then incremented for the next cycle.

Once convergence has been reached or too many cycles have occurred, flow proceeds to the error analysis section. The matrix of coefficients to the normal equations is first output. The inverse of this matrix is proportional to the parameter variance-covariance matrix according to Equation (A.13). Then, as described in Section A.2.2, this matrix is diagonalized by EIG2 (described below) and the eigenvectors, the standard errors of these "eigen parameters" and their probable errors are output. Finally, subroutine MQ2DIFF (see below) is used to simulate the multiple quantum spectrum from the refined parameter values.

Subroutine HAMIL5 is used to set up the Hamiltonian in a simple product basis set. The operation of this routine is based in large part on the methods developed by J. Murdoch [67]. The 2^N simple product states are actually the integers from zero to 2^N-1 in which each bit represents one nucleus. The numbering of these "nuclei" follows that of the dipolar and scalar couplings used. A zero for a particular bit represents one of the two spin-$\frac{1}{2}$ states (α or β) and a one means the other state. Thus, checking the value of a particular bit determines the spin state of that nucleus. For example, with four spins, a simple product state $\alpha\beta\alpha\beta$ is represented by the integer 5 (0101 binary). Using these "spin states" the Hamiltonian is found in this basis set by "operating" on the states to determine which couplings contribute to each matrix

element. Both the on-diagonal and off-diagonal elements are calculated in this manner. Only the submatrices for each total magnetic quantum number are calculated, all other elements being zero. HAMIL5 uses a definition of dipolar couplings twice that of Reference [18].

After each submatrix of the Hamiltonian in the simple product basis set is calculated, it must be diagonalized to give eigenstates and eigenvectors. If this is the first cycle in an iteration, or if no iteration is desired, this is done immediately by EIG2. For an intermediate stage in the iteration, the Hamiltonian is first subjected to the transformation

$$\underset{\approx}{H}'_{(n)} = \underset{\approx}{S}^{\dagger}_{(n-1)} \underset{\approx}{H}_{(n)} \underset{\approx}{S}_{(n-1)}. \qquad (A.17)$$

In Equation (A.17), the subscripts indicate the cycle number. If the parameters have not changed much on going from cycle (n-1) to cycle (n), then using the method of Equation (A.17) will produce matrix $\underset{\approx}{H}'_{(n)}$ which should be approximately diagonal. Subjecting this transformed matrix to the Jacobi method should require fewer rotations to reach a completely diagonal form. In addition, using Equation (A.17) at every cycle will help preserve the order of the eigenstates.

The subroutine EIG2 produces a diagonal matrix from a real symmetric one by the Jacobi rotation technique [124]. In this approach, the largest off-diagonal element is chosen as a pivotal element about which an orthogonal rotation is done. The angle of rotation is chosen so that this largest off-diagonal element is made to vanish. Orthogonal transformations of this type are repeated until no off-diagonal element is larger than a threshold. The unit matrix is also rotated by the same angle for each transformation. It can be shown that the product of the orthogonal matrices for each rotation is the required eigenvector matrix [118].

As mentioned above, it is necessary to keep the eigenstates in the same order as in the initial diagonalization. This is important to maintain the fit to experiment because the eigenstates will no longer be in the proper order for line assignments and will cause an erroneous divergence [125]. Such a situation is partly avoided in MQITER. Subroutine HAMIL5 calls USWAP which calculates the sum of squared deviations according to

$$\Delta_{ij}^2 = \sum_k ((S_{ki})_{(0)} - (S_{kj})_{(n)})^2. \qquad (A.18)$$

If none of the eigenvectors have changed position then the minimum elements of matrix $\underset{\approx}{\Delta}$ will be along its diagonal. If one of the off-diagonal elements in a particular row is the minimum value of that row, then the eigenstates and eigenvectors are swapped accordingly. This procedure should maintain the line assignments and avoid divergence due to the method of diagonalization. This rearrangement of the eigenvalue sequence is particularly common when the dimension of the submatrix is large and it contains several degenerate states.

Subroutine MQ2DIFF is used to calculate the multiple quantum spectrum from final parameters. As with the other parts of the program, MQ2DIFF will calculate incomplete multiple quantum spectra when not all submatrices of the Hamiltonian have been diagonalized. Since there is no offset term in the Hamiltonian computed by HAMIL5, transition frequencies for each order are calculated relative to the centers of the orders. HAMIL5 also assumes that all chemical shifts are zero and so each order is symmetric about its center. MQ2DIFF only outputs one half of the symmetric spectrum. After the presentation of the spectrum with identifying line numbers and transition states, the frequencies of one

half of each order are presented as a descending list of positive numbers. MQ2DIFF attempts to identify degenerate transitions in this list. The eigenstates may also be scanned for degeneracies to help locate doubly degenerate symmetry representations.

Subroutine SYMSET is called by MQ2DIFF to classify eigenstates by their symmetry relations. The calculation is based on the group theory result stated in the following equations.

$$\text{If} \quad |\langle \Gamma_i | A_1 | \Gamma_j \rangle|^2 \neq 0,$$

$$\text{then} \quad \Gamma_i = \Gamma_j. \tag{A.19}$$

In Equation (A.19), the Γ symbols refer to the irreducible symmetry representations of states i and j. For NMR single quantum transitions, neglecting symmetry breaking relaxation effects, the magnetic dipole transition operators are totally symmetric (i.e., A_1 representation) [36]. Equation (A.19) states that to find states of the same irreducible symmetry representation, the transition element

$$|\langle i | I_x | j \rangle|^2$$

must be found and compared to zero. Instead of I_x, a more convenient operator to use in SYMSET based on the form of the simple product states is I_-. SYMSET loops through all eigenstates and calculates the appropriate matrix element from the expansion of these in terms of simple product states with the eigenvectors from HAMIL5 as coefficients. The resulting matrix elements are compared to a threshold level and if found greater than this level the corresponding states are labelled as belonging to the same irreducible representation. In this manner, all states are classified by representation. An alternative to the approach of

calculating each matrix element individually is to set up the transition operator in the simple product basis and then transform it using the eigenvector matrix.

When not all submatrices have been included in the calculations of HAMIL5, matrix elements of I_- alone are not sufficient to determine all the symmetry relations among eigenstates. The missing submatrix is "bridged" by computing matrix elements of I_-^n where n-1 is the number of submatrices missing. This allows symmetry representations for states below the missing Zeeman manifold to be connected to those above. However, calculations show [126] that matrix elements of I_-^n for states within the same representation may vanish and so this method may omit allowed transitions. The best possible calculation, without expressing the point group of the molecule in the Hamiltonian [127] is to use the single quantum operator I_-.

Once the representations have been determined, MQ2DIFF outputs all the symmetry allowed transitions for the multiple quantum orders of interest. This presentation carries none of the information concerning intensities as they are dependent on experimental parameters as described in the previous chapters. Also output by the program are the eigenstates organized by the symmetry representations found by SYMSET. In this list, states labelled as representation #1 are those for which no non-zero matrix elements were located. States of representation #2 are the totally symmetric (A_1) states. The extreme Zeeman states are always found in this representation. The relationship of the other representations to the actual point group irreducible representations must be made by examination of the dimensions of each Zeeman manifold.

A.2.4 Program Example: Benzene

As an example of the operation of MQITER, consider the case of benzene oriented in a liquid crystal as in previous chapters. The high order transitions produce very simple spectra and the line splitting of the sole five quantum pair is sufficient to determine the entire spectrum when hexagonal ring geometry and scalar couplings are assumed. Because of this, it is not necessary to use MQITER to iterate to a solution for the benzene spectrum. However, it is a well understood and characterized spectrum and so a convenient example to choose. This particular example is for the fit of one calculated spectrum to that of another and so the parameter errors are extremely small. The use of MQITER with actual experimental lines assignments also produces a very good fit with the parameter errors found to be well within the bounds expected on the basis of the digital resolution of the Fourier transform spectrum.

An initial run is necessary to give line numbers for assignment to the "experimental" spectrum. In the second run, the line assignments come from another simulation with a different set of couplings which represents this "experimental" spectrum. As seen in the RMS error calculation, the initial fit is already fairly close. Both D's and J's were varied in the iteration, the parameter sets corresponding to ortho, meta, and para couplings. During the cycles, states are swapped by the method described in the previous section. Note that only degenerate states are affected by this swapping implying that, even without this check, convergence would be obtained because the RMS error would still decrease. The final parameter errors reported are indeed very small. After the refined parameters are output, the variance -covariance matrix and the eigenvectors from its diagonalization are given. This eigenvector matrix

is not completely diagonal indicating strong mixing of the parameters. This is to be expected for the dipolar coupling parameters due to their dependence mentioned above, but in addition, each eigenvector shows significant mixing of dipolar and scalar couplings. Even though no anisotropic (or "pseudo-dipolar") contribution from J_{ij} is included in the Hamiltonian, this eigenvector matrix shows that the D_{ij}'s and J_{ij}'s are not linearly independent.

After the simulation is performed and the frequencies output, a listing of degeneracies found among the eigenstates is given. Following this, the symmetry classifications of eigenstates is shown. The correspondence between these classes and the point group representations is: representation #1, A_2 state; representation #2, A_1 states; representation #3, $E_2^{a,b}$ states; representation #4, B_1 states; representation #5, $E_1^{a,b}$ states; representation #6, B_2 states.

A.2.5 Computer Output for Benzene Example

CASE benziti

benzene iteration example

D(1 2 = -1300.0000
J(1 2 = 6.0000

D(1 3 = -250 1900
J(1 3 = 1.0000

D(1 4 = -162.5000
J(1 4 = 0.5000

D(1 5 = -250.1900
J(1 5 = 1.0000

D(1 6 = -1300 0000
J(1 6 = 6.0000

D(2 3 = -1300.0000
J(2 3 = 6 0000

D(2 4 = -250.1900
J(2 4 = 1.0000

D(2 5 = -162.5000
J(2 5 = 0.5000

D(2 6 = 250 1900
J(2 6 = 1.0000

D(3 4 = -1300.0000
J(3 4 = 6.0000

D(3 5 = -250 1900
J(3 5 = 1.0000

D(3 6 = -162.5000
J(3 6 = 0 5000

D(4 5 = -1300.0000
J(4 5 = 6.0000

D(4 6 = -250 1900
J(4 6 = 1.0000

D(5 6 = -1300.0000
J(5 6 = 6 0000

TOTAL # OF FREQ ENTERED = 32

TMPMOB.LOG;1 4-NOV-1981 16:42:18.28 Page 4

LINE ASSIGNMENTS FOR THE 2 QUANTUM SPECTRUM

LINE #	EXPERIMENTAL FREQUENCY
1	1565.8000
2	4184.9800
3	2332.2100
22	2253.7400
23	2253.7400
25	555.7400
26	555.7400
28	1629.1300
29	1629.1300
37	889.7100
39	-544.7400
41	2423.0200
56	695.8400
58	1321.5000
7	3310.6201

TMPMOB.LOG;1 4-NOV-1981 16:42:18.28 Page 5

LINE ASSIGNMENTS FOR THE 3 QUANTUM SPECTRUM

LINE #	EXPERIMENTAL FREQUENCY
2	3261.5801
4	1827.1400
6	4794.8999
25	1303.0500
26	2143.8999
29	1303.0500
33	2143.8999
36	-806.0700
37	1733.1000
39	-39.6620
64	2008.1000
72	1314.6200
77	1314.6200

TMPMOB.LOG;1 4-NOV-1981 16:42:18.28 Page 6

LINE ASSIGNMENTS FOR THE 4 QUANTUM SPECTRUM.

LINE #	EXPERIMENTAL FREQUENCY
1	1565.8101
2	4184.9800
4	2332.2100

TMPMOB.LOG;1 4-NOV-1981 16:42:18.28 Page 7

LINE ASSIGNMENTS FOR THE 5 QUANTUM SPECTRUM

LINE #	EXPERIMENTAL FREQUENCY
1	2371.8799

```
TMPMCB ICG;1                    4 NOV-1981 16 42:18 2E          Page 6

PROGRAM MQITER - START OF ITERATIVE CALCULATIONS.

    ITERATION #  1   R M S ERROR =   74.303
          SWAPPED STATES:    6 ,    5
          SWAPPED STATES    17 ,   12
    ITERATION #  2   R M S ERROR =    0.011
          SWAPPED STATES:    5 ,    6
          SWAPPED STATES    12 ,   17
          SWAPPED STATES    55 ,   50
    ITERATION #  3   R M S ERROR =    0.007
          SWAPPED STATES    17 ,   12
          SWAPPED STATES    50     55
          SWAPPED STATES:   54 ,   49
          SWAPPED STATES    55 ,   50
    ITERATION #  4   R M S ERROR =    0.007

PARAMETER SET #  1

D12
D23
D34
D45
D56
D16

PARAMETER SET #  2

D13
D24
D35
D46
D15
D26

PARAMETER SET #  3

D14
D25
D36

PARAMETER SET #  4

J12
J23
J34
J45
J56
J16

PARAMETER SET #  5

J13
J24
J35
J46
J15
J26

PARAMETER SET #  6

J14
J25
J36
```

REFINED PARAMETERS . . .

D(1 2) = -1259.9948
J(1 2) = 9.9978

D(1 3) = -242.5051
J(1 3) = 5.0035

D(1 4) = -157.5022
J(1 4) = 1.0065

D(1 5) = -242.5051
J(1 5) = 5.0035

D(1 6) = -1259.9948
J(1 6) = 9.9978

D(2 3) = -1259.9948
J(2 3) = 9.9978

D(2 4) = -242.5051
J(2 4) = 5.0035

D(2 5) = 157.5022
J(2 5) = 1.0065

D(2 6) = -242.5051
J(2 6) = 5.0035

D(3 4) = -1259.9948
J(3 4) = 9.9978

D(3 5) = -242.5051
J(3 5) = 5.0035

D(3 6) = -157.5022
J(3 6) = 1.0065

D(4 5) = -1259.9948
J(4 5) = 9.9978

D(4 6) = 242.5051
J(4 6) = 5.0035

D(5 6) = -1259.9948
J(5 6) = 9.9978

TMPMCB ICG;1 4 NOV-1981 16 42:18.28 Page 12

MATRIX OF COEFFICIENTS FOR THE NORMAL EQUATIONS
(BEFORE DIAGONALIZATION) . .

1)	0 1913E-02	-0 1194E-02	-0 1907E-02	0 1916E-03	0.1304E-03	0 2385E-03
2	-0 1194E-02	0.3664E-02	-0.2905E-03	-0.1974E-03	-0.4772E-03	-0.2328E-02
3)	-0 1907E-02	-0.2905E-03	0 9733E-02	-0.8043E-03	-0.1518E-02	0.1672E-03
4	0 1916E-03	-0.1974E-03	-0 8043E-03	0.3069E-02	-0.1417E-02	-0.2613E-02
5	0 1304E-03	-0 4772E-03	-0 1518E-02	-0 1417E-02	0.2791E-02	0.1599E-02
6	0 2385E-03	-0.2328E-02	0 1672E-03	-0 2613E-02	0.1599E-02	0.6922E-02

EIGENVALUES OF NORMAL EQUATIONS MATRIX .

2561 061 237 698 101.241 745.659 521.499 103.319

TMPMCB ICG;1 4-NOV-1981 16:42:18.28 Page 13

ERROR VECTORS AND STANDARD DEVIATIONS OF EIGENBASIS PARAMETERS . . .

0 5391 0 4817 0.2337 0.4942 0.3315 0.2619
STANDARD ERROR = 0 000
-0 3395 0 7284 -0.0781 -0 5046 0.3956 -0.0057
STANDARD ERROR = 0.001
0 2394 0 0478 0.9412 -0.0462 -0.2167 -0.0748
STANDARD ERROR = 0 001
0 7131 -0.0944 -0.0531 0.5694 0.3623 0.1557
STANDARD ERROR = 0 200
0 1636 -0 3371 0 1821 -0 1782 0.7418 -0.4972
STANDARD ERROR = 0.000
0 2392 -0.3355 0.1320 -0.3818 0.2612 0.8090
STANDARD ERROR = 0 001

TMPMCB ICG;1 4-NOV-1981 16:42:18 28 Page 14

PROBABLE ERRORS OF EIGENBASIS PARAMETER SETS . .

1	0.000
2	0.000
3	0 001
4	0.000
5	0.000
6	0 001

REFINED ENERGIES . . .

EN(1) = -2348.6201

EN(2) = -1126.1205
EN(3) = 23.2569
EN(4) = -1336.4915
EN(5) = -565.8827
EN(6) = -565.8827
EN(7) = -1126.1204

EN(8) = -782.8983
EN(9) = 1756.3574
EN(10) = -16.4116
EN(11) = 1017.7760
EN(12) = -670.4888
EN(13) = -616.3345
EN(14) = 671.6273
EN(15) = 1017.7761
EN(16) = 176.9272
EN(17) = -670.4889
EN(18) = 748.7367
EN(19) = 176.9272
EN(20) = -616.3342
EN(21) = 748.7367
EN(22) = -593.3799

EN(23) = -640.6532
EN(24) = 912.9626
EN(25) = -14.9649
EN(26) = -521.4840
EN(27) = 1121.2855
EN(28) = 2446.2722
EN(29) = 1127.6299
EN(30) = 1127.6301
EN(31) = -21.7477
EN(32) = -570.3831
EN(33) = -570.3832
EN(34) = 1121.2853
EN(35) = 503.0070
EN(36) = 503.0070
EN(37) = 1974.1377
EN(38) = 407.8770
EN(39) = -548.6663
EN(40) = 1178.4855
EN(41) = 407.8772
EN(42) = -548.6665

EN(43) = -782.8983
EN(44) = 1756.3577
EN(45) = -593.3801
EN(46) = -16.4116
EN(47) = 176.9273
EN(48) = -670.4891
EN(49) = 748.7369
EN(50) = 1017.7768
EN(51) = 176.9273
EN(52) = -616.3347
EN(53) = -670.4890
EN(54) = 748.7369

EN(55) = 1017.7764
EN(56) = 671.6282
EN(57) = -616.3344

EN(58) = 23.2569
EN(59) = -1336.4916
EN(60) = -1126.1210
EN(61) = -565.8826
EN(62) = -1126.1201
EN(63) = -565.8828

EN(64) = -2348.6201

1 QUANTUM SPECTRUM CALCULATION . . .

LINE #	FREQUENCY (HZ)	TRANSITION STATES	SYMM
LOWER QUANTUM # = 3 ; UPPER QUANTUM # = 2			
2	2371.8770	3-> 1	2
LOWER QUANTUM # = 2 ; UPPER QUANTUM # = 1			
10	2143.8965	11-> 2	3
12	509.7860	13-> 2	3
14	2143.8967	15 > 2	3
15	1303.0477	16-> 2	3
18	1303.0476	19-> 2	3
19	509.7863	20 > 2	3
22	-806.0652	8-> 3	2
23	1733.1006	9-> 3	2
24	-39.6665	10 > 3	2
43	2008.1188	14-> 4	4
56	-104.6061	12-> 5	5
61	-104.6062	17 > 5	5
62	1314.6194	18-> 5	5
65	1314.6194	21 > 5	5
LOWER QUANTUM # = 1 ; UPPER QUANTUM # = 6			
98	1695.7709	24-> 8	2
100	261.3243	26-> 8	2
112	3229.0876	28-> 8	2
119	-843.3948	24-> 9	2
120	-2277.8416	26-> 9	2
122	689.9148	28 > 9	2
138	929.3742	24-> 10	2
140	-505.0724	26 > 10	2
142	2462.6838	28 > 10	2
163	109.8538	29-> 11	3
164	109.8541	30-> 11	3
166	-1588.1592	32 > 11	3
167	-1588.1592	33-> 11	3
169	-514.7690	35-> 11	3
170	-514.7693	36-> 11	3
181	1791.7743	27-> 12	5
188	1791.7740	34-> 12	5
192	1078.3657	38-> 12	5
193	121.8225	39-> 12	5
195	1078.3660	41-> 12	5
196	121.8223	42-> 12	5
203	1743.9642	29-> 13	3
204	1743.9648	30-> 13	3
206	45.9514	32-> 13	3
207	45.9513	33-> 13	3
209	1119.3416	35-> 13	3
210	1119.3414	36-> 13	3
217	-1312.2885	23-> 14	4
219	-686.5923	25-> 14	4
231	1302.4803	37 > 14	4
263	950.7026	29-> 16	3
264	950.7029	30-> 16	3

266	-747.3104	32-> 16	3
267	-747.3104	33-> 16	3
269	326.0798	35-> 16	3
270	326.0797	36-> 16	3
311	372.5488	27-> 18	5
308	372.5486	34-> 18	5
312	-340.8597	38-> 18	5
313	-1297.4030	39-> 18	5
315	-340.8595	41-> 18	5
316	-1297.4032	42-> 18	5
394	1771.8654	40-> 22	6

FREQ (HZ)	DEGENERACY
3229 0806	1
2462 6838	1
2371 8770	1
2277 8416	1
2143 8965	2
2008 1188	1
1791 7743	2
1771 8654	1
1743 9642	2
1733 1206	1
1695 7709	1
1588 1592	2
1314 6194	2
1312 2805	1
1303 0477	2
1302 4803	1
1297 4030	2
1119 3416	2
1078 3657	2
950 7026	2
929 3742	1
843 3948	1
806 0652	1
747 3104	2
659 9148	1
686 5923	1
514 7690	2
509 7867	2
505 0724	1
372 5488	2
340 8597	2
326 0798	2
261 3243	1
121 8225	2
109 8539	2
104 6061	2
45 9514	2
39 6685	1

TOTAL # UNIQUE FREQ = 38

2 QUANTUM SPECTRUM CALCULATION . . .

LINE #	FREQUENCY (HZ)	TRANSITION STATES	SYMM
LOWER QUANTUM # = 3 ; UPPER QUANTUM # = 1			
1	1565.8119	8-> 1	2
2	4104.9775	9-> 1	2
3	2332.2085	10-> 1	2
LOWER QUANTUM # = 2 ; UPPER QUANTUM # = 0			
22	2253.7502	29-> 2	3
23	2253.7507	30-> 2	3
25	555.7374	32-> 2	3
26	555.7373	33-> 2	3
28	1629.1276	35-> 2	3
29	1629.1274	36-> 2	3
37	699.7057	24-> 3	2
39	-544.7409	26-> 3	2
41	2423.0154	28-> 3	2
56	695.8383	23-> 4	4
58	1321.5265	25-> 4	4
70	3310.5991	37-> 4	4
80	1687.1682	27-> 5	5
87	1687.1680	34-> 5	5
91	973.7597	38-> 5	5
92	17.2164	39-> 5	5
94	973.7599	41-> 5	5
95	17.2162	42-> 5	5
LOWER QUANTUM # = 1 ; UPPER QUANTUM # = -1			
136	-0.0001	43-> 6	2
137	2539.1660	44-> 6	2
139	766.3967	46-> 6	2
151	-2539.1658	43-> 9	2
152	0.0002	44-> 9	2
154	-1772.7690	46-> 9	2
166	-766.3967	43-> 10	2
167	1772.7693	44-> 10	2
169	0.0000	46-> 10	2
185	-840.8488	47-> 11	3
186	0.0002	50-> 11	3
189	-840.8487	51-> 11	3
190	-1634.1100	52-> 11	3
193	0.0004	55-> 11	3
195	-1634.1104	57-> 11	3
201	-0.0004	48-> 12	5
202	1419.2257	49-> 12	5
206	-0.0002	53-> 12	5
207	1419.2257	54-> 12	5
215	793.2618	47-> 13	3
218	1634.1113	50-> 13	3
219	793.2618	51-> 13	3
220	0.0005	52-> 13	3
223	1634.1110	55-> 13	3
225	0.0001	57-> 13	3
239	0.0009	56-> 14	4

TMPMCB LCG;1 4-NOV-1981 16 42:18.2E Page 21

260	0.0001	47-> 16	3
263	840.8496	50-> 16	3
264	0.0001	51-> 16	3
265	-793.2612	52-> 16	3
268	840.8492	55-> 16	3
270	-793.2616	57-> 16	3
291	-1419.2258	48-> 16	5
292	0.0002	49-> 16	5
296	-1419.2257	53-> 16	5
297	0.0002	54-> 16	5
348	-0.0002	45-> 22	6

TMPMQB LCG;1 4-NOV-1981 16:42:18.2E Page 22

FREQ (HZ)	DEGENERACY
4174 9775	1
3310 5991	1
2539 1660	1
2423 7154	1
2332 2085	1
2253 7502	2
1772 769[illegible]	1
1687 1682	2
1634 1100	2
1629 1276	2
1565 8119	1
1419 2257	2
1321 5265	1
973 7597	2
889 7057	1
840 8488	2
793 2619	2
766 3967	1
655 8383	1
555 7374	2
544 7409	1
17 2164	2
0 0001	15

TOTAL # UNIQUE FREQ = 23

TMPMCB ICG;1 4-NOV-1981 16 42:18.28 Page 23

3 QUANTUM SPECTRUM CALCULATION . . .

LINE #	FREQUENCY (HZ)	TRANSITION STATES	SYMM
LOWER QUANTUM # = 3 ; UPPER QUANTUM # = 0			
2	3261.5828	24-> 1	2
4	1827.1361	26-> 1	2
6	4794.8926	28-> 1	2
LOWER QUANTUM # = 2 ; UPPER QUANTUM # = -1			
25	1303.0477	47-> 2	3
28	2143.8972	50-> 2	3
29	1303.2479	51-> 2	3
30	509.7865	52-> 2	3
33	2143.8970	55-> 2	3
35	509.7861	57-> 2	3
36	-806.0652	43-> 3	2
37	1733.1008	44-> 3	2
39	39.6685	46-> 3	2
64	2008.1196	56-> 4	4
71	-104.6064	48-> 5	5
72	1314.6196	49-> 5	5
76	-104.6063	53-> 5	5
77	1314.6196	54-> 5	5

TMPMCB ICG;1 4 NOV-1981 16 42:18.28 Page 24

FREQ (HZ)	DEGENERACY
4794 8926	1
3261 5828	1
2143 8972	2
2008 1196	1
1827 1361	1
1733 1008	1
1314 6196	2
1303 0477	2
806 0652	1
509 7865	2
104 6064	2
39 6685	1

TOTAL # UNIQUE FREQ = 12

TMPMCB LCG;1 4-NOV-1981 16:42:18.28 Page 25

4 QUANTUM SPECTRUM CALCULATION . . .

LINE #	FREQUENCY (HZ)	TRANSITION STATES	SYMM
LOWER QUANTUM # = 3 ; UPPER QUANTUM # = -1			
1	1565.8118	43-> 1	2
2	4104.9780	44-> 1	2
4	2332.2085	46-> 1	2
LOWER QUANTUM # = 2 ; UPPER QUANTUM # = -2			
18	-0.0005	60-> 2	3
20	0.0004	62-> 2	3
22	0.0000	58-> 3	2
25	-0.0001	59-> 4	4
37	0.0001	61-> 5	5
39	-0.0001	63 > 5	5

TMPMCB LCG;1 4 NOV-1981 16:42:18.28 Page 26

FREQ (HZ	DEGENERACY
4104.9780	1
2332.2085	1
1565.8118	1
0.0005	6

TOTAL # UNIQUE FREQ = 4

TMPMQB LCG;1 4-NOV-1981 16:42:18.28 Page 27

5 QUANTUM SPECTRUM CALCULATION . . .

LINE #	FREQUENCY (HZ)	TRANSITION STATES	SYMM
LOWER QUANTUM # = 3 ; UPPER QUANTUM # = -2			
1	2371.8770	58-> 1	2

TMPMCB ICG;1 4-NOV-1981 16:42:18.28 Page 25

0 QUANTUM SPECTRUM CALCULATION . . .

LINE #	FREQUENCY (EZ)	TRANSITION STATES	SYMM
QUANTUM # 2			
QUANTUM # 1			
16	2539.1658	9-> 8	2
17	766.3967	10-> 8	2
30	-1772.7690	10-> 9	2
56	-1634.1105	13-> 11	3
59	-840.8488	16-> 11	3
62	-840.8488	19 > 11	3
63	-1634.1102	20-> 11	3
71	1419.2255	18-> 12	5
74	1419.2255	21 > 12	5
77	1634.1106	15-> 13	3
79	793.2617	16-> 13	3
81	793.2617	19-> 13	3
103	-793.2615	20-> 16	3
QUANTUM # 0			
122	625.6882	25-> 23	4
134	2614.7610	37-> 23	4
141	-1434.4467	26-> 24	2
143	1533.3097	28-> 24	2
169	1989.0726	37-> 25	4
176	2987.7563	28 > 26	2
201	-713.4086	38-> 27	5
202	-1669.9518	39-> 27	5
204	-713.4084	41-> 27	5
205	-1669.9523	42-> 27	5
220	0.0004	30-> 29	3
222	-1698.0129	32-> 29	3
223	-1698.0129	33-> 29	3
225	-624.6227	35-> 29	3
226	-624.6228	36-> 29	3
234	-1698.0133	32-> 30	3
235	-1698.0133	33-> 30	3
237	-624.6231	35-> 30	3
239	-624.6232	36-> 30	3
258	1073.3901	35-> 32	3
259	1073.3901	36-> 32	3
301	-956.5433	39-> 38	5
304	-956.5435	42-> 38	5
306	956.5435	41-> 39	5
QUANTUM # -1			
311	2539.1660	44-> 43	2
313	766.3967	46-> 43	2
326	-1772.7693	46-> 44	2
363	840.8495	50-> 47	3
365	-793.2613	52-> 47	3
368	840.8492	55 > 47	3
370	-793.2617	57-> 47	3

TMPMQB LOG;1 4-NOV-1981 16:42:18.22 Page 30

371	1419.2261	49-> 48	5
376	1419.2261	54-> 48	5
383	-1419.2260	53-> 49	5
388	-840.8495	51-> 50	3
389	-1634.1108	52-> 50	3
394	-1634.1112	57-> 52	3
403	1634.1105	55-> 52	3

QUANTUM # -2

TMPMQB.LOG;1 4-NOV-1981 16:42:18.28 Page 31

FREQ (HZ)	DEGENERACY
2967.7563	1
2614.7610	1
2539.1658	2
1969.2726	1
1772.7690	2
1698.0129	4
1669.9518	2
1634.1105	4
1533.3097	1
1434.4467	1
1419.2255	4
1073.3901	2
956.5433	2
840.8488	2
793.2617	2
766.3967	2
713.4086	2
625.6882	1
624.6227	4
0.0004	1

TOTAL # UNIQUE FREQ = 20

ENERGY DEGENERACY CALCULATION. . .

```
EN(  1  =   -2348 6201
EN(  2)     -1126.1205
EN   3      -23.2569
EN   4  =   -1336.4915
EN(  5)      -565.8827
EN   6       -565.8827     IS DEGENERATE WITH STATE #   5
EN(  7       -1126.1200    IS DEGENERATE WITH STATE #   2
EN(  8)  =    -782.8083
EN   9       1756.3574
EN( 1   =     -16.4116
EN( 11)      1017.7760
EN   12  =    -670.4888
EN( 13   =    -616.3345
EN( 14)       671.6273
EN   15      1017.7761     IS DEGENERATE WITH STATE #  11
EN(  16  =    176.9272
EN   17)     -670.4889     IS DEGENERATE WITH STATE #  12
EN   18       748.7367
EN   19       176.9272     IS DEGENERATE WITH STATE #  16
EN   20)     -616.3342     IS DEGENERATE WITH STATE #  13
EN   21       748.7367     IS DEGENERATE WITH STATE #  18
EN   22   =   -593.3799
EN   23)  =   -640.6532
EN   24   -    912.9626
EN   25   =     -14 9649
EN   26)     -521.4840
EN   27      1121.2855
EN   28   -  2446.2722
EN   29)  -  1127.6298
EN   30      1127.6301
EN   31   -    -21.7479
EN   32)     -570.3831
EN   33      -570.3832     IS DEGENERATE WITH STATE #  32
EN   34   -  1121.2853     IS DEGENERATE WITH STATE #  27
EN(  35)      503 0070
EN   36   -   503.0070     IS DEGENERATE WITH STATE #  35
EN   37   =  1974.1077
EN(  38)      407.8770
EN   39      -548.6663
EN   4    -  1178.4855
EN   41)      407 8772     IS DEGENERATE WITH STATE #  38
EN   42      -549.6665     IS DEGENERATE WITH STATE #  39
EN   43   =   -782.8083
EN   44)  -  1756.3577
EN   45      -593.3801
EN   46   =    -16.4116
EN   47)  -    176 9273
EN   48      -670.4891
EN   49   -    748.7369
EN   50)     1017 7768
EN   51   -    176.9273     IS DEGENERATE WITH STATE #  47
EN   52)  =   -616.3340
EN   53)     -670 4890     IS DEGENERATE WITH STATE #  48
EN   54       748.7369     IS DEGENERATE WITH STATE #  49
EN   55   =  1017.7764     IS DEGENERATE WITH STATE #  50
EN   56)      671 6282
EN   7       -616.3344     IS DEGENERATE WITH STATE #  52
EN   58   -    23.2569
EN   59)    -1336.4916
EN   60     -1126.1210
EN(  61  =   -565.8826
EN(  62  =   1126.1201     IS DEGENERATE WITH STATE #  60
EN   63)  -   -565.8828     IS DEGENERATE WITH STATE #  61
EN   64   -  -2348.6201
```

SYMMETRY CLASSIFICATION OF EIGENSTATES. . .

STATES OF REPRESENTATION # 1

EN(31) = -21.7479

TOTAL NUMBER OF STATES = 1

STATES OF REPRESENTATION # 2

EN(1) = -2348.6291
EN(3) = 23.2569
EN 8 = -782.8083
EN(9) = 1756.3574
EN(10) = -16.4116
EN 24 = 912.9626
EN(26) = -521.4847
EN(28) = 2446.2722
EN 43 = -782.8083
EN 44 = 1756.3577
EN(46) = -16.4116
EN 59 = 23.2569
EN(64) = 2348.6291

TOTAL NUMBER OF STATES = 13

STATES OF REPRESENTATION # 3

EN(2) = -1126.1205
EN(7) = -1126.1200
EN 11 = 1017.7760
EN 13 = -616.3345
EN(15) = 1017.7761
EN 16 = 176.9272
EN(19) = 176.9272
EN 20) = -616.3342
EN 29 = 1127.6298
EN(30) = 1127.6301
EN(32) = -570.3831
EN 33 = -570.3832
EN(35) = 503.0070
EN(36) = 503.0070
EN 47 = 176.9273
EN 50 = 1017.7768
EN(51) = 176.9273
EN 52 = -616.3340
EN(55) = 1017.7764
EN(57) = -616.3344
EN 60 = -1126.1210
EN(62) = 1126.1201

TOTAL NUMBER OF STATES = 22

STATES OF REPRESENTATION # 4

EN(4) = -1336.4915
EN(14) = 671.6273
EN 23 = -640.8532
EN(25) = 14.9649
EN(27) = 1974.1077
EN 56 = 671.6282
EN(59) = -1336.4916

TOTAL NUMBER OF STATES = 7

```
TMPMQB LOG:1                    4-NOV-1981 16:42:18.28          Page 35

     STATES OF REPRESENTATION #  5
EN    5        -565.8827
EN(  6  =       565.8827
EN(  12)       -670.4888
EN   17  =     -670.4889
EN(  18) =      748.7367
EN(  21)        748.7367
EN   27        1121.2855
EN(  34) =     1121.2853
EN(  38) =      407.8770
EN(  39        -542.6663
EN(  41  =      407.8772
EN(  42) -     -542.6665
EN   48        -670.4891
EN(  49  =      748.7369
EN(  53) -     -670.4890
EN   54         748.7369
EN   61  =     -565.8826
EN   63  =     -565.8828

          TOTAL NUMBER OF STATES =  18

     STATES OF REPRESENTATION #  6
EN(  22)       -593.3799
EN   40        1178.4855
EN(  45  =     -593.3801

          TOTAL NUMBER OF STATES =   3
FORTRAN STOP
  PINENUTS     job terminated at  4 NOV-1981 16:42:18.15

  Accounting information:
  Buffered I/O count            72      Peak working set size:    200
  Direct I/O count             236      Peak virtual size:        454
  Page faults:                 404      Mounted volumes:            0
  Elapsed CPU time:     0 00:01:12.97   Elapsed time:     0 00:15:12.15
```

APPENDIX B

Programs to Calculate Biphenyl Dipolar Couplings

The proton dipole-dipole couplings of a biphenyl group with either D_2 or D_4 symmetry are calculated with programs BIPH4PARA or BIPH5PARA. Program BIPH4PARA calculates couplings for any particular set of molecular parameters. This program will also increment one of the parameters to produce a series of couplings. Program BIPH5PARA computes a least-squares fit of the calculated couplings to a set of experimental couplings which are given as part of the input. Both programs calculate the A_1 symmetry lines allowed in the six and seven quantum transitions. BIPH4PARA writes these line frequencies to a disk file which is later used to produce variation plots like these shown in Chapter 4.

The following sections outline the coupling constant calculation and give a brief description of each program.

B.1 Dipolar Couplings for Biphenyl

The form of the coupling constant equations is essentially the same when either D_2 or D_4 symmetry is assumed. The more general case is the one with less symmetry: the D_2 point group. This is the symmetry assumed in the equations below. The D_4 couplings are derived by first transforming the order tensor from coordinate system #1 (see Fig. 4.5) and then proceeding with the equations for D_2 symmetry. This transformation may be written as

$$\underset{\approx}{S}^{(2)} = \underset{\approx}{R}^{T} \underset{\approx}{S}^{(1)} \underset{\approx}{R} \qquad \text{(B.1)}$$

where $\underset{\approx}{S}^{(1)}$ and $\underset{\approx}{S}^{(2)}$ refer to the order tensors in molecular coordinate system #1 and #2 respectively. The transformation matrix $\underset{\approx}{R}$ is given in

Equation (2.3). For the transformation required, angle $\alpha = +\phi/2$ and $\beta = \gamma = 0$. The non-zero order parameters in coordinate system #2 in terms of coordinate system #1, are then

$$(S_{xx}^{(2)} - S_{yy}^{(2)}) = (S_{xx}^{(1)} - S_{yy}^{(1)})(\cos^2\phi/2 - \sin^2\phi/2) \tag{B.2a}$$

$$S_{xy}^{(2)} = (S_{xx}^{(1)} - S_{yy}^{(1)})\ \cos\phi/2\sin\phi/2 \tag{B.2b}$$

$$S_{zz}^{(2)} = S_{zz}^{(1)} \tag{B.2c}$$

The equations for the coupling constants are given below. Since coordinate system #2 is used throughout, the superscript 2 is dropped. These equations all contain the average couplings for conformations, with $\pm\phi$. The numbering is according to Figure (4.5). The following definitions are used in the coupling constant equations. The internuclear distances when the dihedral angle ϕ is zero are denote as r_{260}, r_{150}, r_{160}, and r_{250}. The angles $\alpha,\beta,\gamma,\gamma',\delta$, and δ' are given by the following trigonometric relations.

$$\sin\alpha = \frac{r_{67}-r_{23}}{2r_{260}} \tag{B.3a}$$

$$\sin\beta = \frac{r_{58}-r_{14}}{2r_{150}} \tag{B.3b}$$

$$\sin\gamma = \frac{r_{14}-r_{67}}{2r_{160}} \tag{B.3c}$$

$$\sin\gamma' = \frac{r_{58}-r_{23}}{2r_{250}} \tag{B.3d}$$

$$\sin\delta = \frac{r_{14}-r_{23}}{2r_{12}} \tag{B.3e}$$

$$\sin\delta' = \frac{r_{58}-r_{67}}{2r_{56}} \tag{B.3f}$$

Finally, with the constant related to nuclear properties, $K = -\gamma_p^2 h/4\pi^2$, the coupling constants are given below. For Ring A:

$$D_{12} = \frac{K}{r_{12}^3}\left[S_{zz}(3\cos^2\delta-1) + (S_{xx}-S_{yy})(\cos^2\phi-\sin^2\phi)\sin^2\delta + 4S_{xy}\cos\phi\sin\phi\sin^2\delta\right] \quad \text{(B.4a)}$$

$$D_{14} = \frac{K}{r_{14}^3}\left[(S_{xx}-S_{yy})(\cos^2\phi-\sin^2\phi) + 4S_{xy}\cos\phi\sin\phi\right] \quad \text{(B.4b)}$$

$$D_{23} = D_{14}\left(\frac{r_{14}}{r_{23}}\right)^3 \quad \text{(B.4c)}$$

$$D_{13} = \frac{K}{r_{13}^3}\left[S_{zz}(3\cos^2\theta_{13z}-1) + (S_{xx}-S_{yy}) \times \sin^2\theta_{13z}(\cos^2\phi-\sin^2\phi) + 4S_{xy}\sin^2\theta_{13z}\cos\phi\sin\phi\right]. \quad \text{(B.4d)}$$

For Ring B:

$$D_{56} = \frac{K}{r_{56}^3}\left[S_{zz}(3\cos^2\delta'-1) + (S_{xx}-S_{yy})\sin^2\delta'\right] \quad \text{(B.5a)}$$

$$D_{58} = \frac{K}{r_{58}^3}\left[(S_{xx}-S_{yy}) - S_{zz}\right] \quad \text{(B.5b)}$$

$$D_{67} = D_{58}\left(\frac{r_{58}}{r_{67}}\right)^3 \quad \text{(B.5c)}$$

$$D_{57} = \frac{K}{r_{57}}\left[S_{zz}(3\cos^2\theta_{57z}-1) + (S_{xx}-S_{yy})\sin^2\theta_{57z}\right] \quad \text{(B.5d)}$$

where

$$\cos\theta_{13z} = \frac{r_{12}\cos\delta}{r_{13}}$$

$$\cos\theta_{57z} = \frac{r_{56}\cos\delta'}{r_{57}}$$

For inter-ring couplings, the full equation for D_{ij} in terms of internuclear distances, order parameters and direction cosines (Eq. 2.3) must be used as they do not reduce simply as with the intra-ring couplings. The cosines of the angles $\theta_{ij\alpha}$ defining internuclear vectors in the molecular axis frame are calculated from the trigonometric relations in Equation (B.3) and the r_{ij} values. These are then used in Equation (2.3) to obtain inter-ring couplings. These inter-ring couplings are for an average of the conformations with dihedral angles $\pm\phi$. To calculate the four-conformation average ($+\phi$, $-\phi$, $\pi+\phi$, $\pi-\phi$) the following equations are used.

$$\bar{D}_{15} = \bar{D}_{18} = \bar{D}_{45} = \bar{D}_{48} = \frac{D_{15}+D_{18}}{2} \tag{B.6a}$$

$$\bar{D}_{16} = \bar{D}_{17} = \bar{D}_{46} = \bar{D}_{47} = \frac{D_{16}+D_{17}}{2} \tag{B.6b}$$

$$\bar{D}_{26} = \bar{D}_{27} = \bar{D}_{36} = \bar{D}_{37} = \frac{D_{26}+D_{27}}{2} \tag{B.6c}$$

$$\bar{D}_{25} = \bar{D}_{28} = \bar{D}_{35} = \bar{D}_{38} = \frac{D_{25}+D_{28}}{2} \tag{B.6d}$$

B.2 Program BIPH4PARA

Program BIPH4PARA calculates biphenyl dipolar couplings from Equation (B.4-6). For D_4 symmetry, the input parameters are r_{12}, r_{14}, r_{23}, r_{260} (distance r_{26} at $\phi = 0$), $S_{zz}^{(1)}$, $(S_{xx}^{(1)} - S_{yy}^{(1)})$, and angle ϕ. Since the second ring (Ring B) is equivalent to the first, its geometric parameters are set equal to those above. For D_2 symmetry, the added parameters required as input are r_{67}, r_{58}, and r_{56}. The order parameters required for coordinate system #2 are $S_{zz}^{(2)}$, $(S_{xx}^{(2)} - S_{yy}^{(2)})$, and $S_{xy}^{(2)}$. The calculation of couplings is done in coordinate system two regardless of which symmetry is assumed and, for D_4, the order tensor is first transformed according to Equation (B.2).

After calculating the D_{ij}'s, BIPH4PARA sets up the Hamiltonian (assuming no offset and chemical shift terms) in the simple product basis set for the submatrices with magnetic quantum numbers M = ± 4, ± 3, and ± 2. These submatrices are then diagonalized. The totally symmetric (A_1) eigenstates are identified as follows. The coefficients of each eigenvector from the diagonalization are summed. It can be shown that this sum will vanish unless the state is of A_1 symmetry [34]. A_1 symmetry states found in this manner are labelled and printed out. From this symmetry determination, the A_1 symmetry transitions expected in the six and seven quantum regions are calculated.

BIPH4PARA will perform the coupling constant and frequency calculations for a series of parameters by incrementing one of them over a given range. Two files are created containing the six and seven quantum A_1 spectra calculated for each set of couplings. These may later be plotted by another program. This is the method used to produce the variation plots shown in Chapter 4.

B.3 Program BIPH5PARA

This program performs the same coupling constant and A_1 subspectra calculations as BIPH4PARA. Instead of varying just one parameter, any or all parameters for either symmetry case can be varied in a least squares fit of the calculated couplings to experimental ones given as input. The intermediate couplings are not printed and the A_1 subspectra simulation is only done at the completion of the iterative process.

The least squares iterative procedure used to fit the couplings is essentially the same as that for program MQITER and most if the discussion given in Appendix A applies to BIPH5PARA as well. The method of calculation for the derivatives of the D_{ij}'s with respect to order

parameters and geometric quantities is noteworthy. Rather than giving the derivatives from Equation (B.4-6) explicitly, they are estimated as a change in the D_{ij}'s with a one percent change in the parameter:

$$\frac{\partial D_{ij}}{\partial p_k} \approx \frac{\Delta D_{ij}}{\Delta p_k} \tag{B.7}$$

where

$$\Delta D_{ij} = D_{ij} - D'_{ij}$$

$$\Delta p_k = 0.01(p_k) \tag{B.8}$$

In Equation (B.8) D_{ij} is the coupling constant calculated with parameter p_k and D'_{ij} is the constant with $p_k + |\Delta p_k|$. This is the method of estimating derivatives adopted in the more general program SHAPE written by Diehl and Bosiger [128].

APPENDIX C

Disk Based Fourier Transform Programs

The core memory capacity of the Data General Nova 820 computer used for operating the spectrometer described in Chapter 5 allows the calculation of a Fourier transform of up to 8192 points (complex). For the typical linewidths and spectral range required in a non-selective multiple quantum experiment on a large spin system, this is not of adequate length. As an example, considering the spectra presented in Chapter 4, the transform size required (32k) already equals the memory available, leaving no room for the executable program. As a solution, a set of programs were written to allow the calculation of the transform in pieces performing phase shifts and transpositions on the intermediate result. This appendix describes the algorithm used, discusses the possible errors induced by the calculation, and presents a description of the programs.

C.1 Disk Based FFT Algorithm

(The description presented here follows closely that given in Ref. [129].)

The discrete Fourier transform of a time series d(j) may be written

$$D(k) = \sum_{j=0}^{N_1-1} d(j)\, W^{jk} \qquad (C.1)$$

where d(j) is N_1 points long, D(k), the transform, is N_2 points long, and

$$W^{jk} = \exp[(i2\pi/N_2)jk]$$

$$k = 0,1, \ldots, N_2-1. \qquad (C.2)$$

We assume

$$N_1 = N_2 = N = C_0C_1 = C_0C_2 \tag{C.3}$$

where C_0 is the amount of core storage available to hold a fraction of d(j). We then write d(j) in composite indices

$$\begin{aligned} d(j) &= d(j_0,j_1) \\ j &= j_0 + j_1C_0 \\ j_0 &= 0, 1, \ldots, C_0-1 \\ j_1 &= 0, 1, \ldots, C_1-1 \end{aligned} \tag{C.4}$$

Likewise, D(k) may be indexed,

$$\begin{aligned} D(k) &= D(k_2,k_0) \\ k &= k_2 + k_0C_2 \\ k_0 &= 0, 1, \ldots, C_0-1 \\ k_2 &= 0, 1, \ldots, C_2-1 \end{aligned} \tag{C.5}$$

Rewriting Equation (C.1) with these indices gives

$$D(k_2,k_0) = \sum_{j_0=0}^{C_0-1} \sum_{j_1=0}^{C_1-1} d(j_0,j_1)\, W^{(k_2+k_0C_2)(j_0+j_1C_0)} \tag{C.6}$$

Expanding the exponential factor and noting that $W^N = 1$, Equation (C.6) reduces to

$$D(k_2,k_0) = \sum_{j_0=0}^{C_0-1} \sum_{j_1=0}^{C_1-1} d(j_0,j_1)\, W^{(j_0+j_1C_0)k_2+j_0k_0C_2}. \tag{C.7}$$

For the case where $C_2 = C$, and using the notation

$$W_0 = \exp(i2\pi/C_0), \tag{C.8a}$$

$$W_1 = \exp(i2\pi/C_1), \tag{C.8b}$$

$$W = \exp(i2\pi/N), \tag{C.8c}$$

Equation (C.7) becomes

$$D(k_2,k_0) = \sum_{j=0}^{C_0-1} \sum_{j_1=0}^{C_1-1} d(j_0,j_1)\, W^{j_0k_2} W_1^{j_1k_2}\, W_0^{j_0k_0}$$

$$= \sum_{j_0=0}^{C_0-1} W_0^{j_0k_0} \left[W^{j_0k_2} \sum_{j_1=0}^{C_1-1} W_1^{j_1k_2}\, d(j_0,j_1) \right] \tag{C.9a}$$

$$D(k_2,k_0) = \sum_{j_0=0}^{C_0-1} W_0^{j_0k_0}\, B(j_0,k_2), \tag{C.9b}$$

with

$$B(j_0,k_2) = W^{j_0k_2}\, A(k_2) \tag{C.9c}$$

$$A(k_2) = \sum_{j_1=0}^{C_1-1} W_1^{j_1k_2}\, d(j_0,j_1) \tag{C.9d}$$

Equation (C.9) shows that if we first do C_0,C_1-point Fourier transforms of $d(j_0,j_1)$, phase shift each section of the result according to Equation (C.9c), and finally do a C_0-point Fourier transform, we will obtain the desired frequency spectrum.

If Equation (C.9) is written in matrix form, we can readily see what is required of computer calculations. First, the program must Fourier transform the columns of the input matrix $\underset{\approx}{d}$:

$$\underset{\approx}{A} = \underset{\approx}{W}_1 \underset{\approx}{d}. \tag{C.10}$$

Next, the matrix $\underset{\approx}{A}$ is phase shifted according to Equation (C.9c) and the transpose of this matrix is Fourier transformed to complete the calculations:

$$\underset{\approx}{D} = \underset{\approx}{W}_0 \underset{\approx}{B}^T. \tag{C.11}$$

Matrix $\underset{\approx}{D}^T$ is written to the output file to facilitate later calculations and display.

C.2 Errors

For the acquisition system employed in the spectrometer, data is represented and stored as fixed point (integer) numbers in the range $\pm$32767 (only 10 bits are actually digitized). It has been shown [130] that an upper bound to the ratio of the RMS error to that of the root mean squared value of the result for the Cooley-Tukey FFT algorithm is

$$\frac{\text{RMS(error)}}{\text{RMS(result)}} = \frac{2^{(M+3)/2} 2^{-B} (0.3)}{\text{RMS(initial timefunction)}} \tag{C.12}$$

In Equation (C.12), the number of points in the transform is $N = 2^M$ and B is the number of bits for single precision integer arithmetic (B = 15 for a 16 bit-word computer operating in twos complement mode). For an 8 K, complex FFT on a Nova 820, the numerator on the right side of Equation (1.12) evaluated to 2.34×10^{-3}. This is generally sufficiently small to be ignored. The ratio of Equation (C.12) increases as $\sqrt{N}$ and, even for the transform size required in the multiple quantum experiments, it is not considered to contribute to errors in the analysis.

The factors contributing to Equation (C.12) are i) the propagation of errors present in the input time series, ii) errors induced by the mathematical requirements of the FFT algorithm and iii) the necessity to scale the transform calculation occasionally intermediate to the final

result. This last contribution also arises because the RMS value of the intermediate result in the FFT algorithm increases from one cycle to the next [130]. This tendency for the RMS magnitude of the spectrum to increase during the FFT calculation effects the programming approach significantly. If the entire calculation were to be performed on integers, provisions would have to be made to detect overflow during both transforms and the phase shifting of Equation (C.9c). With transform lengths above 16 K, the typical methods of bit shifting to scale the calculations during overflow is no longer adequate. The highest intensity lines become small with the many divisions by two and, for the usual cases where the full dynamic range available from the acquisition is desired, low intensity lines are completely lost.

The solution to this problem and one that removes the contribution to Equation (C.12) from scaling is to perform all computations in floating point arithmetic. In addition, using floating point numbers removes errors associated with multiplication and addition. Errors in intensity and frequency determinations from the final spectrum are then almost completely a result of errors propagated from the experimental time series.

C.3 Programs

Besides the programs DSKFFT, DSKFT1, and DSKFT2 which do the actual transformation, several other programs are necessary to produce tau-averaged spectra such as those presented in Chapter 4. CONVERT takes the original integer data and converts it to floating point representation. DSKSCL, DSKMAG, DSKBASE and DSKBADD are used to scale, take magnitudes, baseline correct and co-add the data and calculated spectra. Finally,

RETSPC is designed to re-convert the floating point spectrum to integers by truncation.

These programs were written specifically for the Data General commercial operating system RDOS but could be modified to run on almost any mini- or micro-computer. A memory size of 32 K words and a moderate amount of disk storage are required. Calculations of a 32 K Fourier transform on the NOVA system described in Chapter 5 requires about one-half hour. The operation of all the disk programs is described in more detail elsewhere [117]. Because these programs are quite lengthy, a listing (~80 pages) is not given here. Copies may be obtained from the author upon request.

APPENDIX D

COMPUTER PROGRAM LISTINGS

```
C
C       MQITSET
C
C       SETS UP DATA FOR MQITIR
C
C       OUTPUT FILE IS MQITER.DAT
C
        integer mqit(10),iparam(15),flcntl
        integer title(72),case(40),mqo(10)
        real d(45),cj(45
        logical yans

        data mqit   10*-1 /, iparam / 15*0 /, title / 72*0 /
        data d / 45*0.0/, cj / 45*0.0 /
        data case / 40*0 /

        iu 0
        maxparp=15
        maxlin=230

c
c       this section opens up appropriate file and sets up
c       initial data
c

        open(unit=01,name='mqiter.dat',type='new')
c
        type 1 1
        accept 102, case
        write(1,103) case
c
        flcntl=0
        type 104
        if yans(iu)) flcntl=1

c
c       data initialization section
c

        type 105
        accept 106, title
        write(1,107) title
 2      type 108
        accept *, n
        if(n  ge  1 .and  n  le. 10) go to 3
        type 407
        go to 2
 3      loword=0
        if(n  eq  9) loword=7
        if(n .eq  10  loword=6
        nm1=n-1
        ncp=n*nm1/2
        type 2 1. n,loword
        accept *. loword
        if n .eq  9 .and. loword .lt. 7) loword=7
        if(n .eq  10 .and. loword .lt. 6) loword=6

        iter=0
        type 203
        if yans(iu)) iter=1
        write(1,*) n,loword,iter,flcntl

c
```

```
c       the next section handles input of the coupling corstarts
c

        if flcntl .eq. 1  go to 200

        type 205
        k=1
        do 100 i=1,nm1
        ip1=i+1
        do 100 j=ip1,n
        type 206, i,j
        accept *  d(k)
        type 208, i,j
        accept *, cj(k)
        k=k+1
 100    continue

        do 150 i=1,ncp
 150    write(1,*) d(i)
        do 160 i=1,ncp
 160    write(1,*) cj(i)

c
c       if iter = 1 then enter the line assignment
c       data
c

 200    if(iter  eq  0) go to 500

        nwline=1
        nord=0
        type 301
        accept *, ni
        type 304
        if( not  yans(iu)) nwline=0
        if nwline .ne. 1  go to 180
        type 303
        accept *, nord
        type 305
        accept *  (mqit(i), i=1,nord)
        if(flcntl .eq. 0  go to 180
 120    write(1,*) ni,nord,nwline
        if nwline .eq. 0) go to 195
        write(1,*) (mqit(i), i=1,10)
        type 307
        do 190 i=1,nord
        type 308, mqit(i
        do 170 j=1,maxlin
        type 309
        accept *, lnum,frq
        write(1,*) lnum,frq
        if(lnum  eq. 0) go to 190
 170    continue
 190    continue

c
c       data input for parameter sets
c

 195    type 403
        accept *, nos
        write(1,*) nos
        type 405
```

```
      do 300 i=1,nos
      do 290 j=1,maxparp
290   iparam(j)=0
      type 406, i
      do 350 j=1,maxparp
340   type 309
      accept *, ip
      if(ip .lt. 99) go to 344
      type 407
      go to 340
344   if(ip .eq. 0) go to 355
      iparam(j)=ip
350   continue
355   write(1,408) (iparam(j), j=1,maxparp)
360   continue


500   type 409
      idbirr=0
      if(yars(iu)) idbirr=1
      type 502
      accept *,nmqo
      write(1,*) idbirr,nmqo
      if(nmqo .le. 0) go to 425
      type 503
      accept *,(mqo(i), i=1,nmqo)
      write(1,*) (mqo(i), i=1,nmqo)
425   type 505
      thr=0
      if yans(iu)) thr=-1.0
      if thr .eq. -1.0 go to 450
      type 506
      accept *, thr

450   write(1,*) thr

      close(unit=01)
c
c     format statments
c

101   format( ,1x,'Program MQITSIT',/
     1  ,1x,'Data collection for program MQITER.'//,
     1  1x 'What is the case name (data file name) for this run?')
102   format(40a1)
103   format(1x,40a1)
104   format(1x,'Has this case been handled before with',/,
     1  1x 'the same data file? ',$)
105   format 1x,'Enter a case title (up to 72 char):')
106   format(72a1)
107   format(1x,72a1)
108   format(/,1x,'How many spins in this case? ',$)
201   format' ,1x,'For ',i2,' spins, the lowest order for',/,
     1  1x.'which a complete frequency calculation is possible',/,
     2  1x 'is the ',i2,' quantum spectrum.  Other orders',/,
     3  1x.'may be calculted but will be missing some allowed',/,
     4  1x 'transitions.',/,
     5  1x 'Enter the lowest order for which a complete frequency,',/,
     6  1x 'calculation is desired  ',$)
203   format(1x,'Is this an iterative run? ',$)
205   format(/,1x,'Enter the coupling constants (in Hz) . . .',//)
206   format( 10x,'D(',i2,',',i2,') = ',$)
208   format(12x,'J(',i2,',',i2,') = ',$)
```

```
 301    format(/1x,'How many iterative cycles are to be allowed? ',$)
 303    format( 1x,'Line assignment input.'/,
     1  1x 'How many orders contain line assignments? ',$)
 304    format(1x,'Is this a new set of line assignments',/,
     1  1x.'for this case? ',$)
 305    format(1x,'Enter these orders: ',$)
 307    format( 1x,'After the prompt, enter the line numbers from',/,
     1  1x 'the simulation and the experimental frequencies',/,
     2  1x 'assigned to them (enter each pair with a CR).  A zero',/,
     3  1x 'for a lire number terminates input.  A total of 230',/,
     4  1x.'lines are allowed.'//)
 308    format(/' Line assignments for the ',12,' quantum spectrum:'/)
 309    format(' >> ',$)
 403    format(/1x,'Perameter set input.',/,
     1  1x.'How mary parameter sets are there? ',$)
 405    format(/1x,'After the prompt, enter each of the parameters',/,
     1  1x 'in a set   Each entery should be a two digit number',/,
     2  1x.'corresponding to the nuclei i and j coupled.',/,
     3  1x '(A zero means nucleus ten and the lower number nucleus',/,
     4  1x 'is the first digit in the pair.)',/,
     5  1x.'Positive numbers refer to D''s ard negative numbers',/,
     6  1x 'refer to J''s',//)
 406    format(1x,'Perameter set # ',12,/)
 407    format( ' Say what?' )
 408    format(1514)
 409    format(1x,'Do you wish tc include a search for doubly',
     1  ' degenerate', ,' eigerstates in freq calculation? ',$)
 502    format(1x,'How mary orders do you want calcualted?',/,
     1  1x ''-1 mears all orders) ',$)
 503    format(1x,'Enter the orders you want in the order',/,
     1  1x 'they are tc be calculated: ',$)
 505    format(1x,'Is the default value (1.0e-4) of the threshold',/,
     1  1x.'for allowed frequencies to be used? ',$)
 506    format(1x,'Erter the threshold to be used (positive number) '
     1   $

c
c
c       end of program
c

        stop
        end
```

```
C         PROGRAM MQITER
C
C        VAX VMS VERSION.
C
C
C        THIS PROGRAM SIMULATES THE MULTIPLE QUANTUM NMR SPECTRUM FOR UP
C        TO 10 COUPLED SPINS 1/2.  THE PROGRAM CAN EITHER SIMPLY SIMULATE
C        THE SPECTRUM FROM GIVEN COUPLING CONSTANTS OR ITERATE ON A SET
C        OF INITIAL PARAMETERS TO FIT AN EXPERIMENTAL SPECTRUM.
C
C        FOR UP TO EIGHT SPINS THE ENTIRE SPECTRUM (ALL MQ ORDERS) CAN
C        BE CALCULATED.  FOR NINE SPINS THE SEVEN QUANTUM SPECTRUM AND
C        ABOVE ARE COMPLETE.  FOR TEN SPINS THE LOWEST COMPLETE SPECTRUM
C        IS THE EIGHT QUANTUM SPECTRUM.  LOWER ORDERS THAN THESE ARE
C        POSSIBLE, BUT NOT ALL EIGENSTATES AND FREQUENCIES ARE CALCULATED
C
C
C
C        IF ITER=0 JUST THE SIMULATION IS DONE.
C        IF ITER GT 0 THE PROGRAM IS ITERATING ON INPUT PARAMETERS.
C        A TOTAL OF NI ITERATIONS WILL BE PERFORMED IF CONVERGENCE
C        IS NOT REACHED FIRST.  CONVERGENCE IS REACHED WHEN THE RELATIVE
C        PERCENT CHANGE IN THE R.M.S. ERROR OF THE FIT BETWEEN THEORY
C        AND EXPERIMENTAL SPECTRA FOR SUCCESSIVE ITERATIONS IS LESS THAN
C        ONE PERCENT.
C
C
         DIMENSION SIGMA(28),PROBER(28)
         INTEGER L(28),M(28),TITLE(72),FLCNTL,CASE(42)
         INTEGER IMQO(11),FIND(7)
C
         COMMON / CFILE / ISC,FLIND,IFP
         COMMON   CSTATE   N,LST(2,1024),N0(11),NSM(11),
     1                     NSP(11),MAXMAT,NST
C
         COMMON D(45),CJ(45),EN(256),ITER,NOS,IPARAM(28,15),
     1   ELMB(256,28),MQIT(2,10),LASS(230),IFPER(230),
     2   IC(230,28),B(230),V(784),BV(28),WORK(4900)
         EQUIVALENCE (SIGMA,BV),(PROBER,D)
C
C        OPEN SCRATCH DATA FILES
         ISC=3
         OPEN(UNIT=03,TYPE='SCRATCH',ACCESS='DIRECT',INITIALSIZE=1,
     1   EXTENDSIZE=1,RECORDSIZE=1,RECORDTYPE='FIXED',
     2   ASSOCIATEVARIABLE=IFP)
         OPEN(UNIT=04,TYPE='SCRATCH',ACCESS='DIRECT',INITIALSIZE=1,
     1   EXTENDSIZE=1,RECORDSIZE=1,RECORDTYPE='FIXED',
     2   ASSOCIATEVARIABLE=IFP2)
C
C        READ IN CASE TITLE.
         OPEN(UNIT=01,NAME='MQITER.DAT',TYPE='OLD')
         READ(1,401) CASE
         WRITE(6,402) CASE
         READ(1,701) TITLE
          RITE(6,702) TITLE
C
C        READ IN CONTROL VARIABLES AND PERFORM INITIAL CALCULATIONS.
         READ(1,*  N,LOWORD,ITER,FLCNTL
         ER1=10000.0
         NPARPS=15
         NM1=N-1
         NP1=N+1
C
```

```
C       CALCULATE BINOMIAL COEFFICIENTS, AND NSP
        N@(1)=1
        NSP(1)=1
        DO 2@ J=1,N
        JP1=J+1
        JD N+1-J
        N@ JP1)=(N@(J)*JD /J
 2      NSP(JP1)=NSP(J)+N@(JP1)
C
C       DETERMINE MAXMAT, NSM, NST. NFILE, FIIND
        NT-NP1-LOWORD
        IF (MOD(N,2) - MOD(LOWORD,2)) .EQ. @ NT=NT+1
        NT NT/2
        MAXMAT=1
        DO 12 J=1,NT
        MAXMAT=MAX@(N@(J ,MAXMAT
 12     MAXMAT=MAX@(N@(J+LOWORD),MAXMAT)
        NST=2
        NFILE=@
        NSM(1)=1
        K=1
        DO 13 J=2,N
        IF N@(J) .GT  MAXMAT) GO TO 13
        K=K+1
        NSM(K)=NSM(K-1)+N@(J)
        NST=NST+N@(J)
        FIIND(K-1)=N@(J)*N@(J)
        NFILE=NFILE+1
 13     CONTINUE
        NSM(K+1)=NSM(K)+1


C
        NCP=N*NM1/2
C       READ IN COUPLING CONSTANTS
        IF FLCNTL) 4.5,4
 4      OPEN(UNIT=@2.NAME=CASE,TYPE='OLD')
        READ(2,*) (D(K), K=1,NCP)
        READ(2,*  (CJ(K), K=1,NCP)
        GO TO 1@
 5      READ(1,*) (D(J), J=1,NCP)
        READ(1,*  (CJ(J), J=1,NCP)
        DO 6 J=1 NCP
        D(J)=D(J) 4.@
 6      CJ J =CJ(J /4.@
        OPEN(UNIT=@2,NAME=CASE,TYPE='NEW')
        WRITE(2,*) (D(K), K=1,NCP)
        WRITE(2,*) (CJ(K , K=1,NCP
 1      CALL CNTOUT(D,CJ,N)
C
        FICNTI=@
        IF ITER  EQ. 2 GO TO 55
C       READ IN EXPERIMENTAL LINES
        READ 1,*  NI,NORD,NWLINE
        DO 31 I=1.1@
        MQIT(1.I)=-1
 31     MQIT(2.I =@
        DO 15 I=1,23@
        IASS(I)=@
 15     EXPER(I =@.@
C
        NEXPER-1
        IF NWLINE .EQ. @  GO TO 37
```

```
      READ(1,*) (MQIT(1,I), I=1,10)
      DO 35 I=1,NORD
 27   READ(1,*  LNUM,FRQ
      IF LNUM .LE. 0  GO TO 35
      IASS(NEXPER)=LNUM
      EXPER(NEXPER =FRQ
      MQIT(2 I =MQIT(2.I)+1
      NEXPER=NEXPER+1
      IF NEXPER .GE. 231  GO TO 32
      GO TO 27
 35   CONTINUE
 32   CALL LINORD(NORD
C
C     WRITE MQIT,LASS,EXPER TO DISK FILE
      WRITE(2,*  ((MQIT(I,K), I=1,2), K=1,10
      WRITE(2,*) (LASS(K), K=1,230)
      WRITE(2,*) (EXPER(K), K=1,230)
      GO TO 38
C
C     READ IN OLD LINE ASSIGNMENTS
 37   READ(2,*  ((MQIT(I,K , I=1,2), K 1,10
      READ(2,*) (LASS(K , K=1,230)
      READ(2,*) (EXPER(K), K=1,230)
      DO 39 JC=1,10
 39   NEXPER=NEXPER-MQIT(2,JC
 38   NEXPER=NEXPER-1
      WRITE(6,724  NEXPER
C
C     WRITE LINE ASSIGNMENTS TO OUTPUT
C
      IF NVLINE .NE  0  GO TO 365
      NORD=0
      DO 360 I=1,10
 360  IF MQIT(1,I) .NE. -1  NORD=NORD+1
 365  K=0
      DO 380 JC=1,NORD
      WRITE(6,739) MQIT(1,JC
      J=MQIT(2,JC)
      DO 370 I=1,J
      K=K-1
      WRITE(6,740) IASS(K),EXPER(K)
 370  CONTINUE
 380  CONTINUE
C
C     READ IN PARAMETER SET DATA
      READ 1 *  NOS
      READ(1 *) ((IPARAM(I,J), J 1,NPARPS), I=1,NOS)
      WRITE(6,741
C
C
C     ENTER ITERATIVE LOOP.
 55   CALL HAMILS
      IF ITER  EQ  0) GO TO 500
C
C     LEAST SQUARES ROUTINES
C
      CALL CONDIT
      CALL ERRIT(ER1,NI,NEXIT,NEXPER)
      CALL NORMAL(NEXPER)
      IF NEXIT .EQ. 0  GO TO 400
      CALL MINV(V,NOS,DET,L,M
      IF DET  EQ. 0 0) WRITE(6,729)
      CALL CORREC
```

```
      ITER=ITER+1
      GO TO 55
C     END OF ITERATION LOOP
C
C     OUTPUT REFINED PARAMETERS
 400  DO 407 I=1,NOS
      WRITE(6,728) I
      DO 405 J=1,NPARPS
      K=IPARAM(I,J)
      KOUT=IABS(K)
      IF(K) 411,407,413
 411  WRITE(6,737) KOUT
      GO TO 405
 413  WRITE(6,738) KOUT
 405  CONTINUE
 407  CONTINUE
      WRITE(6,730)
      CALL CNTOUT(D,CJ,N)
C
C
C     ERROR ANALYSIS.
C
C     OUTPUT COEFF OF NORMAL EQUATIONS
C      D=-TRANS * DC **(-1)
      DO 471 I=1,784
 471  WORK(I)=V(I)
      CALL MINV(WORK,NOS,DET,L,M)
      IF(DET .EQ. 0.0) WRITE(6,729)
      WRITE(6,751)
      DO 409 NS=1,NOS
      IICW=(NS-1)*NCS
      IHIGH=IICW+NOS
      ILOW=ILOW+1
      IF(NOS-14) 416,416,417
 416  WRITE(6,752) NS,(WORK(K), K=IICW,IHIGH)
      GO TO 409
 417  WRITE(6,753) NS,(WORK(K), K=IILOW,IHIGH)
 409  CONTINUE
      CALL GENSYM(V,NOS)
      SIGMA(1)=V(1)
      IF(NCS .EQ. 1) GO TO 420
      CALL EIG2(V,WORK,SIGMA,0,NCS,0)
      WRITE(6,754)
      IF(NOS-14) 516,516,517
 516  WRITE(6,755) (SIGMA(K), K=1,NOS)
      GO TO 420
 517  WRITE(6,756) (SIGMA(K), K=1,NCS)
 420  FNL=NFIPER
      FNOS=NOS
      DEV=(ER1*ER1*FNL)/(FNL-FNOS)
      DO 435 J=1,NOS
 435  PROBER(J)=0.0
      WRITE(6,734)
      ICOLMN=0
      DO 450 NS=1,NCS
      ER2=SQRT(DEV*SIGMA(NS))
      INDX=ICOLMN*NOS
      IHIGH=INDX+NOS
      ILOW=INDX+1
      WRITE(6,732) (WORK(K), K=ILOW,IHIGH)
      WRITE(6,735) ER2
      DO 445 J=1,NOS
 445  PROBER(NS)=PROBER(NS)+(WORK(INDX+J)*ER2)**2
```

```
      ICOLMN=ICOLMN+1
  450 CONTINUE
      DO 460 J=1,NOS
  460 PROBIR(J)=0.6745*SQRT(PROBIR(J))
      WRITE(6,733) (J,PROBIR(J), J=1,NCS)
      WRITE(6,736)
      CALL ECUT(N,MAXMAT,EN,N0)
C
C
C     CALCULATE ALLOWED MQ LINES
C
  500 READ(1,*  IDBIRR,NMQO
      IF NMQO  LE. 0  GO TO 55
      READ(1,*) (IMQO(I), I=1,NMCC)
  550 READ(1,*  THR
      CALL MQ2IFP'THR,IDBIRR.NMCC,IMQC)
      CLOSE(UNIT=01)
      CLOSE(UNIT=02
      CLOSE(UNIT=03
      STOP
C
  401 FORMAT'40A1)
  402 FORMAT'1H1,10X,' CASE:',5X 40A1/)
  701 FORMAT 72A1
  702 FORMAT(/10X,72A1,//)
  724 FORMAT(' TOTAL # OF FREQ ENTERED =',I4, )
  728 FORMAT(' ,' PARAMETER SET # ',I2, )
  729 FORMAT(/,
     1' !!! DETERMINANT OF MATRIX TO BE INVERTED IS ZERO !!!', )
  730 FORMAT(1H1,/,' REFINED PARAMETERS .   .',/)
  732 FORMAT(5X,<MAX'14,NOS)>F8.4)
  733 FORMAT(1F1, ,' PROBABLE ERRORS OF EIGENBASIS ',
     1'PARAMETER SETS . . .',//,
     2(5X I2 5X,F10.3 )
  734 FORMAT(1F1, ,' ERROR VECTORS AND STANDARD DEVIATIONS '
     1.'OF EIGENBASIS PARAMETERS . . .',/)
  735 FORMAT(1?X,'STANDARD ERROR = ',F8 3)
  736 FORMAT(1H1, ,' REFINED ENERGIES   . .', )
  737 FORMAT(' J',I2
  738 FORMAT(' D',I2
  739 FORMAT(1H1, ,' LINE ASSIGNMENTS FOR THE ',I2,
     1' QUANTUM SPECTRUM.',//5X,'LINE #'.10X,'EXPERIMENTAL FREQUENCY'
     1 / 1?,46('-'),/
  740 FORMAT'5X,I4,14X,F12 4)
  741 FORMAT(1F1,/.
     1' PROGRAM MQITER - START OF ITERATIVE CALCULATIONS.',//)
  751 FORMAT(1H1, ' MATRIX OF COEFFICIENTS FOR THE NORMAL EQUATIONS'
     1.   ' 'BEFORE DIAGONALIZATION  . .   '//)
  752 FORMAT(2X,I2,') ',<NOS>I<MIN(12, 126/NCS))>.4/)
  753 FORMAT(2X,I2,') ',14F9.3,/,<NCS-14>F9.3/)
  754 FORMAT(/.2X,'EIGENVALUES OF NORMAL EQUATIONS MATRIX . . .'/)
  755 FORMAT(6X,<NCS>F<MIN(12,(126/NCS))>.3/)
  756 FORMAT'6X,14F9.3, ,<NOS-14 F9.3 )
      END
```

```
      SUBROUTINE LINCRD(NORD)
C
C
C
C
C     THIS SUBROUTINE ORDERS THE LINE ASSIGNMENTS OF EXPERIMENTAL
C     LINES THAT ARE INPUT FROM THE TTY FOR AN ITERATIVE RUN.
C
C
      COMMON D(45),CJ(45),EN(256),ITER,NOS,IPARAM(28,15),
     1 IIMB(256,28),MQIT(2,10),IASS(230),EXPER(230),
     2 DC(230,29),B(230),V(784),BV(28),WORK(4900)
C
      INDEX=0
      DO 100 I=1,NORD
      NL=MQIT(2,I)
      IF(NL .EQ. 1) GO TO 99
      NLM1=NL-1
      DO 50 J=1,NLM1
      JM=J+INDEX
      JP1=J+1
      DO 45 K=JP1,NL
      KM=K+INDEX
      IF(IASS(JM) .LE. IASS(KM)) GO TO 45
      IT=IASS(JM)
      IASS(JM)=IASS(KM)
      IASS(KM)=IT
      EX=EXPER(JM)
      EXPER(JM)=EXPER(KM)
      EXPER(KM)=EX
   45 CONTINUE
   50 CONTINUE
   99 INDEX=INDEX+MQIT(2,I)
  100 CONTINUE
C
      RETURN
      END
```

```
      SUBROUTINE CNTOUT(AR1,AR2,N)
C
C
C
C     OUTPUTS COUPLING CONSTANTS TO LPR.
C
      DIMENSION AR1(1),AR2(1)
C
      NM1=N-1
      K=1
      DO 30 I=1,NM1
      IP1=I+1
      DO 30 J=IP1,N
      IOUT=AR1(K) * 4.0
      CJOUT=AR2(K) * 4.0
      WRITE(6,731) I,J,IOUT,I,J,CJOUT
30    K=K+1
C
731   FORMAT(' D(',I2,',',I2,') = ',F12.4,/
     1,' J(',I2,',',I2,') = ',F12.4,//)
      RETURN
      END
```

```
      SUBROUTINE HAMIL5
C
C              VAX-VMS VERSION.
C
C     THIS PROGRAM SETS UP AND CALLS FOR THE DIAGONALIZATION OF THE
C     FREE-INDUCTION HAMILTONIAN OF AN N SPIN 1/2 SYSTEM (N LESS THAN 11).
C     ONLY DIPOLAR AND SCALAR COUPLING CONSTANTS ARE INCLUDED IN
C     THE HAMILTONIAN.  THE SUBROUTINE IS CALLED BY MQITER.
C     ALSO CALCULATED IS THE MATRIX OF DERIVATIVES OF THE
C     EIGENVALUES WITH RESPECT TO THE PARAMETERS BEING ITERATED
C     UPON   THIS IS MATRIX DLMB.
C
C     SUBROUTINES CALLED ARE NUMSRT, EIG2, UNTRAN, AND MATID
C     ALSO CALLED ARE READMS AND WRITMS
C
C
      DIMENSION H(2485),S(4900),ST(4900)
      INTEGER NUMB(2,1024),IST(70),ISP(10),IFLIP(2),FLIND(7)
C
      COMMON / CFILL / ISC,FLIND,IFP
      COMMON   CSTATE   N,LST(2,1024),N0(11),NSM(11),
     1                  NSP(11),MAXMAT,NST
C
      COMMON D(45),CJ(45),EN(256),ITER,NOS,IPARAM(28,15),
     1 DLMB(256,28),MQIT(2,10 ),IASS(230),EXPER(230),
     2 DC(230,29),B(230),V(784),BV(28),WORK(4900)
      EQUIVALENCE (WORK,ST),(H(1),DC(1,1)),(S(1),DC(1,12))
C
      NPARPS=15
      NM1=N-1
      NSTATE=2**N
      NCP=N*NM1/2

C
      IF ITER .EQ. 0) GO TO 31
      DO 25 I=1,NOS
      DLMB(1,I)=0.0
      DO 24 J=1,NPARPS
      K=IPARAM(I,J)
      IF(K) 10,15,10
 10   DLMB(1,I) =DLMB(1,I)+1.0
 24   CONTINUE
 15   DLMB(NST,I)=DLMB(1,I)
 25   CONTINUE
 31   ECP=0.0
      DO 35 I=1,NCP
 35   ECP=ECP+D(I)*CJ(I)
      EN(1)=ECP
      EN(NST)=ECP
 37   NST=1
      CALL NUMSRT(NUMB,N,NSTATE)
      IST(1,1)=NUMB(1,NSTATE)
      IST(2,1)=NUMB(2,NSTATE)
      IST(1,NSTATE)=NUMB(1,1)
      IST(2,NSTATE)=NUMB(2,1)
      KKK=1
C
      IF 0
C     MAIN LOOP
      DO 100 JS=1,NM1
      IND 0
C
      IS=N JS
```

```
      KK=0
      DO 40 J=1,NSTATE
      IF(NUMB(2,J) .NE. IS) GO TO 40
      KK KK+1
      KKK=KKK+1
      IF(KK  LE. MAXMAT) IST(KK)=NUMB(1,J)
      IST(1,KKK)=NUMB(1,J)
      LST(2,KKK)=IS
 40   CONTINUE
      IF(KK  GT. MAXMAT) GO TO 100
      IF IF+1
C
      MST=KK
      MM MST*MST
 45   IM=0
C
      DO 80 M=1,MST
      DO 80 L=1,M
      IM IM+1
      IF L .NE. M) GO TO 60
C     DIAGONAL ELEMENTS
      MSK=1
      DO 50 K=1,N
      ISP(K)=-1
      IF((IST(I) .AND. MSK) .NE. 0) ISP(K)=1
      MSK=MSK*2
 5    CONTINUE
      H(IM)=0.0
      IF(IND .NE. 0) GO TO 56
      KK=0
      DO 55 I=1,NM1
      IP1=I+1
      DO 55 J=IP1,N
      KK KK+1
      H(LM =H(LM)+(D(KK)+CJ(KK))*ISP(J)*ISP(I)
 55   CONTINUE
      GO TO 80
 56   DO 59 I=1,NPARPS
      K=IPARAM(IND,I)
      IF(K  57.80,57
 57   ICP1=IABS(K/10)
      IF(ICP1  EQ. 0) ICP1=10
      ICP2=MOD(IABS(K),10)
      IF(ICP2 .EQ. 0) ICP2=10
 59   H(LM =H(IM)+ISP(ICP1)*ISP(ICP2)
      GO TO 80
C
C     OFF DIAGONAL ELEMENTS.
 60   JW=1
      JSP=0
      H(LM =0.0
      MSK=1
      DO 75 K=1,N
      IF((IST(I) .AND. MSK) - (IST(M) .AND. MSK)) 70,75,70
 70   JSP=JSP+1
      IFLIP(J =K
      JW=2
 75   MSK=MSK*2
      IF JSP .NE. 2) GO TO 80
      K5=(2*N-IFLIP(1))*(IFLIP(1)-1)/2 - IFLIP(1)+IFLIP(2)
      IF(IND  NE. 0) GO TO 77
      H(LM = -D(K5)+2.0*CJ(K5)
      GO TO 80
```

```
 77     DO 95 I=1,NPARPS
        K=IPARAM(IND,I)
        IF(K .EQ. 0) GO TO 80
        ICP1=IABS(K/10)
        IF(ICP1 .EQ. 0) ICP1=10
        ICP2=MOD(IABS(K),10)
        IF(ICP2 .EQ. 0) ICP2=10
        K6 = (2*N-ICP1)*(ICP1-1)/2 - ICP1 + ICP2
        IF(K6 .NE. K5) GO TO 95
        IF(K) 83,80,85
 83     H(LM)=H(LM)+2.0
        GO TO 95
 85     H(IM)=H(IM)-1.0
 95     CONTINUE
C
 80     CONTINUE
C
C
        IF(ITER .LE. 1 .AND. IND .EQ. 0) GO TO 87
        IF(IND .NE. 0) GO TO 91
        CALL READMS(IF,ISC,S,FLIND,IFP)
C       ROUGE DIAGONALIZATION
        CALL UNTRAN(E,S,MST,ST)
C
 87     CALL BIG2(E,S,EN,MST0,MST,ITER)
C
        CALL WRITMS(IF,ISC,S,FLIND,IFP)
        IF(ITER .LE. 0) GO TO 98
        IF ITER .NE. 1) GO TO 988
        CALL WRITMS(IF,ISC+1,S,FLIND,IFP)
        GO TO 97
 988    CALL USWAP(ST,S,EN,MST,MST0,IF)
        GO TO 97
C
 91     CALL UNTRAN(E,S,MST,ST)
        DO 9 I=1,MST
        II=MAT(I,I)
 90     DL=B(MST0+I,IND)=E(II)
 97     IND=IND+1
        IF(IND .LE. NOS) GO TO 45
 98     MST0=MST0+MST
 100    CONTINUE
        IF(ITER .NE. 0) RETURN
        WRITE(6,402)
        CALL EOUT(N,MAXMAT,EN,NP)
        RETURN
C
 402    FORMAT('1',/,' ENERGIES (HZ) . . .'/)
        END
```

```
      SUBROUTINE NUMSRT(NUMB,N,NN)
C
C     TABULATES THE NUMBER OF ONES IN THE BINARY REPRESENTATION OF INTEGERS.
C
      DIMENSION NUMB(2,NN)
      DO 20 J=1,NN
      JJ J-1
      NUMB(1.J =JJ
      KK 1
      LL=0
      DO 12 K=1,N
      IF((JJ  AND. KK)  NE. 0) LI=LI+1
      KK=2*KK
 10   CONTINUE
      NUMB(2,J)=II
 20   CONTINUE
C
      RETURN
      END
```

```
      SUBROUTINE EIG2(H,S,EN,MST0,N,ITER)
C
C     SUBPROGRAM EIGEN - VERSION '2
C
C     THIS SUBROUTINE DIAGONALIZES AN N BY N SYMMETRIC MATRIX H BY THE
C     JACOBI METHOD.  THE UPPER TRIANGULAR ELEMENTS OF H (H(I,J)? J .GE. I)
C     ARE ENTERED COLUMN-WISE IN A 1-D ARRAY.  THE SUBROUTINE OUTPUTS THE
C     EIGENVALUES IN THE VECTOR EN.  THE TRANSFORMATION MATRIX IS
C     OUTPUT IN VECTOR S (H = S*H-DIAG*S-INV).  DEPENDING ON THE VALUE OF
C     ITER, S IS EITHER SET EQUAL TO THE UNIT MATRIX OR LEFT AS INPUT
C     WITH SUCCESIVE JACOBI ROTATIONS BEING MULTIPLIED INTO IT.
C
C     THE SUBROUTINE IS ADAPTED FROM SUBROUTINE "EIGEN" IN THE IBM
C     SYSTEM/360 SCIENTIFIC SUBROUTINE PACKAGE.
C
      DIMENSION H(1 ),S(1),EN(1
      ON=N
      RANGE=1 0E-6
      IF(ITER-1) 10,10,25
 1    IJ=?
      DO 20 J=1,N
      DO 20 I=1,N
      IJ=IJ+1
      S(IJ)=0 0
 20   IF I .EQ. J) S(IJ)=1.0
C
 25   ANORM=0 0
      DO 30 J=2,N
      JM1=J-1
      DO 30 I=1,JM1
      IJ MAT(I.J)
 3    ANORM=ANORM + H(IJ)*H(IJ)
      ANORM=SQRT(2.0*ANORM)
      IF(ANORM .LT. RANGE) GO TO 125
      ANORMX=ANORM * RANGE / ON
      IND=0
      THR=ANORM
C
 4    THR=THR ON
C
 5    DO 100 M=2,N
      MM1=M-1
      DO 100 L=1,MM1
      IM MAT(L.M)
      IF(ABS(H(LM)) .LT. THR) GO TO 100
C
      IND=1
      LL MAT(L,L)
      MM=MAT(M,M)
      LLFF=H(MM)-H(LL)
      IF(DIFF  EQ. 0.0) DIFF=1.0E-30
      AA 0.5*ATAN(2.0*H(LM)/DIFF
      SINA=SIN(AA)
      COSA=COS(AA)
      SINA2=SINA*SINA
      COSA2=COSA*COSA
C
      DO 70 K=1,N
      IF(K-L) 61,70,62
 61   KL MAT(K,L)
      KM MAT K,M)
      GO TO 65
 62   IF(K-M) 63,70,64
```

```
 63     KL=MAT(L,K)
        KM=MAT(K,M)
        GO TO 65
 64     KL=MAT(L,K)
        KM=MAT(M,K)
 65     BB    = COSA*B(KI) - SINA*B(KM)
        B(KM) =SINA*B(KL) + COSA*B(KM)
        B(KL) =BB
 70     CONTINUE
C
        SS=2.0*SINA*COSA*B(LM)
        BB    = COSA2*B(LL) + SINA2*B(MM) - SS
        B(MM) =SINA2*B(LL) + COSA2*B(MM) + SS
        B(LL) =BB
        B(IM) =-DIFF*SINA*COSA + B(IM)*(COSA2 - SINA2)
C
        DO 80 I=1,N
        II = (L-1)*N + I
        IM = (M-1)*N + I
        SS    = COSA*S(IL) - SINA*S(IM)
        S(IM)=SINA*S(II) + COSA*S(IM)
        S(IL) =SS
 80     CONTINUE
C
 100    CONTINUE
C
        IF(IND .EQ. 0) GO TO 120
        IND=0
        GO TO 57
C
 120    IF(THR .GT. ANORM) GO TO 40
C
 125    DO 130 I=1,N
        II = MAT(I,I)
        J=I+MST2
        B(J)=B(II)
 130    CONTINUE
C
        RETURN
        END
```

```
      SUBROUTINE UNTRAN(A,U,N,ST)
C
C     THIS SUBROUTINE CALCULATES THE UNITARY TRANSFORMATION
C     (U-ADJOINT)*A*(U) FOR THE SPECIAL CASE WHERE A IS REAL SYMME-
C     TRIC AND U-ADJOINT=U-TRANSPOSE.
C
C     RESULT RETURNED IN A
C     N IS THE DIMENSION OF A,U AND NSQ=N**2.
C     STORAGE MODE OF MATRICES IS SINGLE SUBSCRIPT VECTOR WITH ONLY
C     UPPER TRIANGLE HALF OF A STORED.
C
C     ST IS A WORK MATRIX.
C
      DIMENSION ST(1),A(1),U(1)
C
      NSQ=N*N
      DO 10 IST=1,NSQ
   10 ST(IST)=0.0
C
C     FORM PRODUCT AU AND STORE IN ST
      DO 50 IDX1=1,N
      DO 50 IDX2=1,N
      IN3=MATVEC(IDX1,IDX2,N)
      DO 50 I=1,N
      IF(IDX1-I) 30,20,20
   20 IN2=MAT(I,IDX1)
      GO TO 40
   30 IN2=MAT(IDX1,I)
   40 IN1=MATVEC(I,IDX2,N)
      ST(IN3)=ST(IN3)+A(IN2)*U(IN1)
   50 CONTINUE
C
C     FORM PRODUCT U-TRANSPOSE*ST AND STORE IN A
      DO 100 IDX1=1,N
      DO 100 IDX2=IDX1,N
      IN1=MAT(IDX1,IDX2)
      A(IN1)=0.0
      DO 100 I=1,N
      IN2=MATVEC(I,IDX2,N)
      IN3=MATVEC(I,IDX1,N)
      A(IN1)=A(IN1)+U(IN3)*ST(IN2)
  100 CONTINUE
C
C
      RETURN
      END
```

```
      SUBROUTINE CONDIT
C
C               VAX/VMS VERSION.
C
C     THIS SUBROUTINE FORMS THE EQUATIONS OF CONDITION FOR A LEAST
C     SQUARES ITERATIVE FIT OF AN EXPERIMENTAL SPECTRUM TO THEORY.
C     QUANTITIES CALCULATED IN THIS SUBPROGRAM ARE SUM(PARTIAL DERIV.
C     OF NU(I) W.R.T. PARAMETER P(J)) AND (NU(OBS) - NU(CALC)) WHERE
C     THE NU'S ARE FREQUENCIES (EITHER EXPERIMENTAL OR THEORETICAL)
C     AND THE PARAMETERS P ARE THE INITIAL PARAMETERS BEING ITERATED
C     UPON.  THE SUM IS RETURNED (IN COMMON) IN ARRAY DC AND THE
C     "RESIDUALS" ARE RETURNED IN ARRAY B.
C
C
C               THIS SUBROUTINE IS MODELED AFTER THAT FOUND IN THE
C     PROGRAM "LAOCOON3."
C
C
      INTEGER ORDER,UES,DML,DMU
C
      COMMON / CSTATE / N,LST(2,1024),N0(11),NSM(11),
     1                  NSP(11),MAXMAT,NST
C
      COMMON P(45),CJ(45),EN(256),ITER,NOS,IPARAM(28,15),
     1 IIMP(256,28),MQIT(2,10),LASS(230),EXPER(230),
     2 DC(230,28),B(230),V(784),BV(28),WORK(4900)
C
      NP1=N+1
      KK=0
C
      DO 300 IORD=1,N
      NL=MQIT(2,IORD)
      ORDER=MQIT(1,IORD)
      IF(ORDER .EQ. -1) GO TO 400
C
C     LOOP OVER ZEEMAN SUBMATRICES
      IIME=0
      KZ1=1
      DO 200 IZ=1,N
      IF(ORDER .EQ. 0 .AND. IZ .EQ. 1) GO TO 200
      IF(IZ+ORDER) .GT. NP1) GO TO 250

C     SUBMATRIX DIMENSIONS

      DML=N0(IZ)
      DMU=N0(IZ+ORDER)
      IF(DML .LE. MAXMAT) GO TO 134
      KZ1=KZ1+1
      GO TO 200

  134 IF(DMU .GT. MAXMAT) GO TO 200
      KZ2=1
      DO 136 I=1,ORDER
      IF(N0(IZ-I) .LE. MAXMAT) GO TO 136
      KZ2=KZ2+1
  136 CONTINUE

C     LOOP OVER LOWER EIGENSTATES
      LES=0
      IF(IZ .NE. 1) LES=NSM(IZ-KZ1)
      NTOP=DML
      IF(ORDER .EQ. 0) NTOP=NTOP-1
      DO 100 J=1,NTOP
```

```
      LES=LES+1

C     LOOP OVER UPPER EIGENSTATES
      UES=NSM(IZ-KZ2+ORDER
      NU=1
      IF(ORDER .NE. 0) GO TO 135
      NU=J+1
      UES=UES+J
  135 DO 95 JST=NU,DMU
      UES=UES+1

C     LINE NUMBER COUNTER
      LINE=LINE+1
      KKK=KK
      DO 80 NC=1,NL
      KKK=KKK+1
      IF(LASS(KKK) .NE. LINE) GO TO 60
      E(KKK)=EXPER(KKK) - (EN(UES)-EN(LES))
      DO 70 K=1,NOS
   70 DC(KKK,K)=DLMB(UES,K) - DLMB(LES,K)
   80 CONTINUE
C
   95 CONTINUE
  100 CONTINUE
  200 CONTINUE
C
  250 KK=KK+NL
  300 CONTINUE
C
  400 RETURN
      END
```

```
      SUBROUTINE ERRIT(ER1,NI,NEXIT,NL)
C
C             VAX VMS VERSION.
C
C     EVALUATES R.M.S. ERROR FOR A VECTOR OF RESIDUALS FROM ONE
C     ITERATIVE CYCLE IN NMR ITERATIVE PROGRAM.  THIS VERSION IS MODIFIED
C     FROM PROGRAM "LAOCOON."
C
C     B IS THE VECTOR OF RESIDUALS.
C     ITER IS THE NUMBER OF THE PRESENT ITERATIVE CYCLE.
C     ER1 IS THE RMS ERROR FROM THE LAST CYCLE.
C     NI IS THE TOTAL NUMBER OF ITERATIONS ALLOWED.
C     NEXIT IS A PARAMETER TO BE USED IN DETERMINING WHETHER
C             FURTHER ITERATIVE CYCLES SHOULD BE RUN.
C             IF NEXIT=0 RETURNED NO FURTHER ITERATIONS NECESSARY.
C             IF NEXIT=1, FUTHER CYCLES ARE REQUIRED.
C     NL IS THE NUMBER OF RESIDUALS CONTAINED IN B.
C
C
      REAL MINERR
C
      COMMON D(45),CJ(45),IN(256),ITER,NOS,IPARAM(28,15),
     1  ILAB(256,28),MQIT(2,10),LASS(230),EXPER(230),
     2  IC(230,29),B(230),V(784),BV(28),WORK(4900)
C
      MINERR = 1.0E-8
      ER2=0.0
      FNL=NL
C
      DO 4 K=1,NL
    4 ER2=ER2+B(K)*B(K)
      ER2=SQRT(ER2/FNL)
      IF(ER2 .GE. MINERR) GO TO 5
      WRITE(6,401) ER2
      GO TO 8
    5 WRITE(6,301) ITER,ER2
C
      IF((ER1-ER2)/ER1-0.01) 8,8,10
    8 NEXIT=0
      ER1=ER2
      RETURN
C
   10 IF(ITER-NI) 110,8,8
  110 ER1=ER2
      NEXIT=1
      RETURN
C
  301 FORMAT(5X,'ITERATION # ',I2,3X,'R M S ERROR = ',F8.3)
  401 FORMAT(/,' ITERATION CYCLE TERMINATED -',/,
     1' RMS ERROR LESS THAN MINIMUM ALLOWED!',/,
     2' ERROR = ',E16.4, )
      END
```

```
      SUBROUTINE NORMAL(NL)
C
C              VAX VMS VERSION.
C
C     THIS SUBROUTINE SETS UP THE NORMAL EQUATIONS FOR A LEAST
C     SQUARES ITERATIVE PROCEDURE.
C     THE MATRIX PRODUCTS DC-TRANS*DC AND DC*B ARE FORMED WHERE DC IS THE
C     MATRIX OF DERIVATIVES OF FREQUENCIES WITH
C     RESPECT TO PARAMETERS AND B IS THE MATRIX OF RESIDUALS
C     BETWEEN CALCULATED AND OBSERVED FREQUENCIES.
C
C
      COMMON D(45),CJ(45),EN(256 ,ITER,NOS,IPARAM(28,15),
     1 ILMB(256 28),MQIT(2,10),LASS(230 ,EXPER(230),
     2 IC(230,28),B(230),V(784),BV(28),WORK(4900)
C
      DO 210 NS1=1,NOS
      DO 206 NS2=NS1,NOS
C
      INDX1=MATVEC(NS2,NS1,NOS)
      INDX2=MATVEC(NS1,NS2,NOS)
C
      V(INDX1)=0.0
      DO 205 LEQ=1,NL
  205 V(INDX1)=V(INDX1)+DC(LEQ,NS1)*DC(LEQ,NS2)
  206 V(INDX2)=V(INDX1)
C
      BV(NS1)=0.0
      DO 210 LEQ=1,NL
  210 BV(NS1)=BV(NS1)+DC(LEQ,NS1)*B(LEQ)
C
      RETURN
      END
```

```
      SUBROUTINE CORREC
C
C             VAX/VMS VERSION.
C
C     THIS SUBROUTINE APPLIES CORRECTIONS TO PARAMETERS THAT
C     ARE BEING ITERATED UPON.  IT IS DESIGNED TO BE CALLED FROM
C     THE MAIN PROGRAM MQITER.
C
C
C
      COMMON / CSTATE / N,LST(2,1024),N0(11),NSM(11),
     1                  NSP(11),MAXMAT,NST

      COMMON D(45),CJ(45),EN(256 ,ITER,NOS,IPARAM(28,15),
     1  ILMB(256 28),MQIT(2,10),LASS(230),EXPER(230),
     2  IC(230,28),B(230),V(784),BV(28),WORK(4900)
C
      NPARPS=15
      DO 310 NS=1,NOS
C
      CORR=0.0
      DO 200 NSB=1,NOS
      INDX=MATVEC(NS,NSB,NOS)
  200 CORR=CORR + V(INDX)*BV(NSB)
C
      DO 309 K=1,NPARPS
      KC=IPARAM(NS,K)
      ICP1=IABS(KC/10)
      IF(ICP1 .EQ. 0) ICP1=10
      ICP2=MOD(IABS(KC),10)
      IF(ICP2 .EQ. 0) ICP2=10
      ICPC=(2*N-ICP1)*(ICP1-1)/2-ICP1+ICP2
      IF(KC) 306,310,308
  306 CJ(ICPC)=CJ(ICPC)+CORR
      GO TO 309
  308 I(ICPC)=I(ICPC)+CORR
  309 CONTINUE
  310 CONTINUE
C
      RETURN
      END
```

```
      SUBROUTINE GENSYM(ARR,IDIM)
C
C           THIS SUBROUTINE RE-ARRANGES A 1D VECTOR ARRAY
C     (REAL) REPRESENTING A GENERAL REAL MATRIX INTO THE STORAGE
C     MODE WHERE ONLY THE UPPER TRIANGULAR HALF OF THE ARRAY IS KEPT.
C     THIS REDUCES STORAGE REQUIREMENTS FOR REAL SYMMETRIC ARRAYS.
C
      DIMENSION ARR(1)
C
      MATCNT=1
C
      DO 100 ICOLMN=1,IDIM
      INDX=(ICOLMN-1)*IDIM
C
      DO 100 IROW=1,ICOLMN
      ARR(MATCNT)=ARR(INDX+IROW)
      MATCNT=MATCNT+1
C
  100 CONTINUE
C
      RETURN
      END
```

```
      SUBROUTINE MINV(A,N,D,L,M)
C
C     INVERTS A MATRIX
C
      DIMENSION A(1),L(1),M(1)
      REAL A,D,BIGA,HOLD
C
      D=1.0
      NK=-N
      DO 80 K=1,N
      NK=NK+N
      L(K)=K
      M(K)=K
      KK=NK+K
      BIGA=A(KK)
      DO 20 J=K,N
      IZ=N*(J-1)
      DO 20 I=K,N
      IJ=IZ+I
      IF(ABS(BIGA)-ABS(A(IJ))) 15,20,20
15    BIGA=A(IJ)
      L(K)=I
      M(K)=J
20    CONTINUE
C
      J=L(K)
      IF(J-K) 35,35,25
25    KI=K-N
      DO 30 I=1,N
      KI=KI+N
      HOLD=-A(KI)
      JI=KI-K+J
      A(KI)=A(JI)
30    A(JI)=HOLD
C
35    I=M(K)
      IF(I-K) 45,45,38
38    JP=N*(I-1)
      DO 40 J=1,N
      JK=NK+J
      JI=JP+J
      HOLD=-A(JK)
      A(JK)=A(JI)
40    A(JI)=HOLD
C
45    IF(BIGA) 48,46,48
46    D=0.0
      RETURN
48    DO 55 I=1,N
      IF(I-K) 50,55,50
50    IK=NK+I
      A(IK)=A(IK)/(-BIGA)
55    CONTINUE
C
      DO 65 I=1,N
      IK=NK+I
      HOLD=A(IK)
      IJ=I-N
      DO 65 J=1,N
      IJ=IJ+N
      IF(I-K) 60,65,60
60    IF(J-K) 62,65,62
62    KJ=IJ-I+K
```

```
      A(IJ)=HOLD*A(KJ) + A(IJ)
65    CONTINUE
C
      KJ=K-N
      DO 75 J=1,N
      KJ=KJ+N
      IF(J-K) 70,75,70
70    A(KJ)=A(KJ)/BIGA
75    CONTINUE
C
      I=D*BIGA
C
      A(KK)=1.0/BIGA
80    CONTINUE
C
      K=N
100   K=K-1
      IF(K) 150,150,105
105   I=L(K)
      IF(I-K) 120,120,108
108   JQ=N*(K-1)
      JR=N*(I-1)
      DO 110 J=1,N
      JK=JQ+J
      HOLD=A(JK)
      JI=JR+J
      A(JK)=-A(JI)
110   A(JI)=HOLD
120   J=M(K)
      IF(J-K) 100,100,125
125   KI=K-N
      DO 130 I=1,N
      KI=KI+N
      HOLD=A(KI)
      JI=KI-K+J
      A(KI)=-A(JI)
130   A(JI)=HOLD
      GO TO 100
150   RETURN
      END
```

```
      subroutine uswap(s1,s2,en,idim,mst0,if)

c     Checks a metrix (s2) ageinst a previously stored
c     matrix or unit isc+1   Check is for minimum RMS
c     difference in elements of rows with one another.
c     The sum of (s1(j,k)-s2(i,k))**2 for all k from
c     1 to idim is calculated.  This is stored as DJI(i).
c     The minimum of this vector is then found and
c     if that minimum if not for j=i ther the corresponding
c     columns of s2 are interchanged.  Also the elements
c     en(mst0+j) and en(mst0+i) are swapped.
c
c     This routine is designed to keep the order of eigenstates
c     and eigenvectors the same for succesive cycles in the
c     iterative portion of mqiter.  This will help convergence
c     in the case where the diagonalization of the Hamiltonian
c     may inadvertently swap eigenstates.

      dimension dji(700),s1(1),s2(1),en(1)
      integer flind(7),st1,st2
      common / cfile / isc,flind,ifp


c     read in original matrix
      call readms(if,isc+1,s1,flind,ifp)

c     loop over columns by j
      do 500 j=1,idim
      joff=(j-1)*idim

c     loop over columns by i
      do 200 i=1,idim
      dji(i)=0.0
      ioff=(i-1)*idim

      do 100 k=1,idim
  100 dji(i)=dji(i) + (s1(joff+k) - s2(ioff+k))**2

  200 continue

c     find minimum
      small=dji(1)
      kkk=1
      do 300 kk=2,idim
      if (dji(kk) .ge. small) go to 300
      kkk=kk
      small=dji(kk)
  300 continue

      if(kkk .eq. j) go to 500

c     swap eigenvectors

      koff=(kkk-1)*idim
      do 400 k=1,idim
      indx1=joff+k
      indx2=koff+k
      temp=s2(indx1)
      s2(indx1)=s2(indx2)
      s2(indx2)=temp
  400 continue

c     swap eigenvalues
```

```
      st1=j+mst0
      st2=kkk+mst0
      temp=er(st1)
      er(st1)=er(st2)
      er(st2)=temp

C     output swapped states
      write(6,101) st1,st2

  500 continue

      return

  101 format(10x,' SWAPPED STATES ',14,' , ',14)
      end
```

```
      subroutine eout(n,maxmat,en,n0)

c     This subroutine outputs the contents of energy vector
c     en in f12.4 format.  States in each Zeeman manifold
c     are seperated by a blank line.  N is the number of spins,
c     maxmat is the size of the largest Zeeman manifold
c     contained in en and n0 is the array containing the
c     binomial coefficients (dimensions of the Zeeman manifolds).

      dimension en(1),n0(1)

      np1=n-1
      nb=1

      do 500 j=1,np1

      if(n0(j) .gt. maxmat) go to 500
      nt=nb+n0(j)-1
      write(6,401) (ieng,en(ieng) , ieng=nb,nt)
      nb=nb+n0(j)

  500 continue

      return

  401 format(//(4x,'EN(',i3,') = ',f12.4))
      end
```

```
      subroutine mq2diff(thr,idbirr,nmqo,imqo)

c     multiple quantum frequency calculating routine.
c     version 6.      VAX/VMS version.
c
c     This subroutine calculates allowed (by symmetry)
c     lines in a multiple quantum spectrum.  Any allowed order
c     can be calculated.  Orders for which not all eigenvector
c     matrices have been calculated will not be complete.
c
c     subroutine symset is called to classify eigenstates
c     by symmetry.
c
c     thr is the minimum allowed threshold for allowed
c     transitions.
c
c     idbirr is the flag for degeneracy checking
c             idbirr=1 eigenstates scanned for degeneracies
c             idbirr=0 eigenstates not scanned.
c
c     nmqo is the number of orders to calculate.
c     mqo is the vector containing the orders to calculate
c     Elements of mqo define what order spectra are calculated in.
c     If nmqo=-1, all orders are calculated starting with 1
c     through r and then the zero quantum.
c
c     this version allows up to 10 spins.
c
      dimension s2(4900),s1(3136),freq(1000)
      integer deg,idbl(256),isym(256),sym
      integer ideger(1000),imqo(1),dml,dmu,ues,flird(7)
      logical tophef,half,lcs

      commor   cfile   isc,flird,ifp
      commor / cstate / n,lst(2,1024),n0(11),nsm(11),
     1                  nsp(11 ,maxmat,nst

      commor d(45),cj(45),er(256),iter,nos,iparam(20,15),
     1  dlmb(256,26),mqit(2,10),lass(230 ,exper(230),
     2  dc(230 26),b(230 ),v(784),bv(28),work(4900)

      equivalerce (work,s2),(idbl(1),dlmb(1,1)),
     1   s1(1 .dlmb(1,2)

c     :n tialize
      if thr  eq. -1) thr=1.0e-4
      rfreq=
      rstate-2**r
      rpl=n+1
      rml=r-1
      do 3 ii=1,256
3     idbl ii  0
      lcs= f lse.
      half= false.
      if idbirr .eq. 0  go to 1
      kk=1
      itop=rml
      do 6 i=1,itop
      jtop=n (i+1)
      if jtop  gt. maxmat) go to 6
      do 5 j-1,jtop
      kk kk-1
      if(idbl(kk)  re. 0 .or  j  eq. jtop) go to 5
```

```
      i1 100.0*en(kk)
      jp1=j+1
      kkk kk
      do 4 k=jp1,jtop
      kkk=kkk+1
      i2=100.0*en(kkk)
      if(i1 .eq. i2  idbl(kkk)=kk
 4    continue
 5    continue
 6    continue
c
c     calculate symmetries
c
 1    call symset(s1,s2,isym,nrep,thr)

      if(mod(r,2) .ne. 0) half=.true.
      if(nmqn .gt. 0) go to 111
      do 212 i=1,r
212   imqo(i)=i
      imqo(npl)=0
      nmqo=npl

c
c     MAIN LOOP OVER ORDERS TO CALCULATE
c
111   do 600 mq=1,nmqo
      mqo=imqo(mq)
      write(6,705) mqo
      kk=1
      line=0
      tophalf=.false.
      do 10 j=1,1000
      freq(j)=0.0
10    idegen(j)=0
      mlow=r/2+1
      if(half) mlow=mlow+2
      nt=npl-mqo
      if(mod(r,2)-mod(mqo,2) .eq. 0) nt=nt+1
      nt=nt/2
      do 13 j=1,nt
      if(n0(j) .le. maxmat .and. n0(j+mqo) .le. maxmat)
     1   go to 13
      write(6,722)
      go to 133
13    continue
133   write(6,723)
      write(6,723)

c     loop over sets of zeeman submatrices.

      kz1=1
      do 200 iz=1,r
      mlow=mlow-1
      if(half) mlow=mlow-1
      mup=mlow-mqo
      if(half) mup=mlow-2*mqo

      if(mqo .eq. 0 .and. iz .eq. 1) go to 200
      if((iz-mqo) .gt. npl) go to 300

c     dimensions of lower and upper submatrices.

      dml=n0(iz)
```

```
      dmu=n0(iz+mqo)

      if (dml .gt. dmu) tophaf=.true.
      if (tophaf .and. (.not. lcs)) go to 300
      if (dml .le. maxmat) go to 134
      kz1=kz1+1
      go to 200

 134  if (dmu .gt. maxmat) go to 200
      kz2=1
      do 136 i=1,mqo
      if (n0(iz+i) .le. maxmat) go to 136
      kz2=kz2+1
 136  continue
      if (mqo .ne. 0) go to 276
      if(half) go to 275
      write(6,603) mlow
      go to 278
 275  write(6,604) mlow
      go to 278
 276  if (half) go to 277
      write(6,601) mlow,mup
      go to 278
 277  write(6,602) mlow,mup

c     loop over lower eigenstates

 278  les=0
      if (iz .ne. 1) les=nsm(iz-kz1)
      ntop=dml
      if (mqo .eq. 0) ntop=ntop-1
      do 100 j=1,ntop
      les=les+1

c     loop over upper eigenstates

      ues=nsm(iz-kz2+mqo)
      nu=1
      if (mqo .ne. 0) go to 135
      nu=j+1
      ues=ues+j
 135  do 95 jst=nu,dmu
      ues=ues+1
c     line # counter
      line=line+1
      if (idblrr .ne. 0 .and. idbl(les) .ne. 0)go to 95
c     eigenstates of same symmetry?
      if (isym(les) .ne. isym(ues)) go to 95
c     possible degenerete situation for zero quantum?
      if (idblrr .ne. 0 .and.
     1  idbl(ues) .eq. les .and. mqo .eq. 0)) go to 95
c     yes, output freq
      freq(kk)=en(ues)-en(les)
      sym=isym(les)+1
      write(6,501) line,freq(kk),ues,les,sym
      kk=kk+1
      if(kk .lt. 1001) go to 95
      write(6,706)
      go to 300

c     END of loops over upper,lower eigenstates and
c     over sets of submatrices.
```

```
 95     continue
 100    continue
 200    continue

c       calculate degeneracies
 300    itop=kk-1
        rfreq=1
        if(itop .le. 1) go to 8000
        write(6,709)
        do 170 icnt=1,itop
        if(ideger(icnt) .eq. -1) go to 170
        i1 = 1.0e2*freq(icnt)
        deg=1
        icp1=icnt+1
        if(icp1 .gt. itop) go to 165
        do 160 jcnt=icp1,itop
        if(ideger(jcnt) .eq. -1) go to 160
        i2 = 1.0e2*freq(jcnt)
        if(iabs(i1) .ne. iabs(i2)) go to 160
        ideger(jcnt)=-1
        if(i1 .eq. i2) deg=deg+1
 160    continue
 165    rfreq=rfreq+1
        ideger(icnt)=deg
 170    continue

c       output frequencies.  If there are no chemical
c       shifts, then only the absolute values output.

        if lcs  go to 666
        do 555 i = 1,1000
 555    freq(i) =abs(freq(i))
 666    call frqout(freq,ideger,itop)
        write(6,707) rfreq

c       END main loop over orders.

 800    continue

c       output results of degeneracy search of eigenstates.
        if(idbirr .eq. 0) go to 741
        write(6,714)
        do 740 ii=1,nst
        if(idbl(ii)) 743,745,743
 743    write(6,716) ii,er(ii),idbl(ii)
        go to 740
 745    write(6,715) ii,en(ii)
 740    continue
 741    write(6,717)
c
c       output symmetry classifications
c
        kk = 0
        nrep=nrep+1
        do 770 jj=1,nrep
        write(6,718) jj
        kkk=0
        do 760 ii=1,nst
        if isym(ii) .ne. kk) go to 760
        write(6,715) ii,en(ii)
        kkk=kkk+1
 760    continue
        write(6,719) kkk
```

```
      kk kk+1
770   continue

c     FORMAT STATEMENTS

501   format(4x,i4,13x,f12.4,17x,i3,'->',i3,13x,i2)
703   format(6x,'LINE #',10X,'FREQUENCY',4X,'(HZ)'
     1,8X,'TRANSITION STATES',5X,'SYMM',/)
705   FORMAT(1H1,,10X,I2,' QUANTUM SPECTRUM CALCULATION . . .',/)
706   FORMAT(' 1000 FREQ HAVE BEEN CALCULATED!')
707   FORMAT(/,' TOTAL # UNIQUE FREQ =',I5,/)
709   FORMAT(1H1, ,7X,'FREQ (HZ)',11X,'DEGENERACY',/,
     11X,46('-'),)
714   FORMAT(1H1,10X,'ENERGY DEGENERACY CALCULATION. . .',/)
715   FORMAT(' EN(',I3,') = ',F12.4)
716   FORMAT(' EN(',I3,') = ',F12.4
     1,5X,'IS DEGENERATE WITH STATE #',I4)
717   FORMAT(1H1, ,10X,
     1' SYMMETRY CLASSIFICATION OF EIGENSTATES. . .'/)
718   FORMAT(/,5X,' STATES OF REPRESENTATION #',I3)
719   FORMAT( ,10X,' TOTAL NUMBER OF STATES = ',I3)
722   FORMAT(17X,'(INCOMPLETE SPECTRUM)',/)
723   FORMAT(1X,79('-' )
801   FORMAT( ' LOWER QUANTUM # = ',I2,' ; UPPER QUANTUM # = '
     1,I2/
802   FORMAT(/' LOWER QUANTUM # = ',I2,'/2',
     1' ; UPPER QUANTUM # = ',I2,' 2'/)
803   FORMAT(/' QUANTUM # = ',I2/)
804   FORMAT(/' QUANTUM # = ',I2,'/2'/)

      return
      end
```

```
      subroutine symset(s1,s2,isym,nrep,thres)

c
c     Determines symmetry relationships among eigenstates
c     stored on disk.  Matrix elements of I minus are
c     calculated and non-zero results are taken to represent
c     two states in the same representation.
c
c     s1 and s2 are input matrices used for the eigenvector
c     matrices read from disk.
c
c     n is the number of spins
c
c     iurt is the unit number read on for eigenvector matrices.
c
c     r0 is the vector of binomial coefficients.
c     nsm is the sum of dimensions of allowed submatrices.
c     nsp is the sum of dimensions of all submatrices.
c     maxmat is the largest allowed submatrix dimension.
c     nst is the total number of eigenstates.
c     lst is the two dimensional matrix of simple product
c     states and the number of "one" spins in each.
c
c     thres is the minimum allowed threshold for allowed
c     transitions
c
c     On exit, ISYM contains the numbers from 1 to NREP which
c     identify the representations found for the eigenstates.
c
c     A symmetry number of one (1) indicates a totally
c     symmetric state (A1 symmetry).
c
c     neither eigenstates or eigenvectors are rearranged.
c
c

      dimension s1(1),s2(1),isym(1)
      real lv(70),uv(70)
      integer spl(70),spu(70),dml,dmu,dmp,ustate,utmp,usp
      integer uf,skip,ues,flind(7)
      logical tophaf

      common / cfile / isc,flind,ifp
      common / cstate / n,lst(2,1024),r0(11),rsm(11),
     1                  nsp(11),maxmat,nst

c     initialize

      do 7 i=1,nst
    7 isym(i)=0
      isym(1)=1
      isym(nst)=1
      nm1=n-1
      tophaf=.false.
      irep=1
      np1=n+1
      skip=0
      izs=0
      do 90 i=1,np1
      if(r0(i).le.maxmat) go to 90
      go to 91
   90 continue
      go to 93
```

```
 91     izs=i-1
        do 92 j=i,npl
        if(n0(j) .le. mexmat) go to 93
        skip=skip+1
 92     continue

c       MAIN LOOP

 93     kz 1
        thr=abs(thres)
        if(thr .lt. 1) thr=1.0/thr
        do 5000 iz=2,nml

c       file numbers
        lf iz-kz
        uf=lf-1
        jump=0
        if(iz .eq. izs) jump=skip
c       power of I minus operator.
        imp=jump+1

c       dimension of lower submatrix
        dml=r0(iz)
        if dml .le. mexmat) go to 94
        kz=kz-1
        go to 5000

c       dimension of upper submatrix
 94     dmu=n0(iz+imp)
c       dimension of operator matrix
        dmp=n0(npl-imp)
        ip=nsp(npl-(imp+1))
c       pointers to beginning of simple product states.
        lsp=nsp(iz-1)
        usp=nsp(iz-1+imp)

c       collect spin product states
        do 80 kk=1,dml
 80     spl(kk) =lst(1,lsp+kk)
        do 85 kk=1,dmu
 85     spu(kk)=lst(1,usp+kk)

        if(dml .gt. dmu) tophaf=.true.

        if(tophaf) go to 10
c       read lower submatrix into s1; upper into s2
        call readms(lf,isc,s1,flind,ifp)
        call readms(uf,isc,s2,flind,ifp)
        go to 11
c       read lower submatrix into s2; upper into s1
 10     call readms(lf,isc,s2,flind,ifp)
        call readms(uf,isc,s1,flind,ifp)

c       loop over lower eigenstates

 11     les=nsm(iz-kz)
        do 400 kl=1,dml
        les=les+1

c       move eigervector to lv

        il (kl-1 *dml
        if(tophaf) go to 25
```

```
      do 50 kk=1,dml
 50   lv kk =s1(il+kk)
      go to 52
 25   do 51 kk 1,dml
 51   lv kk =s2(il+kk

c     quick check to see if this eigerstate is totally symm.

 52   if isym(les) .ne. 0) go to 30
      sum=0
      do 20 kk=1,dml
 20   sum=sum-lv(kk)
      iters=abs(100.0*sum)
      if(iters .ne  0) isym(les)=1

c     loop over upper eigenstates

 30   ues nsm(iz-kz)+dml
      do 300 ku=1,dmu
      ues=ues+1

c     move eigenvector to uv

      iu=(ku-1)*dmu
      if topbaf) go to 35
      do 60 kk=1,dmu
 60   uv(kk)=s2(iu+kk)
      go to 62
 35   do 61 kk=1,dmu
 61   uv(kk)=s1(iu+kk)

c     quick check to see if this eigenstate is totally symm.

 62   if isym(ues) .ne  0) go to 75
      sum=0 0
      do 70 kk 1,dmu
 7.   sum=sum+uv(kk)
      itens=abs(100.0*sum)
      if(iters .ne. 0) isym(ues)=1

c     check for possible previous symmetry calculatior
c     both totally symm. (irep=1) only possibility.

 75   if isym(les) .ne  0 .and. isym(ues) .ne. 0) go to 300

c     matrix elemert calculation section.
      sum=0.0

c     loop over simple product states of lower eigerstate

      do 200 ml=1,dml
      lstate=spl(ml)

c     loop over simple product states of upper eigenstate

      do 100 mu=1,dmu
      ustate=spu(mu)

c     loop over comporerts of I minus operator
c      I minus to imp power)

      do 150 ruc=1,dmp
c     chose operator
```

```
      imin=lst(1,ip+nuc)
c     imin|ustate> = 0 ?
      if (ustate .and. imin) .ne. 0) go to 150
c     utmp = imin|ustate>
      utmp=ustate + imir
c     <lstate|utmp> = <lstate|imin|ustate> = 0 ?
      if(lstate .ne. utmp) go to 150
      sum=sum+lv(ml)*uv(mu)
      go to 100
  150 continue

  100 continue
  200 continue

c     | <les| (I minus **imp |ues> |**2

      itens=thr*(sum*sum)

      if(itens .eq. 0) go to 300
c     non-zero matrix element; check to see if one of
c     these eigenstates previously classified.

      if isym(les) .eq. 0 .and. isym(ues) .eq. 0) go to 175
      if(isym(les) .eq  0) go to 162
      isym(ues)=isym(les)
      go to 300
  162 isym(les =isym(ues)
      go to 300

c     new representation.

  175 irep=irep+1
      isym(les)=irep
      isym(ues =irep

  300 continue
  400 continue

 5000 continue
      nrep=irep

      return
      end
```

```
      subroutine frqout(freq,idegen,itop)

c     this subroutine outputs frequencies from vector freq
c     nd their associated "statistical" degeneracies from
c     ideger   Itop is the maximum number of frequencies in
c     freq.  Frequencies with a degeneracy of -1 are
c     skipped   On completion, idegen is set to -1
c     in all elements.

      dimension freq(1 ),idegen(1

c     find first freq

 175  do 180 i=1,itop
      if idegen(i  .eq. -1) go to 180
      k=i
      go to 182
 180  continue
c     ll done
      returr

c     find next maximum freq

 182  curr=freq(k)
      do 185 i=k,itop
      if idegen(i  .eq. -1 .or. freq(i  .le. curr)
     1 go to 185
      k=i
      go to 182
 185  cortinue
c     maximum found, output
      write(6,601  freq(k),ideger(k)
      ideger(k =-1
      o to 175

 601  format 4x,f12.4,15x,13
      end
```

```
      subroutine readms(irec,iu,inp,flind,ifp)
c
c     Reads in data from file open on unit # iu.
c     File must be opened for sequential, direct access.
c     Record size should be 4 bytes.
c
c     Data is read into real array inp with unformatted,
c     direct access reads.  Irec determines which section
c     of the file to read and flind is an integer
c     array containing the number of records in each section.
c     Ifp is the "associated variable" for the file.
c

      real inp(1)
      integer flind(1)

c
c     determine initial record #
c

      init=1
      if (irec .eq. 1) go to 20
      nt irec-1

      do 10 i=1,nt
 10   init=init+flind(i)

c
c     position file pointer to initial record
c

 20   find(iu'init

c
c     read data
c

      nt=flind(irec)
      do 100 i 1,nt
      read(iu'init  inp(i)
      init=init+1
 100  continue

      return
      end
```

```
      subroutire writms(irec,iu,out,flind,ifp)

c     writes data to file opened on unit # iu.
c     File must be opened for sequential, direct access.
c     Record size should be 4 bytes.
c
c     Data is written from real array out with unformatted,
c     direct access writes   Irec determines the section
c     of the file to receive the data and flind is an integer
c     array cortaining the number of records in each section.

      real out(1)
      integer flind(1)

c
c     determine initial record #
c

      init=1
      if(irec  eq. 1) go to 20
      nt irec-1
      do 10 i=1,nt
 1.   init=irit+flird(i

c
c     write data
c

 20   nt flind(irec)
      do 100 i-1,nt
      write(iu'irit) out(i)
      init=irit+1
 100  continue

      returr
      end
```

```
      FUNCTION MAT(I,J)
C
C      THIS IS A FUNCTION TO COMPUTE THE INDEX FOR AN ARRAY LOCATION
C      WHEN ONLY THE UPPER HALF TRIANGLE OF A TWO DIMENSIONAL ARRAY
C      IS STORED.  THE ARGUMENTS I AND J ARE THE NORMAL 2D INDEXES.
C      J MUST BE GT I FOR THE COMPUTAION TO BE CORRECT.
C
      MAT=J*(J-1) 2 + I
C
      RETURN
      END


      FUNCTION MATVEC(I,J,N)
C
C
C
C      THIS IS A FUNCTION TO COMPUTE THE INDEX FOR AN ARRAY LOCATION
C      WHEN A GENERAL 2D ARRAY IS STORED AS A SINGLE VECTOR.
C      ARGUMENTS I AND J ARE THE NORMAL 2D INDEXES.  N IS THE DIMEN-
C      SION OF THE 2D ARRAY.
C
      MATVEC=(J-1)*N + I
C
      RETURN
      END
```

```
      program biph4para
c
c     calculates coupling constants for a biphenyl
c     with asymmetrically distorted rings.
c          ==========
c
c     Coodirate system #1;  D4 symmetry:
c     The origin is at the center of teh c-c inter ring bridge.
c     The x-axis bisects the dihedral angle, the z-axis is along
c     the benzene para bonds to the substituents.
c
c     Coordirate system #2;  D2 symmetry:
c     The z-axis passes through the biphenyl para bonds,
c     the origin is located in ring "2" (with protons 5,6,7,8),
c     the x-axis lies in the plane of this ring and the y-axis
c     is normal to it
c
c     This version (# 4) does not "symmetrize" the hamiltonian
c     before diagonalization (i.e. bph4ham is called instead
c     of bphham).
c
c     this version increments various parameters for differnt passes
c
c     input  (in common "geom")
c
c     r12, r14, r23, r260, r67, r58, r56,
c     szz  (sxx-syy)=s2p, sxy, delta
c
      implicit double precision (a-h,o-z)
      double precision th(16),lxy(4),lyx(4),s(5)
      real d(28),cj(28),cs(8),en(256),woff,freq(50),cjd4(28)
      real w1mx,w2mx,w1mn,w2mn,zmx,w1(50)
      integer isym(256),n0(6)
      logical yans
      common / geom / r12,r14,r260,r67,r58,r56,szz,s2p,sxy,delta
      common / coup / d,cj,cs,woff
      common / cstate / n,lst(2,256)
      data cjd4 / 2.0,0.0,0.5,4*0.0,0.5,5*0.0,2.0,8*0.0,
     1            2.0,0.0,0.5,0.5,0.0,2.0 /
      data n0 / 1,8,28,28,8,1 /

c     get input

      do 1 j=1,256
      en(j)=0.0
 1    isym(j)=0
      do 2 i=1,8
 2    cs(i)=0.0
      n=8
      woff=0.0
      type *,' Which coord  system? (1 or 2)'
      accept *,icoord
      type *,' INPUT OF INITIAL PARAMETERS:'
      type *,' enter r12: '
      accept *,r12
      type *,' enter r14: '
      accept *,r14
      type *,' enter r23: '
      accept *,r23
      type *,' enter r260: '
      accept *,r260
      if icoord .eq. 1 go to 6066
      type *,' enter r67: '
```

```
      accept *,r67
      type *,' enter r58: '
      accept *,r58
      type *,' enter r56: '
      accept *,r56
6066  type *,' enter szz: '
      accept *,szz
      type *,' enter (sxx-syy)  '
      accept *,s2p
      if(icoord .eq. 1  go to 6067
      type *,' enter sxy:'
      accept *,sxy
6067  type *,' enter delta: '
      accept *,delta
      type *,' which parameter do you wish to vary?'
      type *,'         szz = 1         r12 = 7'
      type *,'  (sxx-syy) = 2         r23 = 8'
      type *,'         sxy = 3         r58 = 9'
      type *,'       delta = 4        r260 = 10'
      type *,'         r14 = 5         r56 = 11'
      type *,'         r67 = 6'
      accept *,iper
      type *,' what is the increment in this parameter?'
      accept *,sinc
      type *,' how many values?'
      accept *,narg

      type *,' are the d4 j''s to be used in the simulation?'
      if(yes(idum)) go to 11
      do 12 i=1,20
12    cj i =0.0
      go to 13
11    do 14 i=1,20
14    cj i =cjd4(i

13    rad=4  d00*dater(1.0d00)
      dk -2 0d00*(245.017d00**2.2)

      w1mx=0 0
      w2mx=0 0
      w1mn=0 0
      w2mn=0.0
      imx=1 1
      iwflag=0
      open(unit=1,name='spif1.da',type='new')
      open(unit=2,name='spif2.da',type='new')
      nq 6
      write(1,602) narg,nq
      nq 7
      write(2,602) narg,nq

c     main loop over order parameters
      do 5000 nd=1,narg

c     compute delta in rads
      rdel=delta*rad 100.0d00

      if(icoord .eq. 2  go to 5050
c
c     coordinate system #1
      s(1 =szz
      s(2 =s2p*((dcos(rdel/2.0d00))**2-(dsin(rdel/2.0d00))**2)
      s(3)=s2p*(dcos(rdel/2.0d00)*dsin(rdel/2.0d00))
```

```
        s(4 =0 0d00
        s(5)=0 0d00
        r67=r23
        r58=r14
        r56=r12
        go to 6060
c
c       cocrdirate system #2
 5050   s(1)=szz
        s(2 =s2p
        s(3)=sxy
        s(4)=0 0d00
        s(5 =0.0d00

c       compute trig functions of delta
 6060   csdl=dcos(rdel)
        sndl=dsin(rdel)

c       output initial parameters
        print 201, r12,r14,r23,r260,r67,r56,r56,(s(i), i=1,3),delta
 201    format('1program biph3 - initial parameters . . .'//
     1' r12 = ',e14.4/,' r14 = ',e14.6/,' r23 = ',e14.6/,
     2' r260 = ',e14.6 ,' r67 = ',e14.6/,' r58 = ',e14.6/,
     3' r55 = ',e14.6//,' szz = ',e14.6/,' (sxx-syy) = ',e14.6/,
     4' sxy = ',e14.6//,' DELTA = ',f10.4///)

c       compute reeded distances at delta=0

        rx1 (r14 r23 /2.0d00
        rx2=(r58-r67)/2.0d00
        rx3=(r58-r14 /2.0d00
        rx4=(r14 r67)/2.0d00
        rx5=(r58-r23)/2.0d00
        rx6=(r67-r23 /2.0d00

c       compute trig functions of reeded angles

        srd=rx1 r12
        csd=dsqrt(1.0d00-snd**2.0)
        sn =rx6/r260
        csa=dsqrt(1 0d00-sna**2.0)
        sndp=rx2 r56
        csdp=dsqrt(1 0d00-sndp**2.0)

        ry4=r260*csa
        ry1=r12*csd+ry4
        ry2=r56*csdp+ry4
        ry3=ry1+ry2-ry4

c       calculate internuclear distances for delta=0

        r160=dsqrt(ry1**2.0+rx2**2 0)
        r150=dsqrt(ry3**2 0+rx3**2 0)
        r250=dsqrt(ry2**2.0+rx5**2.0)

        srg=rx4/r160
        csg=ry1 r160
        sngp=rx5/r250
        csgp=ry2/r250
        snb=rx3 r150
        csb=ry3/r150

        print 101, sra,srb,srg srgp,snd,sndp,r160,r150,r250
```

```
 101    format('1program biph3 - calculation of 6,7 quantum',
     1' for para substituted bipheryl.',///,
     2' trig values:',//,' sna = ',e14.6,/,' snb = ', e14.6,/,
     3' sng = ',e14.6,/,' sngp = ',e14.6,/,' snd = ',e14.6,/,
     4' srdp = ',e14.6,/,' r160 = ',e14.6,/,' r150 = ',e14.6,/,
     5' r250 = ',e14.6///)

c       calculate lxy's and lyx's

        lxy(1)=r14*srdl
        lyx(1)=r14*csdl

        lxy(2)=r23*sndl
        lyx(2)=r23*csdl

        lxy(3)=0.0d00
        lyx(3)=r67

        lxy(4)=0.0d00
        lyx(4)=r58

c       calculate th's

        th(1)=(lyx(1)-lyx(3))/2.0d00
        th(2)=(lxy(1)-lxy(3))/2.0d00

        th(3)=(lyx(2)-lyx(3))/2.0d00
        th(4)=(lxy(2)+lxy(3))/2.0d00

        th(5)=(lyx(1)-lyx(4))/2.0d00
        th(6)=(lxy(1)+lxy(4))/2.0d00

        th(7)=(lyx(2)+lyx(3))/2.0d00
        th(8)=(lxy(2)-lxy(3))/2.0d00

        th(9)=(lyx(1)+lyx(4))/2.0d00
        th(10)=(lxy(1)-lxy(4))/2.0d00

        th(11)=(lyx(1)+lyx(3))/2.0d00
        th(12)=(lxy(1)-lxy(3))/2.0d00

        th(13)=(lyx(2)-lyx(4))/2.0d00
        th(14)=(lxy(2)+lxy(4))/2.0d00

        th(15)=(lyx(2)+lyx(4))/2.0d00
        th(16)=(lxy(2)-lxy(4))/2.0d00

c       calculate internuclear distances for delta not=0

        r17=dsqrt(ry1**2.0 + th(11)**2.0 + th(12)**2.0)
        r16=dsqrt(ry1**2.0 + th(1)**2.0 + th(2)**2.0)
        r25=dsqrt(ry2**2.0 + th(13)**2.0 + th(14)**2.0)
        r26=dsqrt(ry2**2.0 + th(15)**2.0 + th(16)**2.0)
        r24=dsqrt(ry4**2.0 + th(3)**2.0 + th(4)**2.0)
        r15=dsqrt(ry3**2.0 + th(5)**2.0 + th(6)**2.0)
        r27=dsqrt(ry4**2.0 + th(7)**2.0 + th(8)**2.0)
        r18=dsqrt(ry3**2.0 + th(9)**2.0 + th(10)**2.0)
        r13=dsqrt(((r23+r14)/2.0d00)**2.0 + (ry1-ry4)**2.0)
        r57=dsqrt(((r67+r58)/2.0d00)**2.0 + (ry2-ry4)**2.0)

c       output interrulcear distances
        print *,' r17 = ',r17
        print *,' r16 = ',r16
```

```
      print *,' r25 = ',r25
      print *,' r28 = ',r28
      print *,' r26 = ',r26
      print *,' r15 = ',r15
      print *,' r27 = ',r27
      print *,' r18 = ',r18
      print *,' r13 = ',r13
      print *,' r57 = ',r57

c     calculate angles between internuclear vectors and
c     moleculer axis system.

      rpd2=rad 2.0d00

      ang13=rpd2-datan(2.0d00*(ry1-ry4)/(r23+r14))
      th13z=dcos(ang13)
      th13x=csd1*dsin(ang13)
      th13y=snd1*dsin(ang13)

      ang57=rpd2-datan(2.0d00*(ry2-ry4)/(r67+r58))
      th57z=dcos(ang57)
      th57x=dsin(ang57
      th57y=  d00

      th56z=csdp
      th56x=sndp
      th56y=  d00

      th12z=csd
      th12x=csd1*snd
      th12y=snd1*snd

      th16z=ry1 r16
      th16x=th(1)/r16
      th16y=th(2)/r16

      th26z=ry4 r26
      th26x=th(3)/r26
      th26y=th(4)/r26

      th15z=ry3 r15
      th15x=th(5)/r15
      th15y=th(6)/r15

      th27z=ry4 r27
      th27x=th(7)/r27
      th27y=th(8)/r27

      th18z=ry3 r18
      th18x=th(9)/r18
      th18y=th(10)/r18

      th17z=ry1 r17
      th17x=th(11)/r17
      th17y=th(12)/r17

      th25z=ry2 r25
      th25x=th(13)/r25
      th25y=th(14)/r25

      th28z=ry2 r28
      th28x=th(15)/r28
      th28y=th(16)/r28
```

```
c       calculate couplirgs

        d12=dk*coupi(th12z,th12x,th12y,s,r12)
        d23=dk*coupi(0.0d00,csdl,sndl,s,r23)
        d14=dk*coupi(0.0d00,csdl,sndl,s,r14)
        d13=dk*coupi(th13z,th13x,th13y,s,r13)

        d56=dk*coupi(th56z,th56x,th56y,s,r56)
        d67=dk*coupi(0.0d00,1.0d00,0.0d00,s,r67)
        d58=dk*coupi(0.0d00,1.0d00,0.0d00,s,r58)
        d57 dk*coupi(th57z,th57x,th57y,s,r57)

        d26=coupi(th26z,th26x,th26y,s,r26)
        d27=coupi(th27z,th27x,th27y,s,r27)
        ad26=dk* d26 + d27)/2.0d00

        d15 coupi(th15z,th15x,th15y,s,r15)
        d18=coupi(th18z,th18x,th18y,s,r18)
        ad15=dk* d15 + d18)/2.0d00

        d25=coupi(th25z,th25x,th25y,s,r25)
        d28=coupi(th28z,th28x,th28y,s,r28)
        ad25=dk* d25 + d28)/2.0d00

        d16 coupi(th16z,th16x,th16y,s,r16)
        d17=coupi(th17z,th17x,th17y,s,r17)
        ad16=dk* d16 + d17)/2.0d00

c       output result
        print *,' RING A'
        print *,' d12 = ',d12
        print *,' d23 = ',d23
        print *,' d14 = ',d14
        print *,' d13 = ',d13
        print *,' RING B'
        print *,' d56 = ',d56
        print *,' d67 = ',d67
        print *,' d58 = ',d58
        print *,' d57 = ',d57
        print *,' INTER RING COUPLINGS (AVERAGED OVER CONFORMATICNS)'
        print *,' d26 = ',ad26
        print *,' d15 = ',ad15
        print *,' d25 = ',ad25
        print *,' d16 = ',ad16

c       rearrarge couplirgs to orderirg used in simulations.

        d(1 =d12/4.0
        d(2 =d13/4.0
        d(3)=d14 4.0
        d(4 =ad15/4.0
        d(5 =ad16/4.0
        d(6)=ad16/4.0
        d(7 =ad15/4.0
        d(8)=d23/4.0
        d(9)=d13 4.0
        d(10 =ad25/4.0
        d(11 =ad26/4.0
        d(12)=ad26/4.0
        d(13 =ad25/4.0
        d(14 =d12/4.0
        d(15)=ad25/4.0
```

```
      d(16)=ad26/4.0
      d(17)=ad26/4.0
      d(18)=ad25/4.0
      d(19)=ad15/4.0
      d(20)=ad16/4.0
      d(21)=ad16/4.0
      d(22)=ad15/4.0
      d(23)=d56/4.0
      d(24)=d57/4.0
      d(25)=d58/4.0
      d(26)=d67/4.0
      d(27)=d57/4.0
      d(28)=d56/4.0

c     calculate spectrum
      call cntprt(d,cj,8)
      call bph4ham(en,isym)
      call peout(5,28,en,isym,n0)

c     output spectrum
      print 103
  103 format('1              A1 subspectra . . .'///)
      print 104
  104 format(' SIX QUANTUM LINES'/)
      print 105
  105 format('1x,17(' '), /,10x,'|M| = 4 to |M| = 2'/)
      k=1
      l1=n0(1)+n0(2)+1
      h1=l1+n0(3)-1
      do 550 jc=l1,h1
      if(isym(jc) .ne. 1) go to 550
      freq(k)=abs(en(1)-en(jc))
      k=k-1
  550 continue
      call desfrq(freq,k-1)
      nf1=k-1
      do 556 i=1,nf1
      w1(i)=freq(i)
      wimx=amax1(w1(i),wimx)
  556 wimn=amin1(w1(i),wimn)
      print 108
  108 format(//10x,'|M| = 3 to |M| = 3'/)
      k=1
      l1=n0(1)+1
      h1=l1+n0(2)-1
      l2=n0(1)+n0(2)+n0(3)+n0(4)+1
      h2=l2+n0(5)-1
      do 555 jc1=l1,h1
      if(isym(jc1) .ne. 1) go to 555

      do 555 jc2=l2,h2
      if(isym(jc2) .ne. 1) go to 555
      freq(k)=er(jc1)-er(jc2)
      if ifix(10.0*abs(freq(k))) .eq. 0) go to 555
      k=k-1
  555 continue
      call desfrq(freq,k-1)
      nf2=(k-1)/2
      np=nf1+nf2
      do 557 i=1,nf2
      w1(i+nf1)=freq(i)
      wimx=amax1(freq(i),wimx)
  557 wimn=amin1(freq(i),wimn)
```

```
      write(1,602) np
      write(1,604) (w1(i), i=1,np)
      write(1,604) (zmx, i=1,np)
      print 107
107   format(  ' SEVEN QUANTUM LINES',/,19('_')//,
     210X,'|M| = 4 to |M| = 3'/)
      k=1
      l1 n0(1)+1
      h1 l1+n0(2)-1
      do 560 jc=l1,h1
      if(isym(jc) .ne. 1) go to 560
      freq(k =abs(en(jc -en(1))
      w2mx=amax1(freq(k),w2mx)
      w2mn=amin1(freq(k),w2mn)
      k=k-1
560   continue
      call desfrq(freq,k-1)
      np k-1
      write(2,602) np
      write(2,604) (freq(i), i=1,np)
      write(2,604) (zmx, i=1,np)

c     end main loop

      go to
     1          (5001,5002,5003,5004,5005,5006,5007,5008,
     2           5009,5010,5011)
     3                              ipar

5001  szz=szz+sinc
      go to 5000

5002  s2p=s2p+sinc
      go to 5000

5003  if iccord .eq  1) stop
      sxy=sxy+sinc
      go to 5000

5004  delta=delta+sinc
      go to 5000

5005  r14=r14+sinc
      go to 5000

5006  r67=r67+sinc
      if icoord .eq. 1  r23=r67
      go to 5000

5007  r12=r12+sinc
      go to 5000

5008  r23=r23-sinc
      go to 5000

5009  r58=r58+sinc
      if(icoord .eq. 1  r14=r58
      go to 5000

5010  r260=r260+sinc
      go to 5000

5011  r56=r56+sinc
```

```
      if(icoord .eq. 1  r12=r56

 5000 continue

      write(1,602) iwflag
      write(1,604) w1mx,w1mn,zmx
      write(2,602) iwflag
      write(2,604) w2mx,w2mn,zmx
      close(unit=1)
      close(unit=2)
 602  format(i6)
 604  format(e14.6)
      end



      double precision function coupi
     1            (thz,thx,thy,s,r)

      implicit double precision (a-h,o-z)
      dimension s(5

c     calculates anisotropic couplings after formulas
c     of Emsley and Lindon

      szz=s(1
      s2p=s(2
      sxy=s(3)
      sxz=s(4
      syz=s(5

      coupi=( szz*(3.0d00*thz**2.0-1.0d00)
     1       -s2p*(thx**2.0-thy**2.0)
     2       +4.0d00*(  sxy*(thx*thy)
     3                 +sxz*(thx*thz)
     4                 +syz*(thy*thz)  ) )
      coupi=coupi / (r**3.0)

      return
      end
```

```
      subroutine bph4ham(en,isym
c     this is a version of hamil written for
c     the special symmetry of a para-substituted
c     biphenyl with D4 symm.
c     Only the A1 symmetry eigenstates are labeled in
c     symmetry vector isym.
c
c
c     sets up and diagonalizes free induction decay
c     hamiltonian of N spins 1 2 (N less than 9).

      common / coup / d(28),cj(28),cs(8),woff
      common / cstate / n,lst(2,256)

      dimension h(406),s(784),en(1),numb(2,256),n0(6)
      dimension ist(70),isp(8),iflip(2),icst(4,12,4)
      dimension c(784),work(784),isym(1)
      data  n0 / 1,8,28,28,8,1 /
      data  icst / 1,8,2*0, 2,7,2*0, 3,6,2*0, 4,5,2*0, 32*0,
     1 1,28,2*0  7,3*0, 8,11,17,26, 14,23,2*0, 19,3*0, 2,5,18,27,
     2 9,10,21,24, 15,20,2*0, 3,4,22,25, 16,3*0, 6,13,2*0,
     3 12,3*0  1,28,2*0, 22,3*0, 3,12,19,21, 6,15,2*0, 10,3*0,
     4 2,11,24,27, 5,8,19,20, 9,14,2*0, 4,7,25,26, 13,3*0,
     5 16,23,2*0, 17,3*0, 1,8,2*0, 2,7,2*0, 3,6,2*0,
     6 4,5,2*0, 32*0 /


      narrat=28
      nst=74
      nm1=n-1
      ncp=n*nm1/2

      do 15 i=1,nst
15    isym(i)=0
      isym(1)=1
      isym(nst)=1
       cs=0.0
      do 32 i=1,n
32    acs=acs+cs(i)
      ecp=0.0
      do 35 i=1,ncp
35    ecp=ecp+d(i)*cj(i)
      en(1)=-n*woff+ecp-acs
      en(nst)=n*woff+ecp+acs
      nst0=1
      call numsrt(numb,n,256)
      lst(1,1)=numb(1,256)
      lst(2,1)=numb(2,256)
      lst(1,256)=numb(1,1)
      lst(2,256)=numb(2,1)
      kk=1

      if
      do 100 is=1,nm1

      is=n-is
      isp=2*is+n
      kk=0
      do 40 j=1,256
      if(numb(2,j).ne.is) go to 40
      kk=kk+1
      kkk=kkk+1
```

```
      lst(kk)=numb(1,j)
      lst(1,kk)=numb(1,j)
      lst(2,kk)=is
 40   continue
      mst=kk
      lm=0

      if mst .gt. maxmat) go to 100
      if=if+1

      do 60 m=1,mst
      do 80 l=1,m
      lm=lm+1
      if(l .ne. m) go to 60
c     diagonal elements
      msk=1
      do 50 k=1,n
      isp(k)=-1
      if((ist(l) .and. msk) .ne. 0) isp(k)=1
      msk=msk*2
 50   continue
      h(lm) = woff*tsp
      kk=0
      do 55 i=1,nm1
      ip1=i+1
      do 55 j=ip1,n
      kk=kk+1
      h(lm)=h(lm) + (d(kk)+cj(kk))*isp(j)*isp(i)
 55   continue
      do 57 i=1,n
 57   h(lm)=h(lm) - cs(i)*isp(i)
      go to 80

c     off-diagonal elements
 60   jw=1
      jsp=0
      h(lm)=0
      msk=1
      do 75 k=1,n
      if((ist(l) .and. msk) - (ist(m) .and. msk)) 70,75,70
 70   jsp=jsp+1
      iflip(jw)=k
      jw=2
 75   msk=msk*2
      if(jsp .ne. 2) go to 80
      k5=(2*n-iflip(1))*(iflip(1)-1)/2-iflip(1)+iflip(2)
      h(lm)=-d(k5)+2.0*cj(k5)
 80   continue
c
      idim=n/(if+1)

c     diagonalize
      call eig2(h,s,en,mst0,idim,0)
c     find A1 states
      call elsymm(s,isym,mst0,idim)
      mst0=mst0+idim
 100  continue

      return
      end
```

```
      subroutine peout(n,maxmat,en,isym,n0)

c     this subroutine outputs the contents of energy vector
c     en in f12.4 format.  States in each Zeeman manifold
c     are separated by a blank line.  N is the number of spins,
c     maxmat is the size of the largest Zeeman manifold
c     contained in en and n0 is the array containing the
c     binomial coefficients (dimensions of the Zeeman manifolds).

      dimension en(1),n0(1),isym(1)

      np1=n+1
      nb=1

      do 500 j=1,np1

      if(n0(j).gt.maxmat) go to 500
      nt=nb+n0(j)-1
      print 401, (ieng,en(ieng),isym(ieng), ieng=nb,nt)
      nb=nb+n0(j)

  500 continue

      return

  401 format(//(4x,'EN(',i3,') = ',f12.4,2x,i1))
      end
```

```
      subroutine eisymm(s,isym,nen,dim)
c
c     locates totally symmetric eigenvectors in S of
c     dimension dim   Output isym contains 1's for these
c     states  unaffected for others.  First element of
c     isym to use is nen+1.
c

      integer isym(1),test,dim
      dimension s(1)

c     loop over eigenvectors
      thr=1000.0
      l=nen
      do 1000 ieig=1,dim
      il=(ieig-1)*dim
      l=l+1
      if(isym(l).ne.0) go to 1000
c     sum coefficients of eigenvector
      sum=0.0
      do 500 jc=1,dim
  500 sum=sum+s(il+jc)

      test=abs(thr*sum)
      if(test.ne.0) isym(l)=1

 1000 continue

      return
      end
```

```
      subroutine desfrq(freq,itop)

c     this subroutine outputs frequencies from vector freq
c     in descending order.
c     itop is the maximum number of frequencies in freq.

      dimension freq(1

      if(itop .le. 0) return
      itp=itop-1
      do 185 k=1,itp
      ilow=k+1
      do 185 kk=ilow,itop
      rmax=amax1(freq(k),freq(kk))
      freq(kk)=amin1(freq(k),freq(kk))
      freq(k)=rmax
  185 continue

      print 601, (freq(k), k=1,itop)

  601 format(4x,f12.4)
      return
      end
```

```
      SUBROUTINE CNTPRT(AR1,AR2,N)
C
C
C
C     CUTPUTS COUPLING CONSTANTS TO LPR.
C
      DIMENSION AR1(1),AR2(1)
C
      NM1=N-1
      K=1
      PRINT 732
      DO 30 I=1,NM1
      IP1=I+1
      DO 30 J=IP1,N
      IOUT=AR1(K) * 4.0
      CJOUT=AR2(K) * 4.0
      PRINT 731, I,J,DOUT,I,J,CJOUT
   30 K=K+1
C
  731 FORMAT(' D(',I2,',',I2,') = ',F12.4,/
     1' J(',I2,',',I2,') = ',F12.4,//)
  732 FORMAT('1H1')
      RETURN
      END
```

```
      program biph5para
c
c     calculates coupling constarts for a biphenyl
c     with asymmetrically distorted rings.
c          ==============
c
c     this version has error analysis where errors in parameters
c     are propagated from variance - covariance matrix of spectral
c     simulation.  this is input at beginning of program.
c
c     Coodinate system #1;  D4 symmetry:
c     The origin is at the center of teh c-c inter ring bridge.
c     The x-axis bisects the dihedral angle, the z-axis is along
c     the benzene para bonds to the substituents
c
c     Coordinate system #2;  D2 symmetry
c     The z-axis passes through the biphenyl para bonds,
c     the origin is located in ring '2' (with protons 5,6,7,8),
c     the x-axis lies in the plare of this ring and the y-axis
c     is normal to it.
c
c     This version (# 4) does not "symmetrize" the hamiltonian
c     before diagonalization (i.e. bph4ham is called instead
c     of bphham').
c
c     This version performs a linear least squared fit of calculated
c     couplings to experimental couplings.  The initail input
c     geometry and order parameters are varied in the iteration.
c
c     input  (in common "geom'
c
c     r12, r14, r23, r2B0, r67, r58, r56,
c     szz, (sxx-syy =s2p, sxy, delta
c
      implicit double precision (a-h,o-z)
      double precision dnew(12 ,dlast(12 ,dexp(12 ,dc(12,11)
      double precision b 12),v(144),para(11),bv(11)
      double precision a(11,12 ,cx(12,12),vcy(11,11),ap(11)
     1 d(28),cj(28 ,cs(8),en 256 ,woff,freq(50),cjd4(28)
      integer isym(256 ,n0(6),l(12),m(12),ipar(11)
      logical yans
      character*4 dname(12)/'D12 ','D13 ','D14 ','D15 ',
     1                      'D16 ','D23 ','D26 ','D25 ',
     2                      'D56 ','D57 ','D58 ','D67 '
      common / geom / szz,s2p,sxy,delta,r14,r67,r12,r23,r58,r2B0,r56
      common / geom2 / r13,r57
      common   coup   d,cj,cs,woff
      common / cstate / n,lst(2,256)
      common / cit / para,ipar,dc,b,v,bv
      data cjd4 / 2.0,0.0,0.5,4*0.0,0.5,5*0.0,2.0,8*0.0,
     1            2.0,0.0,0.5,0.5,0.0,2.0 /
      data n0   1,0,28,28,8,1
      equivalence (para,szz)

c     get input

      do 1 j=1.256
      en j)=0.0
 1    isym j =0
      do 2 i=1.8
 2    cs i)=0.0
      r=0
      woff=0.0
```

```
      type *,' Which coord. system? (1 or 2)'
      accept *,icoord
      type *,' INPUT OF INITIAL PARAMETERS '
      type *,' enter r12: '
      accept * r12
      r56=r12
      type *,' enter r14: '
      accept * r14
      r58=r14
      type *,' enter r23: '
      accept *,r23
      r67=r23
      type *,' enter r260: '
      accept *,r260
      ncoup=7
      if icoord .eq. 1  go to 6066
      ncoup=12
      type *,' enter r67: '
      accept *,r67
      type * ' enter r58  '
      accept *,r58
      type *,' enter r56: '
      accept *,r56
6066  type *,' enter szz: '
      accept *,szz
      type *,' enter (sxx-syy) '
      accept *,s2p
      sxy=0.0d00
      if icoord .eq  1  go to 6067
      type *,' enter sxy: '
      accept *,sxy
6067  type * ' enter delta  '
      accept *,delta
      do 122 i=1,11
122   ip r(i =0
      type *,' The parameters which can be varied are . . .'
      if icoord .eq  2  go to 6068
      type *,'          szz = 1          r12 = 7'
      type *,'  (sxx-syy) = 2          r23 = 8'
      type *,'      delta = 4         r260 = 10'
      type *,'          r14 = 5'
      go to 6069
6068  type *,'          szz = 1          r12 = 7'
      type *,'  (sxx-syy) = 2          r23 = 8'
      type *,'          sxy = 3          r58 = 9'
      type *,'      delta = 4         r260 = 10'
      type *,'          r14 = 5          r56 = 11'
      type *,'          r67 = 6'
6069  type *,' How many of these do you wish to have vary?'
      accept *,npar
      type *,' From the table above, which parameters are to vary?'
      accept *,(ipar(i , i=1,npar)
      type * ' Enter total # of iterative cycles to be allowed:'
      accept *,ncyc
      ieran=0
      type * ' Do you wish to include error analysis?'
      if yans(idum)) ieran=1

      type *,' are the d4 j''s to be used in the simulation?'
      if yans(idum ) go to 11
      do 12 i=1,20
12    cj i =0.0
      go to 13
```

```
 11     do 14 i=1,20
 14     cj(i)=cjd4(i)

c       input of experimental couplings
 13     type *,' Enter experimental dipolar couplings   . .'
        do 15 i=1,ncoup
        dexp(i)=0.0d00
        type 801,dname(i
 801    format(10x,a4,'= ',$)
 15     accept *,dexp(i)
c       output initial parameters
 17     print 201, r12,r14,r23,r260,r67,r58,r56,szz,s2p,sxy,delta
 201    format('1program biph5para - initial parameters . . .'//
     1' r12 = ',e14.4/,' r14 = ',e14.6 ,' r23 = ',e14.6 ,
     2' r260 = ',e14 6/,' r67 = ',e14.6/ ' r58 = ',e14.6/,
     3' r56 = ',e14 6  ,' szz = ',e14.6/,' (sxx-syy) = ',e14.6 ,
     4' sxy = ',e14.6//,' DELTA = ',f10.4///

        print 802, (dname(i),dexp(i), i=1,ncoup)
 802    format('10x,'experimental couplings . . .', ,
     1          '15x,a4,'= ',f10.4)
c       enter iterative loop
        iter=1
        er1=1.0d04
c
c       calculate couplings
 9899   call biphd(dlast,icoord)
        if iter .ne. 1 go to 9899
        call derd(d,dlast,icoord)
        call cntprt(d,cj,8)
        print 333
 333    format(1h1)
c
c       least squares routines
c
c       calculate derivatives
 9899   do 5560 np=1 npar
        nap=ipar(np)
        xinc=0.01d00*dabs(para(nap))
        para(nap)=para(nap)+xinc
        call biphd(dnew,icoord)
        para(nap)=para(nap)-xinc
        call deriv(dlast,dnew,xinc,np,ncoup)
 5560   continue

c       calculate residuals
        do 5565 k=1,ncoup
 5565   d(k)=dexp(k)-dlast(k)
        call exit2(er1,ncyc,nexit,ncoup,iter
        call norm2(ncoup)
        det=0.0d00
        call dminv(v,npar,det,l,m)
        print *,'                    DET = ',det
        if det .eq. 0.0d00 print 729
 729    format('1x,'DETERMINANT OF MATRIX TO BE INVERTED IS ZERO!!'//)
        if nexit .eq 0) go to 5000
c
c       correction of parameters
        do 310 ns=1,npar
        corr=0.0d00
        do 210 nsb=1,npar
        indx=matvec(ns,nsb,npar)
 210    corr=corr+v(indx)*bv(nsb)
```

```
      para(ipar(ns))=para(ipar(ns))+corr
  310 continue
      iter=iter+1
      go to 9898
c     end of iteration loop

c     output final parameters
c     output internulcear distances
 5000 print 334
  334 format(///' FINAL PARAMETERS:'  )
      print *,' r12 = ',r12
      print *,' r13 = ',r13
      print *,' r14 = ',r14
      print *,' r23 = ',r23
      print *,' r260 = ',r260
      print *,' r56 = ',r56
      print *,' r57 = ',r57
      print *,' r58 = ',r58
      print *,' r67 = ',r67
      print *,' szz = ',szz
      print *,' (sxx-syy) = ',s2p
      print *,' sxy = ',sxy
      print *,' delta = ',delta
      if ierar .eq  0) go to 5050
c
c     error analysis
c
      type *,' Enter variance - covariance matrix from simulation:'

      do 9002 j=1,ncoup
      do 9002 i=j,ncoup
      type 9003, j,i
      accept *,vcx(j,i
      vcx(i,j)=vcx(j,i
 9002 continue
 9003 format(1x,'CX(',i2,',',i2 ') = ',$

      do 9000 np=1,npar
      do 9000 nc=1,ncoup
      dc(np nc)=0 0d00
      do 9000 i=1,npar
      npi=matvec(np,i,npar
 9000 dc(np nc)=a(np,nc  + v(npi)*dc(nc i)

      do 9050 i=1,npar

      do 9045 m2=1,npar
      vcy(i,m2)=0.0d00
      do 9040 j=1,ncoup
      ap j =0.0d00
      do 9030 k=1,ncoup
 9030 ap j =ap(j) + vcx(j,k)*a(m2,k)

 9040  cy(i,m2 =vcy(i,m2  - ap(j *a(i,j)

 9045 continue
 9050 continue

c
c     utput variance - covariance matrices
      print 333
      print *,'     variance - covariance matrix from simulation'
      print 810, (j,(vcy(j,k), k=1,ncoup), j=1,ncoup)
```

```
 810    format( 2x,i3,' :   ',(ncoup/2)e14.6,/10x,
     1(ncoup/2+mod(ncoup,2))e14.6/
        print 333
        print *,'     variance - covariance matrix for parameters'
        print 809, (j,(vcy(j,k), k=1,npar), j=1,npar)
 809    format(/2x,i3,'     ',(npar/2)e14.6,/10x,
     1'(npar 2+mod(npar,2))e14.6 )
c
c       calculate spectrum

 5 5    call dord(d,dlast,icoord)
        call cntprt(d,cj,8)
        call bph4ham(en,isym
        call peout(5,26,en,isym,n0

c       output spectrum
        print 103
 1(3    format('1            A1 subspectra . . .'///)
        print 104
 104    format(' SIX QUANTUM LINES'/)
        print 105
 105    format(1x,17('_'), /,10x,' M| = 4 to |M| = 2' )
        k=1
        l1 n2(1)=n0(2)+1
        h1 l1+n0(3)-1
        do 550 jc=l1,h1
        if isym(jc) .ne. 1) go to 550
        freq(k)=abs(en(1)-en(jc))
        k=k+1
 55     continue
        call desfrq(freq,k-1)
        nf1=k-1
        print 108
 108    format(' 10x,'|M| = 3 to |M| = 3')
        k=1
        l1 n2(1)+1
        h1 l1+n0(2)-1
        l2 n0(1)+n0(2)+n0(3)-n0(4)+1
        h2 l2+n0(5)-1
        do 555 jc1=l1,h1
        if isym(jc1) .ne. 1) go to 555

        do 555 jc2=l2,h2
        if isym(jc2) .ne. 1) go to 555
        freq(k)=en(jc1)-en(jc2)
        if ifix(10 0*abs(freq(k))) .eq  0) go to 555
        k=k+1
 555    continue
        call desfrq(freq,k-1)
        print 107
 107    format(///' SIVEN QUANTUM LINES' /,1(('_')//,
     210X,'|M| = 4 to |M| = 3' )
        k=1
        l1 n2(1  1
        h1 l1+n0(2)-1
        do 560 jc=l1,h1
        if isym(jc) .ne. 1) go to 560
        freq(k)=abs(en(jc)-er(1))
        k=k+1
 56     continue
        call desfrq(freq,k-1)
        end
```

```
c
      subroutine dord(d,d2,icoord)
      double precision d2(1)
      real d(1)

c     rearrange couplings to ordering used in simulations.


      d(1)=d2(1)/4.0
      d(2)=d2(2)/4.0
      d(3)=d2(3)/4.0
      d(4)=d2(4)/4.0
      d(5)=d2(5)/4.0
      d(6)=d2(5)/4.0
      d(7)=d2(4)/4.0
      d(8)=d2(6)/4.0
      d(9)=d2(2)/4.0
      d(10)=d2(8)/4.0
      d(11)=d2(7)/4.0
      d(12)=d2(7)/4.0
      d(13)=d2(8)/4.0
      d(14)=d2(1)/4.0
      d(15)=d2(8)/4.0
      d(16)=d2(7)/4.0
      d(17)=d2(7)/4.0
      d(18)=d2(8)/4.0
      d(19)=d2(4)/4.0
      d(20)=d2(5)/4.0
      d(21)=d2(5)/4.0
      d(22)=d2(4)/4.0
      d(23)=d2(9)/4.0
      d(24)=d2(10)/4.0
      d(25)=d2(11)/4.0
      d(26)=d2(12)/4.0
      d(27)=d2(10)/4.0
      d(28)=d2(9)/4.0

      return
      end
```

```
      subroutine biphd(d,icoord)
c
c     calculates coupling constants for a biphenyl
c     with asymmetrically distorted rings.
c
c
c     Coordinate system #1;  D4 symmetry:
c     The origin is at the center of teh c-c inter ring bridge.
c     The x-axis bisects the dihedral angle, the z-axis is along
c     the benzene para bonds to the substituents.
c
c     Coordinate system #2;  D2 symmetry:
c     The z-axis passes through the biphenyl para bonds,
c     the origin is located in ring "2" (with protons 5,6,7,8),
c     the x-axis lies in the plane of this ring and the y-axis
c     is normal to it.
c
c
      implicit double precision (a-h,o-z)
      double precision th(16),lxy(4),lyx(4),s(5),d(12)
      common   geom   szz,s2p,sxy,delta,r14,r67,r12,r23,r58,r268,r56
      common / geom2 / r13,r57

      do 1 j=1,12
 1    d(j)=0.0d00
      rad=4.d0*datan(1.0d00)
      dk=-2.0d00*(245.017d00**2.0)

c     compute delta in rads
      rdel=delta*rad/180.0d00

      if(icoord .eq. 2) go to 5050
c
c     coordinate system #1
      s(1)=szz
      s(2)=s2p*((dcos(rdel/2.0d00))**2-(dsin(rdel/2.0d00))**2)
      s(3)=s2p*(dcos(rdel/2.0d00)*dsin(rdel/2.0d00))
      s(4)=0.0d00
      s(5)=0.0d00
      r67=r23
      r58=r14
      r568=r12
      go to 6060
c
c     coordinate system #2
 5050 s(1)=szz
      s(2)=s2p
      s(3)=sxy
      s(4)=0.0d00
      s(5)=0.0d00

c     compute trig functions of delta
 6060 csdl=dcos(rdel)
      snol=dsin(rdel)


c     compute needed distances at delta=0

      rx1=(r14-r23)/2.0d00
      rx2=(r58-r67)/2.0d00
      rx3=(r58-r14)/2.0d00
      rx4=(r14-r67)/2.0d00
      rx5=(r58-r23)/2.0d00
```

```
      rx6=(r67 r23)/2.0d00

c     compute trig functions of needed angles

      snd=rx1/r12
      csd=dsqrt(1.0d00-snd**2.0)
      sna=rx6 r260
      csa=dsqrt(1.0d00-sna**2.0)
      sndp=rx2/r56
      csdp=dsqrt(1.0d00-sndp**2.0)

      ry4=r260*csa
      ry1=r12*csd+ry4
      ry2=r56*csdp+ry4
      ry3=ry1+ry2-ry4

c     calculate internuclear distances for delta=0

      r160=dsqrt(ry1**2.0+rx2**2 0)
      r150=dsqrt(ry3**2.0+rx3**2.0)
      r250=dsqrt(ry2**2.0+rx5**2 0)

      sng=rx4 r160
      csg=ry1/r160
      sngp=rx5/r250
      csgp=ry2 r250
      snb=rx3/r150
      csb=ry3/r150

c     calculate lxy's and lyx's

      lxy(1 =r14*snd1
      lyx(1) r14*csd1

      lxy(2 =r23*snd1
      lyx(2 =r23*csd1

      lxy(3)=0 0d00
      lyx(3  r67

      lxy(4 =0 0d00
      lyx(4)=r56

c     calculate th's

      th(1)=(lyx(1)-lyx(3))/2.0d00
      th(2)=(lxy(1)+lxy(3))/2.0d00

      th 3)=(lyx(2)-lyx(3) /2.0d00
      th 4)=(lxy(2)+lxy(3))/2.0d00

      th(5)=(lyx(1)-lyx(4))/2.0d00
      th 6)=(lxy(1)+lxy(4))/2.0d00

      th(7)=(lyx(2)+lyx(3))/2.0d00
      th(8)=(lxy(2)-lxy(3))/2.0d00

      th 9)=(lyx(1)+lyx(4))/2.0d00
      th(10)=(lxy(1)-lxy(4))/2.0d00

      th(11) (lyx(1)+lyx(3))/2.0d00
      th 12)=(lxy(1)-lxy(3))/2.0d00
```

```
      th(13)=(lyx(2)-lyx(4))/2.0d00
      th(14)=(lxy(2)+lxy(4))/2.0d00

      th(15)=(lyx(2)+lyx(4))/2.0d00
      th(16)=(lxy(2)-lxy(4))/2.0d00

c     calculate internuclear distances for delta not=0

      r17=dsqrt(ry1**2.0 + th(11)**2.0 + th(12)**2.0)
      r16=dsqrt(ry1**2.0 + th(1)**2.0 + th(2)**2.0)
      r25=dsqrt(ry2**2.0 + th(13)**2.0 + th(14)**2.0)
      r26=dsqrt(ry2**2.0 + th(15)**2.0 + th(16)**2.0)
      r26=dsqrt(ry4**2.0 + th(3)**2.0 + th(4)**2.0)
      r15=dsqrt(ry3**2.0 + th(5)**2.0 + th(6)**2.0)
      r27=dsqrt(ry4**2.0 + th(7)**2.0 + th(8)**2.0)
      r18=dsqrt(ry3**2.0 + th(9)**2.0 + th(10)**2.0)
      r13=dsqrt(((r23+r14)/2.0d00)**2.0 + (ry1-ry4)**2.0)
      r57=dsqrt(((r67+r58)/2.0d00)**2.0 + (ry2-ry4)**2.0)


c     calculate angles between internuclear vectors and
c     molecular axis system.

      rpd2=rad/2.0d00

      th13z=(ry1-ry4)/r13
      sn13=(r14+r23)/(2.0d00*r13)
      th13x=csd1*sn13
      th13y=snd1*sn13

      th57z=(ry2-ry4)/r57
      th57x=(r67+r58)/(2.0d00*r57)
      th57y=0.0d00

      th56z=csdp
      th56x=snd
      th56y=0.0d00

      th12z=csd
      th12x=csd1*snd
      th12y=snd1*srd

      th16z=ry1/r16
      th16x=th(1)/r16
      th16y=th(2)/r16

      th26z=ry4/r26
      th26x=th(3)/r26
      th26y=th(4)/r26

      th15z=ry3/r15
      th15x=th(5)/r15
      th15y=th(6)/r15

      th27z=ry4/r27
      th27x=th(7)/r27
      th27y=th(8)/r27

      th18z=ry3/r18
      th18x=th(9)/r18
      th18y=th(10)/r18

      th17z=ry1/r17
```

```
      th17x=th(11)/r17
      th17y=th(12)/r17

      th25x=ry2/r25
      th25x=th(13)/r25
      th25y=th(14)/r25

      th28z=ry2/r28
      th28x=th(15)/r28
      th28y=th(16)/r28

c     calculate couplings

      d12=dk*coupi(th12z,th12x,th12y,s,r12)
      d23=dk*coupi(0.0d00,csd1,srd1,s,r23)
      d14=dk*coupi(0.0d00,csd1,snd1,s,r14)
      d13=dk*coupi(th13z,th13x,th13y,s,r13)

      d56=dk*coupi(th56z,th56x,th56y,s,r56)
      d67=dk*coupi(0.0d00,1.0d00,0.0d00,s,r67)
      d58=dk*coupi(0.0d00,1.0d00,0.0d00,s,r58)
      d57=dk*coupi(th57z,th57x,th57y,s,r57)

      d26=coupi(th26z,th26x,th26y,s,r26)
      d27=coupi(th27z,th27x,th27y,s,r27)
      ad26=dk*(d26 + d27)/2.0d00

      d15=coupi(th15z,th15x,th15y,s,r15)
      d18=coupi(th18z,th18x,th18y,s,r18)
      ad15=dk*(d15 + d18)/2.0d00

      d25=coupi(th25z,th25x,th25y,s,r25)
      d28=coupi(th28z,th28x,th28y,s,r28)
      ad25=dk*(d25 + d28)/2.0d00

      d16=coupi(th16z,th16x,th16y,s,r16)
      d17=coupi(th17z,th17x,th17y,s,r17)
      ad16=dk*(d16 + d17)/2.0d00

c     rearrange couplings to ordering used in simulations.

      d(1)=d12
      d(2)=d13
      d(3)=d14
      d(4)=ad15
      d(5)=ad16
      d(6)=d23
      d(7)=ad26
      d(8)=ad25
      d(9)=d56
      d(10)=d57
      d(11)=d58
      d(12)=d67

      end



      double precision function coupi
     1                  (thz,thx,thy,s,r)

      implicit double precision (a-h,o-z)
```

```
      dimension s(5)

c     calculates anisotropic couplings after formulas
c     of Emsley and Lindon.

      szz=s(1)
      s2p=s(2)
      sxy=s(3)
      sxz=s(4)
      syz=s(5)

      coupi=( szz*(3.0d00*thz**2.0-1.0d00)
     1        +s2p*(thx**2.0-thy**2.0)
     2        +4.0d00*(  sxy*(thx*thy)
     3                  +sxz*(thx*thz)
     4                  +syz*(thy*thz) ) )
      coupi=coupi / (r**3.0)

      return
      end
```

```
      SUBROUTINE DMINV(A,N,D,L,M
C
C     INVERTS A MATRIX
C
      IMPLICIT DOUBLE PRECISION (A-H,O-Z)
      DIMENSION A(1),L(1),M(1)
C
      I=1 0D00
      NK -N
      DO 80 K=1,N
      NK NK+N
      L(K)=K
      M(K)=K
      KK=NK+K
      BIGA=A(KK)
      DO 20 J=K,N
      IZ N*(J-1)
      DO 20 I=K,N
      IJ IZ+I
      IF(DABS(BIGA)-DABS(A(IJ))) 15,20,20
15    BIGA=A(IJ)
      L(K)=I
      M(K)=J
20    CONTINUE
C
      J=L(K)
      IF(J-K) 35,35,25
25    KI K-N
      DO 30 I=1,N
      KI KI+N
      HOLD=-A(KI)
      JI KI-K+J
      A(KI)=A(JI)
30    A(JI)=HOLD
C
35    I=M(K)
      IF I-K  45,45,38
38    JP=N*(I-1)
      DO 40 J=1,N
      JK NK-J
      JI=JP+J
      HOLD=-A(JK)
      A(JK)=A(JI)
40    A(JI)=HOLD
C
45    IF BIGA  46,46,48
46    I=  0D00
      RETURN
48    DO 55 I=1,N
      IF(I-K  50,55,50
50    IK NK+I
      A(IK)=A(IK)/(-BIGA)
55    CONTINUE
C
      DO 65 I=1,N
      IK=NK+I
      HOLD=A(IK)
      IJ I-N
      DO 65 J=1,N
      IJ IJ+N
      IF I-K  60,65,60
60    IF J-K  62,65,62
62    KJ IJ-I+K
```

```
      A(IJ =HOLD*A(KJ) + A(IJ)
65    CONTINUE
C
      KJ K-N
      IO 75 J=1,N
      KJ KJ+N
      IF(J-K  70,75,70
70    A(KJ)=A(KJ)/BIGA
75    CONTINUE
C
      I=I*BIGA
C
      A(KK =1.0D00/BIGA
80    CONTINUE
C
      K=N
100   K=K-1
      IF(K) 150,150,105
105   I=L(K
      IF(I-K  120,120,108
108   JQ N*(K-1)
      JP N*(I-1)
      IO 110 J=1,N
      JK JQ+J
      HOLD=A JK)
      JI JP-J
      A(JK)=-A(JI)
110   A(JI =HOLD
120   J=M(K
      IF(J-K) 100,100,125
125   KI K-N
      IO 130 I=1,N
      KI KI+N
      HOLD=A KI)
      JI KI-K+J
      A(KI)=-A(JI)
130   A(JI =HOLD
      GO TO 100
150   RETURN
      END
```

```
      subroutine deriv(dlast,dnew,xinc,ipx,ncoup)
c
c     computes derivatives of biphenyl couplings w.r.t.
c     iteration parameters   Derivatives are estimated as
c     the ratio of the change in couplings with a 1 % change
c     in a particular parameter.
c
c
c     dlast is the initial (cycle # iter) couplings
c     dnew is the couplings calculated at para = para + xinc
c     ipx is the index in the matrix dc for this dependence
c     ncoup is the number of couplings (ncoup=7 for D4 symm,
c     and =12 for D2 symm)
c
      implicit double precision (a-h,o-z)
      double precision dlast(1),dnew(1)
      common / cit / npar,ipar(11),dc(12,11),b(12),v(144),bv(11)

      do 100 k=1,ncoup
      dc(k,ipx)=(dnew(k)-dlast(k))/xinc
100   continue

      return
      end
```

```
      SUBROUTINE ERIT2(ER1,NI,NEXIT,NL,ITER)
C
C              VAX/VMS VERSION.
C
C     EVALUATES R.M.S. ERROR FOR A VECTOR OF RESIDUALS FROM ONE
C     ITERATIVE CYCLE.
C
C     THIS IS A DOUBLE PRECISION VERSION.
C
C     B IS THE VECTOR OF RESIDUALS.
C     ITER IS THE NUMBER OF THE PRESENT ITERATIVE CYCLE.
C     ER1 IS THE RMS ERROR FROM THE LAST CYCLE.
C     NI IS THE TOTAL NUMBER OF ITERATIONS ALLOWED.
C     NEXIT IS A PARAMETER TO BE USED IN DETERMINING WHETHER
C             FURTHER ITERATIVE CYCLES SHOULD BE RUN.
C             IF NEXIT=0 RETURNED NO FURTHER ITERATIONS NECESSARY.
C             IF NEXIT=1, FUTHER CYCLES ARE REQUIRED.
C     NI IS THE NUMBER OF RESIDUALS CONTAINED IN B.
C
C
      IMPLICIT DOUBLE PRECISION (A-H,O-Z)
      DOUBLE PRECISION MINERR
C
      COMMON   CIT   NPAR,IPAR(11),DC(12,11),B(12),V(144),BV(11)
C
      MINERR = 1.0D-8
      ER2=0.0D0
      FNL=NL
C
      DO 4 K=1,NL
 4    ER2=ER2+B(K)*B(K)
      ER2=DSQRT(ER2/FNL)
      IF(ER2 .GE. MINERR) GO TO 5
      PRINT 401, ER2
      GO TO 8
 5    PRINT 301, ITER,ER2
C
      IF((ER1-ER2)/ER1-0.01D00) 8,8,10
 8    NEXIT=0
      ER1=ER2
      RETURN
C
 10   IF(ITER-NI) 110,8,8
 110  ER1=ER2
      NEXIT=1
      RETURN
C
 301  FORMAT(5X,'ITERATION # ',I2,3X,'R M S ERROR = ',F8.3)
 401  FORMAT(/,' ITERATION CYCLE TERMINATED -',/,
     1' RMS ERROR LESS THAN MINIMUM ALLOWED!',/,
     2' ERROR    ',D16.4, )
      END
```

```
      SUBROUTINE NORM2(NL)
C
C              VAX/VMS VERSION.
C
C     THIS SUBROUTINE SETS UP THE NORMAL EQUATIONS FOR A LEAST
C     SQUARES ITERATIVE PROCEDURE.
C     THE MATRIX PRODUCTS DC-TRANS*DC AND DC*B ARE FORMED WHERE DC IS THE
C     MATRIX OF DERIVATIVES OF FREQUENCIES WITH
C     RESPECT TO PARAMETERS AND B IS THE MATRIX OF RESIDUALS
C     BETWEEN CALCULATED AND OBSERVED FREQUENCIES.
C
C
      IMPLICIT DOUBLE PRECISION (A-H,O-Z)
      COMMON   CIT   NPAR,IPAR(11),DC(12,11),B(12),V(144),BV(11)
C
      NOS=NPAR
      DO 210 NS1=1,NOS
      DO 206 NS2=NS1,NOS
C
      INDX1=MATVEC(NS2,NS1,NOS)
      INDX2=MATVEC(NS1,NS2,NOS)
C
      V(INDX1)=0.0D00
      DO 205 LEQ=1,NL
  205 V(INDX1)=V(INDX1)+DC(LEQ,NS1)*DC(LEQ,NS2)
  206 V(INDX2)=V(INDX1)
C
      BV(NS1)=0.0D00
      DO 210 LEQ=1,NL
  210 BV(NS1)=BV(NS1)+DC(LEQ,NS1)*B(LEQ)
C
      RETURN
      END
```

References

1. E. Merzbacher, Quantum Mechanics (Wiley, New York, 1970), p. 172.

2. C. P. Slichter, Principles of Magnetic Resonance (Springer-Verlag, Berlin-Heidelberg-New York, 1978).

3. R. M. Wilcox, J. Math. Phys. 8, 962 (1967).

4. A. Abragam, The Principles of Nuclear Magnetism (Oxford, London, 1961).

5. Reference 1, Chapter 9.

6. U. Haeberlen, "High Resolution NMR in Solids: Selective Averaging," Advances in Magnetic Resonance, Supplement 1 (Academic, New York, 1976).

7. B. L. Silver, Irreducible Tensor Methods (Academic, New York, 1976).

8. M. E. Rose, Elementary Theory of Angular Momentum (Wiley, New York, 1957).

9. Reference 2, Chapter 9.

10. Reference 2, Chapter 3.

11. Reference 6, p. 9.

12. A. Saupe, Z. Naturforsch. 19a, 161 (1964).

13. M. Mehring, High Resolution NMR Spectroscopy in Solids (Springer-Verlag, Berlin-Heidelberg-New York, 1976), Appendix C.

14. Reference 13, Chapter 2.

15. R. G. Griffin, J. D. Ellet, M. Mehring, J. G. Bullit, and J. S. Waugh, J. Chem. Phys., 57 2147 (1972).

16. S. Chandrasekhar, Liquid Crystals (Cambridge University Press, Cambridge, 1977).

17. Liquid Crystals and Ordered Fluids, Ed. J. F. Johnson and R. S. Porter (Plenum, New York-London, 1973), Vol. 2.

18. J. W. Emsley and J. C. Lindon, NMR Spectroscopy Using Liquid Crystal Solvents (Pergamon, Oxford, 1975).

19. R. Ader and A. Lowenstein, Mol. Phys. 24, 455 (1972); J. W. Emsley, J. C. Lindon, and J. Tabony, Mol. Phys. 26, 1499 (1973); A. Lowenstein, Chem. Phys. Lett. 38, 543 (1976); R. Ader and A. Lowenstein, Mol. Phys. 30, 199 (1975).

20. A. Frey and R. R. Ernst, Chem. Phys. Lett. 49, 75 (1977).

21. G. F. Pedulli, C. Zannoni, and A. Alberti, J. Mag. Res. 10, 372 (1973).

22. E. E. Burnell and C. A. DeLange, J. Mag. Res. 39, 461 (1980).

23. J. W. Emsley and G. R. Luckhurst, Mol. Phys. 41, 19 (1980).

24. Reference 1, p. 479.

25. Reference 2, Chapter 2.

26. R. Besset, J. Horowitz, A. Messiah, and J. Winter, J. Phys. Radium, 15, 251 (1954).

27. W. A. Anderson, R. Freeman, and C. A. Reilly, J. Chem. Phys. 39, 1518 (1963).

28. S. Yatsiv, Phys. Rev. 113, 1522 (1959).

29. W. A. Anderson, Phys. Rev. 104, 850 (1956); J. I. Kaplan and S. Meiboom, Phys. Rev. 106, 499 (1957).

30. G. Bodenhausen, Progress in NMR Spec. 14, 137 (1981).

31. A. Wokaun and R. R. Ernst, Mol. Phys. 36, 317 (1978).

32. J. S. Waugh, L. M. Huber, and U. Haeberlen, Phys. Rev. Lett. 20, 180 (1968).

33. W. S. Warren, Ph.D. Thesis, University of California, Berkeley (1980, published as LBL Report 11885).

34. R. G. Jones, "The Use of Symmetry in Nuclear Magnetic Resonance," in NMR: Basic Principles and Progress, Ed. P. Diehl, E. Fluck, and R. Kosfeld (Springer-Verlag, Berlin-Heidelberg-New York, 1969), Vol. 1, pp. 97-174.

35. M. Tinkham, Group Theory and Quantum Mechanics (McGraw-Hill, New York, 1964), p. 82.

36. M. D. Harmony, Introduction to Molecular Energies and Spectra (Holt, New York, 1972), p. 346.

37. W. Warren and A. Pines, J. Am. Chem. Soc. 103, 1613 (1981).

38. David E. Wemmer, Ph.D. Thesis, University of California, Berkeley (1978, Published as LBL Report 8042).

39. J. C. Rowell, W. D. Phillips, L. R. Melby, and M. Panar, J. Chem. Phys. 43, 3442 (1965).

40. P. Diehl and A. Tracey, Mol. Phys. 30, 1917 (1975).

41. J. W. Emsley, S. K. Khoo, and G. R. Luckhurst, Mol. Phys. 37, 959 (1979).

42. B. Deloche and J. Charvolin, J. Phys., Paris, Lett. 41, 39 (1980).

43. S. Hsi, H. Zimmermann, and Z. Luz, J. Chem. Phys. 69, 4126 (1978).

44. Z. Luz, R. C. Hewitt, and S. Meiboom, J. Chem. Phys. 61, 1758 (1974).

45. Gary P. Drobny, Ph.D. Thesis, University of California, Berkeley (1981).

46. E. E. Burnell and P. Diehl, Mol. Phys. 24, 489 (1972).

47. Reference 7, Chapter 5.

48. Z. Luz and S. Meiboom, J. Chem. Phys. 59, 275 (1973).

49. L. C. Snyder, J. Chem. Phys. 43, 4041 (1965).

50. A. Saupe, Z. Naturforsch. 19a, 161 (1964).

51. Reference 18, p. 16.

52. J. W. Emsley and G. R. Luckhurst, Mol. Phys. 41, 19 (1980).

53. E. E. Burnell and C. A. DeLange, J. Mag. Res. 39, 461 (1980).

54. N. Boden, L. D. Clark, R. J. Bushby, J. W. Emsley, G. R. Luckhurst, and C. P. Stockley, Mol. Phys. 42, 565 (1981).

55. E. E. Burnell and C. A. DeLange, Chem. Phys. Lett. 76, 268 (1980).

56. W. D. Aue, E. Bartholdi, and R. R. Ernst, J. Chem. Phys. 64, 2229 (1976).

57. H. Hatanaka, T. Terao, and T. Hashi, J. Phys. Soc. Japan, 39, 835 (1975); H. Hatanaka and T. Hashi, J. Phys. Soc. Japan, 39, 1139 (1975).

58. A. Pines, D. Wemmer, J. Tang, and S. Sinton, Bull. Am. Phys. Soc. 21, 23 (1978).

59. G. Drobny, A. Pines, S. Sinton, D. Weitekamp, and D. Wemmer, Faraday Div. Chem. Soc. Symposium, 13, 49 (1979).

60. G. Bodenhausen, R. L. Vold, and R. R. Vold, J. Mag. Res. 37, 93 (1980).

61. S. Vega and A. Pines, J. Chem. Phys. 66, 5624 (1977); S. Vega, J. Chem. Phys. 68, 5518 (1978).

62. A. Wokaun and R. R. Ernst, J. Chem. Phys. 67, 1752 (1977).

63. A. Wokaun and R. R. Ernst, Chem. Phys. Lett. 52, 407 (1977).

64. W. S. Warren, S. Sinton, D. P. Weitekamp, and A. Pines, Phys. Rev. Lett. 43, 1791 (1979); W. S. Warren, D. P. Weitekamp, and A. Pines, J. Mag. Res. 40, 581 (1980); W. S. Warren, D. P. Weitekamp, and A. Pines, J. Chem. Phys. 73, 2084 (1980); W. S. Warren and A. Pines, J. Chem. Phys. 74, 2808 (1981).

65. G. Drobny, A. Pines, S. Sinton, W. S. Warren, and D. P. Weitekamp, Phil. Trans. R. Soc. Lond. A, 299, 585 (1981).

66. J. B. Murdoch, W. S. Warren, D. P. Weitekamp, and A. Pines, in submission.

67. J. B. Murdoch, Ph.D. Thesis, University of California, Berkeley (1981).

68. P. D. Buckley, K. W. Jolley, and D. N. Pinder, Progress in NMR Spectroscopy, 10, 1 (1975).

69. D. P. Weitekamp, Ph.D. Thesis, University of California, Berkeley (1981).

70. E. L. Hahn, Phys. Rev. 80, 580 (1950).

71. J. B. Murdoch, private discussion.

72. W. K. Rhim, A. Pines, and J. S. Waugh, Phys. Rev. B, 3, 684 (1971).

73. J. R. Garbow, D. P. Weitekamp, and A. Pines, in preparation.

74. R. L. Vold and R. R. Vold, "Progress in NMR Spectroscopy," 12, 79 (1978).

75. A. Kumar, J. Mag. Res. 30, 227 (1978).

76. A. Kumar and C. L. Khetrapal, J. Mag. Res. 30, 137 (1978); C. L. Khetrapal, A. Kumar, A. C. Kunwar, P. C. Mathias, and K. V. Ramanathan, J. Mag. Res. 37, 349 (1980).

77. A. Carrington and A. D. McLauchlan, Introduction to Magnetic Resonance (Harper and Row, New York-Evenston-London, 1967).

78. S. W. Sinton and J. Murdoch, unpublished work.

79. J. W. Emsley, J. Feeney, and L. H. Sutcliffe, High Resolution NMR Spectroscopy (Pergamon Press, Oxford, 1965), Vol. I, Chapter 8.

80. A. Hargreaves and S. Hasan Rizvi, Acta. Cryst. 15, 365 (1962).

81. I. Fischer-Hjalmars, Tetrahedron, 19, 1805 (1963).

82. G. Casalone, C. Mariani, A. Mugnali, and M. Simonetta, Mol. Phys. 15, 339 (1968).

83. M. J. S. Dewar and A. J. Harget, Proc. Roy. Soc. Lond. A. 315, 443 (1970).

84. A. Gamba, G. F. Tamtardini, and M. Simonetta, Spectrochim. Acta, 28, 1877 (1972).

85. A. Almennigen, O. Bastiansen, and M. Traetteberg, Acta Chem. Scand. 12, 1221 (1958).

86. J. Trotter, Acta Cryst. 14, 1135 (1961).

87. N. J. D. Lucas, Mol. Phys. 22, 147 (1971).

88. S. Sykora, J. Vogt, H. Bosiger, and P. Diehl, J. Mag. Res. 36, 53 (1979).

89. H. Kubota, T. Munakata, T. Hirooka, K. Kuchitsu, and Y. Harada, Chem. Phys. Lett. 74, 409 (1980).

90. V. Galasso, G. DeAlti, and A. Bigotto, Tetrahedron, 27, 991 (1971).

91. C. L. Khetrapal and A. C. Kunwar, Mol. Phys. 28, 441 (1974).

92. P. Bucci, M. Longeri, C. A. Veracini, and L. Lunazzi, J. Am. Chem. Soc. 96, 1305 (1974).

93. J. W. Emsley, D. S. Stephenson, J. C. Lindon, L. Lunazzi, and S. Pulga, J. Chem. Soc., Perkins II, 1541 (1975).

94. F. Lelj, N. Russo, and G. Chindichimo, Chem. Phys. Lett. 69, 530 (1980).

95. A. d'Annibale, L. Lunuzzi, A. C. Boicelli, and D. Macciantelli, J. Chem. Soc. Perkins II, 1396 (1973).

96. W. Niederberger, P. Diehl, and L. Lunazzi, Mol. Phys. 26, 571 (1973).

97. L. D. Field, S. Sterhell, and A. S. Tracey, J. Am. Chem. Soc. 99, 5249 (1977).

98. L. D. Field and S. Sternhell, J. Am. Chem. Soc. 103, 738 (1981).

99. E. Diaz, A. Guzman, M. Cruz, J. Mares, D. J. Ramirez, and P. Joseph-Nathan, Org. Mag. Res. 13, 180 (1980).

100. A. J. Leadbetter, R. M. Richardson, and C. N. Colling, J. de Physique 36, C1-37 (1975); J. E. Lyndon and C. J. Coakley, J. de Physique 36, C1-45 (1975).

101. J. W. Emsley, J. C. Lindon, and G. R. Luckhurst, Mol. Phys. 30, 1913 (1975).

102. N. Boden, L. D. Clark, R. J. Bushby, J. W. Emsley, G. R. Luckhurst, C. P. Stockley, Mol. Phys. 42, 565 (1981).

103. J. W. Emsley, G. R. Luckhurst, G. W. Gray, and A. Mosley, Mol. Phys. 35, 1499 (1978).

104. S. Sinton and A. Pines, Chem. Phys. Lett. 76, 263 (1980).

105. C. J. Reid and M. W. Evans, Mol. Phys. 40, 1523 (1980).

106. Hp. Schad and M. A. Osman, J. Chem. Phys. 75, 880 (1981).

107. J. M. Wacrenier, C. Duron, and D. Lippens, Mol. Phys. 43, 97 (1981).

108. G. W. Gray and A. Mosley, Mol. Cryst. Liquid Cryst. 35, 71 (1976).

109. A. Pines, S. Vega, and M. Merhing, Phys. Rev. B, 18, 112 (1978).

110. J. W. Emsley and D. L. Turner, J. Chem. Soc., Faraday II, 77, 1493 (1981).

111. Reference 18, p. 43.

112. A. O. Cunliffe, "The Calculation of Barriers to Internal Rotation from Torsional Frequencies," in Internal Rotation in Molecules, Orville-Thomas, ed. (Wiley, London, 1974), Chapter 7.

113. D. P. Weitekamp, J. R. Garbow, and A. Pines, in preparation.

114. Radio Amateurs Handbook (American Radio Relay League, Newington, Conn., 1976).

115. V. R. Cross, R. K. Hester, and J. S. Waugh, Rev. Sci. Instrum. 47, 1486 (1976).

116. F. D. Doty, R. R. Inners, and P. D. Ellis, J. Mag. Res. 43, 399 (1981).

117. S. W. Sinton, J. R. Garbow, D. E. Wemmer, D. J. Ruben, and A. Pines, to be published as a Lawrence Berkeley Laboratory Report.

118. P. Diehl, H. Kellerhals, and E. Lustig, "Computer Assistance in the Analysis of High-Resolution NMR Spectra," in NMR: Basic Principles and Progress, Ed. P. Diehl, E. Fluck, and R. Kosfeld (Springer-Verlag, Berlin-Heidelberg-New York, 1972), Vol. 6.

119. A. A. Bothner-By and S. M. Castellano in Computer Programs for Chemistry, Ed. D. F. Detar (Benjamin, New York, 1968), Vol. 1.

120. W. C. Hamilton, Statistics in Physical Science (Ronald, New York, 1964), Chapters 4 and 5.

121. P. Diehl, C. Khetrapal and U. Lienhard, Mol. Phys. 14, 465 (1968).

122. P. Diehl and H. Kellerhals, J. Mag. Res. 1, 196 (1969).

123. IBM System/360 Scientific Subroutine Package, Programmer's Manual (IBM Technical Publications Dept., New York, 1967).

124. Mathematical Methods for Digital Computers, Ed. A. Ralston and H. S. Wilf (Wiley, New York, 1962), Chapter 7.

125. M. Attimonelli and O. Sciacovelli, Org. Mag. Res. 13, 277 (1980).

126. J. Murdoch and S. Sinton, unpublished results.

127. P. L. Corio, Chem. Rev. 60, 363 (1960); A. Quirt and J. Martin, J. Mag. Res. 5, 318 (1971).

128. P. Diehl and H. Bosiger, private communication.

129. N. M. Brenner, IEEE Transactions on Audio and Electroacoustics, 17, 128 (1969).

130. P. D. Welch, IEEE Transactions on Audio and Electroacoustics, 17, 151 (1969).